uOttawa

L'Université canadienne
Canada's university

FACULTÉ DES ÉTUDES SUPÉRIEURES ET POSTOCTORALES

uOttawa

L'Université canadienne
Canada's university

FACULTY OF GRADUATE AND POSDOCTORAL STUDIES

Peiyuan Li

AUTEUR DE LA THÈSE / AUTHOR OF THESIS

Ph.D. (Chemical Engineering)

GRADE / DEGREE

Department of Chemical Engineering

FACULTÉ, ÉCOLE, DÉPARTEMENT / FACULTY, SCHOOL, DEPARTMENT

Adsorption and Separations for Methane, Carbon Dioxide, Nitrogen and Oxygen Gases

TITRE DE LA THÈSE / TITLE OF THESIS

Handan Tezel

DIRECTEUR (DIRECTRICE) DE LA THÈSE / THESIS SUPERVISOR

CO-DIRECTEUR (CO-DIRECTRICE) DE LA THÈSE / THESIS CO-SUPERVISOR

EXAMINATEURS (EXAMINATRICES) DE LA THÈSE / THESIS EXAMINERS

M. Eić

Z. Zhang

B. Kruczek

A. Tremblay

Gary W. Slater

Le Doyen de la Faculté des études supérieures et postdoctorales / Dean of the Faculty of Graduate and Postdoctoral Studies

ADSORPTION AND SEPARATIONS FOR METHANE, CARBON DIOXIDE, NITROGEN AND OXYGEN GASES

PEIYUAN LI

Thesis submitted to the Faculty of Graduate and Postdoctoral Studies

In partial fulfillment of the requirements for the degree of

DOCTOR OF PHILOSOPHY

In Chemical Engineering

Department of Chemical Engineering

Faculty of Engineering

University of Ottawa

Your file Votre référence
ISBN: 978-0-494-32410-3
Our file Notre référence
ISBN: 978-0-494-32410-3

TABLE OF CONTENTS

CHAPTER III

LIST OF TABLES

CHAPTER II

ADSORPTION SEPARATION OF NITROGEN, OXYGEN, CARBON DIOXIDE AND METHANE GASES BY β-ZEOLITE

CHAPTER III

EQUILIBRIUM AND KINETIC ANALYSIS OF CARBON DIOXIDE AND NITROGEN ADSORPTION SEPARATION BY CONCENTRATION PULSE CHROMATOGRAPHY

CHAPTER IV

PURE AND BINARY ADSORPTION EQUILIBRIA OF METHANE AND CARBON DIOXIDE ON SILICALITE

CHAPTER V

PURE AND BINARY ADSORPTION EQUILIBRIA OF CARBON DIOXIDE AND NITROGEN ON SILICALITE

CHAPTER VI

ADSORPTION SEPARATION OF METHANE AND NITROGEN ON SILICALITE

CHAPTER VII

PARAMETRIC ANALYSIS OF ADSORPTION SEPARATION PROCESSES FOR CARBON DIOXIDE / METHANE, CARBON DIOXIDE / NITROGEN AND METHANE / NITROGEN IN SILICALITE

CHAPTER VIII

MEMBRANE GAS SEPARATIONS, THEIR ADSORPTION BEHAVIORS AND SEPARATION MECHANISMS

LIST OF FIGURES

CHAPTER V

PURE AND BINARY ADSORPTION EQUILIBRIA OF CARBON DIOXIDE AND NITROGEN ON SILICALITE

CONTRIBUTIONS OF COLLABORATORS AND/OR CO-AUTHORS

I hereby declare that I am the first author of this thesis working only with my supervisor, Dr. F. Handan Tezel (excluding APPENDICES I and II). Dr. Tezel, Professor of the Department of Chemical Engineering at the University of Ottawa, has provided excellent collaboration throughout this research program. Her helpful comments, suggestions and editorial corrections have significantly improved the quality of this thesis and publications.

Signature: 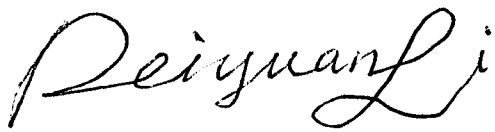 Date: April 6, 2007

ABSTRACT

Adsorption behaviour of different gases were studied in this work for adsorption and adsorbent membrane separations for flue gas, natural gas and landfill gas applications.

Pure adsorption kinetics and equilibrium of CO_2, N_2, CH_4 and O_2 with β-zeolite adsorbent, and CO_2 and N_2 with adsorbents silicalite, NaY and 13X zeolites were studied by using concentration pulse chromatography. Adsorption Henry's Law constants, heats of adsorption, micro-pore diffusion coefficients and corresponding activation energies were determined experimentally and the three different mass transfer mechanisms were discussed. Ideal separation factors were obtained for the adsorption separation applications of the gases studied. Micro-pore diffusion resistance is the definite dominant mass transfer mechanism for most of the adsorbents and separations studied.

Adsorption separations of CO_2/N_2, CO_2/CH_4 and CH_4/N_2 on silicalite were studied by using constant volume and concentration pulse chromatographic techniques. Mixture adsorption isotherms for the binary systems were determined experimentally by using three binary concentration pulse methods. Corresponding x-y adsorption phase diagrams and realistic separation factors were obtained from these experimental binary adsorption isotherms. The results showed that silicalite is a promising adsorbent for the separation of carbon dioxide and nitrogen. Thermodynamic consistency tests between pure and binary gas adsorption systems were performed and results showed reasonable consistency.

Breakthrough curves for dynamic adsorption separation of CO_2/CH_4, CO_2/N_2 and CH_4/N_2 gases with silicalite were determined. Parametric studies, as well as economic assessments were carried out for these separations, using adsorption columns packed with silicalite.

Separations of CO_2/CH_4, CO_2/N_2 and CH_4/N_2 gases with MFI zeolite membrane and separation of CO_2/N_2 gases with two silicone rubber membranes were also studied in this work. Separation factors and permeabilities were measured, adsorption behaviours were analyzed. and separation process mechanisms were discussed. It was concluded that adsorption plays an important role in the separations of these gases with MFI zeolite membrane and silicone rubber membranes.

RÉSUMÉ

Dans cette étude, nous avons examiné le comportement d'adsorption des differents gaz pour l'adsorption et membrane de séparation utilisant des adsorbants pour les applications de gaz combustion, de gaz naturel, et de gaz d'enfouissement.

Nous avons étudié les cinétiques d'adsorption et l'équilibres des gaz pure (CO_2, N_2, CH_4 et O_2) avec β-zéolite et les gaz CO_2 et N_2 avec l'adsorbants silicate et zéolites NaY et 13X en utilisant impulsion de concentration de chromatographie. Les constant de Henri, les énergies d'adsorption, les coefficients de diffusion de micropore, et les correspondantes énergies d'activation sont déterminés expérimentalement, et les trois différents mécanismes de transfert de masse sont discutés. Les facteurs de séparation idéale pour les applications de séparation d'adsorption des gazes étaient obtenus et étudiés. La résistance de diffusion de micropores est le plus dominant mécanisme de transfert de masse pour la plupart des adsorbants et séparations étudier.

Les séparations d'adsorption de CO_2/N_2, CO_2/CH_4 et CH_4/N_2 sur silicate en utilisant un volume constant et les techniques d'impulsion de concentration de chromatographie, sont étudiés. Les isothermes d'adsorption des mixtures pour les systèmes binaires sont déterminées expérimentalement en utilisant trois méthodes de binaires concentration pulse. Les diagrammes de phase d'adsorption en direction x-y correspondant et les facteurs réels de séparation étaient obtenus en utilisant les isothermes binaires d'adsorption déterminée expérimentalement. Les résultats montre que silicate est l'adsorbant avec le plus de prometent pour la séparation de CO_2 et N_2. Les Tests thermodynamiques de consistance entre les systèmes d'adsorption de gaz pure et binaires performé et les résultats sont raisonnables et consistants.

La courbe d'entamer pour la séparation d'adsorption dynamique de CO_2/CH_4, CO_2/N_2 et CH_4/N_2 gazes avec silicate étaient déterminé. Les études paramétriques et d'assessements économiques étaient accomplies pour ces séparations en utilisant des colonnes d'adsorption pleines de silicates.

De plus, nous avons étudié les séparations des gazes CO_2/CH_4, CO_2/N_2 et CH_4/N_2 avec la membrane MFI zéolite et la séparation des gazes CO_2/N_2 avec deux membranes de silicone. Les facteurs de séparation et perméabilité ont étés mesurés, les comportements d'adsorption sont analysés, et les mecanisms de système de séparation sont discutés. Il était conclu que l'adsorption joue un rôle important dans les séparations de ces gazes avec les membranes fabrique de MFI zéolite et de silicone.

ACKNOWLEDGEMENTS

First and foremost, I would like to express my deep gratitude to my supervisor Dr. F. Handan Tezel, who offered me this opportunity to carry out the PhD program. I sincerely appreciate the financial support she has provided which made this work possible. I thank her for her precious time to discuss the research problems during our regular meetings and whenever I went to her office to see her. She not only has shared her knowledge on chemical engineering science. but also educated me how to write scientific papers better, how to use the English language properly, and more importantly, how to become a good scientific researcher. I realize that she has done tremendous work on my behalf. Her valuable instructions, helpful suggestions and beneficial guidance are great contributions to this thesis. I am deeply indebted to her. Her humanism, enthusiasm and professionalism have deeply influenced me and undoubtedly will benefit me forever.

Besides my supervisor, I would like to thank the rest of the staff and professors in the department who have given me assistance and support on the research and in the lab. I also would like to take this moment to thank my colleagues in our group who have helped me a lot during the past four years.

Next, I would like to thank the Natural Sciences and Engineering Research Council of Canada (NSERC), the Ontario Graduate Scholarship (OGS) Program, and the Canadian Society for Chemical Engineering (CSChE) for the scholarships. Their Financial supports are really important for my research.

Last, but not least, I thank my family. I owe tremendous debts to my wife, Xuemei Shen. She has carried on most of our family work so that I could concentrate on this research program. I am also greatly indebted to my daughter, Chuan Silvia Li, to whom I should have devoted more time for her.

CHAPTER I

INTRODUCTION

PREAMBLE

SCOPE OF RESEARCH

THESIS STRUCTURE

REFERENCES

PREAMBLE

The global environment is a major issue today, and global warming in particular is the focus of much attention. Accumulation of greenhouse gases (GHG) in the atmosphere is responsible for increased global warming of our planet. It is supposed that the increasing concentration of carbon dioxide mainly from flue gases, landfill gases and automobile emissions in the atmosphere is the major contributor to this problem with more than 80% of total GHG emissions (Cavenati et al., 2005; Hansen et al., 1988). The emission of carbon dioxide from power plants that burn fossil fuels is the major cause for the accumulation of carbon dioxide in the atmosphere, which causes long-range environmental problems.

Methane is the most important non-CO_2 GHG responsible for global warming making up more than 10% of total GHG emissions. Despite the much smaller amounts of methane released to the atmosphere, the greenhouse warming potential (GWP) of this gas is much higher than carbon dioxide. Therefore, any reduction in methane emissions is important in the short- and medium-term atmosphere reconstruction (Cavenati et al., 2004 and 2005). Landfill gas (LFG) is a multi-component mixture containing mainly methane and carbon dioxide, which constitutes one of the main sources of methane and carbon dioxide emissions, and can be treated as an important resource of directly available methane. This reason, together with a tighter control in emissions to meet Kyoto Protocol targets, puts LFG into consideration for energy production (Cavenati et al., 2004 and 2005).

Separations of carbon dioxide and nitrogen, carbon dioxide and methane, and methane and nitrogen can play a key role in alleviating those problems. The two popular methods for the separation of carbon dioxide and nitrogen from flue gases are adsorption and membranes. These two methods are widely used, as well, in the separation of carbon dioxide and methane for the purification of landfill gas, the upgrade of natural gas and enhanced oil recovery. Nitrogen is needed to be removed from Landfill gas and low grade natural gas for getting new resource of energy, but the separation is really difficult. Because of low selectivities of existing membranes for CH_4/N_2 system, the main technology available for this separation is adsorption (Tabe-Mohammadi, 1999), and to our knowledge, there is no significant improvement until now.

SCOPE OF RESEARCH

In this work, adsorption behaviors for separations, adsorption separation processes and membrane separations with adsorption behaviors have been studied for different gas systems. The scope of research, excluding the two papers in Appendices, includes:

- Main Applications: flue gas, landfill gas, natural gas and enhanced oil recovery;
- Separation Methods: adsorption and membranes;
- Adsorbates: CO_2, N_2, CH_4 and O_2;
- Separations: CO_2/N_2, CO_2/ CH_4, CH_4/ N_2, O_2/ N_2, CO_2/ O_2, and CH_4/ O_2;
- Zeolite Adsorbents: MFI (silicalite and ZSM-5), β-zeolite, NaY and 13X;
- Adsorption: adsorption separations, adsorption behaviors, adsorption mechanism and adsorption applications;
- Adsorption Behavior and Separation: Henry's law constants, heats of adsorption, micro-pore diffusion coefficients, mass transfer mechanisms, equilibrium and kinetic separation factors, equilibrium phase diagrams and integral thermodynamic consistency tests;
- Temperatures of Adsorption Behavior and Separation: 40, 70 and 100 ^{0}C;
- Concentration Pulse Chromatographic Techniques: HT-CPM (Harlick and Tezel Concentration Pulse Method), MTT-CPM (Modified Triebe and Tezel Concentration Pulse Method) and MVV-CPM (Modified Van der Vlist and Van der Meijden Concentration Pulse Method);
- Pure Adsorption Isotherm Models: Langmuir, Freundlich, Sips (Langmuir-Freundlich), Flory-Huggins (vacancy solution theory), Toth, Multisite-Langmuir, and Dualsite-Langmuir;
- Temperature Independent Pure Adsorption Isotherm Models: Toth and Sips (Langmuir- Freundlich);
- Predicted binary isotherm Models: Extended Langmuir, Extended Dualsite Langmuir, Ideal Adsorbed Solution Theory, Statistical Model, Extended Sips (Langmuir-Freundlich) and Flory-Huggins (vacancy solution theory);
- Breakthrough Curves of Adsorption Dynamics: Rosen model, collision integral (Ω_{AB}) in the Lennard-Joned potential-energy function, molecular diffusivity (D_m),

Knudsen diffusivity (D_k) and rates of transfer in the adsorption;

- Parametric Analysis of Adsorption Separation: pressure, particle size, superficial velocity and column length;
- Economic Assessment of Adsorption Separation Processes, including comparison with membrane Processes;
- Membrane Processes: synthesis and separation;
- Types of membranes: MFI zeolite and silicone rubbers (silicone polycarbonate and dimethyl silicone);
- Membrane Separations: permeability, separation factor, ideal separation factor, adsorption behavior and separation mechanisms.

THESIS STRUCTURE

This thesis is presented in paper format. Chapters II and III, the first and the second papers, investigate gas adsorption equilibrium and kinetic separation potential by using concentration pulse chromatography. The systems of the first paper are β-zeolite adsorbent for the separations CO_2/N_2, CO_2/CH_4, CH_4/N_2, O_2/N_2, CO_2/O_2 and CH_4/O_2 and for the gases N_2, O_2, CO_2 and CH_4. The systems of the second paper are silicalite, NaY and 13X adsorbents for the separation CO_2/N_2 and for the gases CO_2 and N_2. In the two papers, adsorption Henry's Law constants and heats of adsorption are obtained by using the Van't Hoff equation. The micro-pore diffusion coefficients and corresponding activation energies are determined experimentally, and the three different mass transfer mechanisms that have to take place for adsorption to occur are discussed. From the equilibrium and kinetic data, the equilibrium and kinetic separation factors are obtained for the gas adsorption separation processes studied. Micro-pore diffusion resistance is the definite dominant mass transfer mechanism for all the systems studied.

Chapters IV, V and VI (the third, the fourth and the fifth papers) study adsorption separation on silicalite by both the concentration pulse chromatographic techniques and the constant volume method for determining pure and mixture adsorption behaviours. The third paper is for the separation of methane and carbon dioxide, the fourth for carbon dioxide and

nitrogen, and the fifth for methane and nitrogen. In these three papers, pure adsorption isotherms are determined by using the constant volume method in the pressure range between 0 and 5 atmospheres at 40, 70 and 100 °C. The ranges of temperature and pressure studied are extended to other operating conditions by using temperature independent isotherm models. Ideal separation factors are obtained from the isotherms of the pure systems. Mixture adsorption isotherms for the binary systems at 40, 70 and 100 °C at 1 atmosphere total pressure are determined experimentally by using three binary concentration pulse methods, HT (Harlick and Tezel) - CPM (Concentration Pulse Method), MTT (Modified Triebe and Tezel) - CPM and MVV (Modified Van der Vlist and Van der Meijden) - CPM. Predicted ideal binary isotherms are compared to the experimental ones. x-y diagrams and separation factors are obtained from the experimental binary isotherms. Applicability of different binary adsorption models for these systems is discussed. The integral thermodynamic consistency tests between pure and binary gas adsorption systems are also shown and discussed. Silicalite is found to be a promising adsorbent for these separations.

Chapter VII, the sixth paper, deals with adsorption dynamics of separating CO_2/CH_4, CO_2/N_2 and CH_4/N_2 with silicalite. Henry's law constants are determined from temperature independent isotherms based on the parameters from Chapters IV, V and VI. Collision integral (Ω_{AB}) in the Lennard-Joned potential-energy function is calculated. And then, in internal (intra-particle) transport processes, molecular diffusivity (D_m), Knudsen diffusivity (D_k), the total diffusivity (D) and the effect diffusivity (D_e) are determined. After that, by using the Rosen Model, the rates of transfer in the adsorption are unravelled and the breakthrough curves of adsorption dynamics of separating the three systems are worked out. Next, the parametric analyses of adsorption separation processes involving CO_2/CH_4, CO_2/N_2 and CH_4/N_2 are carried out. The effects of pressure, temperature, particle size, superficial velocity and column length are discussed. Finally, the economic assessment of PSA is compared with that of membrane separation and it was concluded that adsorption is an economical method for the three separations.

Chapter VIII, the seventh paper, studies the synthesis and applications of MFI (silicalite and ZSM-5) zeolite membrane. The separations of CO_2/N_2, CO_2/CH_4 and CH_4/N_2 with MFI (silicalite and ZSM-5) zeolite membrane and with two types of silicone rubber

membranes (silicone polycarbonate membrane and dimethyl silicone membrane) are investigated. The separation factors and permeability values have been measured. Their adsorption behaviours in the separation processes are analyzed and separation mechanisms are discussed.

Additionally, two more papers given in Appendices I and II, are entitled "Adsorption Separation of CO_2/N_2 and CO_2/CH_4 by Zeolites" and "Binary Adsorption Behaviour of Methane and Nitrogen Gases", respectively. I should mention that I am not the first author of these two papers. Because of that, only the abstracts of them are collected in the thesis and presented in Appendices I and II. Appendix III is entitled "The Unit of Henry's Law Constant and the Relation between the two Henry' Law Constants", which is used in the papers related to this thesis. Appendix IV is entitled "Zero Length Column (ZLC) Method", which is an adequate technique for adsorption kinetic measurements.

REFERENCES

Cavenati, S., C. A. Grande and A. E. Rodrigues, "Adsorption Equilibrium of Methane, Carbon Dioxide, and Nitrogen on Zeolite 13X at High Pressures", Journal of Chemical and Engineering Data **49**, 1095 (2004).

Cavenati, S., C. A. Grande and A. E. Rodrigues, "Upgrade of Methane from Landfill Gas by Pressure Swing Adsorption", Energy and Fuels **19**, 2545 (2005).

Hansen, J., I. Fung, A. Lacis, D. Riud, J. S. Levedeff, R. Ruedy and G. Russell, "Global Climate Changes as Forecast by Goddard Institute for Space Studies Three-Dimensional Model", Journal of Geophysical Research **93,** 9341 (1988).

Tabe-Mohammadi, A., "A Review of the Applications of Membrane Separation Technology in Natural Gas Treatment", Separation Science and Technology **34**, 2095-2111 (1999).

CHAPTER II

ADSORPTION SEPARATION OF NITROGEN, OXYGEN, CARBON DIOXIDE AND METHANE GASES BY β-ZEOLITE

Peiyuan Li and F. Handan Tezel*

Department of Chemical Engineering
Faculty of Engineering
University of Ottawa
161 Louis Pasteur, Ottawa, Ontario K1N 6N5, Canada

Published in Microporous and Mesoporous Materials **98** (2007) 94–101.

Presented at 55th CSChE (Canadian Society for Chemical Engineering) Canadian Chemical Engineering Conference, Toronto, Canada, on Oct. 16-19, 2005, Conference Proceedings 593.

* Corresponding author
Tel: 613-562-5800 Ext. 6099
Fax: 613-562-5172
Emai: Handan.Tezel@uottawa.ca

ABSTRACT

In the present study, adsorption equilibrium and kinetic separation potential of β-zeolite is investigated for N_2, O_2, CO_2 and CH_4 gases by using concentration pulse chromatography. Henry's Law constants and heats of adsorption are obtained by using the Van't Hoff equation. The micro-pore diffusion coefficients are determined, and the three different mass transfer mechanisms, that have to take place for adsorption to occur, are discussed. From the equilibrium and kinetic data, the equilibrium and kinetic selectivities are obtained for the separation of the gases studied.

Regarding β-zeolite, carbon dioxide has the highest Henry's Law constant for all the temperatures studied, followed by methane, nitrogen and oxygen. Micro-pore diffusion is the dominant mass transfer mechanism for all the systems studied. Both equilibrium and kinetic separation factors decrease as column temperature increases. Carbon dioxide separation from oxygen, nitrogen and methane has high equilibrium separation factor. This factor is not very high for methane / nitrogen and methane / oxygen systems and is the lowest for nitrogen / oxygen system. The kinetic separation factors are very small for all the systems studied at high column temperatures. At low temperatures, methane / carbon dioxide system has favourable kinetic separation factor. Nitrogen / carbon dioxide and oxygen / carbon dioxide systems can be separated in kinetic processes with reasonable separation factors. Considering all the observations from this study, it was concluded that β-zeolite is a good candidate to be used for applications in flue gas separations, as well as natural gas and landfill gas purifications.

Keywords: β-Zeolite; Adsorption; Gas separations; Concentration pulse chromatography; Nitrogen Adsorption, Oxygen Adsorption, Carbon Dioxide Adsorption, Methane Adsorption

INTRODUCTION

β-zeolite was discovered before Mobil began the "ZSM" naming sequence. It is the second in an earlier sequence. The structure of β-zeolite consists of intersecting 6.5 X 5.6 and 7.5 X 5.7 Å channels. Up to now, there are no reports on applications of β-zeolite for gas adsorption separations. In the present study, adsorption separation of nitrogen (N_2), oxygen (O_2), carbon dioxide (CO_2) and methane (CH_4) gases using β-zeolite is investigated by studying the equilibrium and kinetic parameters. These gases are very important in many industrial applications, as well as in our daily life. Increasing concentration of carbon dioxide in the atmosphere is a major contributor to the global warming. Separation of CO_2 from air (mostly N_2) is important from that perspective. Separation of CH_4 and CO_2 is important for recovering CH_4 from the landfill gas emissions, as well as for natural gas applications. Enriched oxygen generation from air (a mixture of N_2 and O_2) is an important separation to be used for hospitals, as well as for combustion systems that use enriched oxygen for increasing the efficiency and reducing green house gas emissions.

The use of concentration pulse chromatography for adsorbent screening is very attractive, since it is relatively inexpensive to set up. This technique uses a dynamic method of studying adsorption and measures the response of a chromatographic column to a pulse in adsorbate concentration. The first and second moments of the response peak generated by a pulse in carrier concentration would yield the slope of the isotherm and the diffusivity for any given system. This method has been used in many studies for determination of adsorption capacities and diffusivities, and has been shown to agree well with gravimetric and volumetric data. For the determination of binary adsorption isotherms, this method was found to be simpler and quicker [1-16].

In the concentration pulse chromatographic technique, a pulse of the sample gas is injected into the carrier stream and passed through the column. The response of the column is measured as concentration vs. time at the exit of the column. From this response peak a mean retention time of the sample, μ, defined as the first moment of the chromatogram, is determined experimentally [17]. Dimensionless Henry's Law constants can also be calculated from the corrected first moment of the response peaks as follows [2,3,7]:

$$\mu = \frac{\int_0^t c(t-\mu_D)dt}{\int_0^t cdt} = \frac{L}{v}\left[1+\frac{(1-\varepsilon)K}{\varepsilon}\right] \quad \text{.....(1)}$$

where t is the time, c is the adsorbate concentration measured at the outlet of the column, L is the column length, ε is the bed porosity, v is the interstitial fluid velocity, K is the dimensionless Henry's Law adsorption equilibrium constant, and μ_D is the dead time (the time corresponding to the dead volume).

The dimensionless Henry's Law constants, K, can be converted to a dimensional form, K_p, as follows:

$$K_p = \frac{K}{RT\rho_p} \quad \text{.....(2)}$$

where T is the absolute temperature, ρ_p is the density of the pellets of the adsorbent and K_p is the dimensional Henry's Law adsorption equilibrium constant.

The Van't Hoff equation is given as [18]:

$$K_p = K_0 e^{\frac{\Delta H}{RT}} \quad \text{.....(3)}$$

where T is the column temperature, R is the gas constant, ΔH is the heat of adsorption, and K_0 is the pre-exponential factor. ΔH and K_0 may be obtained from the experimentally determined value of K at several different temperatures. These values can then be used to calculate equilibrium separation factor, the ratio of the Henry's law constants, which is useful in predicting promising separation conditions.

The rate of diffusion in micro-pores can be measured by concentration pulse chromatography from the second moment of the response peak defined as [18]:

$$\sigma^2 = \frac{\int_0^t c(t-\mu)^2 dt}{\int_0^t cdt} \quad \text{.....(4)}$$

where μ is the corrected retention time, t is time, and c is the adsorbate concentration at the outlet of the column [17]. In the low Reynolds number regime (less than 100) $Sh = 2k_f R_p/D_m = 2.0$, assuming spherical geometry, a useful general form for the second moment of the response is [18]:

$$\frac{\sigma^2}{2\mu^2}\cdot\frac{L}{v} = \frac{D_L}{v^2} + \frac{\varepsilon}{(1-\varepsilon)}\left(\frac{R_p^2}{3D_m} + \frac{R_p^2}{15\varepsilon_p D_p} + \frac{r_c^2}{15KD_c}\right) \quad \text{.....(5)}$$

where μ is the corrected retention time (the first moment of the response peak), σ^2 is the second moment of the response peak, L is the column length, ε is the bed porosity, v is the interstitial fluid velocity, K is the dimensionless Henry's law constant, D_l is the axial dispersion coefficient, R_p is the pellet radius, r_c is the crystal radius, ε_p is the pellet porosity, D_p is the macro-pore diffusivity (based on free pore area), D_c is the diffusivity within a crystal (or micro-pore diffusivity), k_f is the external film mass transfer coefficient, and D_m is the molecular diffusivity. The first term on the right hand side of Equation (5) represents the axial dispersion. The last term in parenthesis represents the addition of external film mass transfer, macro-pore diffusion and micro-pore diffusion resistances, respectively. Equation (5) suggests that a plot of the dispersion ($\sigma^2 L/2\mu^2 v$) vs. $1/v^2$ should be approximately linear with slope D_l and intercept given by the last term on the right hand side of Equation (5). Such plots provide a convenient means of extracting the dispersion and mass transfer parameters and establishing which mass transfer resistance is dominant.

The molecular diffusivity, D_m, in $cm^2.s^{-1}$, can be calculated by Chapman-Enskog equation [19-21]:

$$D_m = 1.8583 \times 10^{-3} \times \frac{T^{\frac{3}{2}} \left(\frac{1}{M_A} + \frac{1}{M_B}\right)^{\frac{1}{2}}}{P\sigma_{AB}^2 \Omega_{AB}} \quad \text{.....(6)}$$

where T is the temperature in K, M is the molecular weight, P is the total pressure in atm., σ is a constant in the Lennard-Jones potential-energy function in Å, and Ω is the collision integral (dimensionless). Subscripts A and B refer to components A and B.

The meso-pore and macro-pore diffusivity, D_p, a combination of molecular diffusivity and Knudsen diffusivity, can be calculated by [6]:

$$D_p = \frac{1}{\frac{1}{D_m} + \frac{1}{D_k}} \quad \text{.....(7)}$$

The Knudsen diffusivity, D_k, in $cm^2.s^{-1}$, is given by [6,22]:

$$D_k = 9700 r_p \left(\frac{T}{M}\right)^{\frac{1}{2}} \quad \text{.....(8)}$$

where r_p is the pore radius in cm, M is the molecular weight, and T is temperature in K.

Having predicted the molecular diffusivity from Equation (6) and the macro-pore diffusivity from Equation (7), the micro-pore resistance and the value of D_c/r_c^2 can be calculated experimentally from Equation (5).

When external film mass transfer and macro-pore diffusion resistances are much smaller than micro-pore diffusion resistance, the micropore diffusion is the dominant mass transfer mechanism. When determining the micropore diffusion coefficient, it is important to make sure that this mass transfer resistance is the dominating mechanism. In considering such diffusion processes the value of D_c/r_c^2 can be used to calculate the kinetic separation factor, the ratio of the values of D_c/r_c^2, which is useful in predicting promising separation conditions.

EXPERIMENTAL

Apparatus

A schematic diagram of the experimental apparatus is shown in Figure 2.1.

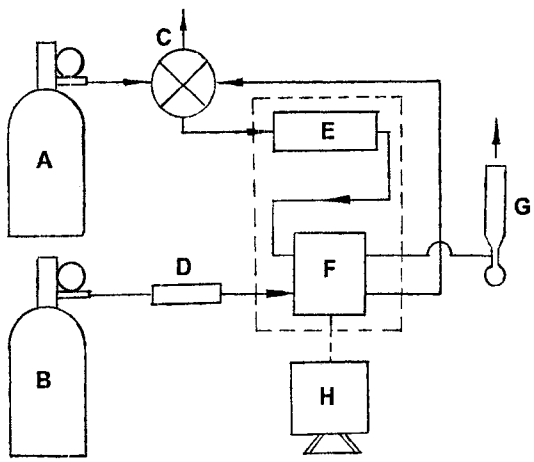

Figure 2.1. Schematic diagram of the experimental set-up.

A – Sample gas; B – Carrier gas;
C – Gas injection valve; D – MKS MFC;
E – Packed adsorption column in GC oven; F – TCD;
G – Bubble meter; H – Computer.

A Varian 3300 gas chromatograph (GC) is equipped with a thermal conductivity detector (TCD), which was used to measure the response of the column to the sample gas injection. The column packed with the β-zeolite adsorbent was fully contained in the GC oven for accurate temperature control. The sampling valve introduced a 1 cc pulse at atmospheric pressure into the helium carrier gas stream. Carrier flow rates were controlled by an MKS mass flow controller (MFC), model number 1259C (0 – 50 sccm range), and measured by a bubble meter at the exit. The carrier helium gas first passed through the reference side of the TCD. It then went through the sample injection valve, where the adsorbate gas sample was injected. After that, the carrier and the sample gases passed through the packed column and the concentration at the outlet of the column was monitored as a function of time. Data acquisition was performed using a National Instruments based data acquisition card and Labview 6.1 on a computer. The adsorbent was regenerated at 101.3 kPa and 350 °C under helium purge (5cc/min at room temperature) for approximately 21 hours before use.

Materials

β-zeolite powder supplied by Professor Neal Tai-Shung Chung from the Department of Chemical and Environmental Engineering at National University of Singapore was mixed with kaolin binder (70% β-zeolite powder and 30% kaolin binder, on a weight % basis) to form 20-60 mesh pellets, and was packed in the column. The sample and carrier gases used in the experiments are listed in Table 2.1.

Specifications and Conditions

The experimental and column specifications and conditions are listed in Table 2.2.

Table 2.1. Details of sample and carrier gases.

Gases	Grade	Purity	Supplier
He (Carrier gas)	Ultra High Purity 5.0	99.999%	Praxair Inc., Ottawa
N_2 (Adsorbate)	Ultra High Purity 5.0	99.999%	Praxair Inc., Ottawa
O_2 (Adsorbate)	Ultra High Purity 4.3	99.993%	Praxair Inc., Ottawa
CO_2 (Adsorbate)	Bone Dry 3.0	99.9%	Praxair Inc., Ottawa
CH_4 (Adsorbate)	Ultra High Purity 3.7	99.97%	Praxair Inc., Ottawa

Table 2.2. Experimental and column specifications and conditions.

Particle Size	20-60 mesh (0.0246-0.0833cm)
Average Particle Diameter, D_p	0.0540 cm
Bed Porosity, ε	0.260
Length of Column, L	10.01 cm
Inner Diameter of Column	0.451 cm
Total Pressure	101.3 kPa
Detector Temperature	110 °C
Detector Initial Attenuation	2
Detector Initial Range	0.50 mV
Detector Filament Temperature	130 °C
Regeneration Temperature	350°C
Regeneration Pressure	101.3 kPa
Regeneration Time	21 hours

RESULTS AND DISCUSSION

Equilibrium Data and Separation Factors

Dimensionless Henry's Law constants, K, are determined from the corrected first moment of the response peaks by using Equation (1) [7], then converted to a dimensional form, K_p, according to Equation (2) [2,3], and listed in Table 2.3 for different adsorbates in the temperature range 40-100°C. Corresponding vant Hoff plots are given in Figure 2.2 as dimensional Henry's Law constants, K_p, as a function of inverse temperature (Equation 3). CO_2 had the highest Henry's Law constant, among the adsorbates studied. One reason for it is that the kinetic diameter of CO_2 molecule is smaller than that of all the other gases studied. The second reason for it is the highest quadropole moment of the CO_2 gas compared to the other ones. Although CH_4 is not a polar molecule, it has high polarizability. This causes CH_4 to have higher Henry's Law constant, compared to N_2 and O_2, which have very similar Henry's Law constant values.

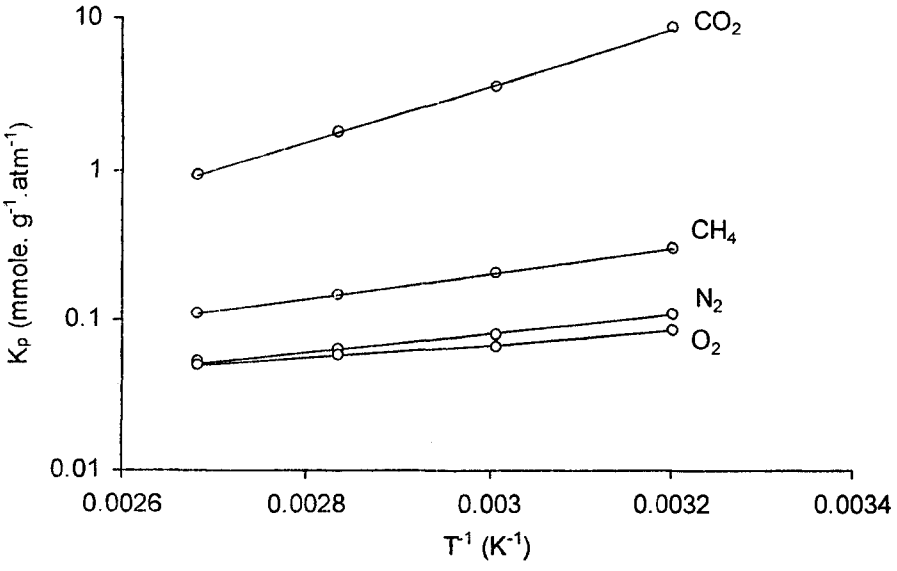

Figure 2.2. Linear regression of the relation between Henry's Law adsorption equilibrium constant (K_p) and inverse of column temperature (1/T): K vs. T^{-1} with different adsorbates for β-zeolite.

Table 2.3. Henry's Law adsorption equilibrium constants given in units of (mmole.g^{-1}.atm^{-1}) for β-zeolite at different temperatures studied.

Adsorbates	39.1 °C	59.3 °C	79.5 °C	99.8 °C
O_2	0.0967	0.0810	0.0754	0.0680
N_2	0.124	0.0969	0.0825	0.0719
CH_4	0.338	0.248	0.190	0.149
CO_2	9.39	4.24	2.25	1.29

Table 2.4 summarizes the parameters, K_0 and ΔH, which give the temperature dependence of K_p according to Equation (3). For all the four gases, Henry's law constants decrease as temperature increases, since adsorption is an exothermic process. As can be seen from Table 2.4. CO_2 has the highest heat of adsorption, again, due to its high quadropole moment. Its interaction with the surface of the β-zeolite is the highest, among the adsorbates studied. The order of the heat of adsorption data follows the same trend as the order of the Henry's Law constants for all the adsorbates.

Table 2.4. β-zeolite adsorption heats and pre-exponential factors.

Adsorbates	K_0 mmole. g^{-1}.atm^{-1}	ΔH kJ.mol^{-1}
O_2	3.44×10^{-3}	-8.27
N_2	1.31×10^{-3}	-11.41
CH_4	6.57×10^{-4}	-15.86
CO_2	1.39×10^{-5}	-34.44

The primary requirement for an economic separation process is an adsorbent with sufficiently high capacity, and selectivity. This selectivity can be based on difference in either adsorption kinetics or adsorption equilibrium. Most of the adsorption processes in current use depend on equilibrium selectivity. In considering such processes it is convenient to define an adsorption equilibrium separation factor:

$$\alpha_{e,A/B} = \frac{x_A / x_B}{y_A / y_B} \quad \text{.....(9)}$$

where x_A, x_B, y_A, and y_B are, respectively, the mole fractions of components A and B in adsorbed and fluid phases at equilibrium. At low concentrations, where Henry's law applies, the separation factor is simply given by the ratio of the Henry's law constants This separation factor, based on equilibrium conditions, is defined as follows:

$$\alpha_{ei,A/B} = \frac{K_{pA}}{K_{pB}} \quad \text{.....(10)}$$

where K_{pA} and K_{pB} are dimensional Henry's Law adsorption equilibrium constant for components A and B, respectively. By using concentration pulse chromatography, we can make sure that the system has the concentrations low enough to follow Henry's law, by injecting a very small amount of the sample gas into the carrier gas stream.

$\alpha_{ei,A/B}$ is the initial equilibrium separation factor, calculated according to Equation (10), and is shown as a function of temperature in Figure 2.3, in which they decrease as column temperature increases. This decrease depends on the relative magnitudes of the heats of adsorption of the 2 components. Following Equations 3 and 10, when T increases, $-(\Delta H_A - \Delta H_B)/RT$ decreases, so $\alpha_{ei,A/B}$ decreases. The highest selectivity values are obtained with CO_2, since it has the highest Henry's Law constant, compared to the other gases. The systems consisting carbon dioxide with oxygen and with nitrogen have good initial equilibrium separation factors, followed by the carbon dioxide/ methane system. Methane/oxygen and methane/nitrogen have small selectivities. For the nitrogen/oxygen system, the values are very close to 1, indicating the difficulty of the separation by equilibrium.

It needs to be emphasized that the separation factors considered here are based on low concentration Henry's Law region adsorption equilibrium properties. Although, realistically speaking, the separation factor should be based on actual capacities under mixture conditions; the one calculated in the Henry's Law region would be an initial indicator of how easy the separation would be.

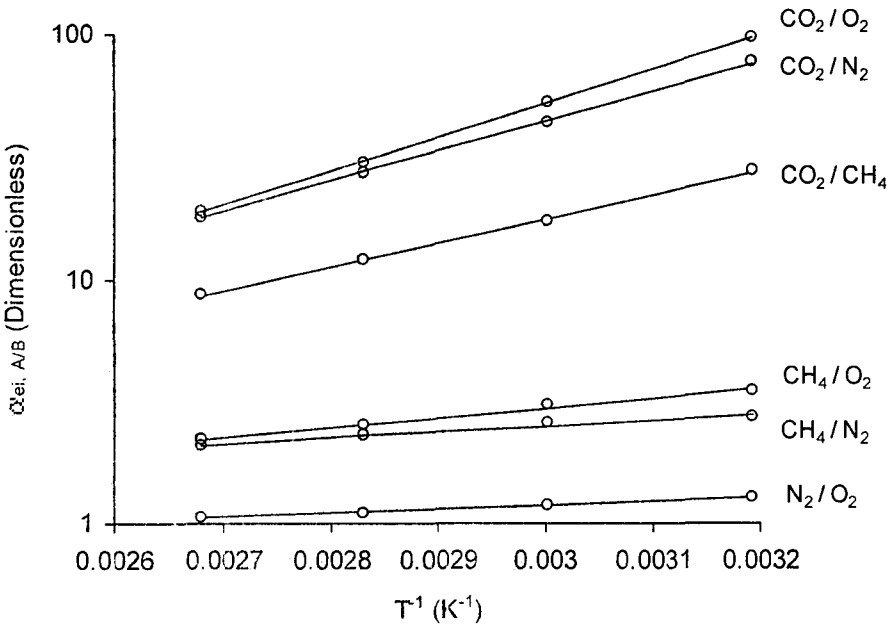

Figure 2.3. The change of adsorption equilibrium separation factor ($\alpha_{ei,\,A/B}$) with column temperature for different adsorbate pairs with β-zeolite.

Comparison of β-zeolite equilibrium data with other zeolite adsorbents, such as silicalite, NaY and 13X [2, 23-26], indicate following:

For CO_2, $K_{p,\text{Silicalite}} < K_{p,\beta\text{-zeolite}} < K_{p,\text{NaY}}$ or $K_{p,13X}$;

For CO_2, $(-\Delta H)_{\text{Silicalite}} < (-\Delta H)_{\beta\text{-zeolite}} \approx (-\Delta H)_{\text{NaY}}$ or $(-\Delta H)_{13X}$;

For CO_2/N_2, $\alpha_{ei,\text{Silicalite}} < \alpha_{ei,\beta\text{-zeolite}} < \alpha_{ei,\text{NaY}} < \alpha_{ei,13X}$.

β-zeolite positions itself between silicalite, which has a ZSM-5 structure, and X and Y zeolites, as far as the Henry' Law constants and heat of adsorption values are considered. The reason for that is the fact that silicalite has no cations in its structure and therefore has a homogeneous surface, whereas β-zeolite, X and Y zeolites have more heterogeneous surfaces. Since CO_2 molecules have quadrupole moment, it is attracted more towards heterogeneous surfaces, increasing the Henry's Law constant and the heat of adsorption for zeolitesβ, X and Y. When the equilibrium separation factors for CO_2 and N_2 are considered for these adsorbents, the trend follows the Si/Al ratio. The lower this ratio is, the higher the

separation factor is. due to more cations in the structure of the adsorbent, making the surface more heterogeneous to attract more CO_2.

Kinetic Data and Estimation of Micro-Pore Diffusion

Equation (5) suggests that a plot of the dispersion $(\sigma^2 L/2\mu^2 v)$ vs. $1/v^2$ should be approximately linear at low flow-rates, with slope D_l and intercept given by the last term of Equation (5) (overall mass transfer resistance). Such plots provide a convenient means of extracting the dispersion and mass transfer parameters. From a comparison of the mass transfer resistances measured under different experimental conditions, it is possible to establish which mass transfer resistance is dominant. A typical linear plot is shown in Figure 2.4.

For CO_2, O_2 and N_2, the contributions of mass transfer resistances, absolute values and percentages to total dispersion resistances are given in Table 2.5, in which, external film mass transfer $(R_p^2/3D_m)$, and macro-pore diffusion resistances $(R_p^2/15\varepsilon_p D_p)$ are estimated by Equations (6-8), and the micro-pore diffusion resistance $(r_c^2/15KD_c)$ is calculated from the difference between column 3 in Table 2.5 and the addition of columns 4 and 6 according to equation (5). As can be seen from the table, the percentages of the resistances of external film mass transfer and macro-pore diffusion to total dispersion were close to zero while the percentages of micro-pore diffusion resistance to total dispersion were close to 100%, so the contributions from external film mass transfer and macro-pore diffusion were negligible with micro-pore diffusion resistance being the definite dominant mass transfer mechanism for all the systems studied. Under these circumstances, micropore diffusion coefficient can be determined with high accuracy. For CH_4, however, the intercepts are so small that it is difficult to obtain accurate values.

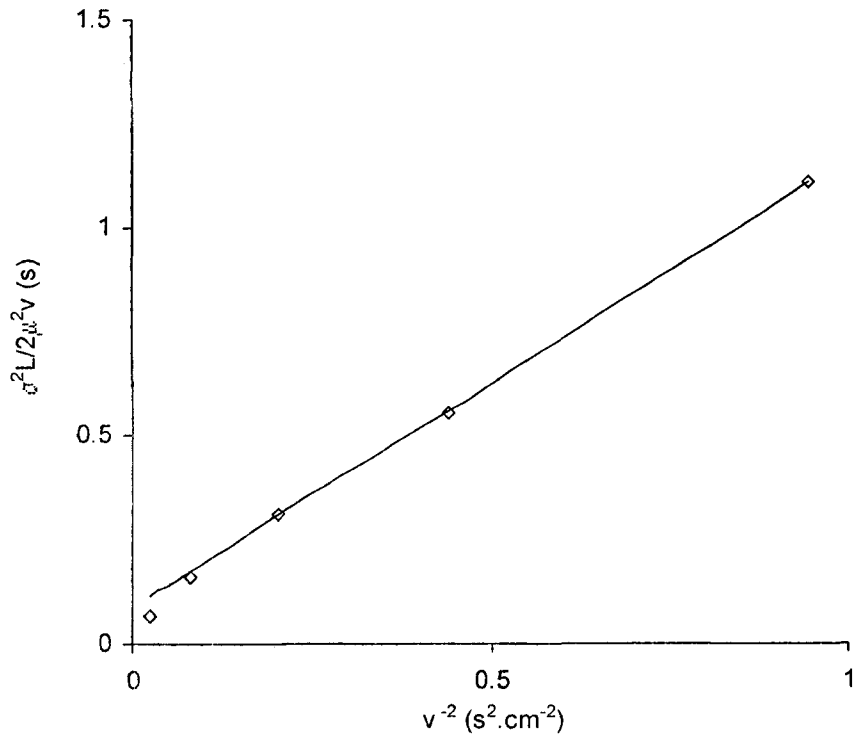

Figure 2.4. Linear relation of $\sigma^2L/2\mu^2v$ vs. v^{-2} in the lower flow rate region for CO_2 in β-zeolite at 40 °C.

The values of the micro-pore diffusion (D_c/r_c^2) for CO_2, O_2 and N_2 are calculated and the results are plotted in Figure 2.5. The corresponding parameters of the Arrhenius type equation:

$$D_c = D_0 \exp(-\frac{E_a}{RT}) \quad \text{.....(11)}$$

or,

$$\frac{D_c}{r_c^2} = \frac{D_0}{r_c^2} \exp(-\frac{E_a}{RT}) \quad \text{.....(12)}$$

are tabulated in Table 2.6, where the activation energy indicates the dependency of the micropore diffusion on temperature and the pre-exponential factor indicates the dependency of the micropore diffusion on other factors. As can be seen from Figure 2.5, at high temperatures (above 80 °C) the diffusivity values are similar for the three gases. At low

temperatures, the values for CO_2 decrease much faster than the other gases, due to its high activation energy. For N_2 and O_2, the activation energy was low. Among the three adsorbates studied, CO_2 had the highest activation energy, which indicated a high dependency of the micropore diffusion on temperature. Apparently, the micropore diffusion of CO_2 increases with temperatures.

Table 2.5. Mass transfer resistances with β-zeolite adsorbent for different gases studied.

Adsorbates	Temperature	Intercept x (1-ε)/ ε	$R_p^2/(3D_m)$		$R_p^2/(15\varepsilon_p D_p)$		$r_c^2/(15KD_c)$	
	°C	second	second	%	second	%	second	%
O_2	39.1	4.78881	0.00037	0.008	0.00077	0.016	4.78767	99.976
O_2	59.3	6.75437	0.00033	0.005	0.00073	0.011	6.75330	99.984
O_2	79.5	5.86026	0.00030	0.005	0.00070	0.012	5.85926	99.983
O_2	99.8	5.93148	0.00028	0.005	0.00068	0.011	5.93052	99.984
N_2	39.1	3.06753	0.00032	0.011	0.00071	0.023	3.06650	99.966
N_2	59.3	4.10427	0.00029	0.007	0.00068	0.016	4.10330	99.976
N_2	79.5	4.17497	0.00026	0.006	0.00065	0.016	4.17406	99.978
N_2	99.8	4.58212	0.00024	0.005	0.00062	0.014	4.58126	99.981
CO_2	39.1	0.24897	0.00038	0.152	0.00088	0.352	0.24772	99.497
CO_2	59.3	0.26194	0.00034	0.130	0.00084	0.320	0.26076	99.551
CO_2	79.5	0.19865	0.00031	0.155	0.00080	0.405	0.19754	99.440
CO_2	99.8	0.29972	0.00028	0.093	0.00077	0.258	0.29867	99.648

Table 2.6. Parameters D_0/r_c^2 and E_a according to Arrhenius Equation (12) with β–zeolite.

Adsorbates	D_0/r_c^2 (s^{-1})	E_a ($kJ.mol^{-1}$)
O_2	0.0195	2.86
N_2	0.0229	2.63
CO_2	185.1	30.4

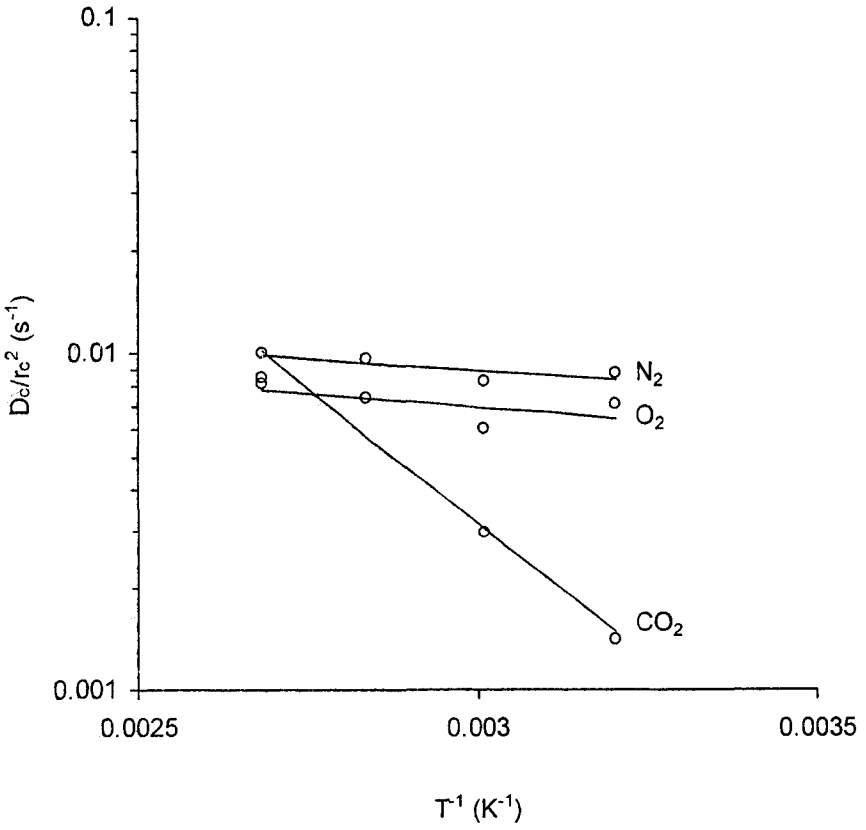

Figure 2.5. Linear regression of the relation between micro-pore diffusivity and temperature: D_c/r_c^2 vs. T^{-1}

In considering such diffusion processes it is convenient to define a kinetic separation factor, which will indicate the ease of separation of any binary gas system based on kinetic parameters:

$$\alpha_{k,A/B} = \frac{D_{c,A}}{D_{c,B}} \quad \text{.....(13)}$$

or

$$\alpha_{k,A/B} = \frac{\left(D_c / r_c^2\right)_A}{\left(D_c / r_c^2\right)_B} \quad \text{.....(14)}$$

Therefore, kinetic separation factors, $\alpha_{k,N2/CO2}$, are shown as a function of temperature in Figure 2.6. The kinetic separation factors decrease as column temperatures increase, depending on the relative magnitudes of diffusional activation energy, E_a. At high column

temperatures, the kinetic separation factors are very small for all the systems studied. At low temperatures, both nitrogen / carbon dioxide and oxygen / carbon dioxide systems can be separated in kinetic processes. These observations are the results of high activation energy for the carbon dioxide. However, it is difficult to separate nitrogen/oxygen systems based on kinetics.

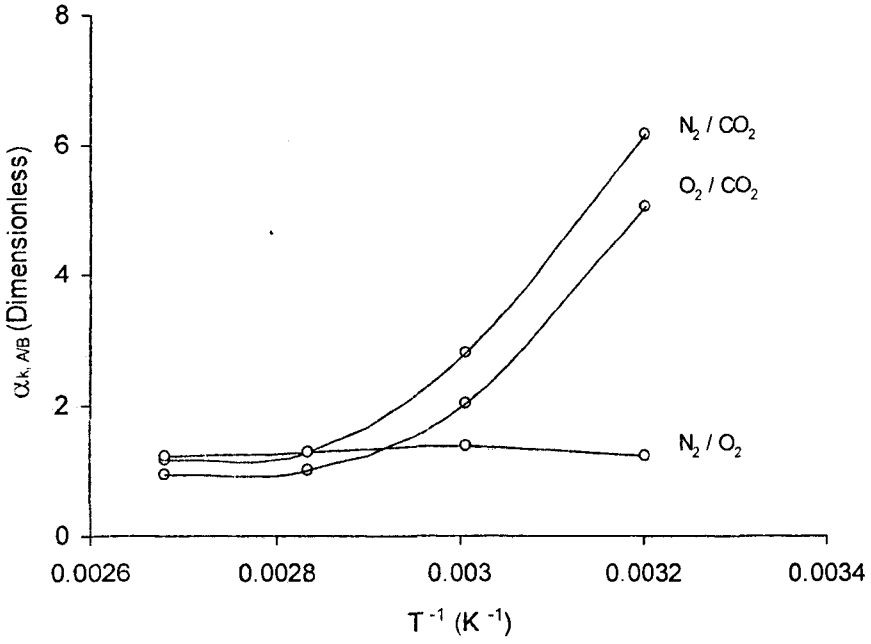

Figure 2.6 The change of kinetic separation factor ($\alpha_{k,A/B}$) with column temperature (T) for different adsorbate pairs with β-zeolite.

CONCLUSIONS

1. Carbon dioxide has the highest Henry's Law constant for the β-zeolite at all the temperatures studied, followed by methane, nitrogen and oxygen. Oxygen and nitrogen Henry's Law constants are very similar to each other.
2. Initial equilibrium separation factors decrease as column temperatures increase.
3. Micro-pore diffusion is the dominant mass transfer mechanism for CO_2.

4. Carbon dioxide separation from oxygen, nitrogen or methane has good equilibrium separation factors. The equilibrium separation factors for methane / nitrogen and methane / oxygen systems are not very high. The equilibrium separation factors are the lowest for nitrogen / oxygen system.
5. The adsorbent studied, β-zeolite, would be a good adsorbent for equilibrium separation of carbon dioxide from oxygen, nitrogen and methane. Therefore, β-zeolite can be expected to be used for applications in flue gas separations, as well as natural gas and landfill gas purifications.

ACKNOWLEDGEMENTS

Authors want to acknowledge Dr. Neal T. S. Chung and his team from National University of Singapore for preparing and supplying the β-zeolite that was used in this work.

NOMENCLATURE

c = Adsorbate concentration, $mol.L^{-1}$

D_c = diffusivity within a crystal (or micro-pore diffusivity), $m^2.s^{-1}$ or $cm^2.s^{-1}$

$D_{c,A}$ = diffusivity within a crystal (or micro-pore diffusivity) of component A, $m^2.s^{-1}$

$D_{c,B}$ = diffusivity within a crystal (or micro-pore diffusivity) of component B, $m^2.s^{-1}$

D_k = Knudsen diffusivity, $m^2.s^{-1}$

D_l = Axial dispersion coefficient, $m^2.s^{-1}$

D_m = molecular diffusivity, $m^2.s^{-1}$

D_p = Macro-pore diffusivity, $m^2.s^{-1}$ or $cm^2.s^{-1}$

D_0 = Pre-exponential factor, $m^2.s^{-1}$ or $cm^2.s^{-1}$

E_a = Diffusional activation energy, $kJ.mol^{-1}$

ΔH = Heat of adsorption, $kJ.mol^{-1}$

ΔH_A = Heat of adsorption of component A, $kJ.mol^{-1}$

ΔH_B = Heat of adsorption of component B, $kJ.mol^{-1}$

K = Henry's Law adsorption equilibrium constant, dimensionless

K_0 = Pre-exponential factor, mmole.g^{-1}.atm^{-1}

K_p = Henry's law adsorption equilibrium constant, mmole.g^{-1}.atm^{-1}

K_{pA} = Henry's Law adsorption equilibrium constant of component A, mmole.g^{-1}.atm^{-1}

K_{pB} = Henry's Law adsorption equilibrium constant of component B, mmole.g^{-1}.atm^{-1}

k_f = External film mass transfer coefficient, m.s^{-1}

L = Column length, cm

M = Molecular weight

M_A = Molecular weight of Component A

M_B = Molecular weight of Component B

P = Total pressure, atm. (in Equation 6)

R = Gas constant, atm.L. mol^{-1}.K^{-1} (0.08206 in Eq. 2)

R_p = Pellet radius, m

r_c = Crystal or micro-particle radius, m,

r_p = Pore radius, cm.

Sh = Sherwood number, dimensionless

t = Time, s

T = Temperature, K

v = Interstitial fluid velocity, cm.s^{-1}

x = Mole fraction in adsorbed phase at equilibrium, dimensionless

x_A = Mole fraction of component *A* in adsorbed phase at equilibrium, dimensionless

x_B = Mole fraction of component B in adsorbed phase at equilibrium, dimensionless

y = Mole fraction in fluid phase at equilibrium, dimensionless

y_A = Mole fraction of component *A* in fluid phase at equilibrium, dimensionless

y_B = Mole fraction of component B in fluid phase at equilibrium, dimensionless

Greek letters

α = Adsorption separation factor or selectivity, dimensionless

$\alpha_{c,A/B}$ = Equilibrium adsorption separation factor, dimensionless

$\alpha_{ci,A/B}$ = Initial equilibrium adsorption separation factor, dimensionless

ε = Bed porosity, dimensionless

ε_p = Pellet porosity, dimensionless

μ = (Corrected) retention time, the first moment of the response peak, s

μ_D = Dead time, s

ρ_P = Pellet density of the adsorbent

σ = Constant in the Lennard-Jones potential-energy function, Å

σ^2 = Second moment of the response peak, s^2

Ω_{AB} = Collision integral between Component A and of Component B, dimensionless

Abbreviations

GC = Gas Chromatograph

MFC = Mass Flow Controller

TCD = Thermal Conductivity Detector

REFERENCES

[1] D.M. Ruthven, R. Kumar, Ind. Eng. Chem. Fundam. 19 (1980) 27.

[2] P. Li, F.H. Tezel, 40th IUPAC Congress, Beijing, P. R. China (2005) 1-O-034 p.61.

[3] P. Li, F.H. Tezel, 55th CSChE Conference, Toronto, Canada (2005) p.593.

[4] J. Nokerman, X. Canet, P. Mougin, S. Limborg-Noetinger, M. Frere, Meas. Sci. Tech. 16 (2005) 1802.

[5] H.W. Haynes, P.N. Sarma, AIChE J. 19 (1973) 1043.

[6] R.T. Yang, Gas Separation by Adsorption Processes, Butterworth Publishers, Stoneham, MA (1987) pp.9-338.

[7] P.J.E. Harlick, F.H. Tezel, Adsorption 6 (2000) 293.

[8] P.J.E. Harlick, F.H. Tezel, CJChE 79 (2001) 236.

[9] P.J.E. Harlick, F.H. Tezel, Adsorption 9 (2003) 275.

[10] P. Schneider, J.M. Smith, AIChE J. 14 (1968) 762.

[11] P. Schneider, J.M. Smith, AIChE J. 14 (1968) 886.

[12] G. Mason, B.A. Buffman, Proc. R. Soc. Lond. A 452 (1996) 1287.

[13] S.H. Hyun, R.P. Danner, AIChE Symp. Ser. 78 (1982) 19.

[14] S.H. Hyun, R.P. Danner, Ind. Eng. Chem. Fundam. 24 (1985) 95.

[15] B.A. Buffman, M. Mason, G.D. Yadav, J. Chem. Soc., Faraday Trans. I 81 (1985) 161.

[16] B.A. Buffman, G. Mason, M.J. Heslop, Ind. Eng. Chem. Fundam. 38 (1999) 1114.

[17] D.B. Shah, D.M. Ruthven, AIChE J. 23 (1977) 804.

[18] D.M. Ruthven, Principles of Adsorption and Adsorption Processes, John Wiley and Sons Inc., New York, NY (1984) pp.1-433.

[19] S. Chapman, T.G. Gowling, Mathematical Theory of Non-Uniform Gases, Second Edition, Cambridge University Press (1951) Chapters 10 and 14.

[20] J.O. Hirschfelder, C.F. Curtiss, R.B. Bird, Molecular Theory of Gases and Liquids, Wiley, New York (1954) p.539.

[21] R.B. Bird, W.E. Stewart, E.N. Lightfoot, Transport Phenomena, John Wiley and Sons Inc., New York, NY (1960) pp.495-518.

[22] W. Kauzmann, Kinetic Theory of Gases, Benjamin, New York, NY (1966), pp.1-248.

[23] V.R. Choudhary and S. Mayadevi, Sep. Sci. Tech. 28 (1993) 2197.

[24] T.C. Golden and S. Sircar, J. Colloid Interface Sci. 162 (1994) 182.

[25] J.A. Dunne, R. Mariwala, M. Rao, S. Sircar, R.J. Gorte, and A.L. Myers, Langmuir 12 (1996) 5888.

[26] J. Pires, M. Brotas de carvalho, F. Ramoa Ribeiro, and E.G. Derouane, J. Mol. Cat. 85 (1993) 295.

CHAPTER III

EQUILIBRIUM AND KINETIC ANALYSIS OF CARBON DIOXIDE AND NITROGEN ADSORPTION SEPARATION BY CONCENTRATION PULSE CHROMATOGRAPHY

Peiyuan Li and F. Handan Tezel*

Department of Chemical Engineering
Faculty of Engineering
University of Ottawa
161 Louis Pasteur, Ottawa, Ontario K1N 6N5, Canada

Accepted to be published in Journal of Colloid and Interface Science in 2007.

Presented at 40th IUPAC (International Union of Pure and Applied Chemistry) World Chemistry Congress, Beijing, China, on Aug. 14-19, 2005, Congress Proceedings 1-O-034.

---

* Corresponding author

Tel: 613-562-5800 Ext. 6099
Fax: 613-562-5172
Emai: Handan.Tezel@uottawa.ca

ABSTRACT

CO_2 and N_2 adsorption kinetics and equilibrium behaviours have been studied on silicalite, NaY and 13X by using concentration pulse chromatography for the separation of these gases in the present study. Adsorption Henry's Law constants, the heat of adsorption values, micro-pore diffusion coefficients and corresponding activation energies are determined experimentally and the three different mass transfer mechanisms are discussed. From the equilibrium data, the corresponding separation factors are obtained for the adsorption separation processes. The heat of adsorption values as well as the Henry's Law adsorption equilibrium constants of CO_2 are much higher than those of N_2 for all the adsorbents studied. 13X, NaY and silicalite all have good separation factors for CO_2/N_2 system based on equilibrium processes. The order of the equilibrium separation factors is 13X (Ceca) > 13X (Zeochem) > NaY (UOP) >> Silicalite (UOP). Equilibrium selectivity favours CO_2 over N_2. Micro-pore diffusion resistance is the definite dominant mass transfer mechanism for CO_2 on silicalite and NaY.

INTRODUCTION

The global environment is a major issue today, and global warming in particular is the focus of much attention. Accumulation of greenhouse gases (GHG) in the atmosphere is responsible for increased global warming of our planet. The increasing concentration of carbon dioxide mainly from flue gas, automobile and landfill emissions in the atmosphere is the major contributor to this problem with more than 80% of total GHG emissions (*1*). For this reason, together with a tighter control in emissions to meet Kyoto Protocol targets, separation of carbon dioxide from nitrogen (representing the major component of air) has been the focus of the present study. A variety of techniques have been used for CO_2-N_2 adsorption separation in the literature (*2-21*).

Adsorption separation of carbon dioxide from nitrogen is investigated by using concentration pulse chromatographic technique, with silicalite, NaY and 13X zeolites as adsorbents, in the present study. Henry's Law constants are calculated from the corrected first moment of the response peaks. The heat of adsorption and the pre-exponential factors are obtained by using the Van't Hoff equation. From the equilibrium data, the equilibrium selectivities are obtained for the adsorption separation process for the four different adsorbents studied. The micro-pore diffusion (D_c/r_c^2) is determined from the corrected first and second moment of the response peaks, and the three different mass transfer mechanisms are discussed.

CONCENTRATION PULSE CHROMATOGRAPHIC TECHNIQUE

The use of concentration pulse chromatography for adsorbent screening is very attractive since it is relatively inexpensive to setup and is very efficient. It is a dynamic method of conducting adsorption measurements, which measures the response of a chromatographic column to a pulse in adsorbate concentration. The first and second moments of the response peak produced by a pulse in carrier gas concentration would yield the initial slope of the adsorption isotherm and the diffusivity. This method, which indirectly measures the adsorption parameters, has been shown to agree well with gravimetric and volumetric data.

Concentration pulse chromatographic technique was found to be simpler and quicker for the determination of binary adsorption isotherms, as well (*8, 22-26*).

In this technique, a pulse of the sample gas is injected into the carrier stream and passes through the column that is packed with the adsorbent. The response of the column to this injection is measured as concentration vs. time at the exit of the column. This response peak gives the mean retention time of the sample, μ, defined as the first moment of the chromatogram, (*27*). Dimensionless Henry's Law constants can be calculated from the corrected (with respect to the dead time) first moment of the response peaks by using following equation (*13, 14, 24*):

$$\mu = \frac{\int_0^\infty c(t-\mu_D)dt}{\int_0^\infty cdt} = \frac{L}{v}\left[1+\frac{(1-\varepsilon)K}{\varepsilon}\right] \quad \text{.....(1)}$$

where t is the time, c is the adsorbate concentration measured at the outlet of the column, L is the column length. ε is the bed porosity, v is the interstitial fluid velocity, K is the dimensionless Henry's Law adsorption equilibrium constant, and μ_D is the correction time for dead volume.

The dimensionless Henry's Law constants, K, can be converted to a dimensional form (*14, 28*) as follows:

$$K_p = \frac{K}{RT\rho_p} \quad \text{.....(2)}$$

where T is temperature, ρ_p is the density of the pellets of the adsorbent and K_p is the dimensional Henry's Law adsorption equilibrium constant given in $mmol.g^{-1}.atm^{-1}$.

The Van't Hoff equation is given as (*29*):

$$K_p = K_0 e^{-\frac{\Delta H}{RT}} \quad \text{.....(3)}$$

where T is the column temperature, R is the gas constant, ΔH is the heat of adsorption, and K_0 is the pre-exponential factor. ΔH and K_0 may be obtained from the experimentally determined K_p values at several different temperatures. These values can then be used to calculate equilibrium separation factor, the ratio of the Henry's law constants, which is useful in predicting promising separation conditions.

The rate of diffusion in micro-pores can be determined by this method from the second moment of the response peak defined as (*27, 29*):

$$\sigma^2 = \frac{\int_0^\infty c(t-\mu)^2 dt}{\int_0^\infty c dt} \quad \text{.....(4)}$$

where μ is the corrected retention time, t is time, and c is the adsorbate concentration at the outlet of the column. At low flow-rates, a useful general form for the second moment of the response peak is given as (*29*):

$$\frac{\sigma^2}{2\mu^2}\cdot\frac{L}{v} = \frac{D_L}{v^2} + \frac{\varepsilon}{(1-\varepsilon)}\left(\frac{R_p^2}{3D_m} + \frac{R_p^2}{15\varepsilon_p D_p} + \frac{r_c^2}{15KD_c}\right) \quad \text{.....(5)}$$

where μ is the corrected retention time (the first moment of the response peak), σ^2 is the second moment of the response peak, L is the column length, ε is the bed porosity, v is the interstitial fluid velocity, K is the dimensionless Henry's law constant, D_L is the axial dispersion coefficient, R_p is the pellet radius, r_c is the crystal radius, ε_p is the pellet porosity, D_p is the macro-pore diffusivity (based on free pore area in the pellet), D_c is the diffusivity within the crystal within the pellet (or micropore diffusivity), and D_m is the molecular diffusivity. The terms on the right hand side of this equation represent different mass transfer resistances that exist for adsorption to take place in a column, packed with adsorbent pellets that are composed of zeolite crystals. The first term represents axial dispersion. The second term represents external film mass transfer. The third and fourth terms represent macropore and micropore diffusion resistances, respectively. According to Equation (5), a plot of the dispersion ($\sigma^2 L/2\mu^2 v$, which is the left hand side) vs. v^{-2} should be approximately linear with slope D_L and intercept given by the summation of the last three terms on the right hand side of Equation (5). By using these plots, the dominant mass transfer mechanisms, as well as the dispersion and mass transfer parameters can be determined.

The molecular diffusivity, D_m, in $cm^2.s^{-1}$, can be estimated by (*30-32*):

$$D_m = 1.8583\times10^{-3}\times\frac{T^{\frac{3}{2}}\left(\frac{1}{M_A}+\frac{1}{M_B}\right)^{\frac{1}{2}}}{P\sigma_{AB}^2\Omega_{AB}} \quad \text{.....(6)}$$

where T is the temperature in K, M is the molecular weight, P is the total pressure in atm., σ is a constant of the Lennard-Jones potential-energy function in Å, and Ω is the collision integral (dimensionless). Subscripts A and B indicate components A and B.

The macro-pore diffusivity, D_p, can be given by a combination of molecular diffusivity and Knudsen diffusivity. It can be estimated by (*23*):

$$D_p = \frac{1}{\frac{1}{D_m} + \frac{1}{D_k}} \quad \text{.....(7)}$$

where D_k is the Knudsen diffusivity in $cm^2.s^{-1}$, which is given by (33, 23):

$$D_k = 9700 r_p \left(\frac{T}{M}\right)^{\frac{1}{2}} \quad \text{.....(8)}$$

where r_p is the pore radius in cm, M is the molecular weight, and T is temperature in K.

After axial dispersion is determined from the slopes of dispersion ($\sigma^2 L/2\mu^2 v$) vs. v^{-2} plots, using the estimated values for molecular diffusivity (from Equation (6)) and the macro-pore diffusivity (from Equation (7)), the micro-pore resistance and the corresponding value of D_c/r_c^2 can be determined experimentally from Equation (5).

If external film mass transfer and macro-pore diffusion resistances are much smaller than micro-pore diffusion resistance, the micro-pore diffusion would be the dominant mass transfer mechanism. These will be the ideal conditions, under which the latter can be determined. Therefore, it is necessary to check the relative values of different mass transfer resistances under the experimental conditions studied.

EXPERIMENTAL

The schematic diagram of the experimental apparatus (Figure 3.S1), as well as the experimental details are given in Supporting Information.

The details about the adsorbents packed in the column are listed in Table 3.1.

Table 3.1. Details of adsorbents packed in the columns.

Type	Commercial Name	Si/Al Ratio	Commercial Number	Shape	Size As Supplied (Diameter)	Supplier
Silicalite	MOLSIV Adsorbents	>1000	HISIV 3000	Cylinder	1/16 inch	Universal Oil Products (UOP) Des Plaines, IL, USA
NaY	MOLSIV Adsorbents	1.8	NAY	Cylinder	1/16 inch	Universal Oil Products (UOP) Des Plaines, IL, USA
13X	Molecular Sieve Adsorbents	1.0 - 1.5	Z10-01	Bead	8x12 mesh	Zeochem Louisville, KY, USA
13X	G5 13X	1.25	GS 13X	Bead	8x12 mesh	Ceca France

The sample and carrier gases used in the experiments are available (in Table 3.S1, Supporting Information). The experimental and column specifications and conditions are available (in Table 3.S2, Supporting Information).

RESULTS AND DISCUSSION

By using Equations (1) and (2) Henry's Law constants are calculated from the corrected first moment of the response peaks (Determination of System Dead Time, Supporting Information). Representative plots for CO_2 and N_2 are shown in Figure 3.1 for all the adsorbents studied. Henry's Law constants are much higher for CO_2 than for N_2 for all the adsorbents. This is due to the fact that, although the molecular weight of CO_2 (44) is larger than that of N_2 (28), its kinetic diameter is smaller (3.3 Å as opposed to 3.64 Å for N_2). Therefore, it can easily get into the pores of the adsorbents. Ceca 13X has significantly larger Henry's Law constants for both of the adsorbates, compared to the other adsorbents studied. N_2 Henry's Law constants were almost identical for silicalite, NaY and Zeochem 13X. Table 3.2 lists the values of ΔH and K_0, which give the temperature dependence of the Henry's Law constants according to Equation (3). From the values of ΔH, it can be seen that CO_2

heats of adsorption values are also higher than those for N_2 with all the adsorbents studied. This is due to the fact that CO_2 has a much higher quadropole moment and a much higher polarizability, compared to N_2, therefore its interaction with the adsorbents are going to be much stronger. The difference in heat of adsorption values is more pronounced with more heterogeneous adsorbents (NaY and 13X), as opposed to silicalite, as expected. In Table 3.2, literature values of heat of adsorption were compared to the ones obtained in the present study. As can be seen from this table, all values agree with the literature, except the values for 13X, for which, the heat of adsorption value seems to be sensitive to the origin of the adsorbent. There was even a discrepancy between the 2 different 13X samples we tried in the present study.

By using the parameters from Table 3.2, the Henry's Law constants at other temperatures were estimated from the experimental data for CO_2 and N_2 and are presented in Table 3.S3 in Supporting Information, in which the data from Harlick and Tezel (*39*) are also listed for CO_2 for comparison. They used nitrogen as the carrier gas while helium was used as the carrier gas in the present study. As can be seen from Table 3.S3 in Supporting Information, Henry's Law constants for CO_2 are very similar for NaY zeolite. For 13X zeolite, on the other hand, the samples obtained from different manufacturers behaved quite differently for CO_2. The Henry's Law constants were the highest for Ceca 13X for all the temperatures studied, followed by UOP 13X, followed by the Zeochem sample.

The primary requirement for an economic separation process is an adsorbent with sufficiently high selectivity, capacity, and life. The selectivity would depend on difference in either adsorption kinetics or adsorption equilibrium. Most of the adsorption processes in current use depend on equilibrium selectivity. In considering such processes it is convenient to define an adsorption equilibrium separation factor as follows:

$$\alpha_{e,A/B} = \frac{x_A / x_B}{y_A / y_B} \quad \text{..... (9)}$$

where x_A, x_B, y_A, and y_B are the mole fractions of components A and B in adsorbed and gas phases at equilibrium, respectively. For Langmuir type favourable adsorption isotherms, the equilibrium separation factor is constant, and is simply given by the ratio of the Henry's Law constants:

$$\alpha_{e.A/B} = \frac{K_{P_A}}{K_{P_B}} \quad \text{.....(10)}$$

where K_{PA} and K_{PB} are Henry's Law adsorption equilibrium constants for components *A* and *B*, respectively. When using concentration pulse chromatography, we can make sure that the system has the concentrations low enough to follow Henry's law, by injecting a very small amount of the sample gas into the carrier gas stream.

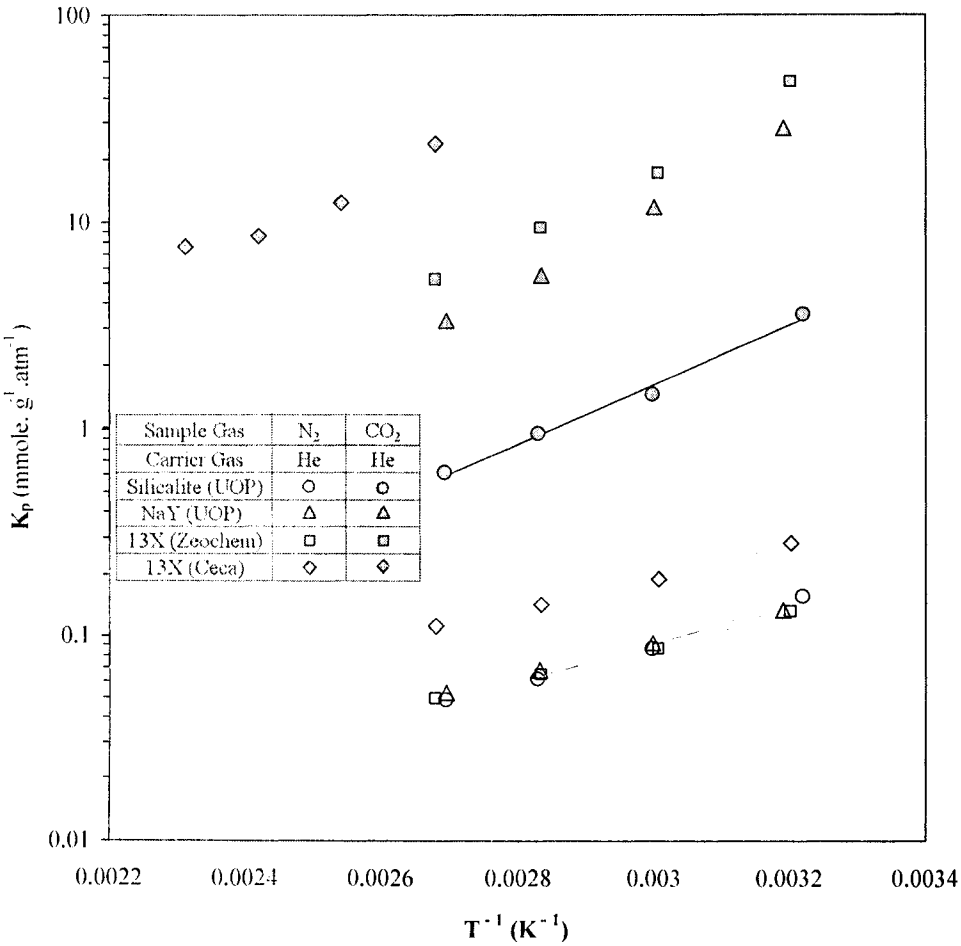

Figure 3.1. Linear regression of the relation between Henry's Law adsorption equilibrium constant (K_p) and column temperature (T):
K_P vs. T^{-1} for different adsorbents and adsorbates.

Table 3.2. Heat of adsorption and pre-exponential factor values and their comparisons with literature.

Adsorbents	Adsorbates	ΔH kJ.mol^{-1}	ΔH (Literature) kJ.mol^{-1}	K_0 mmole. g^{-1}.atm^{-1}
Silicalite	N_2	-18.5	-15.1 (*34*) -17.6 (*35*)	1.14×10^{-4}
	CO_2	-27.4	-21.7 (*36*) -24.1 (*34*) -23.4 (*37*) -27.2 (*35*)	8.18×10^{-5}
NaY	N_2	-15.4	------	3.58×10^{-4}
	CO_2	-33.6	-30 ~ -33 (*38*)	6.33×10^{-5}
13X	N_2	-15.4 (Zeochem) -14.9 (Ceca)	-25.0 (*36*)	3.36×10^{-4} (Zeochem) 9.01×10^{-4} (Ceca)
	CO_2	-34.9 (Zeochem) -26.2 (Ceca)	-36.0 (*36*)	6.43×10^{-5} (Zeochem) 4.58×10^{-3} (Ceca)

The separation factors, determined from the experimental data obtained, are shown as a function of inverse temperature in Figure 3.2. Henry's Law adsorption equilibrium constants and adsorption equilibrium separation factors are given in Table 3.S3 in Supporting Information. The equilibrium separation factors decrease as temperature increases, depending on the relative magnitudes of the heats of adsorption values. Following Equations 3 and 10, the slope of separation factor vs. inverse temperature plot is given by $-(\Delta H_{CO_2} - \Delta H_{N_2})/R$. In this case, since the heat of adsorption of CO_2 is more negative than that of N_2, this plot will have a positive slope, which will cause the separation factor to decrease when T increases. According to the data obtained, all the adsorbents have good

separation factors for CO_2/N_2 system for equilibrium processes. The order of the equilibrium separation factors follows the Si/Al ratio of the adsorbents: 13X (Ceca) > 13X (Zeochem) > NaY (UOP) >> Silicalite (UOP). The reason for that is the homogeneous surface characteristic of the silicalite adsorbent which has a Si/Al ratio in the thousands. The more Al a zeolite will contain, the more cations will be needed to balance the charge difference between Si^{+4} and Al^{+3}, the more heterogeneous its surface will be. Since zeolites X and Y have a much lower Si/Al ratio than silicalite, CO_2 will be more attracted to these adsorbents, because of its higher quadrupole moment, compared to silicalite, resulting in higher heats of adsorption, compared to N_2.

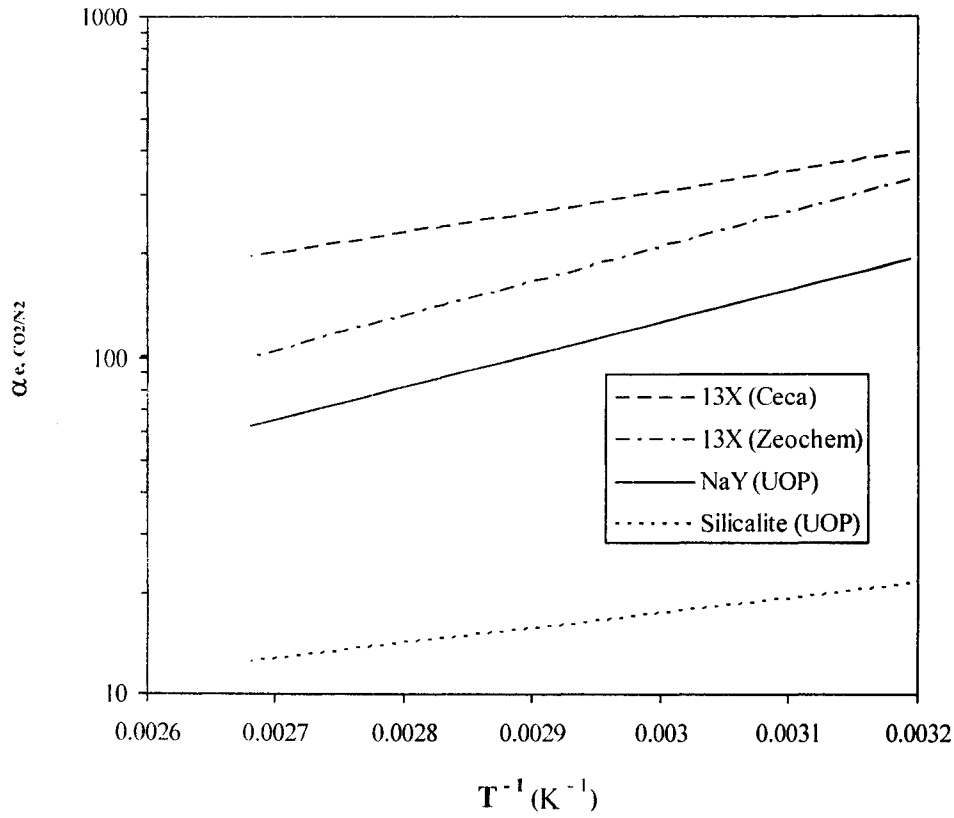

Figure 3.2. The relation between adsorption equilibrium separation factor ($\alpha_{e,CO2/N2}$) and column temperature (T): $\alpha_{e,CO2/N2}$ vs. T^{-1} for different adsorbents studied

It needs to be emphasized that the separation factors considered here are based on pure component data in Henry's Law region. Although, realistically speaking, the separation factor should be based on actual capacities under mixture conditions; the one calculated from the pure component data would be an initial indicator of how easy the separation would be.

Equation (5) suggests that a plot of the dispersion $(\sigma^2 L/2\mu^2 v)$ vs. $1/v^2$ should be approximately linear with slope D_L and intercept given by the last term in Equation (5). Such plots provide a convenient means of extracting the mass transfer parameters. From a comparison of the mass transfer resistances measured under different experimental conditions, it is possible to establish which mass transfer resistance is dominant. A typical plot of dispersion $(\sigma^2 L/2\mu^2 v)$ vs. $1/v^2$ is given in Figure 3.3 for CO_2 with Zeochem 13X adsorbent. These plots are qualitatively similar for all other systems studied.

For CO_2 in silicalite and NaY as the adsorbents, the contributions of different mass transfer resistances to total dispersion are given in Table 3.3, in which, external film mass transfer ($R_p^2/3D_m$ in Column 4), and macro-pore diffusion resistances ($R_p^2/15\varepsilon_p D_p$ in Column 6) are estimated and the micro-pore diffusion resistances ($r_c^2/15KD_c$ in Column 8) are calculated from the difference between column 3 in Table 3.3 (intercept x $(1-\varepsilon)/\varepsilon$) and the addition of columns 4 and 6 according to equation 5. From the table, it can be seen that the contributions from external film mass transfer and macro-pore diffusion are negligible with micro-pore diffusion (with more than 98% of total resistance) being the definite dominant mass transfer mechanism for CO_2 with silicalite and NaY the systems studied. Identical results were reported by Triebe and Tezel (*40*) for different systems. In their work, maximum macropore diffusion resistance consisted of 2 – 4 %. The contribution from external mass transfer was less than 1 %, and micropore diffusional resistance was dominant for CO and N_2 in clinoptilolite. For other systems investigated in this study, the intercepts are so small that it was difficult to obtain accurate values.

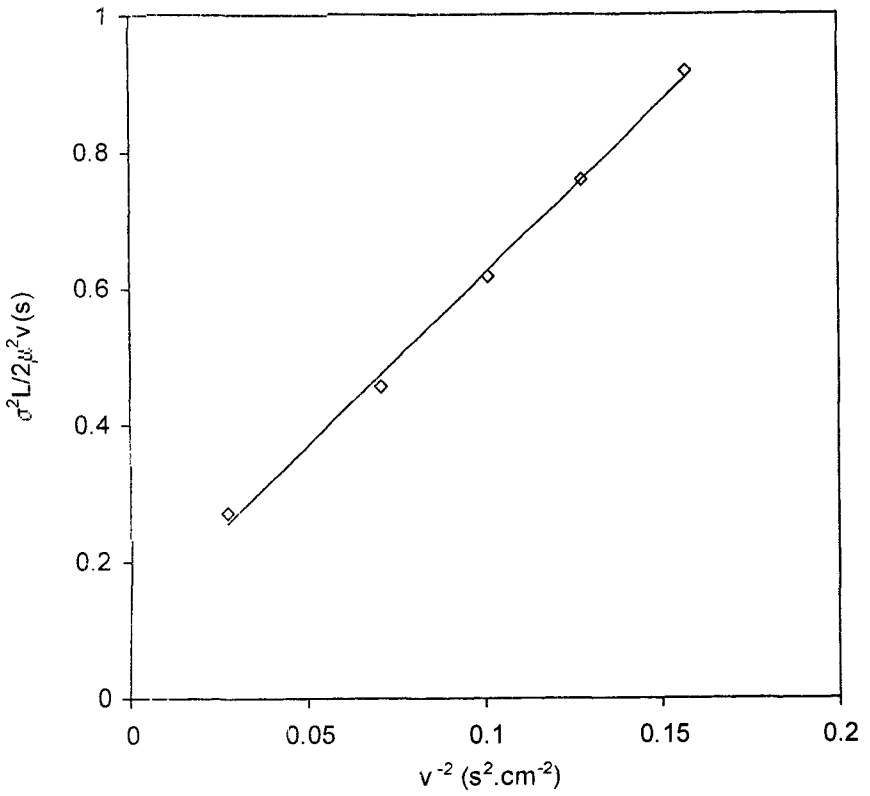

Figure 3.3. Linear relation of $\sigma^2L/2\mu^2v$ vs. v^{-2} in the lower flow rate region for CO_2 with 13X (Zeochem) at 100 °C.

Table 3.3. Mass transfer resistances for CO_2.

Adsorbent	T	Intercept x (1-ε) / ε	$R_p^2/(3D_m)$		$R_p^2/(15\varepsilon_pD_p)$		$r_c^2/(15KD_c)$	
	°C	second	second	%	second	%	second	%
Silicalite (UOP)	40	0.06587	0.00038	0.58	0.00098	1.48	0.06451	97.94
	60	0.06712	0.00034	0.50	0.00093	1.39	0.06586	98.11
	80	0.06800	0.00031	0.45	0.00089	1.31	0.06680	98.23
	100	0.07700	0.00028	0.37	0.00086	1.12	0.07586	98.51
NaY (UOP)	40	0.15563	0.00038	0.24	0.00080	0.51	0.15445	99.24
	60	0.12501	0.00034	0.27	0.00077	0.61	0.12391	99.12
	80	0.09752	0.00031	0.32	0.00074	0.76	0.09648	98.93
	100	0.09865	0.00028	0.29	0.00071	0.72	0.09765	98.99

Knowing the values of K calculated from the first moments, the values of the micro-pore diffusion (D_c/r_c^2) for CO_2 are determined from the micro-pore diffusion resistances calculated at different temperatures and the results are plotted in Figure 3.4. The corresponding parameters of the Arrhenius type equation

$$D_c = D_0 \exp(-\frac{E_a}{RT}) \quad \text{.....(11)}$$

or

$$\frac{D_c}{r_c^2} = \frac{D_0}{r_c^2} \exp(-\frac{E_a}{RT}) \quad \text{.....(12)}$$

are tabulated in Table 3.4. The micro-pore diffusion values (D_c/r_c^2) are given in Table 3.S4 in supporting information for different temperatures studied for CO_2. In Figure 3.4 and Table 3.S4 in Supporting Information, the micropore diffusion (D_c/r_c^2) of CO_2 in silicalite is higher than that in NaY. The reason for that is the homogeneous surface characteristic of the silicalite adsorbent which has a Si/Al ratio in the thousands, so the force between silicalite and CO_2 is smaller than that between NaY and CO_2. Therefore, CO_2 is easier to diffuse through silicalite than NaY so that the micropore diffusion (D_c/r_c^2) of CO_2 in silicalite is higher than that in NaY by more than one order of magnitude.

Based on our study, 1. CO_2 heats of adsorption values are higher than those for N_2 with different adsorbents studied, which agrees with the results from the literature; 2. the Henry's Law adsorption equilibrium constants of CO_2 are much higher than those of N_2 for the different adsorbents studied and equilibrium selectivity favors CO_2 over N_2.; 3. 13X, NaY and silicalite all have good separation factors for CO_2/N_2 system for equilibrium controlled processes. The order of the equilibrium separation factors is 13X Zeolite (Ceca) > 13X Zeolite (Zeochem) > NaY (UOP) >> Silicalite (UOP) for the temperature range studied; 4. the equilibrium separation factors decrease as column temperatures increase for CO_2/N_2 separation for all the adsorbents studied; 5. micro-pore diffusion resistance is the definite dominant mass transfer mechanism for CO_2 with silicalite and NaY. The order of the contributions of three mass transfer resistances is micro-pore diffusion >> macro-pore diffusion > external film mass transfer, which is identical with the results for other similar systems from the literature; 6. the micropore diffusion (D_c/r_c^2) of CO_2 in silicalite is higher

than that in NaY; 7. the adsorbents studied have potential applications for environmental industry, specifically for flue gas separation.

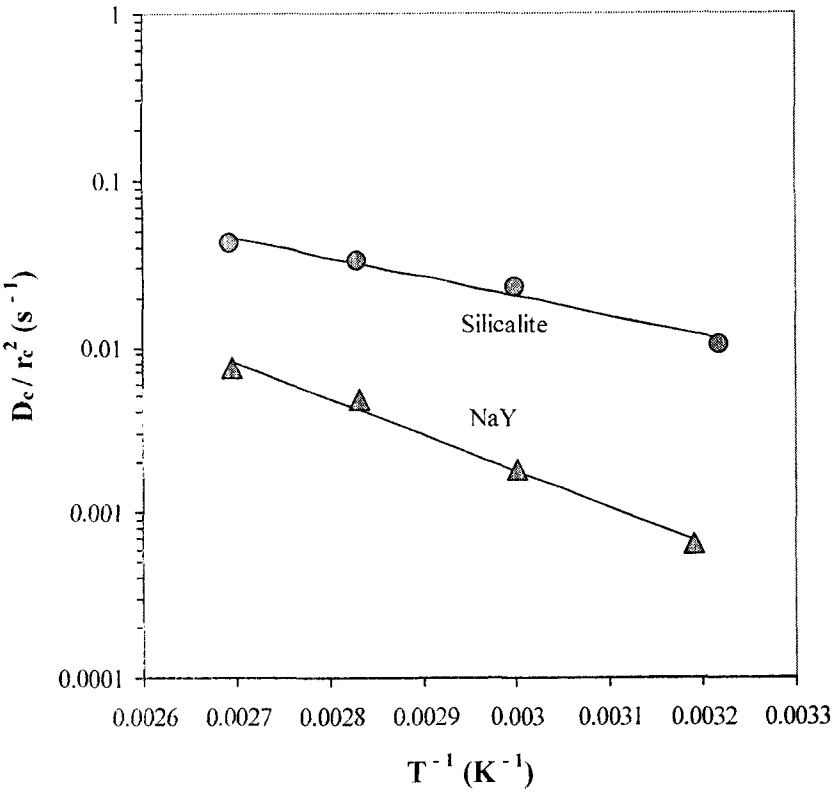

Figure 3.4. Linear regression of the relation between micropore diffusivity and temperature for CO_2.

Table 3.4. Parameters D_0/r_c^2 and E_a of CO_2 according to Arrhenius Equation (12).

Adsorbents	D_0/r_c^2 (s^{-1})	E_a ($kJ.mol^{-1}$)
Silicalite	64.7	22.4
NaY	6606	41.9

ACKNOWLEDGMENTS

Financial supports received from the Natural Sciences and Engineering Research Council of Canada (NSERC) Postgraduate Scholarship, the Ontario Graduate Scholarship (OGS), and the Canadian Society for Chemical Engineering (CSChE) Scholarship are gratefully acknowledged.

Supporting Information Available

Figure 3.S1, Tables 3.S1-3.S4, Experimental details, Determination of System Dead Time and Nomenclature.

REFERENCES

(1) Hansen, J.; Fung, I.; Lacis, A.; Riud, D.; Levedeff, J. S.; Ruedy, R.; Russell, G. Global Climate Changes as Forecast by Goddard Institute for Space Studies Three-Dimensional Model. *J. Geophys. Res.* **1988**, *93*, 9341-9364.

(2) Chue, K. T.; Kim, J. N.; Yoo, Y. J.; Cho, S. H.; Yang, R. T. Comparison of activated carbon and zeolite 13X for CO_2 recovery from flue gas by pressure swing adsorption. *Ind. Eng. Chem. Res.* **1995**, *34*, 591-598.

(3) Diagne, D.; Goto, M.; Hirose, T. New PSA Process with Intermediate Feed Inlet Position Operated with Dual Refluxes: Application to Carbon Dioxide Removal and Enrichment. *J. Chem. Eng. Jap.* **1994**, *27*, 85-89.

(4) Dong, F.; Lou, H.; Kodama, A.; Goto, M.; Hirose, T. The Petlyuk PSA Process for the Separation of Ternary Gas Mixtures: Exemplification by Separation a Mixture of CO_2-CH_4-N_2. *Sep. Purif. Tech.* **1999**, *16*, 159-166.

(5) Dreisbach, F.; Staudt, R.; Keller, J. U. High Pressure Adsorption Data of Methane, Nitrogen, Carbon Dioxide and their Binary and Ternary Mixtures on Activated Carbon. *Adsorption* **1999**, *5*, 215-227.

(6) Harlick, P. J. E.; Tezel, F. H.; Tremblay, A. Y. Carbon Dioxide Removal from Flue Gas Using Pressure Swing Adsorption: Modelling and Optimisation. *51st CSChE Conference* **2001**.

(7) Gomes, V. G.; Yee, W. K. Pressure Swing Adsorption for Carbon Dioxide Sequestration from Exhaust Gases Method. *Sep. Purif. Tech.* **2002**, *28*, 161-171.

(8) Harlick, P. J. E.; Tezel, F. H. CO_2-N_2 and CO_2-CH_4 Binary Adsorption Isotherms with H-ZSM-5: the Importance of Experimental Data Regression with the Concentration Pulse Method. *Can. J. Chem. Eng.* **2001**, *79*, 236-245.

(9) Harlick, P. J. E.; Tezel, F. H. Adsorption of Carbon Dioxide, Methane and Nitrogen: Pure and Binary Mixture Adsorption by H-ZSM-5 with SiO_2/Al_2O_3 Ratio of 30. *Sep. Sci. Tech.* **2002**, *37*, 33-60.

(10) Harlick, P. J. E.; Tezel, F. H. Adsorption of Carbon Dioxide, Methane and Nitrogen: Pure and Binary Mixture Adsorption for ZSM-5 with SiO_2/Al_2O_3 Ratio of 280. *Sep. Purif. Tech.* **2003**, *33*, 199-210.

(11) Hernandez-Huesca, R.; Diaz, L.; Aguilar-Armenta, G. Adsorption Equilibria and Kinetics of CO_2, CH_4 and N_2 in natural zeolites. *Sep. Purif. Tech.* **1999**, *15*, 163-173.

(12) Kikkinides, E. S; Yang, R. T. Aguilar-Armenta, G. Concentration and Recovery of CO_2 from Flue Gas by Pressure Swing Adsorption. *Ind. Eng. Chem. Res.* **1993**, *32*, 2714-2720.

(13) Li, P.; Tezel, F. H. Equilibrium and Kinetic Analysis of CO_2-N_2 Adsorption Separation by Concentration Pulse Chromatography. *40th IUPAC Congress* **2005**, p61, 1-O-034.

(14) Li, P.; Tezel, F. H. Analysis of Adsorption Parameters by Concentration Pulse Chromatography. *55st CSChE Conference* **2005**, 593.

(15) Nishikawa, N. Removing and Recovering of CO_2. *Journal of the Japan Institute of Energy* **1992**, *71*, 1090-1098.

(16) Pakseresht, S.; Kazemeini, M.; Akbarnejad, M. M. Equilibrium Isotherms for CO, CO_2, CH_4 and C_2H_4 on the 5A Molecular Sieve by a Simple Volumetric Apparatus. *Sep. Purif. Tech.* **2002**, *28*, 53-60.

(17) Takamura, Y.; Narita, S.; Aoki, J.; Uchida, S. Application of High-Pressure Swing Adsorption Process for Improvements of CO_2 Recovery System from Flue Gas. *Can. J. Chem. Eng.* **2001**, *79*, 812-816.

(18) Takamura, Y.; Narita, S.; Aoki, J.; Hironaka, S.; Uchida, S. Evaluation of Dual-Bed Pressure Swing Adsorption for CO_2 Recovery from Boiler Exhaust Gas. *Sep. Purif. Tech.* **2001**, *24*, 519-528.

(19) Tezel, F. H.; Harlick, P. J. E.; Sirkecioglu, A. Adsorption of Nitrogen and Carbon Dioxide on ZSM-5. *12th International Zeolite Conference* **1998**.

(20) Tierney, M. J.; Scott, H. S.; Erb, T.; Prasertmanukitch, S. The Purification of Dilute CO_2/Air Solutions with an Annular Bed Adsorber: Numerical and Experimental Investigations. *Sep. Purif. Tech.* **1999**, *17*, 159-171.

(21) Zhang, Z.; Guan, J.; Ye, Z. Prasertmanukitch, S. Separation of a Nitrogen-Carbon Dioxide Mixture by Rapid Pressure Swing Adsorption. *Adsorption* **1998**, *4*, 173-177.

(22) Haynes, H. W.; Sarma, P. N. Prasertmanukitch, S. A Model for the Application of Gas Chromatography to Measurements of Diffusion in Bidisperse Structured Catalysts. *AIChE J.* **1973**, *19*, 1043-1046.

(23) Yang, R. T. *Gas Separation by Adsorption Process*; Butterworth Publishers: Stoneham, MA, 1987; pp. 9-338.

(24) Harlick, P. J. E.; Tezel, F. H. A Novel Solution Method for Interpreting Binary Adsorption Isotherms from Concentration Pulse Chromatography Data. *Adsorption* **2000**, *6*, 293-309.

(25) Harlick, P. J. E.; Tezel, F. H. Use of Concentration Pulse Chromatography for Determining Binary Isotherms: Comparison with Statically Determined Binary Isotherms. *Adsorption* **2003**, *9*, 275-286.

(26) Nokerman, J.; Canet, X.; Mougin, P.; Limborg-Noetinger, S; Frere, M. Comparative Study of the Dynamic Gravimetric and Pulse Chromatographic methods for the Determination of Henry constants of Adsorption for VOC-Zeolite Systems. *Measur. Sci. Tech.* **2005**, *16*, 1802-1812.

(27) Shah, D. B.; Ruthven, D. M. Measurements of Zeolitic Diffusivities and Equilibrium Isotherms by Chromatography. *AIChE J.* **1977**, *23*, 804-810.

(28) Li, P.; Tezel, F. H. Adsorption Separation of N_2, O_2, CO_2 and CH_4 Gases by β-Zeolite. accepted to be published in *Micropor. & Mesopor. Mat.* **2007**, *98*, 94–101.

(29) Ruthven, D. M. *Principles of Adsorption and Adsorption Processes*; John Wiley and Sons Inc.: New York, NY, 1984; pp. 1-433.

(30) Chapman, S.; Gowling, T. G. *Mathematical Theory of Non-Uniform Gases, Second Edition;* Cambridge University Press, 1951; Chapters 10 and 14.

(31) Hirschfelder, J. O.; Curtiss, C. F.; Bird, R. B. *Molecular Theory of Gases and Liquids*; John Wiley and Sons Inc.: New York, NY, 1954; p. 539.

(32) Bird, R. B.; Stewart, W. E.; Lightfoot, E. N. Diffusivity and the Mechanisms of Mass Transport in *Transport Phenomena*; John Wiley and Sons Inc.: New York, NY, 1960; pp. 495-518.

(33) Kauzmann, W. *Kinetic Theory of Gases*; , Benjamin: New York, NY, 1966; pp. 1-248.

(34) Golden, T. C.; Sircar, S. Gas adsorption on silicalite. *J. Colloid Interf.* **1994**, *162*, 182-188.

(35) Dunne, J. A.; Mariwala, R.; Rao, M.; Sircar, S.; Gorte, R. J.; Myers, A. L. Calorimetric heats of adsorption and adsorption isotherms: 1. O_2, N_2, Ar, CO_2, CH_4, C_2H_6, and SF_6 on silicalite. *Langmuir* **1996**, *12*, 5888-5895.

(36) Choudhary, V. R.; Mayadevi, S. Adsorption of methane, ethane, ethylene, and carbon dioxide on high silica pentasil zeolites and zeolite-like materials using gas chromatography pulse technique. *Sep. Sci. Tech.* **1993**, *28*, 2197-2209.

(37) Yamazaki, T.; Katoh, M.; Ozawa, S.; Ogino, Y. Adsorption of CO_2 over univalent cation-exchanged ZSM-5 zeolites. *Mol. Physi.* **1993**, *80*, 313-324.

(38) Pires, J.; Brotas de Carvalho, M.; Ramoa Ribeiro, F.; Derouane, E. G. Carbon dioxide in Y and ZSM-20 zeolites: Adsorption and Infrared Studies. *J. Mol. Cat.* **1993**, *85*, 295-303.

(39) Harlick, P. J. E.; Tezel, F. H. An exprmental adsorbent screening study for CO_2 removal from N_2. *Micropor. Mesopor. Mat.* **2004**, *76*, 71-79.

(40) Triebe, R. W.; Tezel, F. H. Adsorption of nitrogen, carbon monoxide, carbon dioxide and nitric oxide on molecular sieves. *Gas Sep. Purif.* **1995**, *9*, 223-230.

SUPPORTING INFORMATION

Equilibrium and Kinetic Analysis of CO_2-N_2 Adsorption Separation by Concentration Pulse Chromatography

*Peiyuan Li and F. Handan Tezel**

Department of Chemical Engineering, Faculty of Engineering, University of Ottawa

161 Louis Pasteur, Ottawa, Ontario K1N 6N5, Canada

This supporting information contains:

- Figure 3.S1
- Experimental details
- Table 3.S1
- Table 3.S2.
- Determination of System Dead Time
- Table 3.S3
- Table 3.S4
- Nomenclature.

This document contains 12 pages including this cover page.

Figure 3.S1.

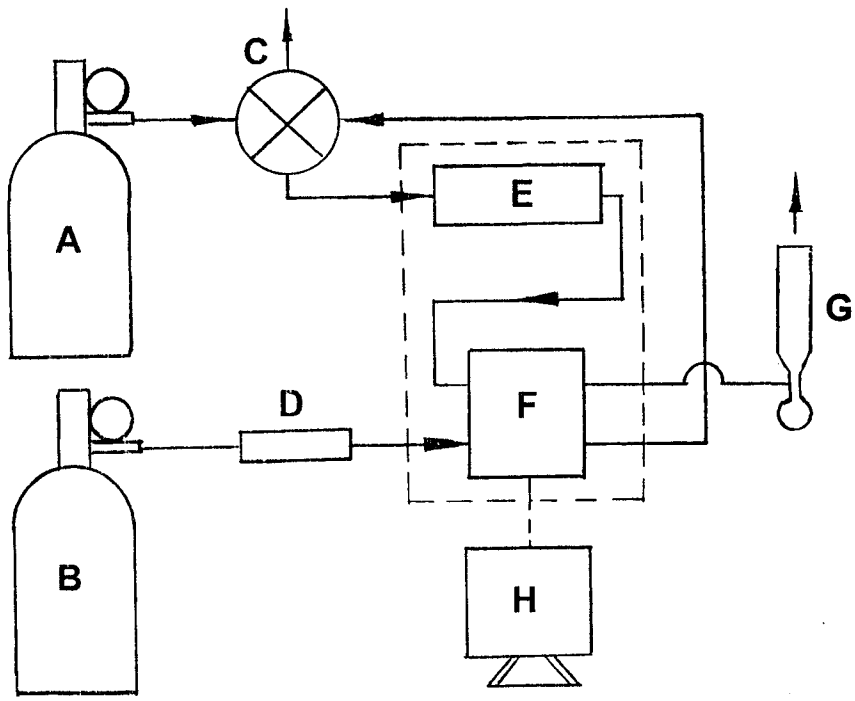

Figure 3.S1. Schematic diagram of the experimental set-up.

A – Sample gas; B – Carrier gas; C – Gas injection valve; D – MKS MFC; E – Packed adsorption column within GC oven; F – TCD; G – Bubble meter; H – Computer.

Experimental Details

Varian 3300 and HP 5730A gas chromatographs (GC) were used for this study. They were both equipped with a thermal conductivity detector (TCD) to measure the composition of the gas at the outlet of the column. The column, packed with the adsorbent, was fully contained in the GC oven for accurate temperature control. Its temperature was measured by a thermocouple with high precision. The injection valve introduced a 1 cc pulse of the sample gas at atmospheric pressure into the carrier stream. Carrier flow rates were controlled by an MKS mass flow controller (MFC), model number 1259C (0 – 50 sccm range), and measured by a bubble meter at the exit. The carrier gas first passed through the reference side of the TCD in the GC. After the injection, the carrier and the sample gases passed together through

the packed column and then the sample side of the TCD. The concentration at the outlet of the column was monitored as a function of time. Data acquisition was performed using a National Instruments based data acquisition card and Labview 6.1 software on an Intel based computer. Before each experimental run, the adsorbent was regenerated at 101.3 kPa and 350 °C under helium purge (5cc/min at room temperature) for approximately 22 hours.

Table 3.S1. Sample and carrier gases used in this study.

Type	Grade	Purity	Supplier
He	Ultra High Purity 5.0	99.999%	Praxair Inc., Ottawa
CO_2	Bone Dry 3.0	99.9%	Praxair Inc., Ottawa
N_2	Ultra High Purity 5.0	99.999%	Praxair Inc., Ottawa

Table 3.S2. Experimental and column specifications and conditions.

Particle Size	20-60 mesh (0.0246-0.0833cm)
Average Particle Diameter, D_p	0.0540 cm
Length of Column 1, L_1	10.56 cm
Inner Diameter of Column 1	0.405 cm
Length of Column 2, L_2	10.01 cm
Inner Diameter of Column 2	0.451 cm
Total Pressure	101.3 kPa
Detector Temperature	110 °C
Regeneration Temperature	350°C
Regeneration Pressure	101.3 kPa
Regeneration Time	22 hours

Determination of System Dead Time

Before Henry's Law constant and micro-pore diffusion are estimated, the real retention time must be determined, so it is very important to determine the system dead time. In order to do that, non-adsorbing glass-beads that have the same size as the adsorbents used (20-60 mesh) were packed in the column, and then dead time was measured at different flow rates and temperatures with different sample and carrier gases. The retention time for glass-beads (dead time), μ_D, decreases as superficial fluid velocity, v_S, increases as shown in Figures 3.S1 – 3.S3 for 3 different conditions used in this study. Column temperature, type of sample gas, and type of carrier gas do not change the relationship between superficial fluid velocity and dead time as expected. From the experimental data, a linear relation of μ_D vs. v_S^{-1} is obtained and shown in Figures 3.S1 – 3.S3. A proportional constant is introduced as follows:

$$\mu_D = \frac{k_C}{v_S}$$

where μ_D is the dead time, v_S is the superficial fluid velocity, and k_C is the proportionality constant.

As a result of the regression, k_C is determined to be 11.10, 8.69 and 22.60, respectively, for the three different conditions used. Therefore, we can use these results and never measure the dead times again at different temperatures and superficial velocities for different sample and carrier gases as long as the same column and particle sizes are used. The proportionality constants are different in Figures 3.S1 and 3.S2 with the same GC due to different sizes of columns and in Figures 3.S2 and 3.S3 with the same size of columns due to different types of GC, as expected.

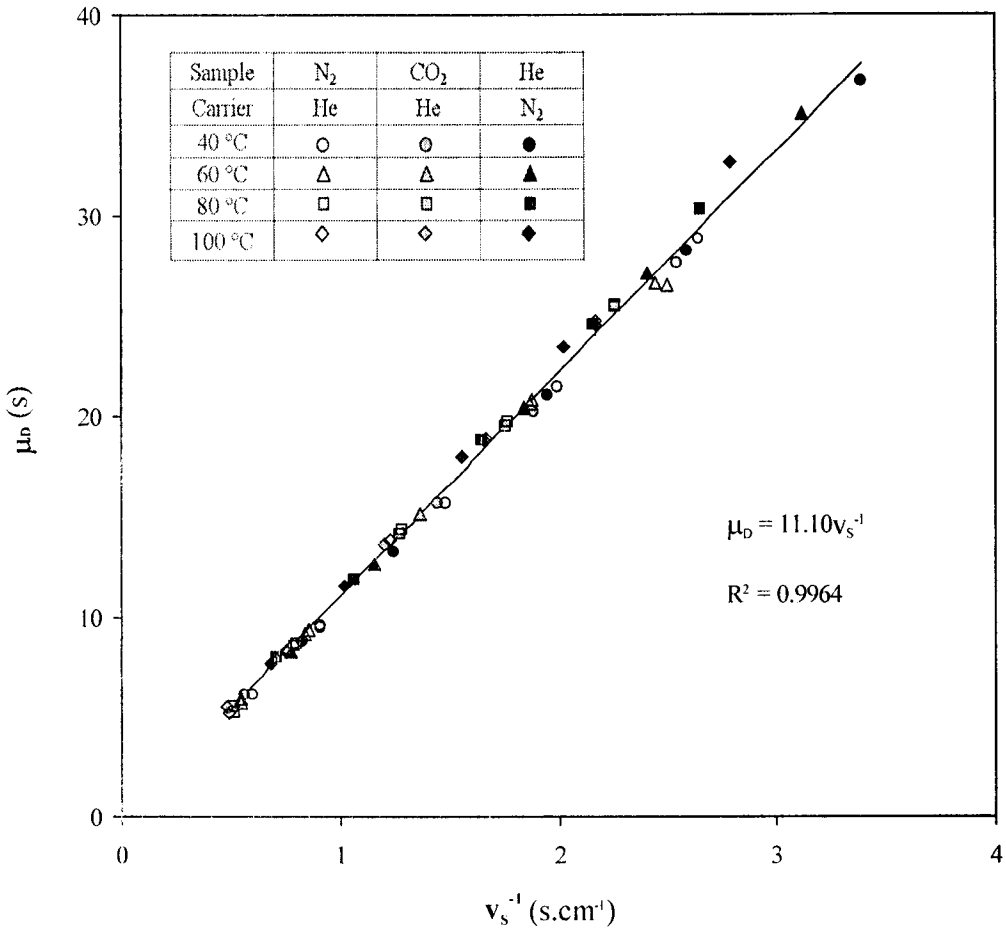

Figure 3.S2. Linear regression of the relation between dead times (μ_D) and superficial fluid velocities (v_S) on Column 1 by HP 5730A with glassbeads.

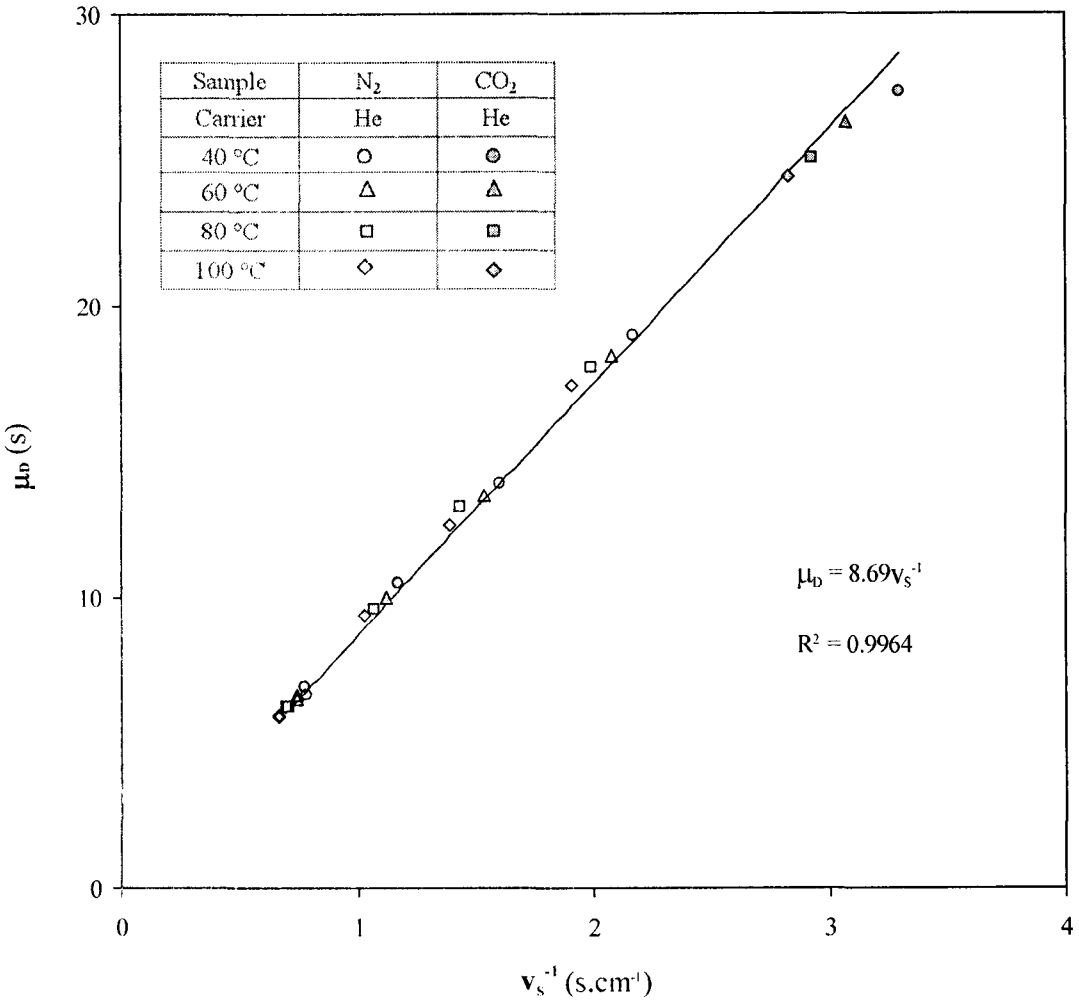

Figure 3.S3. Linear regression of the relation between dead times (μ_D) and superficial fluid velocities (v_S) on Column 2 by HP 5730A with glassbeads.

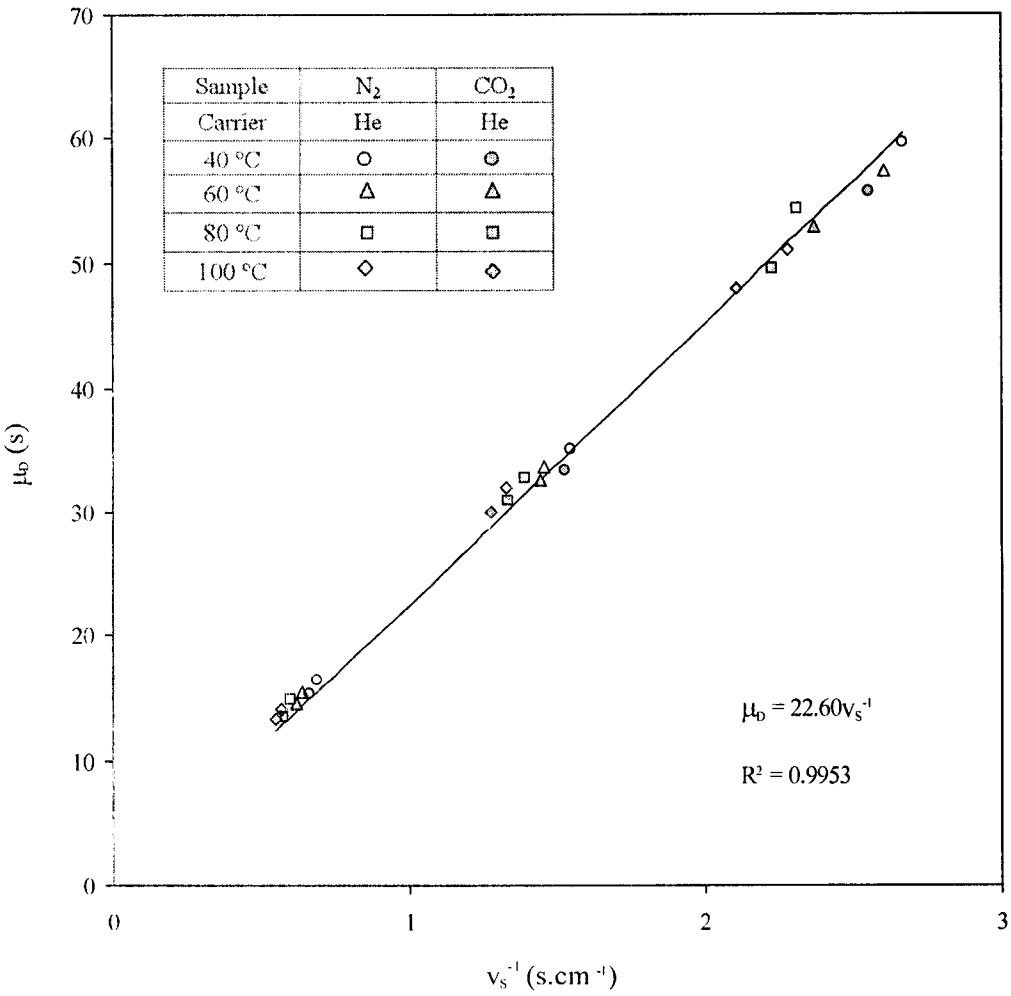

Figure 3.S4. Linear regression of the relation between dead times (μ_D) and superficial fluid velocities (v_S) on Column 2 by Varian 3300 with glassbeads.

Table 3.S3. Henry's Law adsorption equilibrium constants and adsorption equilibrium separation factors.

Adsorbents	Parameters	40 °C	50 °C	60 °C	70 °C	80 °C	90 °C	100 °C
Silicalite (UOP)	$K_{p,N2}$ (mmole. $g^{-1}.atm^{-1}$)	0.1409	0.1130	0.0919	0.0756	0.0629	0.0529	0.0448
	$K_{p,CO2}$ (mmole. $g^{-1}.atm^{-1}$)	3.064	2.212	1.628	1.220	0.930	0.719	0.564
	$\alpha_{e,CO2/N2}$	21.7	19.6	17.7	16.1	14.8	13.6	12.6
NaY (UOP) (Si / Al = 1.8)	$K_{p,N2}$ (mmole. $g^{-1}.atm^{-1}$)	0.1314	0.1095	0.0922	0.0784	0.0673	0.0583	0.0508
	$K_{p,CO2}$ (mmole. $g^{-1}.atm^{-1}$)	25.51	17.11	11.76	8.26	5.91	4.32	3.20
	$\alpha_{e,CO2/N2}$	194.2	156.3	127.5	105.3	87.8	74.0	63.0
NaY (UOP) (Si/Al=5) (*39*)	$K_{p,CO2}$ (mmole. $g^{-1}.atm^{-1}$)	26.9		12.18		5.45		2.97
13X (Zeochem)	$K_{p,N2}$ (mmole. $g^{-1}.atm^{-1}$)	0.1260	0.1049	0.0883	0.0751	0.0644	0.0557	0.0486
	$K_{p,CO2}$ (mmole. $g^{-1}.atm^{-1}$)	42.08	27.80	18.83	13.05	9.23	6.66	4.89
	$\alpha_{e,CO2/N2}$	334	265	213	174	143	119	101
13X (Ceca)	$K_{p,N2}$ (mmole. $g^{-1}.atm^{-1}$)	0.271	0.228	0.193	0.165	0.142	0.124	0.108
	$K_{p,CO2}$ (mmole. $g^{-1}.atm^{-1}$)	108.5	79.5	59.3	45.0	34.7	27.1	21.5
	$\alpha_{e,CO2/N2}$	400	349	308	273	244	219	198
13X (UOP) (*39*)	$K_{p,CO2}$ (mmole. $g^{-1}.atm^{-1}$)	----	----	----	----	18.2	----	7.99

Table 3.S4. Micropore diffusion (D_c/r_c^2) values for CO_2.

Adsorbents	Parameters	40 °C	50 °C	60 °C	70 °C	80 °C	90 °C	100 °C
Silicalite	D_c/r_c^2 (s^{-1})	0.0119	0.0155	0.0199	0.0252	0.0315	0.0389	0.0474
NaY	D_c/r_c^2 (s^{-1})	0.00067	0.00110	0.00176	0.00274	0.00415	0.00615	0.00892

Nomenclature

c = Adsorbate concentration, $mol.L^{-1}$

D = Diffusivity, dispersion coefficient, $m^2.s^{-1}$ or $cm^2.s^{-1}$ (in Equations 5, 6 and 7)

D_0 = Pre-exponential factor, $m^2.s^{-1}$ or $cm^2.s^{-1}$

D_p = Average particle diameter, cm

E_a = Diffusional activation energy, $kJ.mol^{-1}$

ΔH = Heat of adsorption, $kJ.mol^{-1}$

K =Dimensionless Henry's Law adsorption equilibrium constant, dimensionless

K_0 = Pre-exponential factor, dimensionless

K_p = Dimensional Henry's law adsorption equilibrium constant, $mmol.g^{-1}.atm^{-1}$

k = mass transfer coefficient, $m.s^{-1}$

k_C = proportionality constant, dimensionless

L = Column length, cm

M = Molecular weight

P = (Total) pressure, kPa or atm. (in Equation 5)

R = Gas constant, 0.008314 $kJ.mol^{-1}.K^{-1}$ or 0.08206 $atm.l.\ mol^{-1}.K^{-1}$ (in Eq. 2)

R_p = Pellet radius, m

r_c = Crystal or micro-particle radius, m

r_p = Pore radius, cm

Sh = Sherwood number, dimensionless

t = Time, s

T = Temperature, K or °C

v = Interstitial fluid velocity, $cm.s^{-1}$

v_S = Superficial fluid velocity, $cm.s^{-1}$

x = Mole fraction in adsorbed phase at equilibrium

y = Mole fraction in fluid phase at equilibrium

Greek letters

α = Adsorption separation factor or selectivity

ε = (Bed) porosity, dimensionless

μ = (Corrected) retention time, the first moment of the response peak, s

σ = Constant in the Lennard-Jones potential-energy function, Å

σ^2 = Second moment of the response peak, s^2

Ω = Collision integral, dimensionless

Subscripts

A = Component A; adsorbed phase

B = Component B; fluid phase

c = Crystal or micro-particle

D = Dead time

e = Equilibrium process

f = External film

k = Knudsen

L = Axial

m = Molecular

p = Pellet; macro-pore

1 = Column 1

2 = Column 2

Abbreviations

GC = Gas Chromatograph

GHG = Greenhouse gases

HP = Hewlett Packard

MFC = Mass Flow Controller

TCD = Thermal Conductivity Detector

CHAPTER IV

PURE AND BINARY ADSORPTION EQUILIBRIA OF METHANE AND CARBON DIOXIDE ON SILICALITE

Peiyuan Li and F. Handan Tezel*

Department of Chemical Engineering
Faculty of Engineering
University of Ottawa
161 Louis Pasteur, Ottawa, Ontario K1N 6N5, Canada

Accepted to be published in Separation Science and Technology in 2007.

Presented at 2006 AIChE (American Insititute of Chemical Engineers) Annual Meeting, San Francisco, CA, USA, on Nov. 12-17, 2006, Conference Proceedings 333c (Paper is available).

* Corresponding author
Tel: 613-562-5800 Ext. 6099
Fax: 613-562-5172
Emai: Handan.Tezel@uottawa.ca

ABSTRACT

For the separation of CH_4 and CO_2 in landfill gas, pure and binary adsorption was researched at 40, 70 and 100 °C up to 5 atmospheres. Pure adsorption models were considered by the constant volume method. Experimental binary isotherms at different concentrations were determined by using three concentration pulse methods (CPM), among which, HT – CPM is the best one to describe the behaviour of this binary system. Predicted binary isotherms by using six models were compared to the experimental ones. Equilibrium phase diagrams and separation factors were obtained from the experimental binary isotherms. For this system, the integral thermodynamic consistency tests were also shown and discussed.

INTRODUCTION

The global environment is a major issue today, and global warming in particular is the focus of much attention. Accumulation of greenhouse gases (GHG) in the atmosphere is responsible for increased global warming of our planet. It is supposed that the increasing concentration of carbon dioxide mainly from flue gas, automobile and landfill emissions in the atmosphere is the major contributor to this problem with more than 80% of total GHG emissions (1, 2). Besides, methane is the most important non-CO_2 GHG responsible for global warming with more than 10% of total GHG emissions. Despite the much smaller amounts of methane released to the atmosphere, the greenhouse warming potential (GWP) of this gas is 21% higher than carbon dioxide. Therefore, any reduction in methane emissions is important in the short- and medium-term atmosphere reconstruction (1). Landfill gas (LFG) is a multi-component mixture containing mainly methane and carbon dioxide, which constitutes one of the main sources of methane and carbon dioxide emissions, and can be treated as an important resource of directly available methane. This reason, together with a tighter control in emissions to meet Kyoto Protocol targets, puts LFG into consideration for energy production (1, 3).

For CO_2 - CH_4 separation, binary gas isotherms were obtained with two different techniques: gravimetric and volumetric technique (4) and concentration pulse chromatographic technique (5-9). The use of concentration pulse chromatography for adsorbent screening is very attractive since it is relatively inexpensive to setup and easier to operate. A method using the K_p-functions proposed in the literature for determining the binary isotherms from concentration pulse chromatographic data has been given and shown capable of interpreting highly selective binary systems (6, 10-14).

In the work presented in this paper, adsorption separation of carbon dioxide and methane was studied with silicalite adsorbent. Pure and binary isotherms were obtained by the constant volume and the concentration pulse chromatographic techniques. Additionally, the thermodynamic consistency tests between pure and binary gas adsorption systems were discussed.

THEORY

The models for mixed-gas adsorption are crucial to the design of adsorptive gas separation processes. They should be capable of predicting the equilibrium amount adsorbed from pure gas isotherms. Because of the paucity of experimental data, however, none of the theories or models has been extensively tested. In the literature, there are several gas adsorption isotherm models often used to predict binary systems, including extended Langmuir (15), extended dualsite Langmuir (16), extended Sips (17), ideal adsorbed solution theory (18), Flory-Huggins vacancy solution theory (VST) (19) and the statistical model (20).

In the concentration pulse chromatographic technique, a pulse of the sample gas is injected into the carrier gas stream and passes through the column. The response of the column to the injection is measured as concentration vs. time at the exit of the column. From this response peak a mean retention time of the sample, μ, defined as the first moment of the chromatogram, is determined experimentally (10). Dimensionless Henry's Law constant, K, can be determined from the corrected first moment at low concentrations of the response peak as follows (9, 14, 21, 22):

$$\mu = \frac{\int_0^t c(t-\mu_D)dt}{\int_0^t cdt} = \frac{L}{v}\left[1+\frac{(1-\varepsilon)K}{\varepsilon}\right] \quad \text{.....(1)}$$

where t is the time, c is the adsorbate concentration measured at the outlet of the column, L is the column length, ε is the bed porosity, v is the interstitial fluid velocity, K is the dimensionless Henry's Law adsorption equilibrium constant, and μ_D is the dead time.

The dimensionless Henry's Law constants, K, can be converted to a dimensional form, K_p, as follows (22) and gives the slope of the adsorption isotherm for pure component systems.

$$K_p = \frac{K}{RT\rho_p} \quad \text{.....(2)}$$

where T is the absolute temperature, ρ_p is the density of the pellets of the adsorbent and K_p is the dimensional Henry's Law adsorption equilibrium constant.

For the binary mixture systems, the K_p value is related to the slopes of the isotherms of the individual components in the carrier gas mixture. For a binary mixture, the relationship is given as follows (11):

$$K_p = (1 - y_1)\frac{dq_1}{dP_1} + y_1 \frac{dq_2}{dP_2} \quad \text{.....(3)}$$

where $\frac{dq_1}{dP_1}$ and $\frac{dq_2}{dP_2}$ are the slopes of the adsorption isotherms for components 1 and 2 respectively.

This method allows for the experimental evaluation of the binary mixture isotherms when K_p values are determined for different concentrations of the carrier gas (11).

For binary isotherms, both components in the mixed carrier gas are adsorbed and $\frac{dq_2}{dP_2}$ in the last term of Eq. (3) is not constant. The experimental K_p data represent the combined contribution of both components to the isotherms. The interpretation of the binary K_p data has been treated by several methods in the literature (6, 10, 14, 23). Concentration Pulse Chromatographic Methods often used in the literature are listed in Table 4.1.

The thermodynamics of pure and binary gas adsorption systems has been extensively studied using the Gibbsian surface excess (GSE) model (24), which can be differentiated or integrated using different thermodynamic paths in order to generate various thermodynamic consistency tests. For binary gas adsorption systems, it has been used to develop several relationships for checking both the thermodynamic consistency between pure and binary gas equilibrium adsorption data and the internal thermodynamic consistency of the binary adsorption data itself. These relationships of integral and differential consistency tests have been developed for pure and binary gas adsorption data. The integral test requires the measurement of both pure gas and binary gas adsorption isotherms shown below (25):

$$\left(-\int_0^P \frac{q_2^0}{P} dP\right) - \left(-\int_0^P \frac{q_1^0}{P} dP\right) = \int_0^1 \frac{q_1(1-y_1) - q_2 y_1}{y_1(1-y_1)} dy_1$$

or

$$\int_0^P \frac{q_1^0}{P} dP - \int_0^P \frac{q_2^0}{P} dP = \int_0^1 \frac{q_1(1-y_1) - q_2 y_1}{y_1(1-y_1)} \quad \text{.....(4)}$$

Table 4.1. Concentration pulse chromatographic methods often used in the literature.

MVV-CPM (Modified Van der Vlist and Van der Meijden -Concentration Pulse Method) (10, 12, 14)	
4-parameter function	$K_p = A_0 + A_1 y_1 + A_2 y_1^2 + A_3 y_1^3$
Isotherm slope functions	$\frac{dq_1}{dP_1} = B_0 + B_1 y_1 + B_2 y_1^2$ $\quad$ $\frac{dq_2}{dP_2} = C_0 + C_1 y_1 + C_2 y_1^2$
Binary isotherm functions	$q_1 = \left(B_0 y_1 + \frac{B_1}{2} y_1^2 + \frac{B_2}{3} y_1^3 \right) P$ $\quad$ $q_2 = \left[C_0 (1 - y_1) + \frac{C_1}{2}(1 - y_1^2) + \frac{C_2}{3}(1 - y_1^3) \right] P$
MTT-CPM (Modified Triebe and Tezel -Concentration Pulse Method) (23)	
5-parameter function	$K_p = A_{-1}(\beta + y_1) + A_0 + \frac{A_1}{(\beta + y_1)} + \frac{A_2}{(\beta + y_1)^2}$
Isotherm slope functions	$\frac{dq_1}{dP_1} = B_0 + \frac{B_1}{(\beta + y_1)} + \frac{B_2}{(\beta + y_1)^2}$ $\quad$ $\frac{dq_2}{dP_2} = C_0 + \frac{C_1}{(\beta + y_1)} + \frac{C_2}{(\beta + y_1)^2}$
Binary isotherm functions	$q_1 = \left[B_0 y_1 + B_1 \ln \frac{\beta + y_1}{\beta} + \frac{B_2 y_1}{\beta(\beta + y_1)} \right] P$ $\quad$ $q_2 = \left[C_0 (1 - y_1) - C_1 \ln \frac{\beta + y_1}{\beta + 1} + \frac{C_2 (1 - y_1)}{(\beta + 1)(\beta + y_1)} \right] P$
HT-CPM (Harlick and Tezel -Concentration Pulse Method) (6)	
5-parameter function	$K_p = A_1 + A_2 y_1 + A_3 y_1^2 + A_4 \ln\lvert y_1 + \lambda \rvert$
Isotherm slope functions	$\frac{dq_1}{dP_1} = B_1 + 2B_2 y_1 + \frac{B_3}{\lvert y_1 + \lambda \rvert}$ $\quad$ $\frac{dq_2}{dP_2} = C_1 + 2C_2 y_1 + \frac{C_3}{\lvert y_1 + \lambda \rvert}$
Binary isotherm functions	$q_1 = \left[B_1 y_1 + B_2 y_1^2 + B_3 \ln \left\lvert \frac{y_1 + \lambda}{\lambda} \right\rvert \right] P$ $\quad$ $q_2 = \left[C_1 (1 - y_1) + C_2 (1 - y_1^2) - C_3 \ln \left\lvert \frac{y_1 + \lambda}{1 + \lambda} \right\rvert \right] P$

where q^0_1 and q^0_2 are the amount adsorbed of Components *1* and *2* respectively in the pure gas systems, P is the total pressure, q_1 and q_2 are the amounts adsorbed of Components *1* and *2*, respectively in the binary system, y_1 is the mole fraction of Component 1 in the binary system. The two terms of the left side are the potentials of adsorption at P and T for pure gases 2 and 1, respectively. They can be estimated as a function of P at constant T using the pure gas adsorption isotherm. Thus, the quantity on the left side at any given values of P and T can be evaluated from the pure gas adsorption isotherms for the

components in a binary gas mixture. The quantity on the right side at any given values of P and T can be evaluated using the binary gas adsorption isotherm at constant P and T. These two independently measured quantities must be equal; this equality forms the basis for the integral consistency test between pure and binary gas equilibrium adsorption data.

EXPERIMENTAL

Volumetric System

An AccuSorb 2100E Physical Adsorption Analyzer supplied by Micromeritics Instrument Corporation was equipped with high precise pressure transducers and thermocouples. Data acquisition was performed using a National Instruments based data acquisition card and Labview 6.1 on a computer. The adsorbent sample was regenerated at approximately 350 °C under vacuum for approximately 20 hours before use. Helium, with a negligible adsorption on the adsorbent, was used to measure the dead volume in the gas phase.

Concentration Pulse Chromatography

A schematic diagram of the experimental apparatus is shown in Figure 4.1. The flow rates and compositions of the carrier gases (A) were controlled by two MKS mass flow controllers (B), and set to a total flowrate of 15 cc/min. A mixing chamber (C) was installed after the mass flow controllers to ensure a homogeneous mixture in the carrier gas. The carrier gas passed through the reference side of the thermal conductivity detector (TCD) (E) in the system. It then went through the sample injection valve (F), which introduced a 1 cc pulse of adsorbate sample gas (D) at atmospheric pressure into the mixed carrier gas stream. Then, the carrier and the sample passed through the packed column (G) and the sample side of TCD (E), where the response of the column to the sample injection as a voltage was monitored as a function of time. Data acquisition was performed using a National Instruments based data acquisition card and Labview 6.1 on a computer. The adsorbent was regenerated at 101.3 kPa and 350 °C under helium purge for approximately 20 hours before

use. The column was packed with zeolite silicalite adsorbent within a Varian 3300 gas chromatograph.

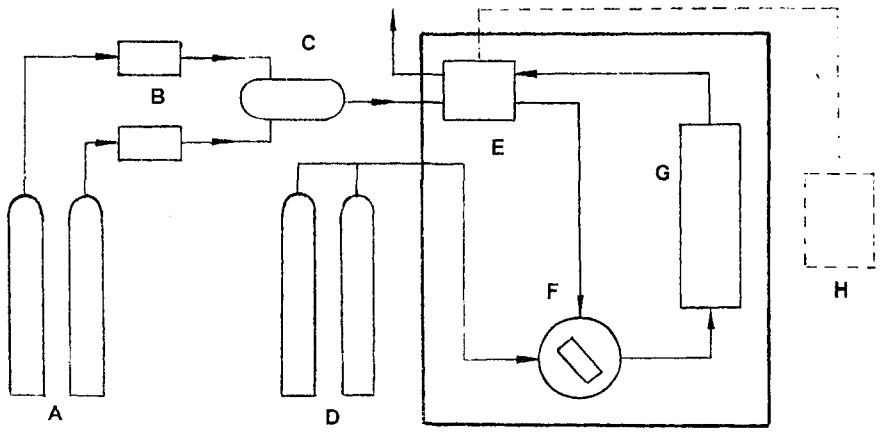

Figure 4.1. Schematic diagram of the experimental apparatus:
A – Carrier gases; B – MKS mass flow controllers;
C – Mixing chamber; D – Sample gases;
E – TCD; F – Gas injection valve;
G – Packed adsorption column within GC oven;
H – Computer data acquisition system.

It is noted that there are two methods to determine the pure isotherms for the end-points of the binary isotherms. The first one is volumetric method, which is traditional, popular and reliable. It was used in this work. The latter is concentration pulse chromatographic method, in which helium is mixed with the adsorbate and used as the carrier gas. The two methods are consistent with each other very well according to our study.

When determining binary isotherms, mixed carriers were used without the He gas. For the CO_2-CH_4 system, CH_4 was used as the primary gas. Samples of each gas were injected into the column at different carrier gas concentrations.

It is important to note that the experimental data represents binary isotherm's effective slope at a particular mixture composition. As the injection volume approaches zero, the K_p values found by both injections should be identical. When CO_2 is injected, the

mixture composition increases slightly in CO_2 concentration. When CH_4 is injected, the mixture composition decreases slightly in CO_2 concentration. Therefore, both adsorbates are injected into the mixed carrier gas and the arithmetic average retention times were found. The arithmetic average retention times found for CO_2 and CH_4 did not vary by more than 5% during this binary study.

Materials

The adsorbent and sample gases used in the experiments are listed in Tables 4.2 and 4.3 respectively. It is noted that the values of adsorbed loading obtained from experiments were corrected taking into account that generally the binder has little adsorption capacity as literature data are mostly obtained with silicalite crystals, without binder.

Table 4.2. Details of the adsorbent studied.

Type	Silicalite
Commercial name	MOLSIV Adsorbents
Commercial number	HISIV 3000
Particle form received	1/16 inch extrudate as received
Size used in the column (Diameter)	Crushed to 20 x 60 mesh
Content of binder	20 wt%
Particle density	1.131 $g.cm^{-3}$
Void fraction	0.39
Supplier	Universal Oil Products, Des Plaines, IL, USA

Table 4.3. Details of the gases used.

Gases	Grade	Purity	Supplier
CO_2	Bone Dry 3.0	99.9%	Praxair Inc., Ottawa
CH_4	Ultra High Purity 3.7	99.97%	Praxair Inc., Ottawa
He	Ultra High Purity 5.0	99.999%	Praxair Inc., Ottawa

Numerical Methods

A non-linear regression was performed in order to determine the parameters for the pure component isotherm fits to the Toth isotherm as well as the K_p regressions. In order to solve the equations given by HT-CPM, MTT-CPM and MVV-CPM, a non-linear equation solver was used. This method was based on Newton's method. In order to determine the optimal values of the B_j and C_j parameters for the HT-CPM, MTT-CPM and MVV-CPM, a non-linear constrained optimization technique was used by using the Solver in MS Excel. This wide range of initial guesses ensured that the absolute and not the local minimum was obtained.

RESULTS AND DISCUSSION

Pure Gas Adsorption of CO_2 and CH_4 by Silicalite

Adsorption equilibrium isotherm data for CO_2 and CH_4 on silicalite pellets were obtained at three different temperatures for pressures up to 5 atm and are given in Figure 4.2 as data points. The curves going through the data points represent Toth isotherm models at the corresponding temperature. The numbered curves are data from the literature (as indicated in the figure), given for comparison with the present study. All the values of adsorbed loading obtained from experiments in this work were corrected taking into account that generally the

binder has little adsorption capacity as literature data are mostly obtained with silicalite crystals, without binder.

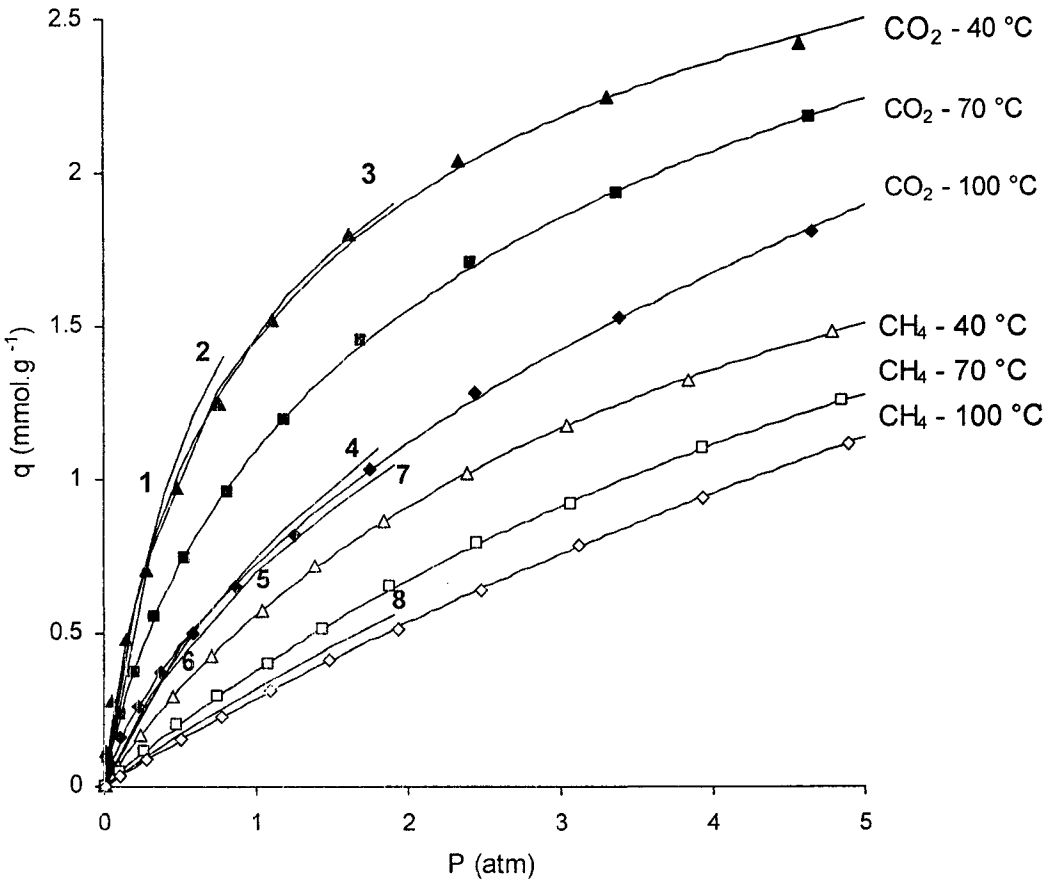

Figure 4.2. Isotherms for CO_2, and CH_4 on silicalite:
The points are experimental data
and the curves through the data points are Toth isotherm model fits.
The numbered curves indicate comparisons with the literature:
1: CO_2 - 25°C (26); **2:** CO_2 - 31°C (27); **3:** CO_2 - 32°C (28); **4:** CO_2 - 80°C (28);
5: CH_4 - 23°C (27); **6:** CH_4 - 25°C (26); **7:** CH_4 - 31°C (28); **8:** CH_4 - 81°C (28).

Although the temperatures are not exactly the same, the qualitative comparison with the literature is excellent, with adsorption capacity increasing with decreasing temperature and/or increasing pressure, for both of the adsorbates, since physical adsorption is always

exothermic. CO_2 is adsorbed more than CH_4 since the quadrupole moment of carbon dioxide is much higher than that of methane. At low pressure, the slopes of the isotherms of carbon dioxide are very high, and then the slopes decrease rather fast with increasing pressure as the adsorbent sample approach to saturation. However, the slopes of the isotherms of methane hardly decease as pressure increases, isotherms being more linear at high temperature.

By using non-linear regressions, the parameters of different isotherm models were obtained and corresponding parameters are shown in Table 4.4. For gauging the quality of the non-linear regressions obtained from the different models used, the RMS (root mean square) deviations ($[\Sigma(q_{data}- q_{curve})^2/n]^{0.5}$) are used and shown in Table 4.4. When two-parameter models, Langmuir and Freundlich, are compared, Langmuir is better than Freundlich. When three-parameter models were considered, it was observed that all of them, Sips, Flory-Huggins Vacancy Solution Theory (VST), Toth and Multisite-Langmuir, are better than the two-parameter models because of their increased flexibility. The four-parameter model, Dualsite-Langmuir Model, is better than all the other models used because of its maximum flexibility among the models applied.

For useful description of adsorption equilibrium data at various temperatures, the temperature independent forms of the Toth and Sips equations were also used. By using the data at the three experimental temperatures simultaneously for curve fitting of both temperature independent Sips and Toth equations, optimal parameters shown in Table 4.5 were obtained. The parameters and RMS deviations at the three temperatures are listed in Table 4.4. From the parameters given in Table 4.5 for temperature independent Toth and Sips isotherms, the experimental data are extended to other temperature and pressures.

By using the Clausius-Clapeyron equation, the isosteric heat of adsorption on silicalite was obtained at the limit of zero coverage at 313-373 K with the volumetric method for pure gases: Q_{CO2} is 28.31 $kJ.mol^{-1}$ (compared with 27.2 $kJ.mol^{-1}$ from Dunne et al (27) and 29.0 $kJ.mol^{-1}$ from Dubinin et al (29)) and Q_{CH4} is 12.52 $kJ.mol^{-1}$ (compared with 12-20 $kJ.mol^{-1}$ from Otto et al (30)).

Table 4.4. Parameters and RMS deviations of adsorption models by non-linear regressions

Models		Parameters	CO_2			CH_4		
			40 °C	70 °C	100 °C	40 °C	70 °C	100 °C
Langmuir (2 param.)	$q = \frac{q_m BP}{1+BP}$	B (atm^{-1})	1.089	0.649	0.332	0.277	0.138	0.071
		q_m ($mmol.g^{-1}$)	2.858	2.834	2.911	2.578	3.128	4.345
		RMS	0.050	0.040	0.038	0.005	0.005	0.003
Freundlich (2 param.)	$q = kP^{\frac{1}{n}}$	k ($mmol.g^{-1}.atm^{-1/n}$)	1.340	1.035	0.713	0.555	0.384	0.292
		n (dimensionless)	2.295	1.938	1.616	1.540	1.306	1.172
		RMS ($mmol.g^{-1}$)	0.106	0.067	0.022	0.037	0.021	0.010
Sips (Langmuir-Freundlich) (3 param.)	$q = \frac{q_m (BP)^{\frac{1}{n}}}{1+(BP)^{\frac{1}{n}}}$	B (atm^{-1})	0.675	0.337	0.065	0.242	0.137	0.060
		q_m ($mmol.g^{-1}$)	3.431	3.697	6.240	2.752	3.134	4.827
		n (dimensionless)	1.256	1.249	1.349	1.039	1.001	1.019
		RMS ($mmol.g^{-1}$)	0.021	0.012	0.009	0.003	0.005	0.003
Toth (3 param.)	$q = \frac{q_m BP}{\left[1+(BP)^n\right]^{\frac{1}{n}}}$	B (atm^{-1})	1.397	0.678	0.100	0.257	0.136	0.053
		q_m ($mmol.g^{-1}$)	3.903	4.885	38.98	2.981	3.166	6.020
		n (dimensionless)	0.604	0.537	0.260	0.864	0.991	0.845
		RMS ($mmol.g^{-1}$)	0.028	0.013	0.011	0.003	0.005	0.003
Flory-Huggins VST (3 param.)	$P = \left(\frac{1}{B}\cdot\frac{q}{1-\frac{q}{q_m}}\right)\exp\left(\frac{\alpha^2\cdot q}{1+\alpha^2\cdot\frac{q}{q_m}}\right)$	B ($mmol.g^{-1}.atm^{-1}$)	3.874	2.608	1.280	0.771	0.434	0.310
		q_m ($mmol.g^{-1}$)	3.082	3.498	5.969	2.976	3.308	5.609
		α_{1v} (dimensionless)	1.020	1.525	2.123	0.806	0.360	0.697
		RMS ($mmol.g^{-1}$)	0.032	0.014	0.019	0.003	0.005	0.003
Multisite Langmuir (3 param.)	$BP = \frac{\frac{q}{q_m}}{\left(1-\frac{q}{q_m}\right)^n}$	B (atm^{-1})	1.002	0.341	0.014	0.180	0.118	0.028
		q_m ($mmol.g^{-1}$)	3.322	6.567	78.01	4.208	3.683	10.97
		n (dimensionless)	1.412	3.881	43.90	2.080	1.248	2.849
		RMS ($mmol.g^{-1}$)	0.049	0.019	0.027	0.003	0.005	0.003
Dualsite Langmuir (4 param.)	$q = \frac{q_{m1} B_1 P}{1+B_1 P} + \frac{q_{m2} B_2 P}{1+B_2 P}$	B_1 (atm^{-1})	0.782	0.393	0.190	0.004	0.002	0.062
		q_{m1} ($mmol.g^{-1}$)	2.822	2.904	3.492	14.05	5.091	4.729
		B_2 (atm^{-1})	36.44	7.003	11.00	0.347	0.144	0.943
		q_{m2} ($mmol.g^{-1}$)	0.217	0.305	0.173	1.989	2.919	0.029
		RMS ($mmol.g^{-1}$)	0.012	0.019	0.027	0.003	0.005	0.003
Temperature Independent Sips	$q = \frac{q_m (BP)^{\frac{1}{n}}}{1+(BP)^{\frac{1}{n}}}$	B (atm^{-1})	0.594	0.343	0.212	0.187	0.143	0.115
		q_m ($mmol.g^{-1}$)	3.614	3.614	3.614	3.108	3.108	3.108
		n (dimensionless)	1.321	1.223	1.149	1.093	1.002	0.936
		RMS ($mmol.g^{-1}$)	0.026	0.026	0.026	0.010	0.016	0.011
Temperature Independent Toth	$q = \frac{q_m BP}{\left[1+(BP)^n\right]^{\frac{1}{n}}}$	B (atm^{-1})	1.617	0.640	0.285	0.262	0.172	0.121
		q_m ($mmol.g^{-1}$)	4.649	4.649	4.649	2.533	2.533	2.533
		n (dimensionless)	0.496	0.570	0.635	1.067	1.160	1.283
		RMS ($mmol.g^{-1}$)	0.031	0.015	0.024	0.012	0.018	0.016

Table 4.5. Optimal parameters determined for the temperature independent Toth and Sips equations for a reference temperature $T_0 = 40°C$

Adsorbates	Parameters	Units	Temperature Independent Toth	Temperature Independent Sips
CO_2	χ	Dimensionless	0	0
	q_{m0}	$mmol.g^{-1}$	4.649	3.614
	B_0	atm^{-1}	1.660	0.603
	Q/RT_0	Dimensionless	10.87	6.439
	n_0	Dimensionless	0.494	1.324
	α	Dimensionless	0.869	0.708
CH_4	χ	Dimensionless	0	0
	q_{m0}	$mmol.g^{-1}$	2.533	3.108
	B_0	atm^{-1}	0.262	0.187
	Q/RT_0	Dimensionless	4.809	3.068
	n_0	Dimensionless	1.067	1.093
	α	Dimensionless	1.065	0.954

The primary requirement for an economic separation process is an adsorbent with sufficiently high selectivity, capacity, and life. The selectivity may depend on a difference in either adsorption kinetics or adsorption equilibrium. Most of the adsorption processes in current use depend on equilibrium selectivity. In considering such processes it is convenient to define an ideal adsorption separation factor:

$$\alpha_{A/B} = \frac{x_A / x_B}{y_A / y_B} \quad \text{..... (5)}$$

where x_A, x_B, y_A, and y_B are, respectively, the mole fractions of components *A* and *B* in adsorbed and fluid phases at equilibrium. If the isotherms are linear or pressure is small enough for the isotherms to keep in the linear range, ideally, the separation factor is given simply by the ratio of the amounts adsorbed in pure components:

$$\alpha_{i,A/B} = \frac{q_A}{q_B} \quad \text{.....(6)}$$

where q_A and q_B are the amounts adsorbed of components *A* and *B*. These equilibrium separation factors are shown as a function of pressure and temperature in Figure 4.3. According to the results, both pressure and temperature are very important for the separation. In general, separation factors increase with decreasing pressure and/or temperature. It is difficult to separate the system at high temperature and/or high pressure. For landfill gas, generally, the separation is easier than other applications as the temperature is between 40 and 50 ^{0}C.

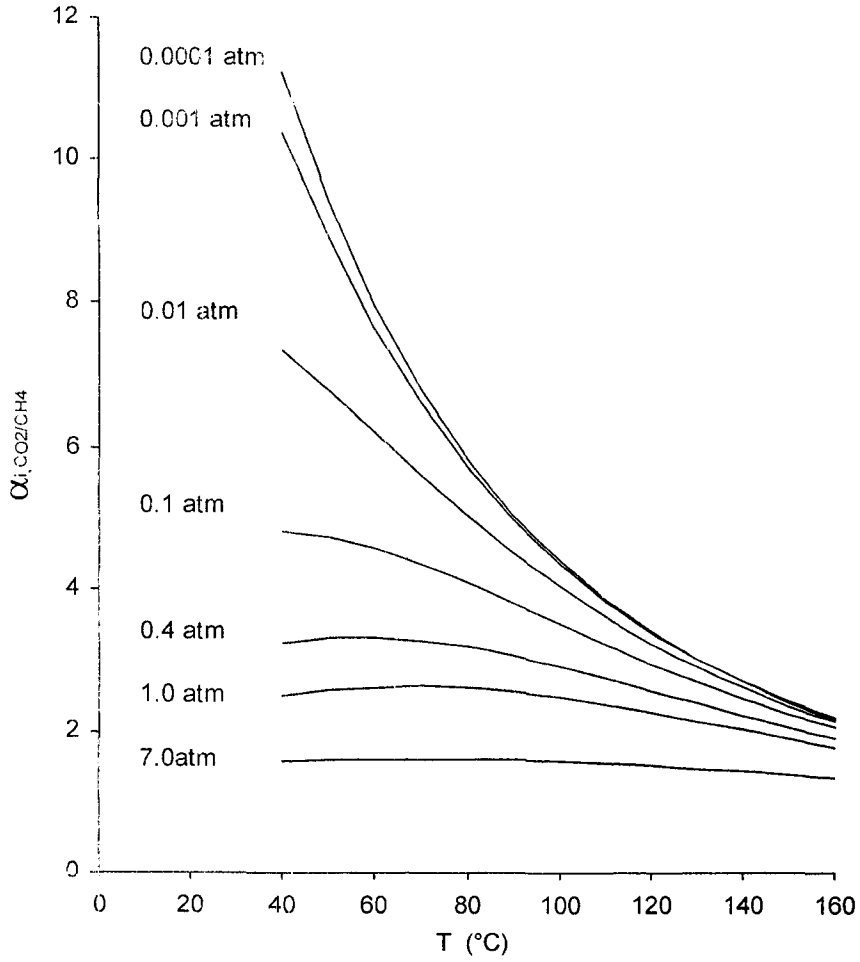

Figure 4.3. Ideal separation factors for CO_2/CH_4, on silicalite

Binary Isotherms

After regenerating the silicalite adsorbent, K_p values were determined by increasing the CO_2 mole fraction in CO_2-CH_4 carrier gas from 0% up to 100%. The samples were injected after attaining equilibrium for each concentration change of the carrier gas by noting that the baseline of the response would be steady. The K_p values, as well as their corresponding curve fits for HT-CPM, MTT-CPM and MVV-CPM, as a function of the gas composition are given in Figure 4.4. It is noted that the increment of y_{CO2} is not used in the calculation because the equations of isotherm slope functions in Table 4.1 are substituted into Equation (3). When y_{CO2} is very small at the beginning, K_p decreases extremely fast, so the taken increment of y_{CO2} is very small for obtaining more accurate results. As can be seen from this figure, the best fit was obtained with the HT-CPM. As was proven before, this method is a more versatile method, which would accommodate more non-ideal systems, where the adsorption capacities of the two adsorbates are very different from each other (5).

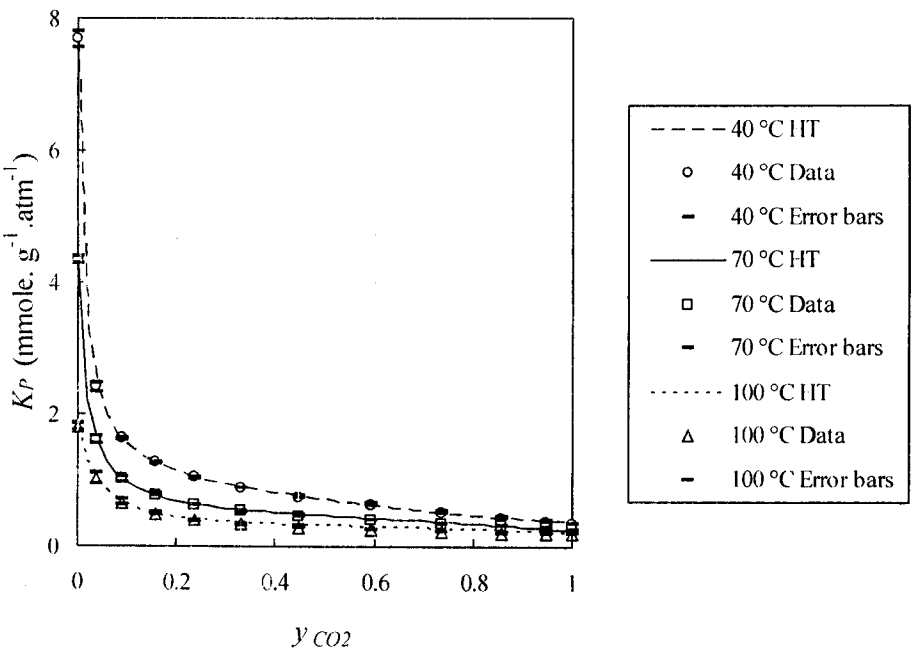

Figure 4.4a. Regressions for CO_2/CH_4, binary K_p with silicalite by HT-CPM at different carrier gas compositions under 1atm. total pressure with error bars.

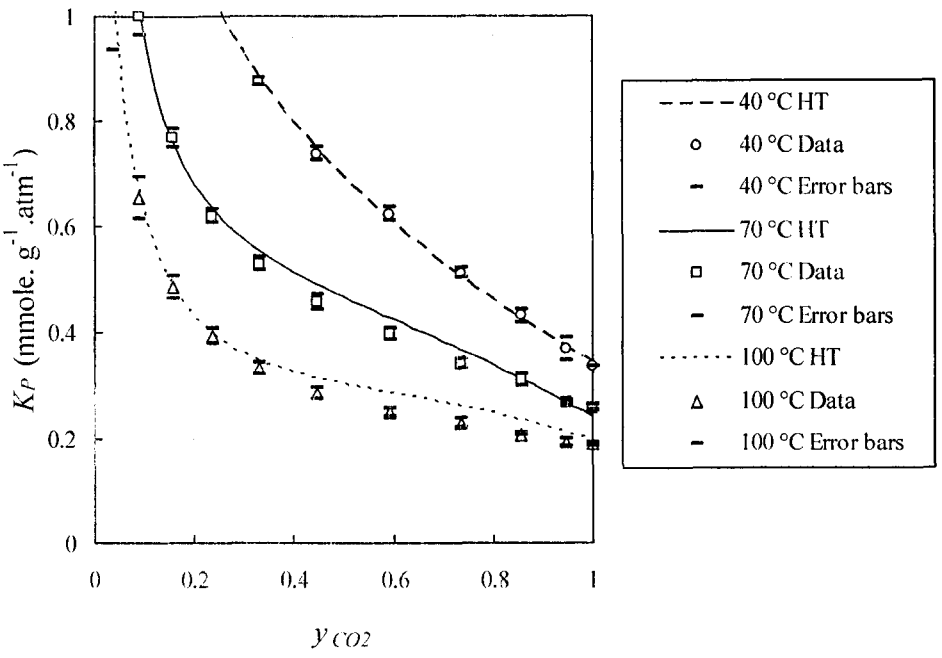

Figure 4.4b. Regressions for CO_2/CH_4, binary K_p with silicalite by HT-CPM at different carrier gas compositions under 1atm. total pressure with error bars. (K_p is in the range between 0 mmol.g^{-1}.atm^{-1} and 1 mmol.g^{-1}.atm^{-1})

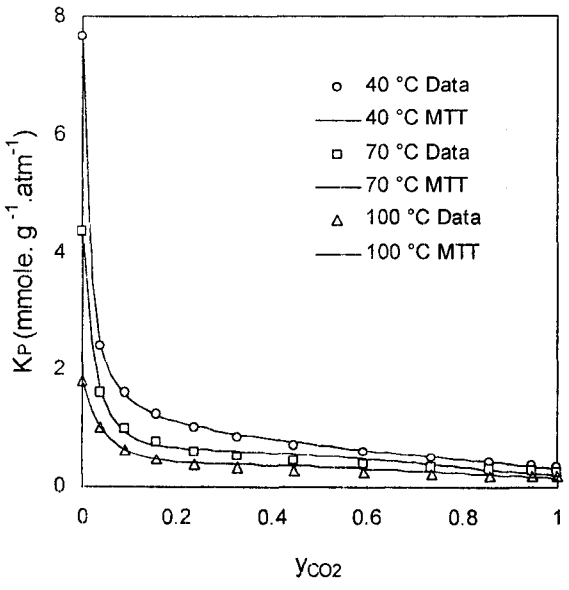

Figure 4.4c. Regressions for CO_2/CH_4, binary K_p with silicalite by MTT-CPM at different carrier gas compositions under 1 atm total pressure.

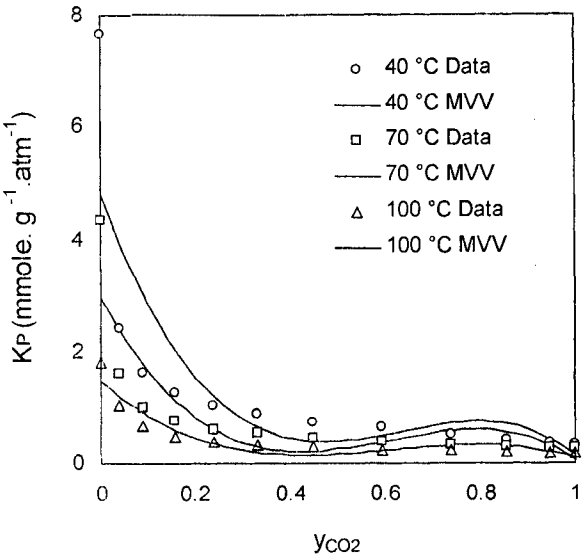

Figure 4.4d. Regressions for CO_2/CH_4, binary K_p with silicalite by MVV-CPM at different carrier gas compositions under 1 atm total pressure.

To quantify the non-linear regressions for these three concentration pulse methods, the RMS (root mean square) deviations ($[\Sigma(K_{p,data}- K_{p,curve})^2/n]^{0.5}$) were used and shown in Table 4.6 and it was observed that the best fit, was actually the HT-CPM method. Therefore, the HT-CPM , shown with error bars in Figures 4.3a and 4.3b, was used to describe these systems for our further study of this binary system.

Table 4.6. RMS deviations ($[\Sigma(K_{p,data}- K_{p,curve})^2/n]^{0.5}$) in $mmole.g^{-1}.atm^{-1}$ of concentration pulse chromatographic methods for CO_2-CH_4 binary system on silicalite.

CPM	40 °C	70 °C	100 °C
HT	0.009	0.019	0.020
MTT	0.027	0.063	0.038
MVV	1.061	0.536	0.152

The experimental binary isotherms for CO_2 - CH_4 with silicalite were obtained at three temperatures and are given in Figure 4.5 in comparison with the predicted ones. When

y_{CO2} increases, the CO_2 adsorption capacity, q_{CO2}, increases and the CH_4 adsorption capacity, q_{CH4}, decreases as expected. The total adsorbed capacity, q_{total}, has a minimum when y_{CO2} is smaller than 0.2, due to a sharp decrease in CH_4 adsorption capacity because of the competitive adsorption by CO_2. The gas composition of CO_2 at which this minimum occurs, increases with temperature. For landfill gas, whose y_{CO2} is around 0.45, the CO_2 adsorption capacity is much higher than that of CH_4; therefore, this trend in adsorption capacities for these gases is very promising for silicalite as an adsorbent for applications in CO_2 removal from landfill gas.

To predict the adsorption behavior of the binary system from pure gas systems, six models were tried: Extended Langmuir, Extended Dualsite Langmuir, Extended Sips, Ideal Adsorbed Solution Theory, Flory-Huggins VST (Vacancy Solution Theory) and Statistical Model. For estimating and comparing the quality of the six binary model predictions, the RMS deviations from the binary experimental data ($[\Sigma(q_{data}- q_{curve})^2/n]^{0.5}$) were used and are listed in Table 4.7. In comparison with the predicted and experimental isotherms, all the six prediction models are similar and there is a rather big difference between the predicted and the experimental isotherms. In Figure 4.5, experimental binary isotherms are compared with their counterparts predicted by the Flory- Huggins VST isotherms. As can be seen from these comparisons, the predicted isotherms over predict the real ones at all temperatures studied.

The phase diagrams at different temperatures were determined from the experimental binary isotherms and are shown in Figure 4.6, together with comparison with the predictions from the Flory-Huggins VST isotherms. Within the temperature range studied, 70°C data gave the best separation, since it was the furthest from the 45° line. Realistic experimental data gave better separation than the Flory-Huggins VST predicted under comparable conditions. Additioanlly, all other five models looked very similar to the Flory-Huggins VST data shown in Figure 4.6 and have considerable differences with the real binary system behaviour obtained. This lack of success for ideal model predictions was also observed for CO_2 - CH_4 with ZSM-5-280 by Harlick and Tezel (8). Therefore, they can only be used for rough estimation for the binary behaviour when there are no binary experimental data.

Table 4.7. RMS deviations ($[\Sigma(q_{data}- q_{curve})^2/n]^{0.5}$) in mmole.g^{-1} of predicted isotherms from the experimental ones for CO_2-CH_4 binary system on silicalite.

Models	Capacity	40 °C	70 °C	100 °C
Extended Langmuir	q_{CO2}	0.096	0.099	0.062
	q_{CH4}	0.158	0.147	0.107
	q_{total}	0.205	0.210	0.148
Extended Dualsite Langmuir	q_{CO2}	0.150	0.135	0.082
	q_{CH4}	0.060	0.062	0.108
	q_{total}	0.093	0.167	0.178
Extended Sips	q_{CO2}	0.098	0.113	0.090
	q_{CH4}	0.163	0.150	0.113
	q_{total}	0.242	0.243	0.193
Ideal Adsorbed Solution Theory	q_{CO2}	0.099	0.098	0.060
	q_{CH4}	0.155	0.148	0.109
	q_{total}	0.205	0.210	0.149
Flory- Huggins VST	q_{CO2}	0.097	0.115	0.078
	q_{CH4}	0.146	0.141	0.105
	q_{total}	0.203	0.231	0.166
Statistical Method	q_{CO2}	0.098	0.097	0.059
	q_{CH4}	0.149	0.145	0.108
	q_{total}	0.193	0.204	0.146

Compared with the literature, at 40 °C the x – y diagram obtained in this study is similar to the ones given by Harlick and Tezel in 2001 (6) for ZSM-5 under the same conditions, since silicalite and ZSM-5 have the same structure.

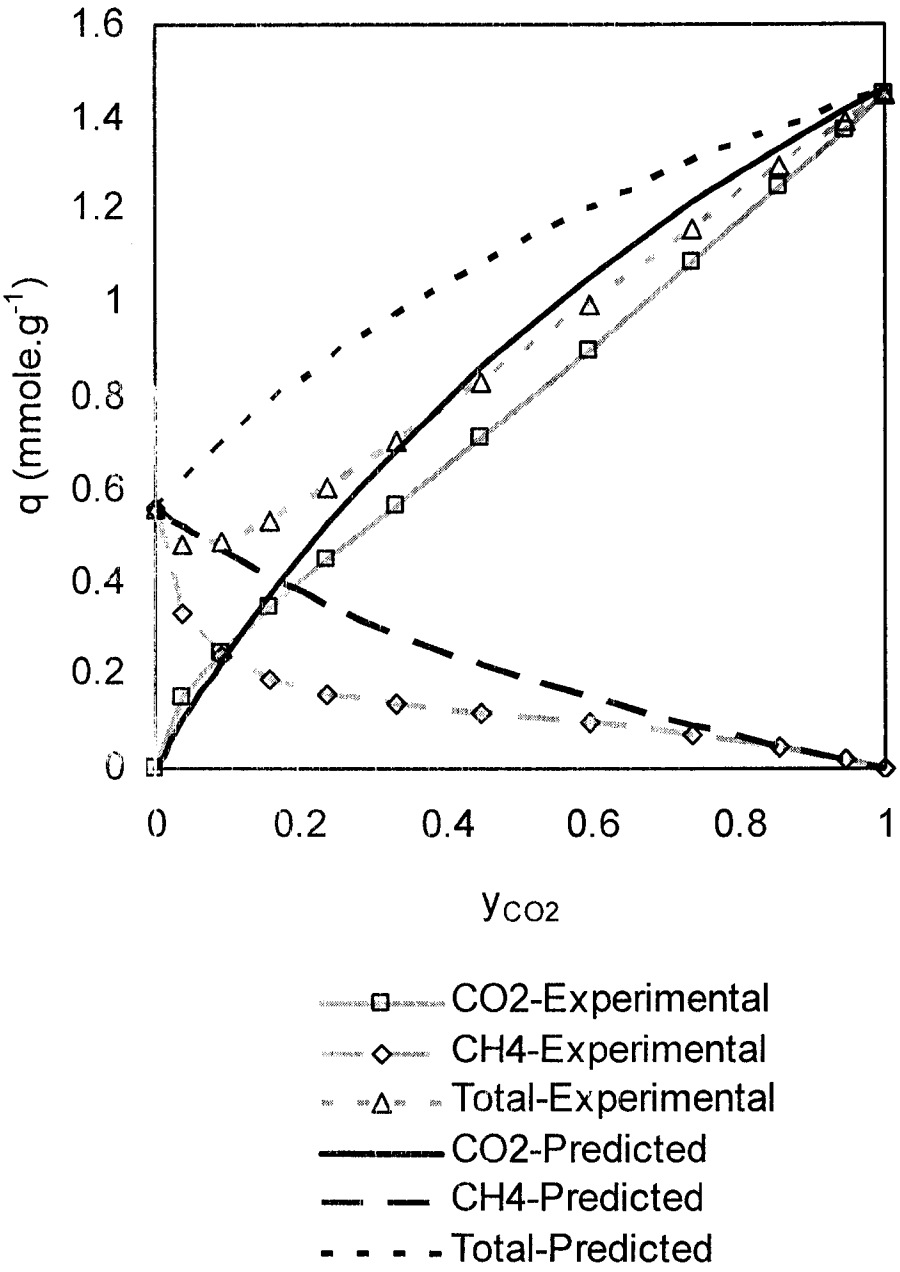

Figure 4.5a. CO_2/CH_4, binary Isotherms with silicalite at 40 °C and at 1atm. total pressure experimental by HT-CPM and predicted by Flory-Huggins VST

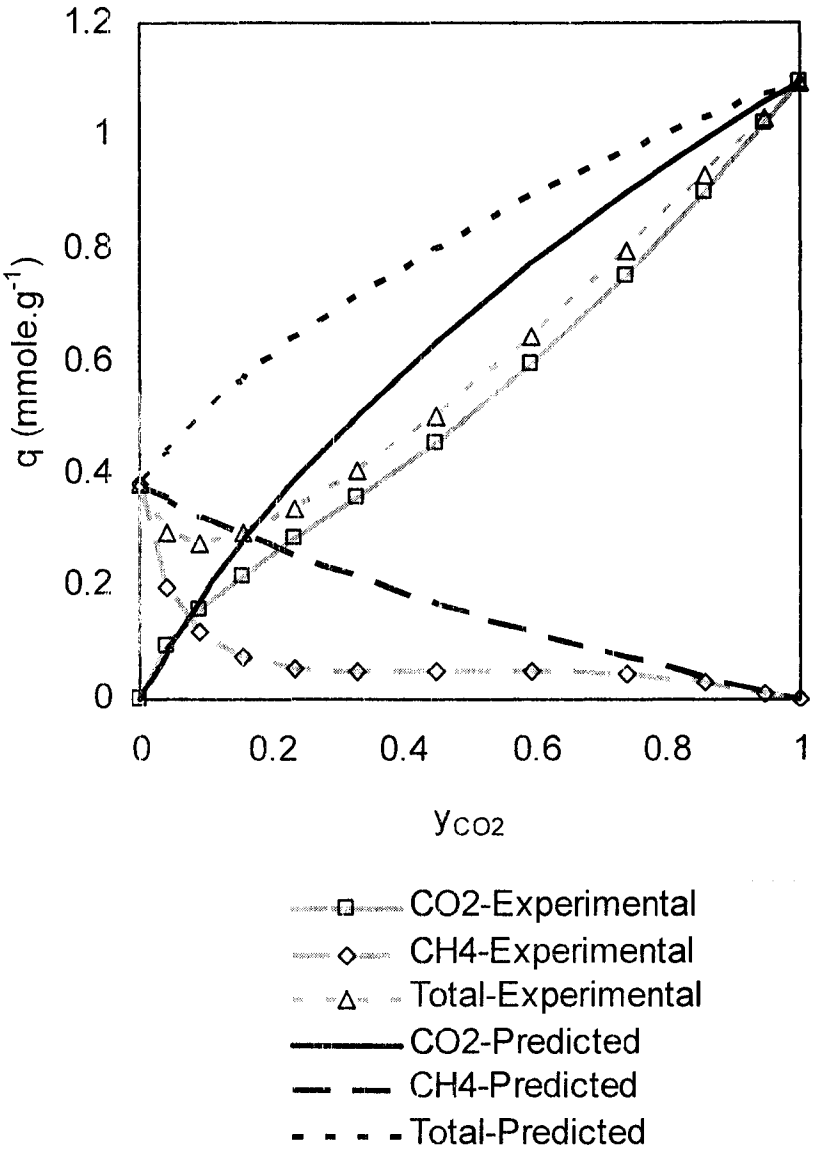

Figure 4.5b. CO_2/CH_4, binary Isotherms with silicalite at 70 °C and at 1atm. total pressure experimental by HT-CPM and predicted by Flory-Huggins VST

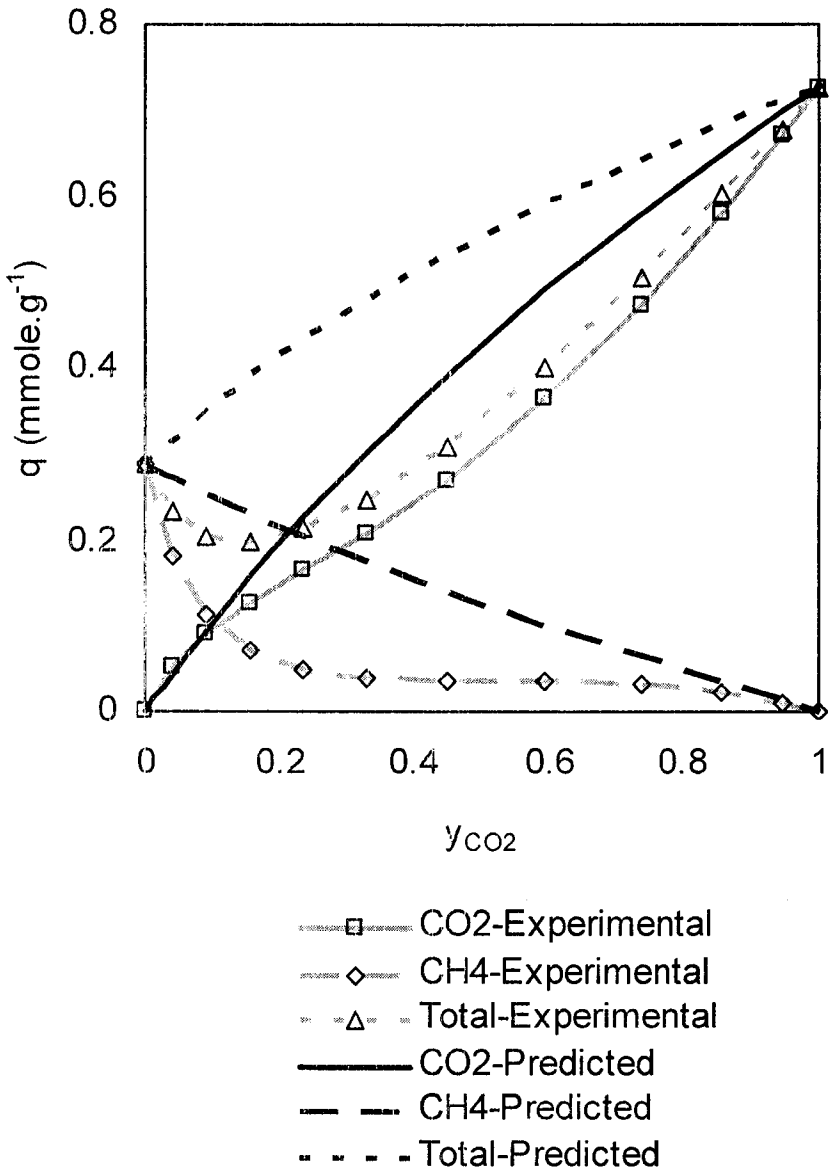

Figure 4.5c. CO_2/CH_4, binary Isotherms with silicalite at 100 °C and at 1atm. total pressure experimental by HT-CPM and predicted by Flory-Huggins VST

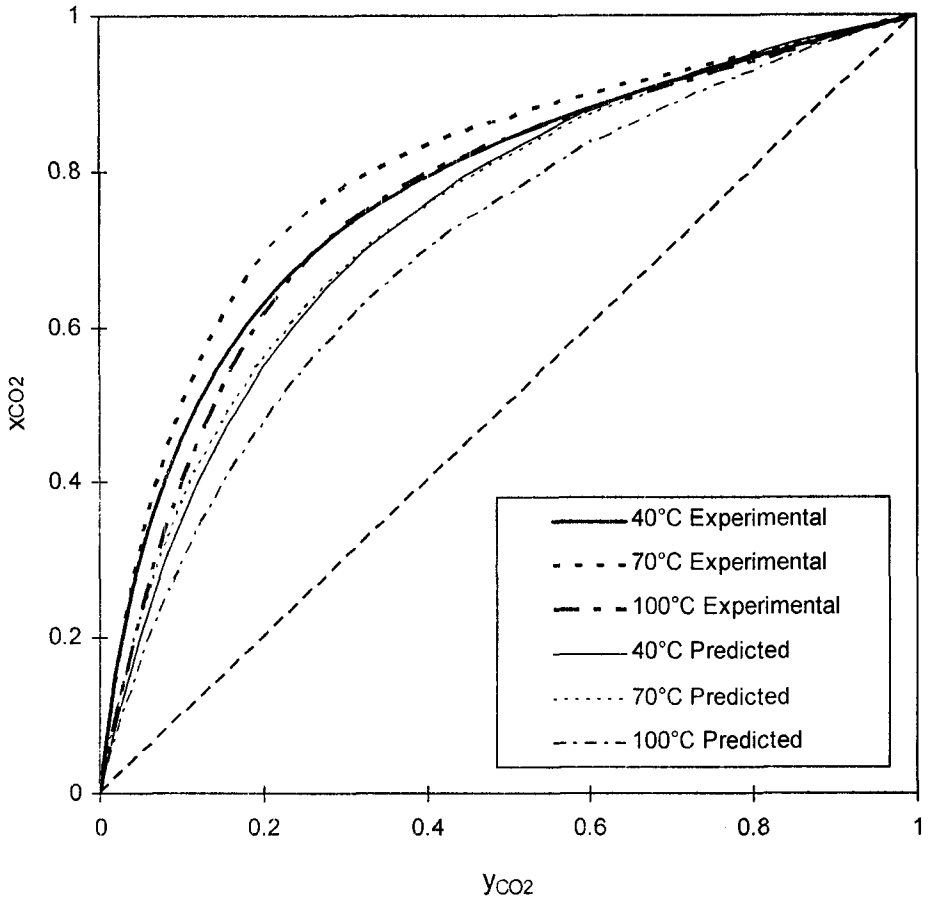

Figure 4.6. x – y diagram for CO_2/CH_4 binary system with silicalite at 1 atm. total pressure experimental by HT-CPM and predicted by Flory-Huggins VST. Harlick and Tezel's data (6) for ZSM-5-30 and ZSM-5-280 gave very similar results to 40°C in this study.

According to Equation (6), the equilibrium separation factors at three temperatures can be calculated for different values of y_{CO_2} and are shown in Figure 4.7. The actual equilibrium separation factors are higher than 5, so the binary system can be separated on silicalite. These separation factors calculated from actual binary behaviour are much better than the ones predicted from the pure isotherms. When the compositions are near pure systems (0 or 1), predicted separation factors are near actual ones. At that time, we can use

predicted separation factors to do rough estimations if we do not have experimental binary data. The actual selectivity is good and temperature influence the separation factor apparently when y_{CO_2} is below 0.6. The actual selectivity decreases with increasing y_{CO_2} when CO_2 concentration in the landfill gas is over 30 %. Therefore, the actual selectivity is better for low CO_2 concentration landfill gas in the real applications. Temperature hardly influences the separation factor when y_{CO_2} is over 0.6. For the practical separation of landfill gases, the system can be separated as the equilibrium separation factors are over 6 when y_{CO_2} is around 0.45 for a typical landfill gas.

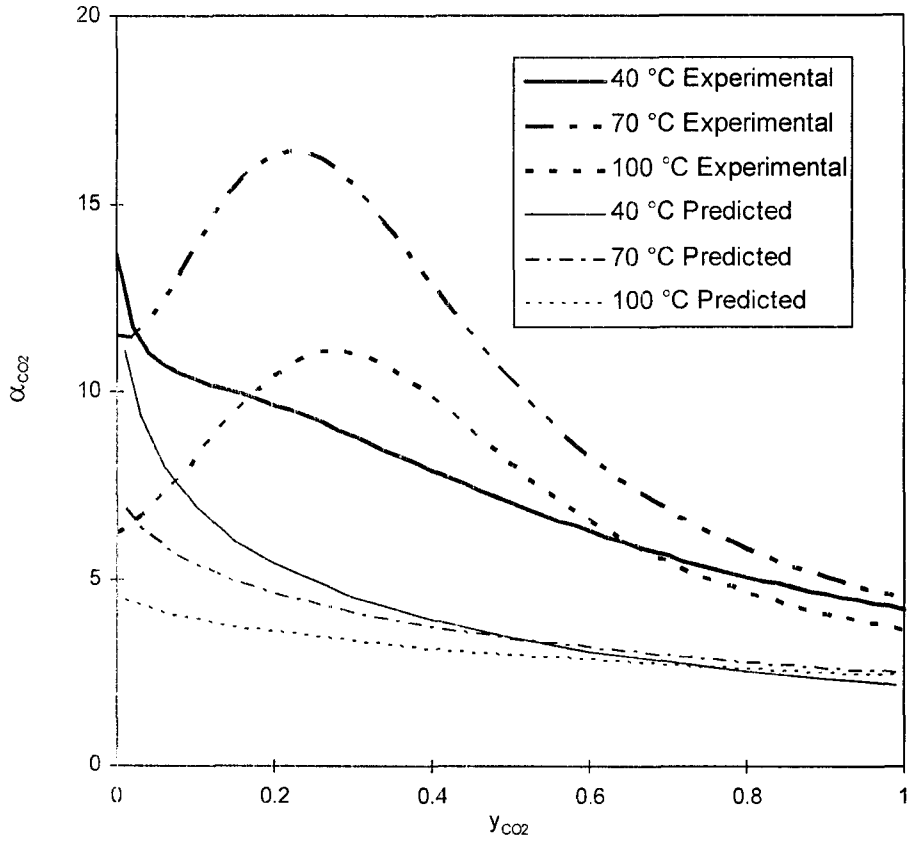

Figure 4.7. Equilibrium separation factor curves for CO_2/CH_4 binary systems: experimental from binary isotherms and predicted from pure isotherms

According to Equation 4, the integral thermodynamic consistency test between pure and binary equilibrium adsorption data is shown in Table 4.8. For the binary systems, the

integrands of the right side as functions of y_1 (y_{CO_2}) can be plotted and the areas under these curves between y_1 (y_{CO_2}) = 0 and y_1 (y_{CO_2}) = 1 are listed. For pure systems, the integrands of the left side as functions of P can be plotted and the areas under these curves between P = 0 and P = 1 atm. are listed. It should be pointed out that the ranges of pressure of the pure systems are the same as the ranges of the partial pressures of the two components as the total pressure of binary system is 1 atm.

Table 4.8. The integral thermodynamic consistency test between pure and binary carbon dioxide (1) -- methane (2) equilibrium adsorption data on silicalite using Equation (4)

Temperature	°C	40	70	100
RHS: $\int_0^1 \frac{q_1(1-y_1)-q_2y_1}{y_1(1-y_1)}d$	mmol.g^{-1}	1.6183	1.0916	0.6168
1st term in LHS: $\int_0^1 \frac{q_1^0}{P}dP$	mmol.g^{-1}	2.3084	1.5809	1.0193
2nd term in LHS: $\int_0^1 \frac{q_2^0}{P}dP$	mmol.g^{-1}	0.6456	0.4036	0.3138
LHS: $\int_0^1 \frac{q_1^0}{P}dP - \int_0^1 \frac{q_2^0}{P}dP$	mmol.g^{-1}	1.6628	1.1771	0.7055
$\left\|\frac{LHS-RHS}{RHS}\right\|$	%	2.75	7.83	14.37

In Table 4.8, it can be seen that the integral thermodynamic consistency test is obeyed fairly well by the binary CO_2-CH_4 adsorption data on silicalite at 40 °C, worse at 70 °C, and worst at 100 °C. Therefore, the binary CO_2-CH_4 adsorption data on silicalite at low temperature satisfy the integral thermodynamic consistency test fairly well. The thermodynamic consistency becomes worse as temperature increases. In addition, the results of the integral thermodynamic consistency test match the results in Figure 4.5 very well. At low temperature, the thermodynamic consistency is good while the difference between

predictions and experimental data is small in Figure 4.5; at higher temperature, the thermodynamic consistency is less satisfied while the difference is big. Thus, we recommend that one key requirement for predicting the adsorption behavior of the binary system from pure gas systems is that they satisfy the integral thermodynamic consistency tests between pure and binary gas adsorption equilibria. Moreover, these data sets can be used to prove the validity of predictive or correlative binary equilibrium models.

CONCLUSIONS

According to the pure gas isotherm data on silicalite, carbon dioxide is adsorbed more than methane. The pure gas adsorption capacity decreases with increasing temperature in the systems of carbon dioxide and methane on silicalite as expected from a physical adsorption system. Among the three concentration pulse chromatographic methods, the HT-CPM is the best one, the MTT-CPM is very well, and the MVV-CPM is not satisfactory for the binary behaviour of CO_2/CH_4 on silicalite. The adsorption capacities for CH_4 and CO_2 are very promising for silicalite as an adsorbent in applications in CO_2 removal from landfill gases. q_{CO2}, q_{CH4} and q_{total} increase with decreasing temperature, so temperature is a very important factor for the separation of this system, particularly when y_{CO2} is very low..For predicting the real binary system of CO_2/CH_4, Flory-Huggins VST, Extended Langmuir, Extended Dualsite Langmuir, Extended Sips, Ideal Adsorbed Solution Theory, and Statistical Model cannot describe the real binary system accurately for silicalite and they can be used only at low temperature or for rough estimation when the experimental binary data are not available. The selectivity is very good for the CO_2/CH_4 binary system on silicalite. The CO_2-CH_4 binary adsorption data on silicalite at low temperature satisfy the integral thermodynamic consistency test fairly well. The thermodynamic consistency becomes better as temperature decreases.

ACKNOWLEDGMENTS

Financial supports received from the Natural Sciences and Engineering Research Council of Canada (NSERC), the Ontario Graduate Scholarship (OGS) Program, and the Canadian Society for Chemical Engineering (CSChE) are gratefully acknowledged.

NOMENCLATURE

A = parameter, dimensionless

B = adsorption affinity constant, usually atm^{-1} (units depending on models); parameter, dimensionless

B_0 = adsorption affinity constant at some reference temperature, atm^{-1}

B_1 = adsorption affinity constant in Site 1, atm^{-1}

B_2 = adsorption affinity constant in Site 2, atm^{-1}

C = parameter, dimensionless

K = dimensionless Henry's law constant, dimensionless

K_P = dimensional Henry's law constant, $mmole.g^{-1}.atm^{-1}$

k = Freundlich adsorption coefficient, $mmol.g^{-1}.atm^{-1/n}$

n = adsorption exponents or number of actives sites, dimensionless

n_0 = adsorption exponents at some reference temperature, dimensionless

P = (total) pressure, atm

P = (total) pressure, atm

P_1 = pressure of Component *1*, atm

P_2 = pressure of Component *2*, atm

P_A = pressure of Component *A*, atm

P_B = pressure of Component *B*, atm

Q = isosteric heat, $J.mol^{-1}$

q = amount adsorbed, $mmol.g^{-1}$

q_A = amount adsorbed of Component *A*, $mmol.g^{-1}$

q_B = amount adsorbed of Component *B*, $mmol.g^{-1}$

q_1 = amount adsorbed of Component *1*, mmol.g^{-1}

q_2 = amount adsorbed of Component *2*, mmol.g^{-1}

q^0_1 = amount adsorbed of Component *1* in pure system, mmol.g^{-1}

q^0_2 = amount adsorbed of Component *2* in pure system, mmol.g^{-1}

q_m = adsorption saturation capacity or maximum amount adsorbed, mmol.g^{-1}

q_{m0} = adsorption saturation capacity or maximum amount adsorbed at some reference temperature, mmol.g^{-1}

q_{m1} = adsorption saturation capacity or maximum amount adsorbed in Site 1, mmol.g^{-1}

q_{m2} = adsorption saturation capacity or maximum amount adsorbed in Site 2, mmol.g^{-1}

R = gas constant, 8.314 J.K^{-1}.mol^{-1}

T = temperature, K

T_0 = reference temperature, K

x = mole fraction in adsorbed phase at equilibrium, dimensionless

x_A = mole fraction of Component *A* in adsorbed phase at equilibrium, dimensionless

x_B = mole fraction of Component B in adsorbed phase at equilibrium, dimensionless

X_i = mole fraction of Component i in adsorbed phase at equilibrium, dimensionless

y = mole fraction in fluid phase at equilibrium, dimensionless

y_A = mole fraction of Component *A* in fluid phase at equilibrium, dimensionless

y_B = mole fraction of Component B in fluid phase at equilibrium, dimensionless

y_1 = mole fraction of Component 1 in fluid phase at equilibrium, dimensionless

Y_i = mole fraction of Component i in fluid phase at equilibrium, dimensionless

Greek letters

α = adsorption constant, adsorption separation factor, dimensionless

$\alpha_{A/B}$ = adsorption separation factor (the ratio of Component A over Component B), dimensionless

$\alpha_{i,A/B}$ = ideal adsorption separation factor (the ratio of Component A over Component B), dimensionless

α = parameter, dimensionless

β = parameter, dimensionless

γ_i = activity coefficient of Component i, dimensionless

θ = fraction of monolayer coverage, dimensionless

λ = parameter, dimensionless

Φ_i = fugacity coefficient of Component i. dimensionless

χ = constant parameter. dimensionless

Abbreviations

CPM = concentration pulse method

DSL = dualsite-Langmuir

GHG = greenhouse gases

GSE = Gibbsian surface excess

GWP = greenhouse warming potential

HT-CPM = Harlick and Tezel - Concentration Pulse Method

LFG = landfill gas

MS = Microsoft

MTT-CPM = Modified Triebe and Tezel - Concentration Pulse Method

MVV-CPM = Modified *Van der Vlist and Van der Meijden* - Concentration Pulse Method

PSA = pressure swing adsorption

RMS = root mean square

SSR = sum of the square residuals

TCD = thermal conductivity detector

TSA = temperature swing adsorption

VST = vacancy solution theory

REFERENCES

1. Cavenati, S., Grande, C. A., and Rodrigues, A. E. (2005) Upgrade of methane from landfill gas by pressure swing adsorption. *Energy and Fuels*, 19: 2545.
2. Hansen, J., Fung, I., Lacis, A., Riud, D., Levedeff, J. S., Ruedy, R., and Russell, G. (1988) Global climate changes as forecast by Goddard Institute for Space Studies three-dimensional model. *Journal of Geophysical Research*, 93: 9341.

3. Cavenati, S., Grande, C. A., and Rodrigues, A. E. (2004) Adsorption equilibrium of methane, carbon dioxide, and nitrogen on zeolite 13X at high pressures. *Journal of Chemical and Engineering Data*, 49: 1095.
4. Buss, E. (1995) Gravimetric measurement of binary gas adsorption equilibria of methane-carbon dioxide mixtures on activated carbon. *Gas Separation and Purification*, 9: 189.
5. Harlick, P. J. E. and Tezel, F. H. (2003) Use of concentration pulse chromatography for determining binary isotherms: comparison with statically determined binary isotherms. *Adsorption*, 9: 275.
6. Harlick, P. J. E. and Tezel, F. H. (2001) CO_2-N_2 and CO_2-CH_4 Binary adsorption isotherms with H-ZSM-5: the importance of experimental data regression with the concentration pulse method. *The Canadian Journal of Chemical Engineering*, 79: 236.
7. Harlick, P. J. E. and Tezel, F. H. (2002) Adsorption of carbon dioxide, methane and nitrogen: pure and binary mixture adsorption by H-ZSM-5 with SiO_2/Al_2O_3 ratio of 30. *Separation Science and Technology*, 37: 33.
8. Harlick, P. J. E. and Tezel, F. H. (2003) Adsorption of carbon dioxide, methane and nitrogen: pure and binary mixture adsorption for ZSM-5 with SiO_2/Al_2O_3 ratio of 280. *Separation and Purification Technology*, 33: 199.
9. Li, P. and Tezel, F. H. (2006) Adsorption separation of methane and carbon dioxide from landfill gas. AICHE (American Institute of Chemical Engineers) Annual Meeting, San Francisco, USA. 64334.
10. Van der Vlist, E. and Van der Meijden, J. (1973) Determination of the adsorption isotherms of the components of binary gas mixtures by gas chromatography. *Journal of Chromatography*, 79: 1.
11. Shah, D. B. and Ruthven, D. M. (1977) Measurement of zeolite diffusivities by chromatography. *AIChE Journal*, 23: 804.
12. Tezel, F. H., Tezel, H. O., and Ruthven, D. M. (1992) Determination of pure and binary isotherms for nitrogen and krypton. *Journal of Colloid and Interface Science*, 149: 197.
13. Heslop, M. J., Buffman, B.A., and Mason, G. A (1996) Test of the polynomial-fitting method of determining binary-gas-mixture adsorption equilibria. *Industrial and Engineering Chemistry Research*, 35: 1456.

14. Harlick, P. J. E. and Tezel, F. H. A (2000) Novel solution method for interpreting binary adsorption isotherms from concentration pulse chromatography data. *Adsorption*, 6: 293.
15. Markham, E. C. and Benton, A. F. (1931) The adsorption of gas mixtures by silica. *Journal of American Chemical Society*, 53: 497.
16. Bowen, T. C. and Vane, L. M. (2006) Ethanol, acetic acid, and water adsorption from binary and ternary liquid mixtures on high-silica zeolites. *Langmuir*, 22: 3721.
17. Tien, Chi (1994) *Adsorption Calculations and Modeling*; Butterworth-Heinemann: Newton, MA.
18. Myers, A. L. and Prausnitz, J. M. (1965) Thermodynamics of mixed-gas adsorption. *AICHE J.*, 11: 121.
19. Cochran, T. W., Kabel R. L., and Danner, R. P. (1985) Vacancy solution theory of adsorption using Flory-Huggins activity coefficient equations, *AICHE J.*, 31: 268.
20. Ruthven, D. M. (1984) *Principles of Adsorption and Adsorption Processes*. John Wiley and Sons: Toronto, Canada.
21. Li, P. and Tezel, F. H. (2007) Adsorption separation of N_2, O_2, CO_2 and CH_4 gases by β-zeolite. *Microporous & Mesoporous Materials*, 98: 94.
22. Li, P. and Tezel, F. H. (2005) Equilibrium and kinetic analysis of CO_2-N_2 adsorption separation by concentration pulse chromatography. 40th IUPAC Congress, Beijing, P. R. China, p61, 1-O-034.
23. Triebe, R. W. and Tezel, F. H. (1995) Adsorption of nitrogen and carbon monoxide on clinoptilolite: determination and prediction of pure and binary isotherms. *The Canadian Journal of Chemical Engineering*, 73: 717.
24. Sircar, S. (1985) Excess properties and thermodynamics of multicomponent gas adsorption. *J. Chem. SOC., Faraday Trans.*, 81: 1527.
25. Rao, M. B. and Sircar, S. (1999) Thermodynamic consistency for binary gas adsorption equilibria. *Langmuir*, 15: 7258.
26. Rees, L. V. C., Bruckner, P., and Hampson, J. (1991) Sorption of N_2, CH_4 and CO_2 in Silicalite-1. *Gas Separation and Purification*, 5: 67.
27. Dunne, J. A., Mariwala, R., Rao, M., Sircar, S. R., Gorte, J., and Myers, A. L. (1996) Calorimetric heats of adsorption and adsorption isotherms. 1. O_2, N_2, Ar, CO_2, CH_4, C_2H_6, and SF_6 on silicalite. *Langmuir*, 12: 5888.

28. Choudhary, V. R. and Mayadevi, S. (1996) Adsorption of methane, ethane, ethylene, and carbon dioxide on Silicalite-1. *Zeolites*, 17: 501.

29. Dubinin, M. M., Rakhmatkariev, G. U., and Isirikyan, A. A. (1989) Heats of adsorption of CO_2 on high-silicon zeolites ZSM-5 and silicalite. *Izv. Akad. Nauk SSSR, Ser. Khim.*, No. 11, 2636.

30. Otto, K., Montreuil, C. N., Todor, O., McCabe, R. W., and Gandhi, H. S. (1991) Adsorption of hydrocarbons and other exhaust hydrocarbons on silicalite. *Ind. Eng. Chem. Res.*, 30: 2333.

CHAPTER V

PURE AND BINARY ADSORPTION EQUILIBRIA OF CARBON DIOXIDE AND NITROGEN ON SILICALITE

Peiyuan Li and F. Handan Tezel*

Department of Chemical Engineering
Faculty of Engineering
University of Ottawa
161 Louis Pasteur, Ottawa, Ontario K1N 6N5, Canada

Submitted to the Journal of Chemical and Engineering Data.

Presented at 56th CSChE (Canadian Society for Chemical Engineering) Canadian Chemical Engineering Conference, Sherbrooke Quebec, October 15-18, 2006, Conference Proceedings 15.

* Corresponding author
Tel: 613-562-5800 Ext. 6099
Fax: 613-562-5172
Emai: Handan.Tezel@uottawa.ca

ABSTRACT

For separation of CO_2 and N_2 in flue gas, pure adsorption isotherms of CO_2 and N_2 on silicalite were determined by using the constant volume system. Binary adsorption behaviour for CO_2 and N_2 mixtures, covering the whole concentration range, were determined by using concentration pulse chromatography at a total pressure of 1 atm. The applicability of seven pure adsorption isotherm models was discussed for the isotherms of both CO_2 and N_2 up to 5 atmospheres between 40 °C and 100 °C. On top of these models, temperature independent Toth and Sips isotherms were also looked at and compared. The ranges of temperature and pressure were extended and ideal separation factors were determined. Mixture adsorption isotherms for the binary system of CO_2 and N_2 at 40 °C, 70 °C and 100 °C at 1 atmosphere total pressure were determined experimentally by using three binary concentration pulse methods, HT - CPM (Harlick and Tezel - Concentration Pulse Method), MTT - CPM (Modified Triebe and Tezel - Concentration Pulse Method) and MVV - CPM (Modified Van der Vlist and Van der Meijden - Concentration Pulse Method). Applicability of six binary adsorption models for this system was discussed. The results obtained showed that temperature independent Toth is a good model for extending the ranges of temperature and pressure for pure systems and HT - CPM is the best one among the three concentration pulse models for CO_2 and N_2 system. Silicalite is a promising adsorbent for the separation of CO_2 and N_2.

INTRODUCTION

The global environment is a major issue today, and global warming in particular is the focus of much attention. Accumulation of greenhouse gases (GHG) in the atmosphere is responsible for increased global warming of our planet. It is supposed that the increasing concentration of carbon dioxide mainly from flue gas and automobile in the atmosphere is the major contributor to this problem.[1, 2] A variety of techniques have been studied for CO_2-N_2 adsorption separation in the literature.[3-22]

Silicalite is widely used as a selective adsorbent. Its intermediate (ten-ring) pore size leads to molecular sieve size selectivity. It has high thermal and hydrothermal stability. Its Si/Al radio is in thousands, so it has hydrophobic and organophilic adsorptive properties.[23]

The volumetric method involves measuring the pressure change in a known volume of gas subjected to an adsorbent sample. As the gas is adsorbed and allowed to come to equilibrium, the measured decrease in the closed system pressure yields the amount of gas adsorbed under the given conditions. This static method has been used extensively to determine adsorption isotherms.[24, 25]

One dynamic method of analysis is the use of the chromatographic technique. In the literature, methods using the *K*p-functions for determining the binary isotherms from concentration pulse chromatographic data have been given and shown capable of interpreting highly selective binary systems.[9, 26-31]

In this current work, adsorption separation of carbon dioxide and nitrogen on silicalite was studied. Pure and binary adsorption isotherms were obtained by the volumetric method and the concentration pulse chromatographic technique, respectively. The thermodynamic consistency tests between pure and binary gas adsorption systems were also discussed.

METHODS

There are many approaches for fitting adsorption isotherms for pure gas systems. Among two-parameter models, the simplest and still the most useful pure gas isotherm is the

Langmuir isotherm.[32, 33] The Freundlich isotherm is another two-parameter model that is commonly used.[34]

Three-parameter adsorption isotherm models are more flexible. For example, Sips (Langmuir-Freundlich) isotherm[35] is superior for data correlation covering wide ranges of pressures and temperatures when both Langmuir and Freundlich isotherms fail.[25] Other three-parameter isotherms that are popular, and satisfy both low and high ends of the pressure range are the Toth and Multisite Langmuir isotherms.[33] Employing Flory-Huggins form of activity coefficient for adsorption, vacancy solution theory is another three-parameter isotherm which was first developed in 1980.[33, 36, 37] Dualsite-Langmuir (DSL) model, a four-parameter isotherm, distinguishes two categories of different active sorption sites in the adsorbent, each one following a Langmuir adsorption behavior.[38]

The temperature independence of equilibrium parameters is required for the purpose of extrapolation or interpolation of equilibrium at other temperatures as well as for the purpose of calculating isosteric heat. For useful description of adsorption equilibrium data at various temperatures, it is important to have the temperature independent form of an isotherm equation. The temperature independence of the Sips and Toth equations for the affinity constants B may take the following form:

$$B = B_0 e^{\frac{Q}{RT_0}\left(\frac{T_0}{T}-1\right)} \qquad \text{.....(1)}$$

where B_0 is the adsorption affinity constant at some reference temperature T_0, Q is the isosteric heat, invariant with the surface loading, and R is gas constant. The saturation capacity of the Sips and Toth equations can be either taken as constant or it can take the following temperature independence:

$$q_m = q_{m0} e^{\chi\left(1-\frac{T}{T_0}\right)} \qquad \text{.....(2)}$$

where q_{m0} is the saturation capacity (maximum amount adsorbed) at the reference temperature T_0 and χ is a constant parameter. The exponent n of the Sips equation may take the following form:

$$\frac{1}{n} = \frac{1}{n_0} + \alpha\left(1 - \frac{T_0}{T}\right) \quad \text{.....(3)}$$

and the form of the exponent n of the Toth equation can be:

$$n = n_0 + \alpha\left(1 - \frac{T_0}{T}\right) \quad \text{.....(4)}$$

where n_0 is the parameter n at the reference temperature T_0 and α is a constant parameter.[33]

Models for mixed-gas adsorption should be capable of predicting the equilibrium amount adsorbed from pure gas isotherms. The simplest theory for binary system is the extended Langmuir model.[39]

$$\theta_A = \frac{q_A}{q_{mA}} = \frac{B_A P_A}{1 + B_A P_A + B_B P_B} \quad \text{.....(5)}$$

where subscripts A and B refer to adsorbates A and B, respectively.

Dual-site extended Langmuir adsorption isotherm was derived from extended Langmuir model.[40] The Sips equation for the pure component adsorption isotherm may be extended to binary systems, as well.[41, 42]

Some thermodynamic equations associated with the ideal solution derive the ideal adsorbed solution theory, which can be used to get the isotherm of a binary system assuming the mixture behave as an ideal solution.[25]

In the concentration pulse chromatographic technique, dimensionless Henry's Law constant, K, can be calculated from the corrected first moment of the response peak as follows.[14, 15, 31, 43]

$$\mu = \frac{\int_0^\infty c(t - \mu_D)dt}{\int_0^\infty c dt} = \frac{L}{v}\left[1 + \frac{(1-\varepsilon)K}{\varepsilon}\right] \quad \text{.....(6)}$$

where t is the time, c is the adsorbate concentration measured at the outlet of the column, L is the column length, ε is the bed porosity, v is the interstitial fluid velocity, K is the dimensionless Henry's Law adsorption equilibrium constant, and μ_D is the dead time. The dimensionless Henry's Law constants, K, can be converted to a dimensional form, K_p.[15]

The K_p value is related to the slopes of the isotherms of the components in the carrier gas mixture. For a binary mixture, the relationship is given as follows.[27]

$$K_p = (1 - y_1)\frac{dq_1}{dP_1} + y_1 \frac{dq_2}{dP_2} \quad \text{.....(7)}$$

Where $\frac{dq_1}{dP_1}$ and $\frac{dq_2}{dP_2}$ are the slopes of the adsorption isotherms for components 1 and 2, respectively.

For binary isotherms, both components in the mixed carrier gas are adsorbed and $\frac{dq_2}{dP_2}$ in the last term of Eq. (7) is not constant. The experimental K_p data represent the combined contribution of both components to the isotherms. The interpretation of the binary Kp data has been treated by several methods[9, 26, 31, 44] shown in Table 5.1.

The following objective function is defined to minimize the sum of the square residuals (*SSR*) with respect to the experimental values for the determination of B and C parameters to obtain the binary isotherms:

$$SSR = \sum_{y_1=0}^{y_1=1} \left(K_{P,Experiment} - K_{P,Equation}\right)^2 \quad \text{.....(8)}$$

The minimization of the sum of the square residuals (SSR) could not be performed with only the data, since a number of solutions exist. 4 constraints are imposed on the system, in order to ensure that the solution reflects what is physically occurring. 2 of these constraints are the 2 end points of the concentration range, which should coincide with the pure isotherms. The other 2 constraints come from the fact that the binary isotherm slopes should always be positive across the entire range of y_1, i.e., no maximum should be seen in the isotherms.[45]

By using these constraints to limit the objective function (Equation (8)), a constrained nonlinear regression could be performed to determine the B. and C parameters. The K curve is defined from the RHS of Equation (7) and the binary isotherms are calculated by binary isotherm functions in Table 5.1 by using B and C coefficients.

The thermodynamics of pure and binary gas adsorption systems has been extensively studied using the Gibbsian surface excess (GSE) model.[46-48] For binary gas adsorption systems, it has been used to develop several relationships for checking both the

thermodynamic consistency between pure and binary gas equilibrium adsorption data and the internal thermodynamic consistency of the binary adsorption data itself. These relationships of integral and differential consistency tests have been developed for pure and binary gas adsorption data. The integral test requires the measurement of both pure gas adsorption isotherms and binary gas adsorption isotherms shown below.[49]

$$\left(-\int_0^P \frac{q_2^0}{P}dP\right)-\left(-\int_0^P \frac{q_1^0}{P}dP\right)=\int_0^1 \frac{q_1(1-y_1)-q_2y_1}{y_1(1-y_1)}d \quad \text{.....(9)}$$

where q^0_1 and q^0_2 are the amount adsorbed of Components *1* and *2* respectively in the pure gas systems, P is both the pressure of pure gas systems and the total pressure of the binary system, q_1 and q_2 are the amounts adsorbed of Components *1* and *2*, respectively in the binary system, y_1 is the mole fraction of Component 1 in the binary system. The two terms of the left side are the potentials of adsorption at P and T for pure gases 2 and 1, respectively. They can be estimated as a function of P at constant T using the pure gas adsorption isotherm. Thus, the quantity on the left side at any given values of P and T can be evaluated from the pure gas adsorption isotherms of the components of a binary gas mixture. The quantity on the right side at any given values of P and T can be evaluated using the binary gas adsorption isotherm at constant P and T. These two independently measured quantities must be equal; this equality forms the basis for the integral consistency test between pure and binary gas equilibrium adsorption data.

EXPERIMENTAL SECTION

The details of volumetric system, concentration pulse chromatography unit and numerical methods are given in our earlier paper.[50] The adsorbent and sample gases used in the experiments are listed in Tables 5.2 and 5.3 respectively. It is noted that the values of adsorbed loading obtained from experiments were corrected taking into account that generally the binder has little adsorption capacity as literature data are mostly obtained with silicalite crystals, without binder.

RESULTS AND DISCUSSION

Fitting with Pure Gas Adsorption Models

Equilibrium isotherm data for CO_2, and N_2 on silicalite pellets were obtained at three different temperatures for pressures up to 5 atm and are given in Figure 5.1 as data points. The curves going through the data points are regressed with Toth isotherm models at the corresponding temperature. The numbered curves are data from the literature for comparison with the present study. All the values of adsorbed loading obtained from experiments in this work were corrected taking into account that generally the binder has little adsorption capacity as literature data are mostly obtained with silicalite crystals, without binder. Our values are a little higher than those of the literature. There are several reasons: the form of our adsorbent was pellets, but that of the literature is crystals; it was assumed that there was no adsorption in the binder; the suppliers of the adsorbent were different. Adsorption capacity increases with decreasing temperature for both of the adsorbates, since physical adsorption is always exothermic. CO_2 is adsorbed more than N_2 since the interaction between CO_2 and silicalite activesites is stronger than that between N_2 and silicalite as the polarizability and quadrupole moment of carbon dioxide is much higher than those of nitrogen. At low pressure, the carbon dioxide isotherm slopes are very high, and then the slopes decrease rather fast with increasing pressure as the adsorbent sample approaches saturation. However, the nitrogen isotherm slopes slightly decease as pressure increases, becoming more linear at high temperature.

By using non-linear regressions, the parameters of different models were obtained and corresponding parameters are shown in Table 5.4. For gauging the quality of the non-linear regressions obtained from the different models used, the RMS (root mean square) deviations ($[\Sigma(q_{data}- q_{curve})^2/n]^{0.5}$) are used and shown in Table 5.4. When two-parameter models, Langmuir and Freundlich, are compared, Langmuir is better than Freundlich. When three or four-parameter models were considered, it was observed that all of them, Toth, Sips, Flory-Huggins Vacancy Solution Theory (VST), Multisite-Langmuir, and Dualsite-Langmuir Model are better than the two-parameter models because of their increased flexibility.

The temperature independent forms of the Toth and Sips equations were also used for description of adsorption equilibrium data at various temperatures,. In Equation 2, χ can be taken as 0 or a parameter. According to our data, all the values of χ obtained are 0 as a parameter for the temperature independent form of the Toth equation; for the temperature independent form of the Sips equation, some values of χ obtained are 0 and some are not. However, there is little difference between them for modeling the isotherms. For one less parameter, we took χ as 0. In other words, the saturation capacities of both Sips and Toth equations were constant, that is $q_m = q_{m0}$. Using the data at the three temperatures simultaneously in the fitting of both Sips and Toth equations, optimal parameters shown in Table 5.5 were obtained. The parameters and RMS deviations at the three temperatures are listed in Table 5.4. From the parameters given in Table 5.5 for temperature independent Toth and Sips isotherms, the experimental data are extended to other temperature and pressures.

The primary requirement for an economic separation process is an adsorbent with sufficiently high selectivity, capacity, and life. The selectivity may depend on a difference in either adsorption kinetics or adsorption equilibrium. Most of the adsorption processes in current use depend on equilibrium selectivity. In considering such processes it is convenient to define an ideal adsorption separation factor:

$$\alpha_{A/B} = \frac{x_A / x_B}{y_A / y_B} \quad \text{.....(10)}$$

where x_A, x_B, y_A, and y_B are , respectively, the mole fractions of components A and B in adsorbed and fluid phases at equilibrium. If the isotherms are linear or pressure is small enough for the isotherms to keep in the linear range, ideally, the separation factor is given simply by the ratio of the amounts adsorbed in pure components:

$$\alpha_{i,A/B} = \frac{q_A}{q_B} \quad \text{.....(11)}$$

where q_A and q_B are the amounts adsorbed of components A and B. These equilibrium separation factors are shown as a function of pressure and temperature in Figure 5.2. For the purpose of extension of the data to other temperatures and pressures, from the curve regressions with the temperature independent Toth model, the ranges of temperature and

pressure were extrapolated and interpolated to estimate the adsorption behaviour at other temperatures and pressures without experimental data in the figure. According to the results obtained, both pressure and temperature are very important for the separation. In general, separation factors increase with decreasing pressure and/or temperature. It is difficult to separate the system at high temperature and/or high pressure.

For the separation of CO_2/N_2, if the separation factor from pure systems can be used for the binary system, the conditions need to be controlled below 100 °C and below the atmospheric pressure. A PSA or a TSA process can be selected. The PSA process can be carried out at room temperature and in the range of pressures between vacuum and 1 atm. If it is done at a temperature higher than 100 °C and in the range of pressure higher than 1 atm, the expected results become worse as the ideal separation factor drops to 6 in Figure 5.2. For a TSA process, it can be done under vacuum at as low pressure as possible and at temperatures as low as possible. Since flue gas temperatures are generally rather high, temperature conditions should be considered.

Binary Isotherms

After regenerating the silicalite adsorbent, K_p values were determined by increasing the CO_2 mole fraction in CO_2-CH_4 carrier gas from 0 % up to 100 %. The samples were injected after attaining equilibrium for each concentration change of the carrier gas by noting that the baseline of the response would be steady. The K_p values, as well as their corresponding curve fits for HT-CPM, MTT-CPM and MVV-CPM, as a function of the gas composition are given in Figure 5.3. As can be seen from this figure, the best fit was obtained with the HT-CPM. As was proven before, this method is a more versatile method, which would accommodate more non-ideal systems, where the adsorption capacities of the two adsorbates are very different from each other.

To quantify the non-linear regressions for these three concentration pulse methods, the RMS (root mean square) deviations ($[\Sigma(q_{data}- q_{curve})^2/n]^{0.5}$) were used and shown in Table 5.6 and it was observed that the best fit, was actually the HT-CPM method. Therefore, the HT-CPM, shown with error bars in Figures 5.3a and 5.3b, was used to describe these systems for our further study of this binary system.

The binary isotherms for CO_2 - N_2 with silicalite were obtained at three temperatures and are given in Figure 5.4 for 40 °C, 70 °C and 100 °C. When y_{CO2} increases, the CO_2 adsorption capacity, q_{CO2}, increases and the N_2 adsorption capacity, q_{N2}, decreases. The total adsorbed capacity, q_{total}, increases as increase of q_{CO2} is more than the decrease of q_{N2}. At the beginning, q_{N2} decreases very fast, while q_{CO2} increases rapidly; when y_{CO2} is higher than 0.2, q_{N2} approaches zero. For flue gas applications, where y_{CO2} is around 0.15, the CO_2 adsorption capacity is much higher than that of N_2; therefore, this trend in adsorption capacities for N_2 and CO_2 is very promising on silicalite as an adsorbent for CO_2 removal from air. q_{CO2}, q_{N2} *and* q_{total} increase with temperatures decreasing since adsorption is exothermic, so temperature is a very important factor for separation. For practical applications, the separation process can be controlled at low temperature to attain good adsorption capacity.

To predict the adsorption behaviour of the binary system from pure gas adsorption data, following six models were used and compared to the real binary adsorption behaviour: Extended Langmuir, Extended Dual-site Langmuir, Ideal Adsorbed Solution Theory, Statistical Model, Extended Sips, and Flory-Huggins of Vacancy Solution Theory. For estimating and comparing the quality of the six binary model predictions, the RMS deviations from the binary experimental data ($[\Sigma(q_{data}- q_{curve})^2/n]^{0.5}$) were used and are listed in Table 5.7. In comparison with the predicted and experimental isotherms, all the six prediction models are similar and there is a rather large difference between the predicted and the experimental isotherms. Therefore, none of the six models can describe the real binary system accurately and they can be used only for rough estimation for the binary system when there are no binary data available. In Figure 5.4, experimental binary isotherms are compared with their counterparts predicted by the Statistical Model isotherms. As can be seen from these comparisons, the predicted isotherms over predict the real ones at all temperatures studied.

The *x-y* phase diagrams at different temperatures studied are shown in Figure 5.5, together with comparison with the ideal predictions from the Extended Langmuir isotherms, using the pure component isotherms. Within the temperature range studied, lower temperature data gave better separation, since the curve was the furthest from the 45° line. Realistic experimental data gave better separation than predicted.

In Figure 5.5, the experimental $x - y$ diagram given at 40 °C by Harlick and Tezel[9] for ZSM-5-30 under the same conditions is compared with the ones obtained in this study. Silicalite and ZSM-5 have the same structure. ZSM-5-30 adsorbent had different Si/Al ratio indicated by the last number in the code of the adsorbent: 30, as opposed to the silicalite for which this ratio is in the thousands. Since the only difference between the adsorbent studied in this work and Harlick and Tezel's adsorbent, was the Si/Al ratio, it is concluded that this ratio influences the binary behaviour of the CO_2-N_2 gas mixture slightly and the separation is better when this ratio is smaller.

The equilibrium separation factors are calculated from the binary isotherms obtained, using Equation (10), and plotted against y_{CO2} in Figure 5.6 at three different temperatures for CO_2/N_2 and silicalite system. The selectivity is good and temperature has a large influence on the separation factor. The selectivity increases with increasing y_{CO_2} and/or decreasing temperature when CO_2 concentration in the flue gas is in the range between 10 % and 20 %. Therefore, the actual selectivity is better for higher CO_2 concentration flue gas at lower temperature in the real applications.

In comparison with experimental and predicted separation factors, these experimental separation factors from actual binary behaviour are much better than the ones predicted from the pure isotherms. When the compositions are near pure systems (0 or 1), predicted separation factors are near actual ones. At that time, we can use predicted separation factors to do rough estimations if we do not have experimental binary data.

According to Equation 9, the integral thermodynamic consistency test between pure and binary equilibrium adsorption data is shown in Table 5.8. For the binary systems, the integrands of the right side as functions of y_1 (y_{CO_2}) can be plotted and the areas under these curves between y_1 (y_{CO_2}) = 0 and y_1 (y_{CO_2}) = 1 are listed in this table. For pure systems, the integrands of the left side as functions of P can be plotted and the areas under these curves between P = 0 atm. and P = 1 atm. are listed in Table 5.8. It should be pointed out that the ranges of pressure of the pure systems are the same as the ranges of the partial pressures of the two components as the total pressure of binary system is 1 atm.

In Table 5.8, it can be seen that the integral thermodynamic consistency test is obeyed fairly well by the binary CO_2-N_2 adsorption data on silicalite at 40 °C, worse at 70 °C, and the worst at 100 °C. Therefore, the binary CO_2-N_2 adsorption data on silicalite at

low temperature satisfy the integral thermodynamic consistency test fairly well. The thermodynamic consistency becomes worse as temperature increases. In addition, the results of the integral thermodynamic consistency test match the results of predicting the adsorption behavior of the binary system from pure gas systems in Figure 5.4 very well. At low temperature, the thermodynamic consistency is good. so the difference of predicting the adsorption behavior of the binary system from pure gas systems is small; at high temperature, the thermodynamic consistency is not satisfied, so the difference of predicting the adsorption behavior of the binary system from pure gas systems is excessive or it is impossible to predict the adsorption behavior of the binary system from pure gas systems accurately. Thus. we recommend that one key requirement for predicting the adsorption behavior of the binary system from pure gas systems is that they satisfy the integral thermodynamic consistency tests between pure and binary gas adsorption equilibria. Moreover, these data sets can be used to prove the validity of predictive or correlative binary equilibrium models.

CONCLUSIONS

1. According to the pure gas isotherm data on silicalite, carbon dioxide is adsorbed much more strongly than nitrogen.
2. The pure gas adsorption capacity decreases with increasing temperature in the systems of carbon dioxide and nitrogen on silicalite.
3. Temperature independent Toth is a useful model for extrapolation and/or interpolation to predict separations at other temperatures and pressures.
4. Among the three concentration pulse chromatographic methods used, the HT-CPM is the best one. the MTT-CPM is very well, and the MVV-CPM is not satisfactory for describing the binary behaviour of CO_2/N_2 with silicalite.
5. The adsorption capacities for N_2 and CO_2 are very promising for silicalite as an adsorbent in applications in CO_2 removal from air for flue gases.
6. q_{CO2}, q_{N2} and q_{total} increase with decreasing temperature. Therefore, temperature is a very important factor for separation, particularly when y_{CO2} is very low.

7. For predicting the binary system of CO_2/N_2, Flory-Huggins of Vacancy Solution Theory is not acceptable. Extended Langmuir, Extended Dualsite Langmuir, Ideal Adsorbed Solution Theory, Statistical Model and Extended Sips cannot describe the real binary system accurately, either, and they can only be used at low temperatures or for rough estimation when the binary data are not available.
8. The selectivity is excellent for the CO_2/N_2 binary system on silicalite.
9. The CO_2-N_2 binary adsorption data on silicalite at low temperature satisfy the integral thermodynamic consistency test fairly well. The thermodynamic consistency becomes less satisfactory as temperature increases.

ACKNOWLEDGMENTS

Financial supports received from the Natural Sciences and Engineering Research Council of Canada (NSERC), the Ontario Graduate Scholarship (OGS) Program, and the Canadian Society for Chemical Engineering (CSChE) are gratefully acknowledged.

NOMENCLATURE

B = adsorption affinity constant, usually atm^{-1} (units depending on models)
B_0 = adsorption affinity constant at some reference temperature, atm^{-1}
B_1 = adsorption affinity constant in Site 1, atm^{-1}
B_2 = adsorption affinity constant in Site 2, atm^{-1}
K = dimensionless Henry's law constant, dimensionless
K_P = dimensional Henry's law constant, mmole. $g^{-1}.atm^{-1}$
n = adsorption exponents or number of actives sites, dimensionless
n_0 = adsorption exponents at some reference temperature, dimensionless
P = (total) pressure, atm
P_1 = pressure of Component *1*, atm
P_2 = pressure of Component *2*, atm

P_A = pressure of Component *A*, atm

P_B = pressure of Component *B*, atm

Q = isosteric heat, J.mol^{-1}

q = amount adsorbed, mmol.g^{-1}

q_A = amount adsorbed of Component *A*, mmol.g^{-1}

q_B = amount adsorbed of Component *B*, mmol.g^{-1}

q_1 = amount adsorbed of Component *1*, mmol.g^{-1}

q_2 = amount adsorbed of Component *2*, mmol.g^{-1}

q^0_1 = amount adsorbed of Component *1* in pure system, mmol.g^{-1}

q^0_2 = amount adsorbed of Component *2* in pure system, mmol.g^{-1}

q_m = adsorption saturation capacity or maximum amount adsorbed, mmol.g^{-1}

q_{m0} = adsorption saturation capacity or maximum amount adsorbed at some reference temperature, mmol.g^{-1}

q_{m1} = adsorption saturation capacity or maximum amount adsorbed in Site 1, mmol.g^{-1}

q_{m2} = adsorption saturation capacity or maximum amount adsorbed in Site 2, mmol.g^{-1}

R = gas constant, 8.314 J.K^{-1}.mol^{-1}

T = temperature, K

T_0 = reference temperature, K

x = mole fraction in adsorbed phase at equilibrium, dimensionless

x_A = mole fraction of Component *A* in adsorbed phase at equilibrium, dimensionless

x_B = mole fraction of Component B in adsorbed phase at equilibrium, dimensionless

y = mole fraction in fluid phase at equilibrium, dimensionless

y_A = mole fraction of Component *A* in fluid phase at equilibrium, dimensionless

y_B = mole fraction of Component B in fluid phase at equilibrium, dimensionless

y_1 = mole fraction of Component 1 in fluid phase at equilibrium, dimensionless

Greek letters

α = adsorption constant, adsorption separation factor, dimensionless

$\alpha_{A/B}$ = adsorption separation factor (the ratio of Component A over Component B), dimensionless

$\alpha_{i,A/B}$ = ideal adsorption separation factor (the ratio of Component A over Component B), dimensionless

θ = fraction of monolayer coverage, dimensionless

χ = constant parameter. dimensionless

Abbreviations

CPM = concentration pulse method

DSL = dualsite-Langmuir

GHG = greenhouse gases

GSE = Gibbsian surface excess

GWP = greenhouse warming potential

LFG = landfill gas

PSA = pressure swing adsorption

RMS = root mean square

SSR = sum of the square residuals

TCD = thermal conductivity detector

TSA = temperature swing adsorption

VST = vacancy solution theory

LITERATURE CITED

(1) Cavenati, S.; Grande, C. A.; Rodrigues, A. E. Upgrade of Methane from Landfill Gas by Pressure Swing Adsorption. *Energy and Fuels.* **2005,** *19*, 2545-2555.

(2) Hansen, J.; Fung, I.; Lacis, A.; Riud, D.; Levedeff, J. S.; Ruedy, R.; Russell, G. Global Climate Changes as Forecast by Goddard Institute for Space Studies Three-Dimensional Model. *Journal of Geophysical Research.* **1988**, *93*, 9341-9364.

(3) Chue, K. T.; Kim, J. N.; Yoo, Y. J.; Cho, S. H.; Yang, R. T. Comparison of Activated Carbon and Zeolite 13X for CO_2 recovery from flue gas by Pressure Swing Adsorption. *Industrial and Engineering Chemistry Research.* **1995,** *34*, 591-598.

(4) Diagne, D.; Goto, M.; Hirose, T. New PSA Process with Intermediate Feed Inlet Position Operated with Dual Refluxes: Application to Carbon Dioxide Removal and Enrichment. *Journal of Chemical Engineering of Japan.* **1994**, *27*, 85-89.

(5) Dong, F.; Lou, H.; Kodama, A.; Goto, M.; Hirose, T. The Petlyuk PSA Process for the Separation of Ternary Gas Mixtures: Exemplification by Separation a Mixture of CO_2-CH_4-N_2. *Separation and Purification Technology.* **1999**, *16*, 159-166.

(6) Dreisbach, F.; Staudt, R.; Keller, J. U. High Pressure Adsorption Data of Methane, Nitrogen, Carbon Dioxide and their Binary and Ternary Mixtures on Activated Carbon. *Adsorption.* **1999**, *5*, 215-227.

(7) Gomes, V. G; Yee, K. W. K. Pressure Swing Adsorption for Carbon Dioxide Sequestration from Exhaust Gases. *Separation and Purification Technology.* **2002,** *28*, 161-171.

(8) Harlick, P. J. E.; Tezel, F. H.; Tremblay, A. Y. Carbon Dioxide Removal from Flue Gas Using Pressure Swing Adsorption: Modelling and Optimisation. Presented at the 51st Canadian Chemical Engineering Conference, Oct. 14-17, **2001**.

(9) Harlick, P. J. E.; Tezel, F. H. CO_2-N_2 and CO_2-CH_4 Binary Adsorption Isotherms with H-ZSM-5: the Importance of Experimental Data Regression with the Concentration Pulse Method. *The Canadian Journal of Chemical Engineering.* **2001,** *79*, 236-245.

(10) Harlick, P. J. E.; Tezel, F. H. Adsorption of Carbon Dioxide, Methane and Nitrogen: Pure and Binary Mixture Adsorption by H-ZSM-5 with SiO_2/Al_2O_3 Ratio of 30. *Separation Science and Technology.* **2002,** *37*, 33-60.

(11) Harlick, P. J. E.; Tezel, F. H. Adsorption of Carbon Dioxide, Methane and Nitrogen: Pure and Binary Mixture Adsorption for ZSM-5 with SiO_2/Al_2O_3 Ratio of 280. *Separation and Purification Technology.* **2003**, *33*, 199-210.

(12) Hernandez-Huesca, R.; Diaz, L.; Aguilar-Armenta, G. Adsorption Equilibria and Kinetics of CO_2, CH_4 and N_2 in natural zeolites. *Separation and Purification Technology.* **1999**, *15*, 163-173.

(13) Kikkinides, E. S.; Yang, R. T. Concentration and Recovery of CO_2 from Flue Gas by Pressure Swing Adsorption. *Industrial and Engineering Chemistry Research.* **1993**, *32*, 2714-2720.

(14) Li, P.; Tezel, F. H.; Chung, T-S N.; Kulprathipanja, S. Analysis of Adsorption Parameters by Concentration Pulse Chromatography. 55th Canadian Chemical Engineering Conference, Toronto, Canada, Oct. 16-19, **2005,** 593.

(15) Li, P.; Tezel, F. H. Equilibrium and Kinetic Analysis of CO_2-N_2 Adsorption Separation by Concentration Pulse Chromatography. 40th IUPAC Congress, Beijing, P. R. China, Aug. 14-19, **2005**, p61, 1-O-034.

(16) Nishikawa, N. Removing and Recovering of CO_2. *Journal of the Japan Institute of Energy.* **1992,** *71*, 1090-1098.

(17) Pakseresht, S.; Kazemeini, M.; Akbarnejad, M. M. Equilibrium Isotherms for CO, CO_2, CH_4 and C_2H_4 on the 5A Molecular Sieve by a Simple Volumetric Apparatus. *Separation and Purification Technology.* **2002**, *28*, 53-60.

(18) Takamura, Y.; Narita, S.; Aoki, J.; Uchida, S. Application of High-Pressure Swing Adsorption Process for Improvement of CO_2 Recovery System from Flue Gas. *The Canadian Journal of Chemical Engineering.* **2001**, *79*, 812-816.

(19) Takamura, Y.; Narita, S.; Aoki, J.; Hironaka, S.; Uchida, S. Evaluation of Dual-Bed Pressure Swing Adsorption for CO_2 Recovery from Boiler Exhaust Gas. *Separation and Purification Technology.* **2001**, *24*, 519-528.

(20) Tezel, F. H.; Harlick, P.; Sirkecioglu, A. Adsorption of Nitrogen and Carbon Dioxide on ZSM-5. Proceedings of the 12th International Zeolite Conference in Baltimore, MD. July 5-10, **1998.**

(21) Tierney, M. J.; Scott, H. S.; Erb, T.; Prasertmanukitch, S. The Purification of Dilute CO_2/Air Solutions with an Annular Bed Adsorber: Numerical and Experimental Investigations. *Separation and Purification Technology.* **1999**, *17*, 159-171.

(22) Zhang, Z.; Guan, J.; Ye, Z. Separation of a Nitrogen-Carbon Dioxide Mixture by Rapid Pressure Swing Adsorption. *Adsorption.* **1998,** *4*, 173-177.

(23) Karger, J.; Ruthven, D. M. Diffusion in Zeolites and Other Microporous Solids. John Wiley and Sons Inc., New York, NY. **1992**, pp. 467-512.

(24) Lewis, W. K.; Gilliland, E. R.; Chertow, B.; Cadogan, W. P. Absorption Equilibria: Hydrocarbon Gas Mixtures. *Industrial and Engineering Chemistry.* **1951**, *42*, 1319-1326.

(25) Yang, R. T. Gas Separation by Adsorption Process. Butterworth Publishers, Stoneham, MA. **1987**, pp. 9-338.

(26) Van der Vlist, E.; Meijden, J. Van der. Determination of the Adsorption Isotherms of the Components of Binary Gas Mixtures by Gas Chromatography. *Journal of Chromatography.* **1973**, *79*, 1-13.

(27) Shah, D. B.; Ruthven, D. M. Measurement of Zeolite Diffusivities by Chromatography. *AIChE Journal.* **1977**, *23*, 804-810.

(28) Tezel, F. H.; Tezel, H. O.; Ruthven, D.M. Determination of Pure and Binary Isotherms for Nitrogen and Krypton. *Journal of Colloid and Interface Science.* **1992**, *149*, 197-207.

(29) Heslop, M.J.; Buffman, B.A.; Mason, G. A Test of the Polynomial-Fitting Method of Determining Binary-Gas-Mixture Adsorption Equilibria. *Industrial and Engineering Chemistry Research.* **1996**, *35*, 1456–1466.

(30) Kabir, H.; Grevillot, G.; Tondeur, D. Equilibria and Activity Coefficients for Non-Ideal Adsorbed Mixtures from Perturbation Chromatography. *Chemical Engineering Science*, **1998,** *53*, 1639–1654.

(31) Harlick, P. J. E.; Tezel, F. H. A Novel Solution Method for Interpreting Binary Adsorption Isotherms from Concentration Pulse Chromatography Data. *Adsorption.* **2000,** *6*, 293–309.

(32) Langmuir, I. The Adsorption of Gazes on Platine Surfaces Glass Mica and Platinum. *Journal of the American Chemical Society,* **1918,** *40,* 1361-1403.

(33) Do, D. D. Adsorption Analysis: Equilibria and Kinetics. Imperial College Press, London, UK. **1998**, pp. 1-148.

(34) Freundlich, H. Of the Adsorption of Gases. Section II. Kinetics and Energetics of Gas Adsorption. Introductory Paper to Section II. *Transactions of the Faraday Society,* **1932,** *28*, 195-201.

(35) Sips, R. On the Structure of a Catalyst Surface. *The Journal of Chemical Physics.* **1948**, *16*, 490-495.

(36) Cochran, T. W.; Kabel, R. L.; Danner, R. P. Vacancy Solution Theory of Adsorption Using Flory-Huggins Activity Coefficient Equations. *AIChE Journal.* **1985**, *31,* 268-277.

(37) Cochran, T. W.; Kabel, R. L.; Danner, R. P. The Vacancy Solution Model of Adsorption - Improvements and Recommendations. *AIChE Journal.* **1985**, *31*, 2075-2082.

(38) Krishna, R.; Vlugt, T. J. H.; Smit, B. Influence of Isotherm Inflection on Diffusion in Silicalite. *Chemical Engineering Science.* **1999**, *54*, 1751-1757.

(39) Markham, E. C.; Benton, A. F. The Adsorption of Gas Mixtures by Silica", Journal of American Chemical Society, **1931,** *53*, 497-507.

(40) Bowen, T. C.; Vane, L. M. Ethanol, Acetic Acid, and Water Adsorption from Binary and Ternary Liquid Mixtures on High-Silica Zeolites. *Langmuir.* **2006,** *22*, 3721-3727.

(41) Tien, Chi. Chapter 4: Multicomponent Adsorption Equilibrium and Calculations, in Adsorption Calculations and Modeling. Butterworth-Heinemann, Newton, MA. **1994**, pp.43-69.

(42) Yang, R. T. Adsorption: Fundamentals and Applications. Wiley-Interscience, Hoboken, New Jersey. **2003**, pp. 18-27.

(43) Li, P.; Tezel, F. H. Adsorption Separation of N_2, O_2, CO_2 and CH_4 Gases by β-Zeolite. *Microporous & Mesoporous Materials.* **2007**, *98,* 94-101.

(44) Triebe, R. W.; Tezel, F. H. Adsorption of Nitrogen and Carbon Monoxide on Clinoptilolite: Determination and Prediction of Pure and Binary Isotherms. *The Canadian Journal of Chemical Engineering.* **1995**, *73*, 717-724.

(45) Calleja, G.; Pau, J.; Calles, J.A. Pure and Multicomponent Adsorption Equilibrium of Carbon Dioxide, Ethylene and Propane on ZSM-5 Zeolites with Different Si/Al Ratios. *Journal of Chemical and Engineering Data.* **1998,** *43*, 994–1003.

(46) Sircar, S. Excess Properties and Thermodynamics of Multicomponent Gas Adsorption. *J. Chem. SOC., Faraday Trans.* **1985**, *I 81*, 1527-1540.

(47) Sircar, S. R&D Note: Data Representation for Binary and Multicomponent Gas Adsorption Equilibria. *Adsorption.* **1996,** *2*, 327-330.

(48) Sircar, S.; Rao, M. B. Heat of Adsorption of Pure Gas and Multicomponent Gas Mixtures on Microporous Adsorbents, In Surfaces of Nanoparticles and Porous Materials, J. A. Schwarz and C. Contescu Eds., Marcel Dekker, New York, NY, **1998**, Chapter 19, pp 501-528.

(49) Rao, M. B.; Sircar, S. Thermodynamic Consistency for Binary Gas Adsorption Equilibria. *Langmuir.* **1999**, *15*, 7258-7267.

(50) Li, P.; Tezel, F. H. Adsorption Separation of Methane and Carbon Dioxide on Silicalite submitted to be published in *Separation Science and Technology,* **2007**.

(51) Rees, L. V. C.; Bruckner, P.; Hampson, J. Sorption of N_2, CH_4 and CO_2 in Silicalite-1. *Gas Separation and Purification.* **1991**, *5*, 67.

(52) Dunne, J. A.; Mariwala, R.; Rao, M.; Sircar, S. R.; Gorte, J.; Myers, A. L. Calorimetric Heats of Adsorption and Adsorption Isotherms. 1. O_2, N_2, Ar, CO_2, CH_4, C_2H_6, and SF_6 on Silicalite. *Langmuir.* **1996**, *12*, 5888.

(53) Choudhary, V. R.; Mayadevi, S. Adsorption of Methane, Ethane, Ethylene, and Carbon Dioxide on Silicalite-1. *Zeolites.* **1996**. *17*, 501.

Table 5.1. Concentration pulse chromatographic methods used.

MVV-CPM (Modified Van der Vlist and Van der Meijden -Concentration Pulse Method)[26]		
4-parameter function	$K_p = A_0 + A_1 y_1 + A_2 y_1^2 + A_3 y_1^3$	
Isotherm slope functions	$\frac{dq_1}{dP_1} = B_0 + B_1 y_1 + B_2 y_1^2$	$\frac{dq_2}{dP_2} = C_0 + C_1 y_1 + C_2 y_1^2$
Binary isotherm functions	$q_1 = \left(B_0 y_1 + \frac{B_1}{2} y_1^2 + \frac{B_2}{3} y_1^3 \right) P$	$q_2 = \left[C_0 (1 - y_1) + \frac{C_1}{2}(1 - y_1^2) + \frac{C_2}{3}(1 - y_1^3) \right] P$
MTT-CPM (Modified Triebe and Tezel -Concentration Pulse Method)[44]		
5-parameter function	$K_p = A_{-1}(\beta + y_1) + A_0 + \frac{A_1}{(\beta + y_1)} + \frac{A_2}{(\beta + y_1)^2}$	
Isotherm slope functions	$\frac{dq_1}{dP_1} = B_0 + \frac{B_1}{(\beta + y_1)} + \frac{B_2}{(\beta + y_1)^2}$	$\frac{dq_2}{dP_2} = C_0 + \frac{C_1}{(\beta + y_1)} + \frac{C_2}{(\beta + y_1)^2}$
Binary isotherm functions	$q_1 = \left[B_0 y_1 + B_1 \ln \frac{\beta + y_1}{\beta} + \frac{B_2 y_1}{\beta(\beta + y_1)} \right] P$	$q_2 = \left[C_0 (1 - y_1) - C_1 \ln \frac{\beta + y_1}{\beta + 1} + \frac{C_2 (1 - y_1)}{(\beta + 1)(\beta + y_1)} \right] P$
HT-CPM (Harlick and Tezel -Concentration Pulse Method)[9, 31]		
5-parameter function	$K_p = A_1 + A_2 y_1 + A_3 y_1^2 + A_4 \ln\lvert y_1 + \lambda \rvert$	
Isotherm slope functions	$\frac{dq_1}{dP_1} = B_1 + 2B_2 y_1 + \frac{B_3}{\lvert y_1 + \lambda \rvert}$	$\frac{dq_2}{dP_2} = C_1 + 2C_2 y_1 + \frac{C_3}{\lvert y_1 + \lambda \rvert}$
Binary isotherm functions	$q_1 = \left[B_1 y_1 + B_2 y_1^2 + B_3 \ln \left\lvert \frac{y_1 + \lambda}{\lambda} \right\rvert \right] P$	$q_2 = \left[C_1 (1 - y_1) + C_2 (1 - y_1^2) - C_3 \ln \left\lvert \frac{y_1 + \lambda}{1 + \lambda} \right\rvert \right] P$

Table 5.2. Details of the adsorbent.

Type	Silicalite
Commercial name	MOLSIV Adsorbents
Commercial number	HISIV 3000
Particle form received	1/16 inch extrudate as received
Size used in the column (Diameter)	Crushed to 20 x 60 mesh
Content of binder	20 wt%
Particle density	1.131 $g.cm^{-3}$
Void fraction	0.39
Supplier	Universal Oil Products, Des Plaines, IL, USA

Table 5.3. Details of sample gases.

Gases	Grade	Purity	Supplier
CO_2	Bone Dry 3.0	99.9 %	Praxair Inc., Ottawa
N_2	Ultra High Purity 5.0	99.999 %	Praxair Inc., Ottawa
He	Ultra High Purity 5.0	99.999 %	Praxair Inc., Ottawa

Table 5.4. Parameters and RMS deviations of adsorption models by non-linear regressions.

Models	Equations	Parameters	CO_2			N_2		
			40 °C	70 °C	100 °C	40 °C	70 °C	100 °C
Langmuir (2 param.)	$q = \frac{q_m BP}{1+BP}$	B (atm^{-1})	1.089	0.649	0.332	0.111	0.045	0.013
		q_m ($mmol.g^{-1}$)	2.858	2.834	2.911	2.094	3.765	9.993
		RMS ($mmol.g^{-1}$)	0.050	0.040	0.038	0.004	0.002	0.002
Freundlich (2 param.)	$q = kP^{\frac{1}{n}}$	k ($mmol.g^{-1}.atm^{-1/n}$)	1.340	1.035	0.713	0.212	0.166	0.129
		n (dimensionless)	2.295	1.938	1.616	1.247	1.112	1.037
		RMS ($mmol.g^{-1}$)	0.106	0.067	0.022	0.011	0.005	0.002
Sips (Langmuir-Freundlich) (3 param.)	$q = \frac{q_m (BP)^{\frac{1}{n}}}{1+(BP)^{\frac{1}{n}}}$	B (atm^{-1})	0.675	0.337	0.065	0.118	0.046	0.0006
		q_m ($mmol.g^{-1}$)	3.431	3.697	6.240	2.014	3.722	176.2
		n (dimensionless)	1.256	1.249	1.349	0.989	0.999	1.035
		RMS ($mmol.g^{-1}$)	0.021	0.012	0.009	0.004	0.002	0.002
Toth (3 param.)	$q = \frac{q_m BP}{\left[1+(BP)^n\right]^{\frac{1}{n}}}$	B (atm^{-1})	1.397	0.678	0.100	0.109	0.041	0.002
		q_m ($mmol.g^{-1}$)	3.903	4.885	38.98	2.125	4.207	84.58
		n (dimensionless)	0.604	0.537	0.260	0.990	0.951	0.598
		RMS ($mmol.g^{-1}$)	0.028	0.013	0.011	0.003	0.002	0.002
Flory-Huggins VST (3 param.)	$P = \left(\frac{1}{B}\cdot\frac{q}{1-\frac{q}{q_m}}\right)\exp\left(\frac{\alpha^2\cdot\frac{q}{q_m}}{1+\alpha^2\cdot\frac{q}{q_m}}\right)$	B ($mmol.g^{-1}.atm^{-1}$)	3.874	2.608	1.280	0.242	0.172	0.129
		q_m ($mmol.g^{-1}$)	3.082	3.498	5.969	3.453	32.29	10.31
		α_{1v} (dimensionless)	1.020	1.525	2.123	1.161	3.085	$4x10^{-7}$
		RMS ($mmol.g^{-1}$)	0.032	0.014	0.019	0.004	0.002	0.002
Multisite Langmuir (3 param.)	$BP = \frac{\frac{q}{q_m}}{\left(1-\frac{q}{q_m}\right)^n}$	B (atm^{-1})	1.002	0.341	0.014	0.013	0.006	0.004
		q_m ($mmol.g^{-1}$)	3.322	6.567	78.01	18.03	30.91	34.74
		n (dimensionless)	1.412	3.881	43.90	10.97	9.177	3.489
		RMS ($mmol.g^{-1}$)	0.049	0.019	0.027	0.003	0.002	0.002
Dualsite Langmuir (4 param.)	$q = \frac{q_{m1} B_1 P}{1+B_1 P} + \frac{q_{m2} B_2 P}{1+B_2 P}$	B_1 (atm^{-1})	0.782	0.393	0.190	0.009	0.045	0.013
		q_{m1} ($mmol.g^{-1}$)	2.822	2.904	3.492	3.570	3.765	9.849
		B_2 (atm^{-1})	36.44	7.003	11.00	0.140	0.919	0.004
		q_{m2} ($mmol.g^{-1}$)	0.217	0.305	0.173	1.442	0	0.0254
		RMS ($mmol.g^{-1}$)	0.012	0.019	0.027	0.004	0.002	0.002
Temperature Independent Sips	$q = \frac{q_m (BP)^{\frac{1}{n}}}{1+(BP)^{\frac{1}{n}}}$	B (atm^{-1})	0.594	0.343	0.212	0.075	0.070	0.065
		q_m ($mmol.g^{-1}$)	3.614	3.614	3.614	2.694	2.694	2.694
		n (dimensionless)	1.321	1.223	1.149	1.046	0.968	0.907
		RMS ($mmol.g^{-1}$)	0.026	0.026	0.026	0.006	0.006	0.006
Temperature Independent Toth	$q = \frac{q_m BP}{\left[1+(BP)^n\right]^{\frac{1}{n}}}$	B (atm^{-1})	1.617	0.640	0.285	0.122	0.092	0.172
		q_m ($mmol.g^{-1}$)	4.649	4.649	4.649	1.801	1.801	1.801
		n (dimensionless)	0.496	0.570	0.635	1.155	1.497	1.804
		RMS ($mmol.g^{-1}$)	0.031	0.015	0.024	0.005	0.004	0.004

Table 5.5. Optimal parameters for the temperature independent Toth and Sips equations for a reference temperature T_0 = 40 °C.

Adsorbate	Parameters	Units	Temperature Independent Toth	Temperature Independent Sips
CO_2	χ	Dimensionless	0	0
	q_{m0}	mmol.g^{-1}	4.649	3.614
	B_0	atm^{-1}	1.660	0.603
	Q/RT_0	Dimensionless	10.87	6.439
	n_0	Dimensionless	0.494	1.324
	α	Dimensionless	0.869	0.708
N_2	χ	Dimensionless	0	0
	q_{m0}	mmol.g^{-1}	1.801	2.694
	B_0	atm^{-1}	0.123	0.075
	Q/RT_0	Dimensionless	3.278	0.881
	n_0	Dimensionless	1.152	1.047
	α	Dimensionless	4.000	0.903

Table 5.6. *RMS* deviations $([\Sigma(K_{p,data} - K_{p,curve})^2/n]^{0.5})$ in mmole.g^{-1}.atm^{-1} of concentration pulse chromatographic methods for CO_2-N_2 binary system on silicalite.

CPM	40 °C	70 °C	100 °C
HT	0.060	0.080	0.059
MTT	0.070	0.111	0.078
MVV	3.303	0.939	0.197

Table 5.7. *RMS* deviations $([\Sigma(q_{data}- q_{curve})^2/n]^{0.5})$ in mmole.g^{-1}

of predicted isotherms from the experimental ones for CO_2-N_2 binary system on silicalite.

Models	Capacity	40 °C	70 °C	100 °C
Extended Langmuir	q_{CO2}	0.081	0.103	0.068
	q_{N2}	0.086	0.071	0.054
	q_{total}	0.122	0.150	0.108
Extended Dualsite Langmuir	q_{CO2}	0.094	0.101	0.096
	q_{N2}	0.016	0.075	0.055
	q_{total}	0.101	0.159	0.147
Extended Sips	q_{CO2}	0.042	0.057	0.140
	q_{N2}	0.091	0.075	0.042
	q_{total}	0.115	0.109	0.131
Ideal Adsorbed Solution Theory	q_{CO2}	0.084	0.102	0.066
	q_{N2}	0.083	0.072	0.056
	q_{total}	0.122	0.150	0.108
Flory- Huggins VST	q_{CO2}	0.081	0.359	0.091
	q_{N2}	0.077	0.206	0.064
	q_{total}	0.127	0.563	0.147
Statistical Method	q_{CO2}	0.084	0.102	0.066
	q_{N2}	0.081	0.071	0.055
	q_{total}	0.119	0.147	0.107

Table 5.8. The integral thermodynamic consistency test between pure and binary carbon dioxide (1) – nitrogen (2) equilibrium adsorption data. on silicalite using Equation (9)

Temperature	°C	40	70	100
RHS: $\int_0^1 \frac{q_1(1-y_1)-q_2y_1}{y_1(1-y_1)}d$	mmol.g^{-1}	2.1231	1.3003	0.7166
1st term in LHS: $\int_0^1 \frac{q_1^0}{P}dP$	mmol.g^{-1}	2.3084	1.5809	1.0193
2nd term in LHS: $\int_0^1 \frac{q_2^0}{P}dP$	mmol.g^{-1}	0.2200	0.1671	0.1298
LHS: $\int_0^1 \frac{q_1^0}{P}dP - \int_0^1 \frac{q_2^0}{P}dP$	mmol.g^{-1}	2.0883	1.4136	0.8895
$\left\|\frac{LHS-RHS}{RHS}\right\|$	%	1.64	8.72	24.13

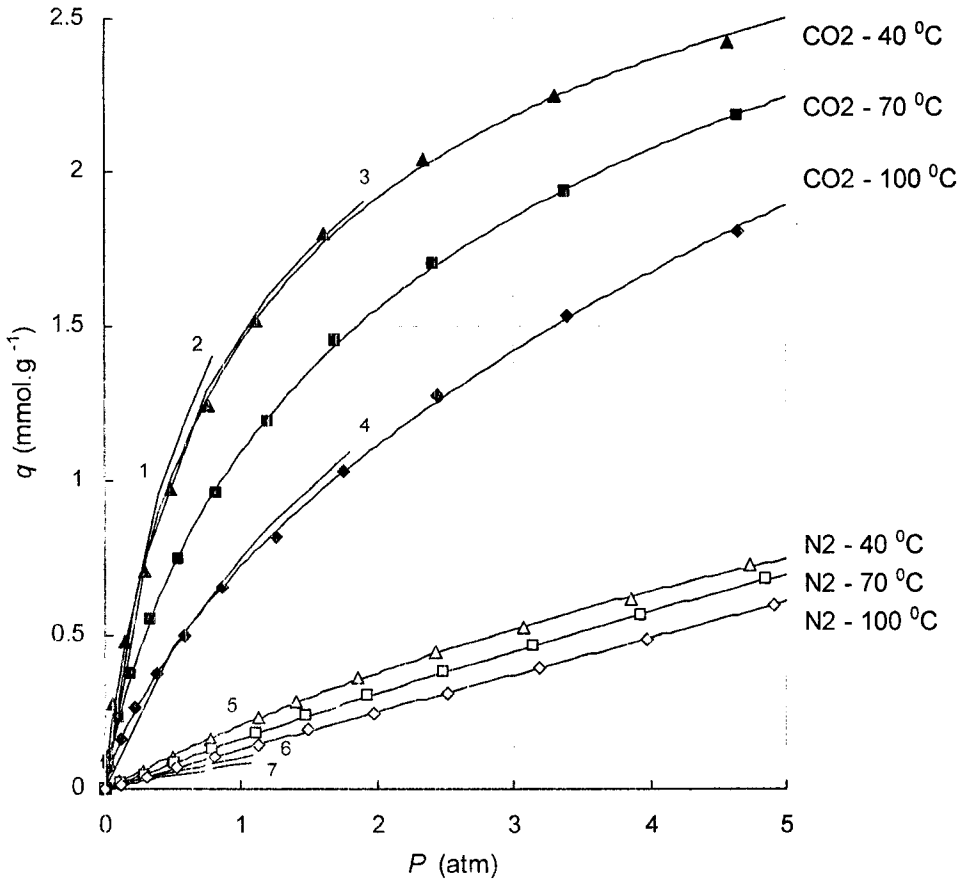

Figure 5.1. Isotherms for CO_2, and N_2 on silicalite:

The points are experimental data and the curves are Toth isotherms.

The numbered curves indicate comparisons with the literature:

1: CO_2 – 25 °C;[51] **2:** CO_2 – 31 °C;[52] **3:** CO_2 – 32 °C;[53] **4:** CO_2 – 80 °C;[53]

5: N_2 – 23 °C;[52] **6:** N_2 – 61 °C;[52] **7:** N_2 – 72 °C;[52]

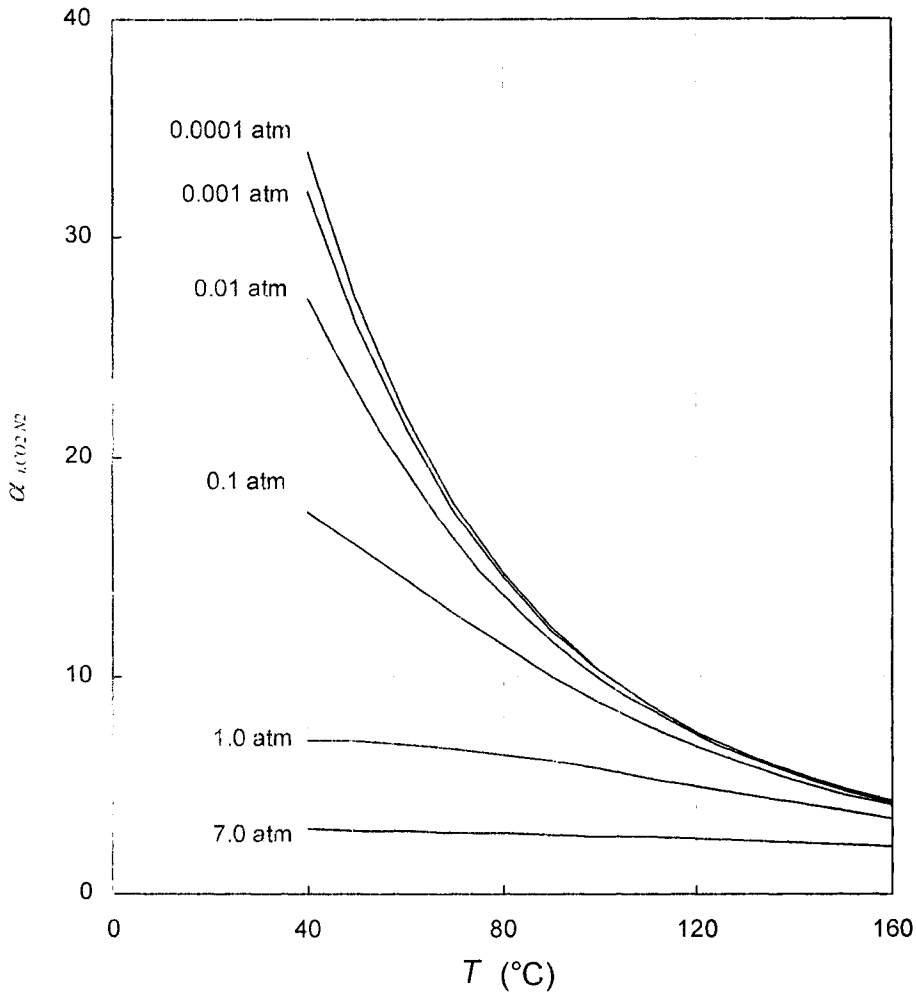

Figure 5.2. Ideal separation factors for CO_2/N_2, on silicalite.

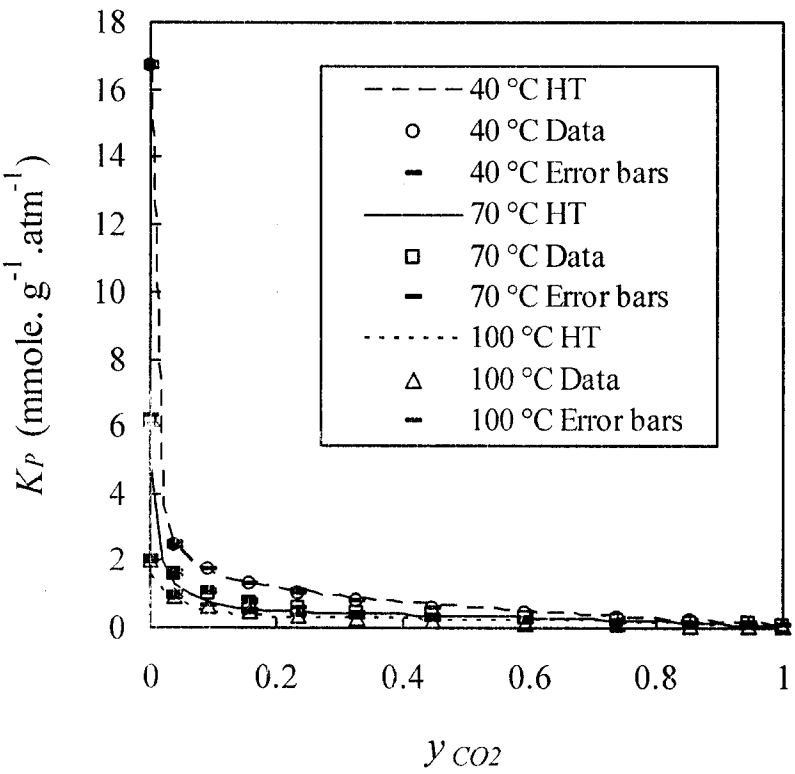

Figure 5.3a. Regressions for CO_2/N_2, binary K_p with silicalite by HT-CPM at different carrier gas compositions at 1 atm. total pressure.

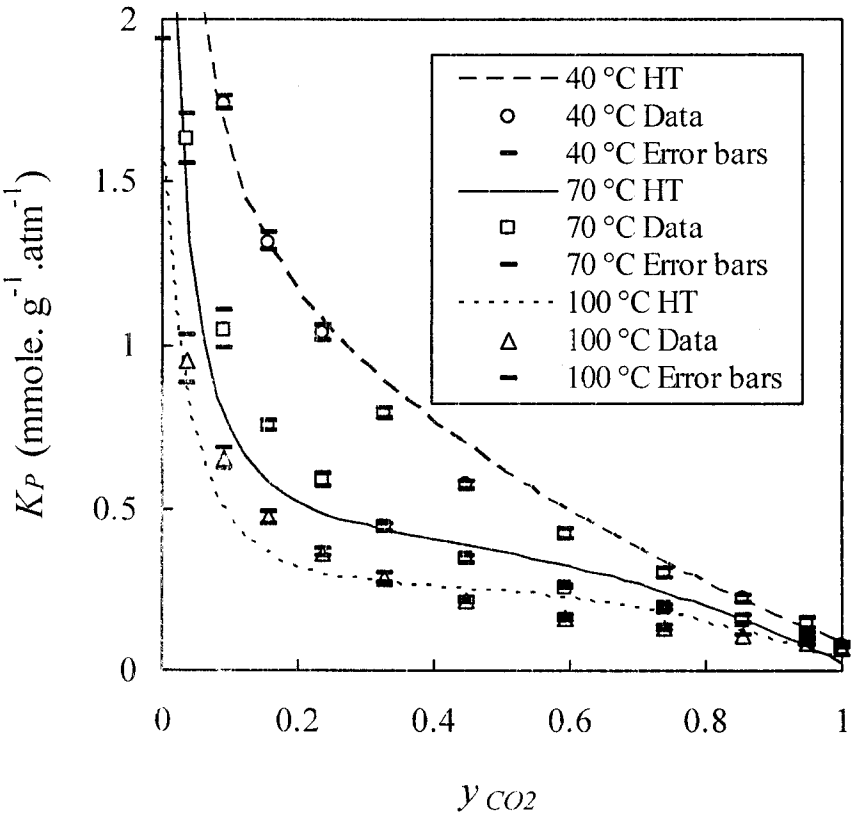

Figure 5.3b. Regressions for CO_2/N_2, binary K_p with silicalite by HT-CPM at different carrier gas compositions at 1 atm. total pressure.
(K_p is in the range between 0 mmol.g^{-1}.atm^{-1} and 0.5 mmol.g^{-1}.atm^{-1})

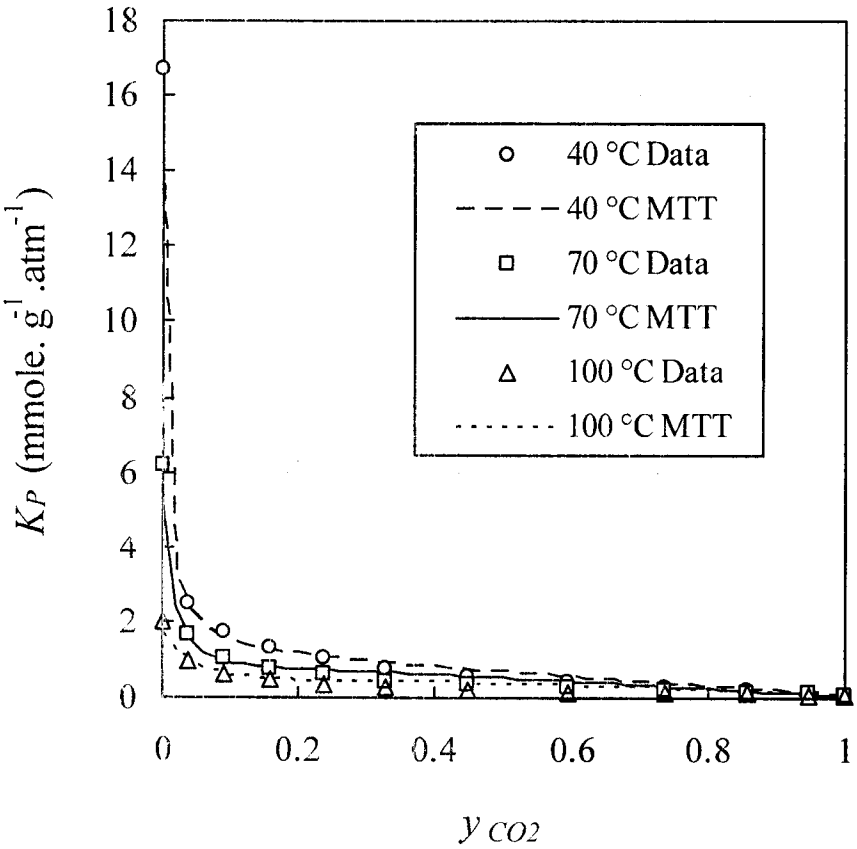

Figure 5.3c. Regressions for CO_2/N_2, binary K_p with silicalite by MTT-CPM at different carrier gas compositions at 1 atm. total pressure.

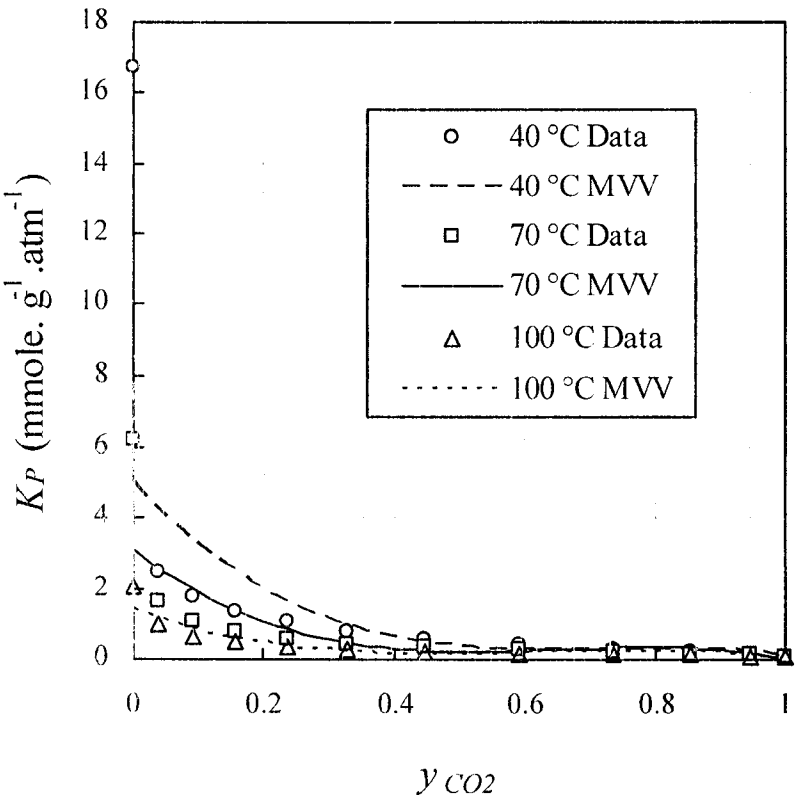

Figure 5.3d. Regressions for CO_2/N_2, binary K_p with silicalite by MVV-CPM at different carrier gas compositions at 1 atm. total pressure.

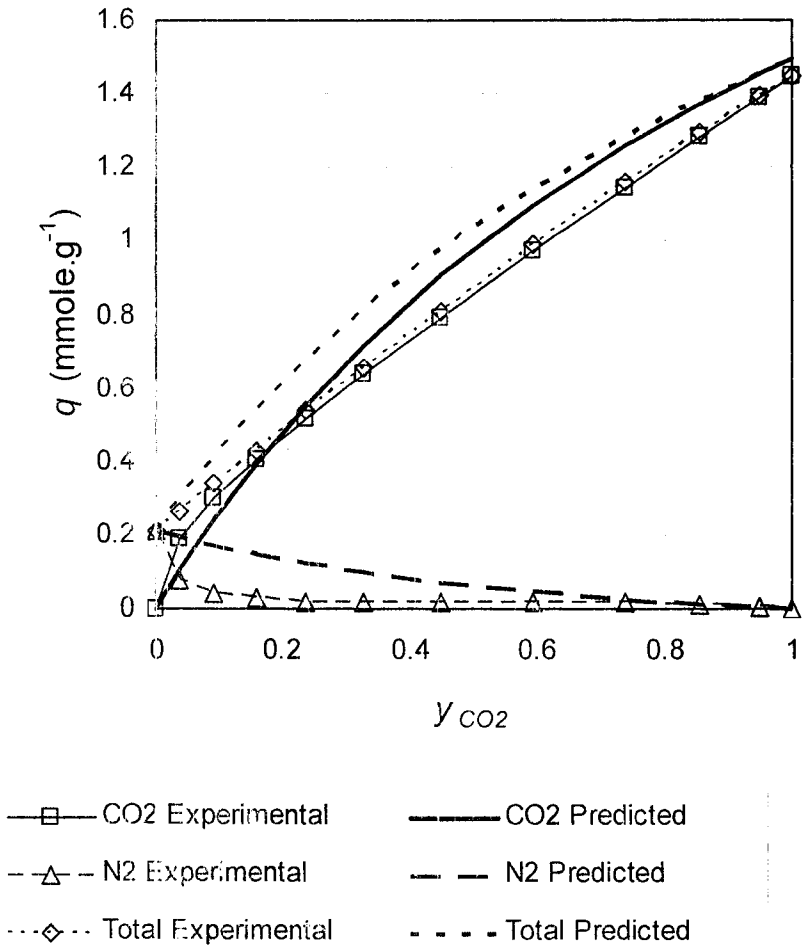

Figure 5.4a. Experimental binary Isotherms from HT-CPM, compared with predicted binary isotherm from Statistical Model for CO_2/N_2 with silicalite at 40 °C and 1 atm. total pressure

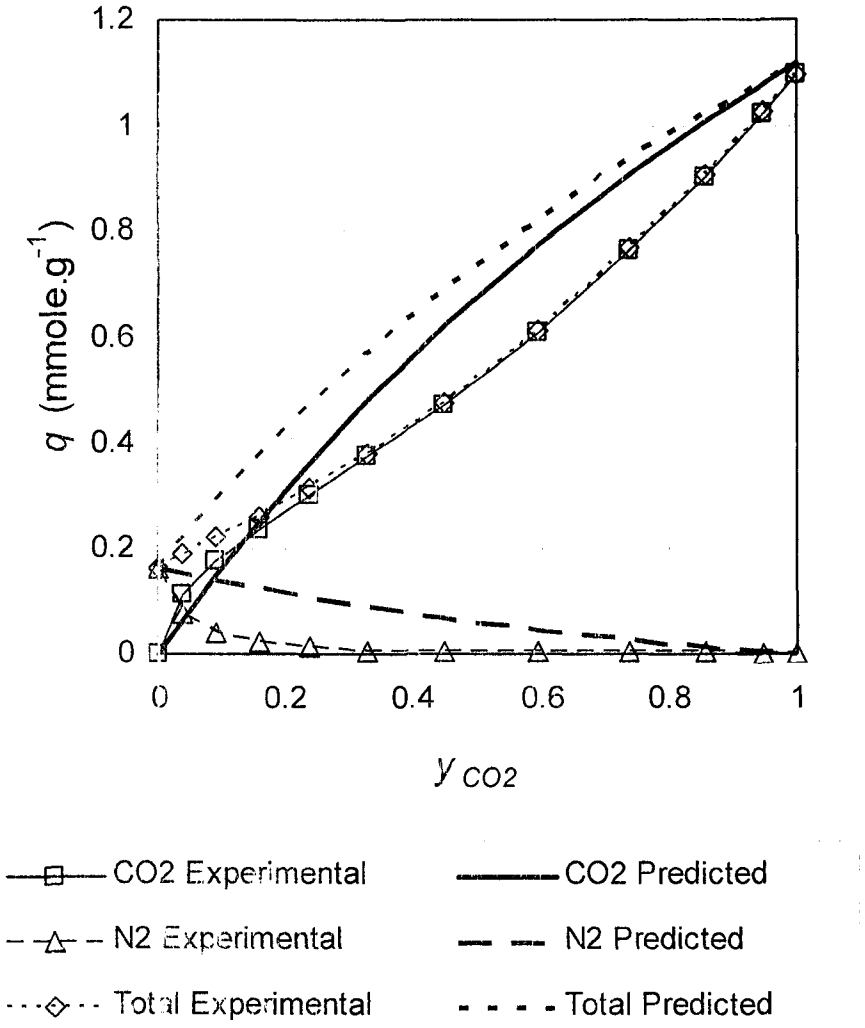

Figure 5.4b. Experimental binary Isotherms from HT-CPM, compared with predicted binary isotherm from Statistical Model for CO_2/N_2 with silicalite at 70 °C and 1 atm. total pressure

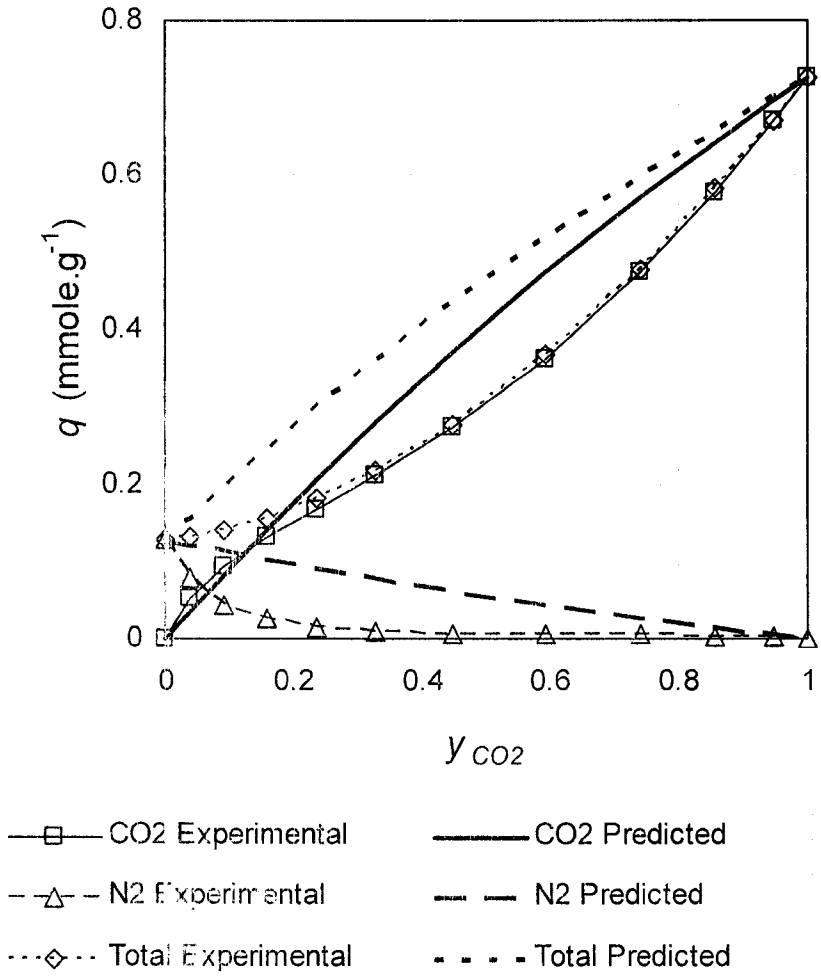

Figure 5.4c. Experimental binary Isotherms from HT-CPM, compared with predicted binary isotherm from Statistical Model for CO_2/N_2 with silicalite at 100 °C and 1 atm. total pressure

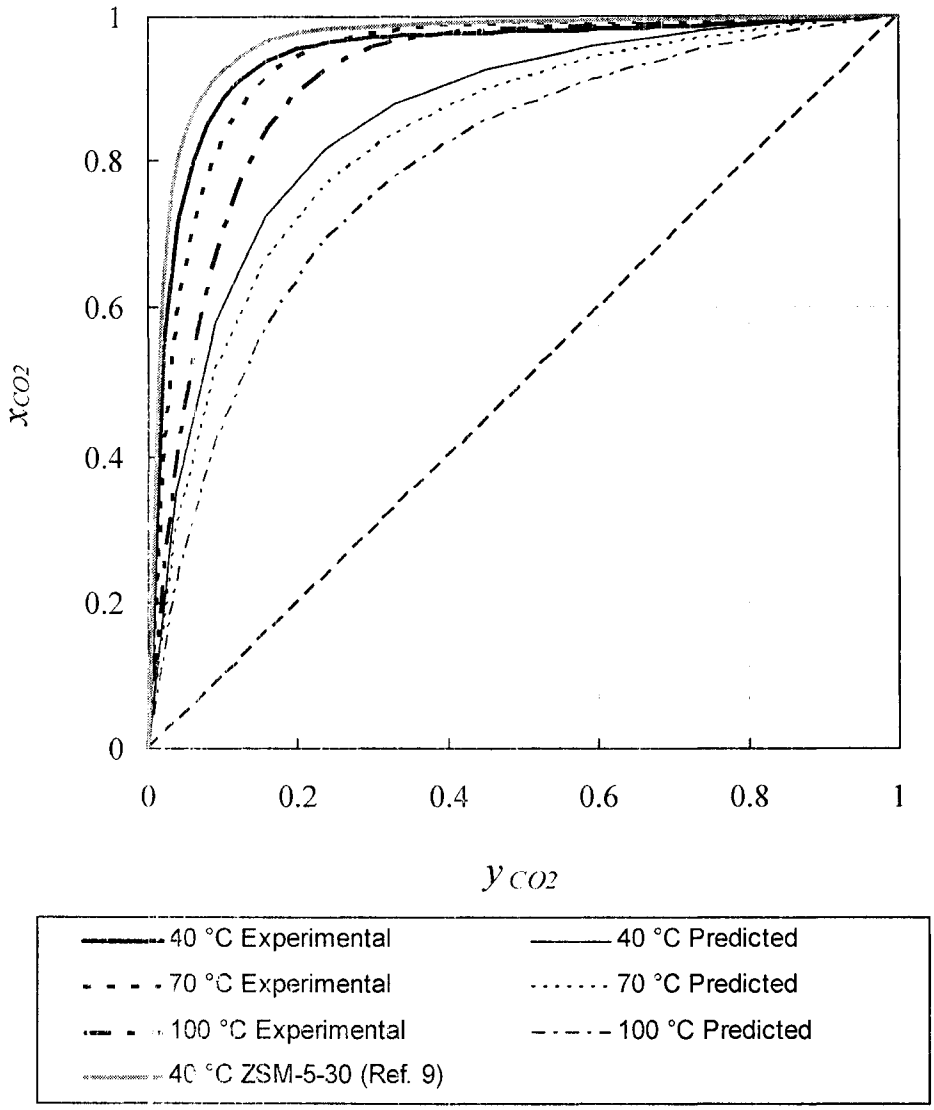

Figure 5.5. $x - y$ diagrams for CO_2/N_2, binary systems with silicalite at 1 atm. total pressure and comparison with the literature values for ZSM-5-30[9]

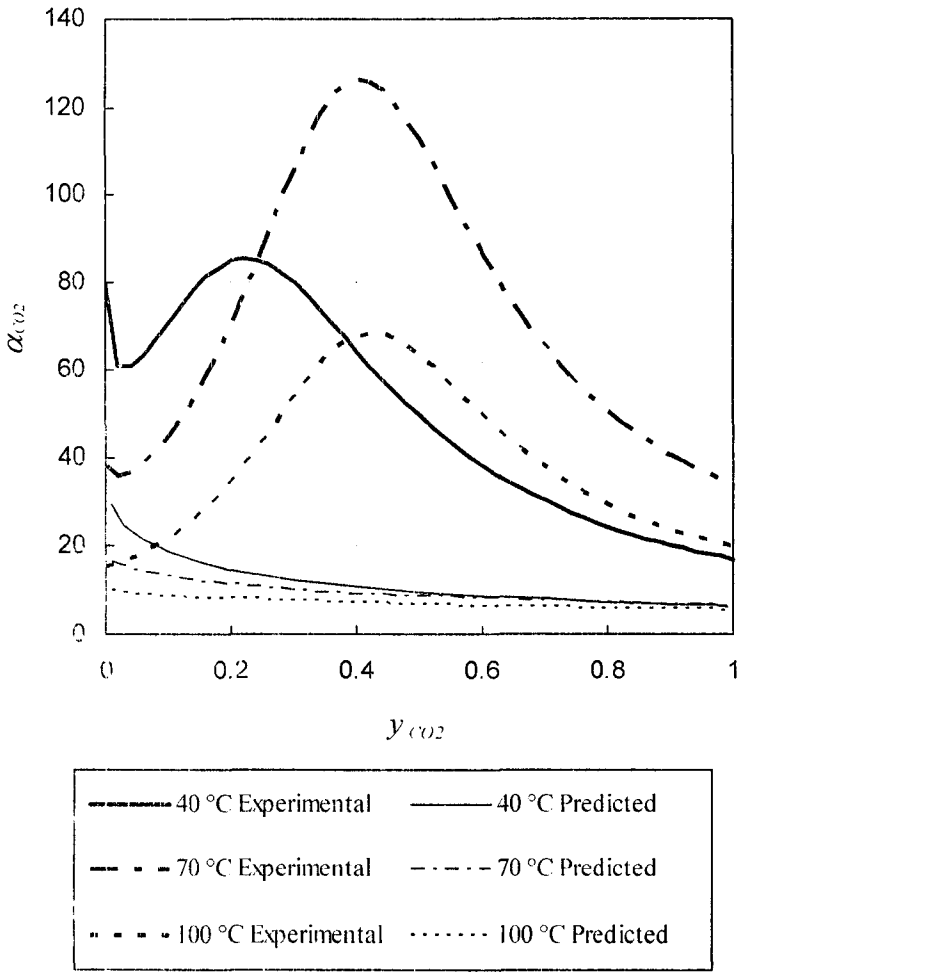

Figure 5.6. Equilibrium separation factor curves
for CO_2/N_2 and silicalite system at different temperatures studied,
experimental from binary adsorption isotherms and predicted from pure gas isotherms

CHAPTER VI

ADSORPTION SEPARATION OF METHANE AND NITROGEN ON SILICALITE

Peiyuan Li and F. Handan Tezel*

Department of Chemical Engineering
Faculty of Engineering
University of Ottawa
161 Louis Pasteur, Ottawa, Ontario K1N 6N5, Canada

It will be submitted to the Journal of Chemical & Engineering Data soon.

Presented at 56th CSChE (Canadian Society for Chemical Engineering) Canadian Chemical Engineering Conference, Sherbrooke Quebec, October 15-18, 2006, Conference Proceedings 360.

* Corresponding author
Tel: 613-562-5800 Ext. 6099
Fax: 613-562-5172
Emai: Handan.Tezel@uottawa.ca

ABSTRACT

Methane is the most important non-CO_2 greenhouse gas (GHG) responsible for global warming with more than 10% of total GHG emissions. The greenhouse warming potential (GWP) of this gas is higher than carbon dioxide. Therefore, any reduction in methane emissions is really important in the atmosphere reconstruction. Nitrogen is needed to be removed from Landfill gas to obtain low grade natural gas as a renewable resource of energy from garbage, but the separation is difficult. Adsorption was considered as a possibility for this separation using silicalite as the adsorbent. Adsorption behaviour of methane and nitrogen on this adsorbent was studied by concentration pulse chromatography and constant volume techniques. Ideal separation factors were obtained from the pure isotherms by using temperature independent Toth isotherm model. Mixture adsorption isotherms for the binary system of methane and nitrogen at 40, 70 and 100 °C and 1 atmosphere total pressure were determined. Corresponding x-y diagrams and separation factors were obtained from these experimental data. The thermodynamic consistency tests between pure and binary gas adsorption systems were also carried out. The separation factors obtained with silicalite for the separation applications of methane and nitrogen gases in this work are much better than those obtained for other systems reported in the literature.

INTRODUCTION

Methane is the most important non-CO_2 GHG responsible for global warming with more than 10% of total GHG emissions. Despite the small amounts of methane released to the atmosphere, the greenhouse warming potential (GWP) of this gas is higher than that of carbon dioxide and the life of methane molecules in the atmosphere is much shorter than carbon dioxide, so any reduction in methane emissions is very important in the short- and medium-term atmosphere reconstruction.[1, 2] Nitrogen needs to be removed from Landfill gas and low grade natural gas for getting new resource of energy, but the separation is difficult. Some papers have been reported on CH_4-N_2 adsorption separation.[3-8] Sheikh et al.[3] studied the adsorption isotherms on a new high specific area active carbon Maxsorb with volumetric and chromatographic methods for this separation. Cavenati et al.[4] obtained the kinetic separation factor on Carbon Molecular Sieve CMS 3K for this separation. Jayaramana et al.[5] researched on selectivity of this system on Clinoptilolites. Their results were not satisfactory, and further improvements are needed before real application can be considered. Warmuzinski and Sodzawiczny[6] did PSA computer simulations on effect of adsorption pressure for the separation. Dong et al.[7] worked on PSA with activate carbon, zeolite 13X and carbon molecular sieve for separating a mixture of carbon dioxide, methane and nitrogen. Harlick and Tezel[9] studied the binary adsorption isotherms of methane and nitrogen by HT-CPM (Harlick and Tezel - Concentration Pulse Method) on ZSM-5 with $SiO_2/Al_2/O_3$ ratio of 280.

In this study, adsorption separation of CH_4 and N_2 gases were considered with silicalite as the adsorbent. Silicalite is one of the most important synthetic zeolites. It is widely used as a selective adsorbent. Its distinctive features include high thermal and hydrothermal stability, hydrophobic and organophilic adsorptive properties and an intermediate (ten-ring) pore size which leads to molecular sieve size selectivity. Its low aluminum content (the Si/Al ratio is in the thousands) is responsible for its hydrophobic nature.[10]

Pure component adsorption isotherms of CH_4 and N_2 were determined on silicalite using constant volume technique. This method involves measuring the pressure change in a known volume of gas subjected to an adsorbent sample. As the gas is adsorbed and allowed

to come to equilibrium, the measured decrease in the system pressure yields the amount of gas adsorbed under the given conditions. This method has been used extensively to determine adsorption isotherms.[11-12] Ideal separation factors were determined from the pure component isotherms obtained.

Binary mixture adsorption behaviour of CH_4 and N_2 on silicalite was determined by using the chromatographic technique at 40, 70 and 100°C and 1 atm total pressure. This dynamic method of analysis can be employed in several ways: tracer gas, step change, and pulse chromatography. The use of concentration pulse chromatography for adsorbent screening is very attractive since it is relatively inexpensive to setup and easy to employ. A method using the slope of the isotherms proposed in the literature for determining the binary isotherms from concentration pulse chromatographic data has been given and shown being capable of interpreting even highly selective binary systems.[9, 13-18]

From the binary isotherms obtained, corresponding phase diagrams and separation factors were determined. The thermodynamic consistency tests between pure and binary gas adsorption systems are also discussed.

THEORY AND EXPERIMENTAL SECTION

There are many models used for adsorption isotherms of pure gas systems. The simplest and still the most useful pure gas isotherm is the Langmuir isotherm:

$$\theta = \frac{q}{q_m} = \frac{BP}{1 + BP} \quad \text{.....(1)}$$

where B is the affinity constant, θ is the fractional coverage, q is the amount adsorbed, q_m is the saturation adsorption capacity or maximum amount adsorbed, and P is the pressure.[19-20]

A three-parameter isotherm that is an empirical and popular one used and satisfies both low and high pressure range is the Toth isotherm:[20]

$$\theta = \frac{q}{q_m} = \frac{BP}{\left[1 + (BP)^n\right]^{\frac{1}{n}}} \quad \text{.....(2)}$$

The temperature independence of equilibrium parameters is required to extrapolate

or interpolate the adsorption equilibrium data to other temperatures and to calculate isosteric heat of adsorption. The temperature independence of the Toth equation for the affinity constants B can be expressed:

$$B = B_0 e^{\frac{Q}{RT_0}\left(\frac{T_0}{T}-1\right)} \quad \text{.....(3)}$$

where B_0 is the adsorption affinity constant at a reference temperature T_0, Q is the isosteric heat of adsorption, invariant with the surface loading, and R is the gas constant. The saturation capacity of the Toth equation can be either taken as constant or it can take the following temperature independence:

$$q_m = q_{m0} e^{\chi\left(1-\frac{T}{T_0}\right)} \quad \text{.....(4)}$$

where q_{m0} is the saturation capacity (maximum amount adsorbed) at the reference temperature T_0 and χ is a constant parameter. The exponent n of the Toth equation may take the following form as a function of temperature:

$$n = n_0 + \alpha\left(1-\frac{T_0}{T}\right) \quad \text{.....(5)}$$

where n_0 is the parameter n at the reference temperature T_0 and α is a constant parameter.[20]

Substituting Equations (3)-(5) into Equation (2) gives a 6-parameter Toth isotherm with temperature independence. The six parameters (B_0, Q, q_{m0}, χ, n_0, α) can be determined by nonlinear regression by using all the isotherm data obtained at several temperatures.

Models for mixed-gas adsorption are crucial to the design of adsorptive gas separation processes. They should be capable of predicting the equilibrium amount adsorbed from pure gas isotherms. Because of the scarcity of experimental data, none of the theories or models has been extensively tested.

The simplest theory for binary system is the Extended Langmuir model:[21]

$$\theta_A = \frac{q_A}{q_{mA}} = \frac{B_A P_A}{1 + B_A P_A + B_B P_B} \quad \text{.....(6)}$$

where subscripts A and B refer to gases A and B, respectively.

In the concentration pulse chromatographic technique, a pulse of the sample gas is injected into the carrier gas stream and passes through the column. The response of the

column to the injection is measured as concentration vs. time at the exit of the column. From this response peak a mean retention time of the sample, μ, defined as the first moment of the chromatogram, is determined experimentally.[14] Dimensionless Henry's Law constant, K, can be calculated from the corrected first moment of the response peak as follows:[9, 22-24]

$$\mu = \frac{\int_0^\infty c(t-\mu_D)dt}{\int_0^\infty cdt} = \frac{L}{v}\left[1+\frac{(1-\varepsilon)K}{\varepsilon}\right] \quad \text{.....(7)}$$

where t is the time, c is the adsorbate concentration measured at the outlet of the column, L is the column length, ε is the bed porosity, v is the interstitial fluid velocity, K is the dimensionless Henry's Law adsorption equilibrium constant, and μ_D is the corrected time due to the dead volume.

The dimensionless Henry's Law constants, K, can be converted to a dimensional form, K_p, as follows:[22]

$$K_p = \frac{K}{RT\rho_p} \quad \text{..... (8)}$$

where T is the absolute temperature, ρ_p is the density of the pellets of the adsorbent and K_p is the dimensional Henry's Law adsorption equilibrium constant.

The K_p value is related to the slopes of the isotherms of the components in the carrier gas mixture. For a binary mixture, the relationship is given as follows:[14]

$$K_p = (1-y_1)\frac{dq_1}{dP_1} + y_1\frac{dq_2}{dP_2} \quad \text{..... (9)}$$

Where $\frac{dq_1}{dP_1}$ and $\frac{dq_2}{dP_2}$ are the slopes of the adsorption isotherms for components 1 and 2, respectively.

This method allows for the experimental evaluation of the binary mixture isotherms when K_p values are determined for different concentrations of the carrier gas.[14]

For binary isotherms, both components in the mixed carrier gas are adsorbed and $\frac{dq_2}{dP_2}$ in the last term of Eq. (9) is not constant. The experimental K_p data represent the combined contribution of both components to the isotherms. The interpretation of the binary K_p data has been treated by several methods.[9, 13, 18, 25]

Three different K_p functional forms have been suggested in the literature to determine the binary isotherms. The most often used form is the 3rd degree polynomial:[9, 13, 15]

$$K_p = A_0 + A_1 y_1 + A_2 y_1^2 + A_3 y_1^3 \quad \text{..... (10)}$$

where the isotherm slopes are given by Eqs. (11) and (12);

$$\frac{dq_1}{dP_1} = B_0 + B_1 y_1 + B_2 y_1^2 \quad \text{..... (11)}$$

$$\frac{dq_2}{dP_2} = C_0 + C_1 y_1 + C_2 y_1^2 \quad \text{..... ....(12)}$$

The isotherm equations are found by the integration of Eqs. (11) and (12).

$$q_1 = \left(B_0 y_1 + \frac{B_1}{2} y_1^2 + \frac{B_2}{3} y_1^3 \right) \quad \text{.....(13)}$$

$$q_2 = \left[C_0 (1 - y_1) + \frac{C_1}{2} (1 - y_1^2) + \frac{C_2}{3} (1 - y_1^3) \right] \quad \text{.....(14)}$$

The following objective function is defined to minimize the sum of the square residuals (SSR) with respect to the experimental values, for the determination of B and C constants:

$$SSR = \sum_{y_1=0}^{y_1=1} \left(K_{P,Experiment} - K_{P,Equation} \right)^2 \quad \text{.....(15)}$$

It was noted that the end-points of the binary isotherms must coincide with the pure gas isotherms:

$$q_1(Binary)\big|_{y_1=1} = q_1(Pure)\big|_{P_{Total}} \quad \text{.....(16)}$$

$$q_2(Binary)\big|_{y_1=0} = q_2(Pure)\big|_{P_{Total}} \quad \text{.....(17)}$$

As no maximum should be seen in the isotherms,[26] so

$$\frac{dq_1}{dP_1} > 0 \quad \text{..... .....(18)}$$

$$\frac{dq_2}{dP_2} > 0 \quad \text{..... .....(19)}$$

By using these constraints to limit the objective function (Equation (15), a constrained nonlinear regression could be performed to determine constants B and C by defining the K curve from the RHS of Equation (9) and writing the slope of the binary isotherms in terms of these constants from Equations (11) and (12). The binary isotherms are then calculated by using Equations (13) and (14). This method, using Equation 10 for curve fitting the experimental data, is referred to as MVV-CPM (Modified Van der Vlist and Van der Meijden -Concentration Pulse Method).

For binary gas adsorption equilibrium, there are only a few published data.[27, 28] However, designing models and optimizing processes require accurate binary adsorption equilibrium data. Because of that, the thermodynamic consistency of experimental binary gas adsorption data and the predictive or correlative models should be checked before they are used for process design purposes.

Sircar et al. studied the thermodynamics of pure and binary gas adsorption systems using the Gibbsian surface excess (GSE) model.[29-31] The model can be differentiated or integrated using different thermodynamic paths in order to generate various thermodynamic consistency tests. The integral test requires the measurement of both pure gas adsorption isotherms and binary gas adsorption isotherms shown below:[28]

$$\left(-\int_0^P \frac{q_2^0}{P}dP\right)-\left(-\int_0^P \frac{q_1^0}{P}dP\right)=\int_0^1 \frac{q_1(1-y_1)-q_2y_1}{y_1(1-y_1)}dy_1 \quad \text{.....(20)}$$

where q^0_1 and q^0_2 are the amount adsorbed of Components *1* and *2* respectively in the pure gas systems, P is both the pressure of pure gas systems and the total pressure of the binary system, q_1 and q_2 are the amounts adsorbed of Components *1* and *2*, respectively in the binary system, y_1 is the mole fraction of Component 1 in the binary system. The two terms of the left side are the potentials of adsorption at P and T for pure gases 2 and 1, respectively. The quantity on the left side at any given value of P and T can be evaluated from the pure gas adsorption isotherms of the components of a binary gas mixture. The quantity on the right side at any given value of P and T can be evaluated using the binary gas adsorption isotherm at constant P and T. These two independently measured quantities form the basis for the integral consistency test between pure and binary gas equilibrium adsorption data.

The details of volumetric system, concentration pulse chromatography unit, adsorbent and numerical methods are given in our earlier paper.[32] The sample gases used in the experiments are listed in Table 6.1.

It is noted that the values of adsorbed loading obtained from experiments were corrected taking into account that generally the binder has little adsorption capacity as literature data are mostly obtained with silicalite crystals, without binder.

RESULTS AND DISCUSSION

Equilibrium isotherm data and corresponding Toth isotherm model fits for CH_4 and N_2 with silicalite pellets had been obtained at three different temperatures for pressures up to 5 atm in our previous work and are given in Figure 6.1.[33, 34] Experimental data are given as data points and Toth isotherm models are shown as curves in this figure. All the values of adsorbed loading obtained from experiments in this work were corrected taking into account that generally the binder has little adsorption capacity as literature data are mostly obtained with silicalite crystals, without binder.

For useful description of adsorption equilibrium data at various temperatures, the temperature independent form of the Toth equation was used. For the purpose of extension of the data to other temperatures and pressures, from the curve regressions with the temperature independent Toth model, the relevant parameters for estimation are obtained. From the parameters, the ranges of temperature and pressure were extrapolated and interpolated to estimate the adsorption behaviour at other temperatures and pressures without experimental data.

For an economic separation process, an adsorbent should have high selectivity and capacity. For comparing selectivity, it is convenient to define adsorption separation factor:

$$\alpha_{A/B} = \frac{x_A / x_B}{y_A / y_B} \quad \text{..... (21)}$$

where x_A, x_B, y_A, and y_B are the mole fractions of components A and B in adsorbed and fluid phases at equilibrium, respectively. If the isotherms are linear or pressure is small enough for the isotherms to keep in the linear range, ideally, the separation factor is given simply by the ratio of the amounts adsorbed for pure components:

$$\alpha_{i.A/B} = \frac{q_A}{q_B} \quad \text{.....(22)}$$

where q_A and q_B are the amounts adsorbed of components *A* and *B*. These equilibrium separation factors are shown as a function of pressure and temperature in Figure 6.2. According to the results, both pressure and temperature are very important for the separation. In general, separation factors increase with decreasing pressure and/or temperature. It is difficult to separate the system at high temperature and/or high pressure. Pressure influences the separation factors more at low temperatures than at high temperatures; however temperature affects the separation factors more at low pressures than at high pressures.

In general, it is difficult to separate CH_4/N_2 if the separation factor is smaller than 3. For this separation, the operating conditions need to be controlled at low temperatures and pressures. PSA or TSA process can be selected. In a PSA process, it can be done at room temperature and in the range of pressure between 0.1 and 3 atm. If the conditions are such that the temperature is higher than 100 °C and/or the pressure higher than 3 atm, the separation is impossible. For a TSA process, it can be done under vacuum at low temperature.

After regenerating the adsorbent, the binary isotherms were determined by increasing the CH_4 mole fraction in CH_4-N_2 carrier gas from 0% up to 100%. The samples were injected after attaining equilibrium at each concentration change for various compositions of carrier gas. Equilibrium of the mixture with the adsorbent was confirmed by noting that the baseline of GC would be steady as equilibrium was approached. The results of the series of runs of the binary study are shown with MVV-CPM with error bars in Figure 6.3, where all the end-points of the binary isotherms were combined and fit to the Toth isotherms of pure gases by the volumetric method.

For estimating and comparing the quality of the non-linear regressions from the three concentration pulse methods we used: MVV-CPM (Modified Van der Vlist and Van der Meijden - Concentration Pulse Method), HT-CPM (Harlick and Tezel - Concentration Pulse Method) and the MTT-CPM (Modified Triebe and Tezel - Concentration Pulse Method), the RMS (root mean square) deviations are obtained. In comparison with the isotherms from the three methods, all the isotherms obtained by MVV-CPM, HT-CPM and the MTT-CPM

match the experimental data very well as there is a rather small difference in the adsorption capacities of the two components in the binary systems so all the three models can be used to describe these systems. Among them, the MVV-CPM is the best one although it cannot be used for the systems with big difference in the adsorption capacities of the two components in the binary systems;[33] therefore, the MVV-CPM was used to describe these systems for our further study in this paper. The parameters for MVV-CPM are listed in Table 6.2.

The experimental binary isotherms for CH_4 - N_2 with silicalite were obtained at three temperatures and are given in Figures 6.4 - 6.6. When y_{CH4} increases, the CH_4 adsorption capacity, q_{CH4}, increases and the N_2 adsorption capacity, q_{N2}, decreases as expected. At 40 °C, the total adsorbed capacity, q_{total}, increases with y_{CH4} as the increase of q_{CH4} is larger than the decease of q_{N2}. At 70 or 100°C, q_{total} has a minimum when y_{CH4} is in the range between 0.2 and 0.4. At the beginning, the increase of q_{CH4} is less than the decease of q_{N2}, and then after the minimum of the total adsorbed capacity, the increase of q_{CH4} is larger than the decease of q_{N2}. Additionally, at the minimum, the drop of q_{total} is smaller at 70 °C than at 100°C. Therefore, it is noted that the drop of q_{total} decreases with temperature in a range of temperature and there is no drop after temperature drops down to a specific one between 40 and 70 °C. Besides, q_{CH4}, q_{N2} *and* q_{total} increase with temperatures decreasing since adsorption is exothermic, so temperature is a very important factor to separate this system. For practical applications, we can control the separation process at low adsorption temperature to attain good capacity.

In the literature, Harlick and Tezel[8] did research on the experimental binary isotherms for CH_4 - N_2 for ZSM-5-280 at 40 °C under the same conditions. Silicalite and ZSM-5 have the same structure. However, their ZSM-5 adsorbents had different Si/Al ratios indicated by the last number in the code of the adsorbent: 280. In the present study, silicalite adsorbent has a Si/Al ratio in the thousands. From both results, a competitive adsorption behavior can be seen. The slopes of the binary isotherms are rather high when y_{CH4} is very low, and then the slopes decrease with increasing y_{CH4}. This suggests that the two adsorbates are attempting to occupy the same active adsorption site.

To predict the adsorption behavior of the binary system from pure gas systems, we tried six models: Extended Langmuir, Extended Dualsite Langmuir, Ideal Adsorbed Solution Theory, Statistical Model, Flory-Huggins of Vacancy Solution Theory and

Extended Sips. They have considerable differences with the real binary system. None of the models predict the binary adsorption behavior completely as same as the work of Harlick and Tezel.[8] Therefore, all the six models cannot describe the real binary system accurately and they can be used only for rough estimation for the binary system when there are no binary data. In Figures 6.4 – 6.6, experimental binary isotherms are compared with their counterparts redicted by the Statistical Model isotherms. As can be seen from these comparisons, the isotherms over predict the real ones at all temperatures studied.

The phase diagrams at different temperatures were determined from the experimental binary isotherms and are shown in Figure 6.7, together with comparison with the predictions from the Statistical Model isotherms. The selectivity decreases with increasing temperature when y_{CH4} is small while it increases with increasing temperature when y_{CH4} is high. Within the temperature range studied, separation can be performed since the curves are far away from the 45° line. Realistic experimental data gave better separation than Statistical Model predicted under comparable conditions. For comparison with others, we searched the literature. However, no other binary phase diagrams were found for the separation of methane and nitrogen.

According to Equation (21), the equilibrium separation factor at three temperatures can be plotted against y_1 and is shown in Figure 6.8. The equilibrium separation factor has a maximum in the range of y_{CH4} between 0.5 and 0.6, where selectivity is good and increases with temperature. In the range of our study, the highest equilibrium separation factor is 11.6 at 100°C and y_{CH4}=0.58.

When the experimental separation factors are compared to the ones predicted from the pure component data, it was observed that the experimental separation factors from actual binary behaviour are much better, as can be seen from Figure 6.8. When the compositions approach pure systems (mole fractions 0 or 1), predicted separation factors are close to actual ones. At that time, predicted separation factors can be used to do rough estimations if experimental binary data do not exist.

For real applications, y_{CH4} is around 0.8. Around that composition range, selectivity increases with increasing temperature and with decreasing y_{CH4} and the equilibrium separation factor is in the range between 4 and 6, giving good selectivity. Sheikh et al.[3] studied the adsorption isotherms on a new high specific area active carbon Maxsorb and

obtained 3 for equilibrium separation factor from volumetric and chromatographic methods at 300K up to a pressure of 550 kPa predicted from pure systems for methane and nitrogen. Cavenati et al.[4] obtained 1.9 of the kinetic separation factor on Carbon Molecular Sieve CMS 3K under 250kPa at 308 K and y_{CH4}=0.57 for this separation. Harlick and Tezel[8] studied the binary system of CH_4/N_2 with ZSM-5-280 as the adsorbent at 40 ^{0}C and 1 atm total pressure by HT-CPM. Based on their data, when separation factor was calculated at y_{CH4}=0.8, a value of 2.9 was obtained, which is lower than the values obtained with silicalite in this work. It is interesting to note that although the individual amounts adsorbed for both of the adsorbates were higher for ZSM-5-280, the separation factors were lower. It is noted that silicalite and ZSM-5 have the same crystalline structure. Harlick and Tezel's ZSM-5 adsorbent had the Si/Al ratio indicated by the last number in the code of the adsorbent: 280. In the present study, silicalite adsorbent has a Si/Al ratio in the thousands. Since the only difference between the adsorbent studied in this work and Harlick and Tezel's adsorbent was the Si/Al ratio, it was concluded that a higher Si/Al ratio gives better selectivity for this system

Because of low selectivities of existing membranes toward CH_4/N_2, the main technology available for CH_4/N_2 separation is only adsorption.[35]

According to Equation (20), the integral thermodynamic consistency test between pure and binary equilibrium adsorption data is shown in Table 6.3. For the binary systems, the integrands of the right side as functions of y_i can be plotted and the areas under these curves between y_i = 0 and y_i = 1 are listed. For pure systems, the integrands of the left side as functions of P can be plotted and the areas under these curves between P = 0 and P = 1 atm. are listed. It should be pointed out that the ranges of pressure of the pure systems are the same as the ranges of the partial pressures of the two components as the total pressure of binary system is 1 atm.

In Table 6.3, it can be seen that the integral thermodynamic consistency test is obeyed fairly well by the binary CH_4-N_2 adsorption data on silicalite at 40 °C and 70 °C, and gets worse at 100 °C. Therefore, the binary CH_4-N_2 adsorption data on silicalite at low temperature satisfy the integral thermodynamic consistency test fairly well. This consistency becomes worse as temperature increases. In addition, the results of the integral thermodynamic consistency test match the results of predicting the adsorption behavior of

the binary system from pure gas systems in Figures 6.4 – 6.6 very well. At low temperature, the thermodynamic consistency is good, so the difference of predicting the adsorption behavior of the binary system from pure gas systems is small; at high temperature, the thermodynamic consistency is not satisfied, so the difference of predicting the adsorption behavior of the binary system from pure gas systems is large or it is impossible to predict the adsorption behavior of the binary system from pure gas systems accurately. Thus, it is recommended that one key requirement for predicting the adsorption behavior of the binary system from pure gas systems is that they satisfy the integral thermodynamic consistency tests between pure and binary gas adsorption equilibria. Moreover, these data sets can be used to prove the validity of predictive or correlative binary equilibrium models. Based on the results obtained in this study, silicalite is an excellent adsorbent for the separation of methane and nitrogen. The separation factors are much better than the ones obtained in the literature for real industrial applications. When y_{CH4} is about 0.8, the separation factors (4-6) are high enough so that the separation of CH_4/N_2 binary system will be possible with silicalite as the adsorbent in the range of temperature at 40-100^{0}C. When y_{CH4} is about 0.58, the separation factors go up to the maximum. In particular, the separation factor is 11.6 at 100^{0}C and y_{CH4}=0.58. This separation factor may be increased further when temperature is increased and/or total pressure is changed.

CONCLUSIONS

1. Temperature independent Toth model is a useful model for extrapolation and/or interpolation to predict separations at other temperatures and pressures.
2. Among concentration pulse chromatographic methods, the MVV-CPM is good for the separation of CH_4-N_2 on silicalite.
3. q_{CH4}, q_{N2} and q_{total} increase with temperatures decreasing, so temperature is a very important factor for us to separate this system.
4. For predicting the real binary system of CH_4/N_2, the six predicted models cannot describe the real binary system accurately and they can be used only at low temperature or for rough estimation when the binary data are not available.
5. The selectivity has a maximum in the range of y_{CH4} between 0.5 and 0.6 for the CH_4-N_2 binary system on silicalite. At the maximum, the selectivity increases with temperature and it is satisfactory at 100 °C.
6. For real applications, the selectivity increases with increasing temperature and with decreasing y_{CH4}.
7. The CH_4-N_2 binary adsorption data on silicalite at low temperature satisfy the integral thermodynamic consistency test fairly well. The thermodynamic consistency is less satisfactory as temperature increases.
8. For real applications, the separation factors are satisfactory with silicalite. When y_{CH4} is about 0.8, the separation factors are 4-6 in the range of temperature between 40-100^{0}C.
9. In the range of our study, the highest equilibrium separation factor is 11.6 at 100^{0}C and y_{CH4}=0.58.

ACKNOWLEDGMENTS

Financial supports received from the Natural Sciences and Engineering Research Council of Canada (NSERC), the Ontario Graduate Scholarship (OGS) Program, and the Canadian Society for Chemical Engineering (CSChE) are gratefully acknowledged.

NOMENCLATURE

B = adsorption affinity constant, usually atm^{-1} (units depending on models)

B_0 = adsorption affinity constant at some reference temperature, atm^{-1}

B_1 = adsorption affinity constant in Site 1, atm^{-1}

B_2 = adsorption affinity constant in Site 2, atm^{-1}

K = dimensionless Henry's law constant, dimensionless

K_P = dimensional Henry's law constant, mmole. $g^{-1}.atm^{-1}$

k = Freundlich adsorption coefficient, $mmol.g^{-1}.atm^{-1/n}$

n = adsorption exponents or number of actives sites, dimensionless

n_0 = adsorption exponents at some reference temperature, dimensionless

P = (total) pressure, atm

Q = isosteric heat, $J.mol^{-1}$

P_1 = pressure of Component *1*, atm

P_2 = pressure of Component *2*, atm

P_A = pressure of Component *A*, atm

P_B = pressure of Component *B*, atm

q = amount adsorbed, $mmol.g^{-1}$

q_A = amount adsorbed of Component *A*, $mmol.g^{-1}$

q_B = amount adsorbed of Component *B*, $mmol.g^{-1}$

q_1 = amount adsorbed of Component *1*, $mmol.g^{-1}$

q_2 = amount adsorbed of Component *2*, $mmol.g^{-1}$

q^0_1 = amount adsorbed of Component *1* in pure system, $mmol.g^{-1}$

q^0_2 = amount adsorbed of Component *2* in pure system, $mmol.g^{-1}$

q_m = adsorption saturation capacity or maximum amount adsorbed, $mmol.g^{-1}$

q_{m0} = adsorption saturation capacity or maximum amount adsorbed at some reference temperature, $mmol.g^{-1}$

q_{m1} = adsorption saturation capacity or maximum amount adsorbed in Site 1, $mmol.g^{-1}$

q_{m2} = adsorption saturation capacity or maximum amount adsorbed in Site 2, $mmol.g^{-1}$

R = gas constant, 8.314 $J.K^{-1}.mol^{-1}$

T = temperature, K

T_0 = reference temperature, K

x = mole fraction in adsorbed phase at equilibrium, dimensionless

x_A = mole fraction of Component *A* in adsorbed phase at equilibrium, dimensionless

x_B = mole fraction of Component B in adsorbed phase at equilibrium, dimensionless

y = mole fraction in fluid phase at equilibrium, dimensionless

y_A = mole fraction of Component *A* in fluid phase at equilibrium, dimensionless

y_B = mole fraction of Component B in fluid phase at equilibrium, dimensionless

y_1 = mole fraction of Component 1 in fluid phase at equilibrium, dimensionless

Greek letters

α = adsorption constant, adsorption separation factor, dimensionless

$\alpha_{A/B}$ = adsorption separation factor (the ratio of Component A over Component B), dimensionless

$\alpha_{i,A/B}$ = ideal adsorption separation factor (the ratio of Component A over Component B), dimensionless

θ = fraction of monolayer coverage, dimensionless

χ = constant parameter, dimensionless

Abbreviations

CPM = concentration pulse method

GHG = greenhouse gases

GSE = Gibbsian surface excess

GWP = greenhouse warming potential

LFG = landfill gas

PSA = pressure swing adsorption

RMS = root mean square

SSR = sum of the square residuals

TCD = thermal conductivity detector

TSA = temperature swing adsorption

VST = vacancy solution theory

LITERATURE CITED

(1) Cavenati, S.; Grande, C. A.; Rodrigues, A. E. Adsorption Equilibrium of Methane, Carbon Dioxide, and Nitrogen on Zeolite 13X at High Pressures. *Journal of Chemical and Engineering Data.* **2004**, *49*, 1095-1101.

(2) Cavenati, S.; Grande, C. A.; Rodrigues, A. E. Upgrade of Methane from Landfill Gas by Pressure Swing Adsorption. *Energy and Fuels.* **2005**, *19*, 2545-2555.

(3) Sheikh, M. A.; Hassan, M. M.; Loughlin, K. F. Adsorption Equilibria and Rate Parameters for Nitrogen and Methane on Maxsorb Activated Carbon. *Gas Separation and Purification.* **1996**, *10*, 161-168.

(4) Cavenati, S.; Grande, C. A.; Rodrigues, A. E. Separation of Methane and Nitrogen by Adsorption on Carbon Molecular Sieve. *Separation Science and Technology*, **2005**, *40*, 2721–2743.

(5) Jayaramana, A.; Hernandez-Maldonadoa, A. J.; Yanga, R. T.; Chinnb, D.; Munsonb, C. L.; Mohrb, D. H. Clinoptilolites for Nitrogen/Methane Separation. *Chemical Engineering Science.* **2004**, *59*, 2407 – 2417.

(6) Warmuzinski, K.; Sodzawiczny, W. Effect of Adsorption Pressure on Methane Purity during PSA Separations of CH4/N2 Mixtures. *Chemical Engineering and Processing.* **1999**, *38*, 55–60.

(7) Dong, F.; Lou, H.; Kodama, A.; Goto, M.; Hirose, T. The Petlyuk PSA Process for the Separation of Ternary Gas Mixtures: Exemplification by Separation a Mixture of CO_2-CH_4-N_2. *Separation and Purification Technology.* **1999**, *16*, 159-166.

(8) Harlick, P. J. E.; Tezel, F. H. Adsorption of Carbon Dioxide, Methane and Nitrogen: Pure and Binary Mixture Adsorption for ZSM-5 with SiO_2 / Al_2O_3 ratio of 280. *Separation and Purification.* **2003**, *33*, 199-210.

(9) Harlick, P. J. E.; Tezel, F. H. A Novel Solution Method for Interpreting Binary Adsorption Isotherms from Concentration Pulse Chromatography Data. *Adsorption.* **2000**, *6*, 293–309.

(10) Karger, J.; Ruthven, D. M. Diffusion in Zeolites and Other microporous Solids. John Wiley and Sons Inc., New York, NY. **1992**, pp. 467-512.

(11) Lewis, W. K.; Gilliland, E. R.; Chertow, B.; Cadogan, W. P. Absorption Equilibria: Hydrocarbon Gas Mixtures. *Industrial and Engineering Chemistry*, **1951**, *42*, 1319-1326.

(12) Yang, R. T. Gas Separation by Adsorption Process. Butterworth Publishers, Stoneham, MA. **1987**. pp. 9-338.

(13) Van der Vlist, E.; Van der Meijden, J. Determination of the Adsorption Isotherms of the Components of Binary Gas Mixtures by Gas Chromatography. *Journal of Chromatography.* **1973**, *79*, 1-13.

(14) Shah, D. B.; Ruthven, D. M. Measurement of Zeolite Diffusivities by Chromatography. *AIChE Journal.* **1977**, *23*, 804-810.

(15) Tezel, F. H.; Tezel, H. O.; Ruthven, D.M. Determination of Pure and Binary Isotherms for Nitrogen and Krypton. *Journal of Colloid and Interface Science*. **1992**, *149*, 197-207.

(16) Heslop, M. J.; Buffman, B. A.; Mason, G. A Test of the Polynomial-Fitting Method of Determining Binary-Gas-Mixture Adsorption Equilibria. *Industrial and Engineering Chemistry Research*. **1996**, *35*, 1456–1466.

(17) Kabir, H.; Grevillot, G.; Tondeur, D. Equilibria and Activity Coefficients for Non-Ideal Adsorbed Mixtures from Perturbation Chromatography. *Chemical Engineering Science*. **1998**, *53*, 1639–1654.

(18) Harlick, P. J. E.; Tezel, F. H. CO_2-N_2 and CO_2-CH_4 Binary Adsorption Isotherms with H-ZSM-5: the Importance of Experimental Data Regression with the Concentration Pulse Method. *The Canadian Journal of Chemical Engineering*. **2001**, *79*, 236-245.

(19) Langmuir, I. The Adsorption of Gases on Platine Surfaces Glass Mica and Platinum. *Journal of the American Chemical Society*. **1918**, *40*, 1361-1403.

(20) Do, D. D. Adsorption Analysis: Equilibria and Kinetics. Imperial College Press, London, UK. **1998** pp. 1-148.

(21) Markham, E. C.; Benton, A. F. The Adsorption of Gas Mixtures by Silica. *Journal of American Chemical Society*, **1931**, *53*, 497-507.

(22) Li, P.; Tezel, F. H. Equilibrium and Kinetic Analysis of CO_2-N_2 Adsorption Separation by Concentration Pulse Chromatography. 40th IUPAC Congress, Beijing, P. R. China. **2005**, p61, 1-O-034.

(23) Li, P.; Tezel, F. H. Adsorption Separation of N_2, O_2, CO_2 and CH_4 Gases by β-Zeolite. Microporous & Mesoporous Materials. **2007**, *98*, 94-101.

(24) Li, P.; Tezel, F. H.; Chung, T-S N.; Kulprathipanja, S. Analysis of Adsorption Parameters by Concentration Pulse Chromatography. 55th Canadian Chemical Engineering Conference, Toronto, Canada. **2005**, 593.

(25) Triebe, R. W.; Tezel, F. H. Adsorption of Nitrogen and Carbon Monoxide on Clinoptilolite: Determination and Prediction of Pure and Binary Isotherms. *The Canadian Journal of Chemical Engineering*. **1995**, *73*, 717-724.

(26) Calleja, G.; Pau, J.; Calles, J. A. Pure and Multicomponent Adsorption Equilibrium of Carbon Dioxide, Ethylene and Propane on ZSM-5 Zeolites with Different Si/Al Ratios. *Journal of Chemical and Engineering Data*. **1998**, *43*, 994–1003.

(27) Valenzuela, D. P.; Myers, A. L. Adsorption Equilibrium Data Book. Prentice Hall, Englewood Cliffs, NJ. **1989**.

(28) Rao, M. B.; Sircar, S. Thermodynamic Consistency for Binary Gas Adsorption Equilibria. *Langmuir*. **1999**, *15*, 7258-7267.

(29) Sircar, S. Excess Properties and Thermodynamics of Multicomponent Gas Adsorption. *J. Chem. SOC., Faraday Trans. I*. **1985**, *81*, 1527-1540.

(30) Sircar, S. R&D Note: Data Representation for Binary and Multicomponent Gas Adsorption Equilibria. *Adsorption*. **1996**, *2*, 327-330.

(31) Sircar, S.; Rao, M. B. Heat of Adsorption of Pure Gas and Multicomponent Gas Mixtures on Microporous Adsorbents, In Surfaces of Nanoparticles and Porous Materials. J. A. Schwarz and C. Contescu Eds. Marcel Dekker, New York, NY. **1998**, Chapter 19, pp 501-528.

(32) Li, P.; Tezel, F. H. Adsorption Separation of Methane and Carbon Dioxide on Silicalite. submitted to be published in *Separation Science and Technology*. **2007**.

(33) Li, P.; Tezel, F. H. Adsorption Separation of Methane and Carbon Dioxide from Landfill Gas. AIChE Annual Meeting, San Francisco, USA. **2006**.

(34) Li, P.; Tezel, F. H. Pure and Binary Adsorption Equilibria of Carbon Dioxide and Nitrogen on Silicalite. submitted to be published in *Journal of Chemical and Engineering Data*. **2007**.

(35) Tabe-Mohammadi, A. A Review of the Applications of Membrane Separation Technology in Natural Gas Treatment. *Separation Science and Technology*. **1999**, *34*, 2095-2111.

Table 6.1. Details of the gases used.

Gases	Grade	Purity	Supplier
CH_4	Ultra High Purity 3.7	99.97%	Praxair Inc., Ottawa
N_2	Ultra High Purity 5.0	99.999%	Praxair Inc., Ottawa
He	Uitra High Purity 5.0	99.999%	Praxair Inc., Ottawa

Table 6.2. Parameters of MVV-CPM for CH_4 - N_2 with silicalite.

CPM Methods	Parameters	Units	40 °C	70 °C	100 °C
MVV-CPM	B_0	mmole. g^{-1}	0.6972	0.3740	0.2251
	B_1	mmole. g^{-1}	-1.2183	-0.8601	-0.7692
	B_2	mmole. g^{-1}	1.4179	1.3033	1.3420
	C_0	mmole. g^{-1}	0.5892	0.6029	0.5320
	C_1	mmole. g^{-1}	-1.4487	-1.6731	-1.5148
	C_2	mmole. g^{-1}	1.0318	1.1905	1.0617

Table 6.3. The integral thermodynamic consistency test between pure and binary methane (1) – nitrogen (2) equilibrium adsorption data on silicalite using Equation (20)

Temperature	°C	39.1	69.4	99.8
RHS: $\int_0^1 \frac{q_1(1-y_1)-q_2 y_1}{y_1(1-y_1)} dy_1$	$mmol.g^{-1}$	0.4170	0.2283	0.1404
1st term in LHS: $\int_0^1 \frac{q_1^0}{P} dP$	$mmol.g^{-1}$	0.6456	0.4036	0.3138
2nd term in LHS: $\int_0^1 \frac{q_2^0}{P} dP$	$mmol.g^{-1}$	0.2200	0.1671	0.1298
LHS: $\int_0^1 \frac{q_1^0}{P} dP - \int_0^1 \frac{q_2^0}{P} dP$	$mmol.g^{-1}$	0.4256	0.2365	0.1841
$\left\lvert \frac{LHS-RHS}{RHS} \right\rvert$	%	2.07	3.65	31.15

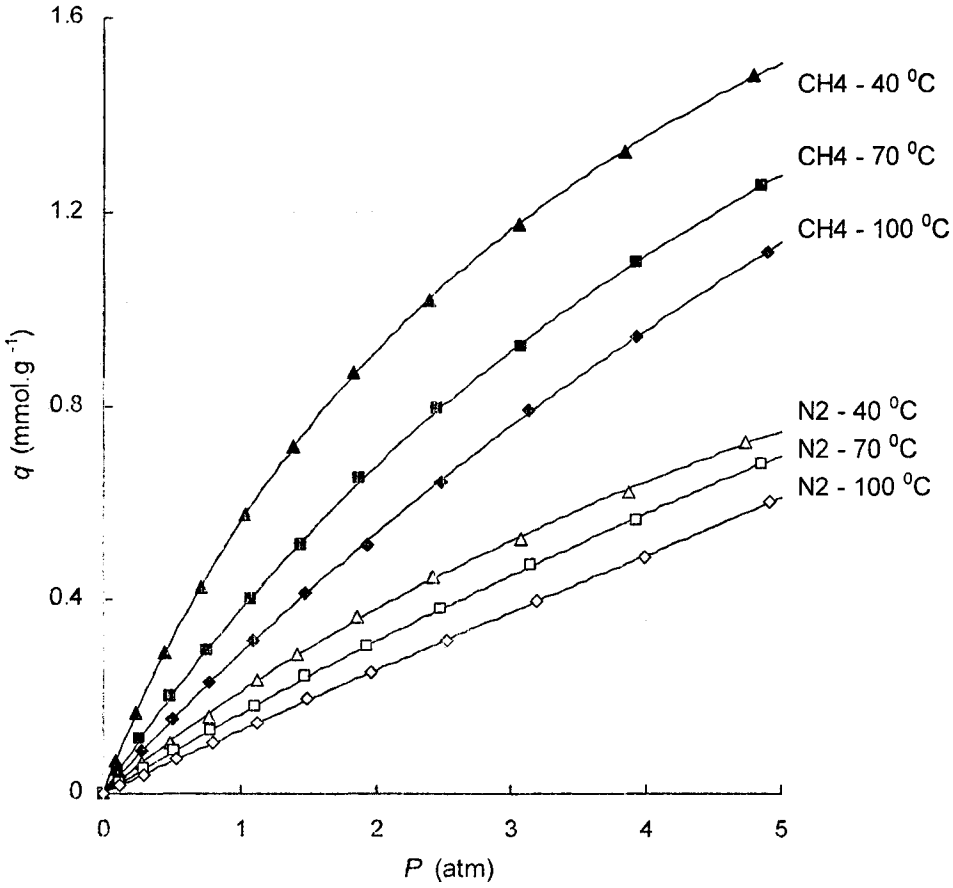

Figure 6.1. Isotherms for CH_4 and N_2 on silicalite:

The points are experimental data and the curves are Toth isotherm models

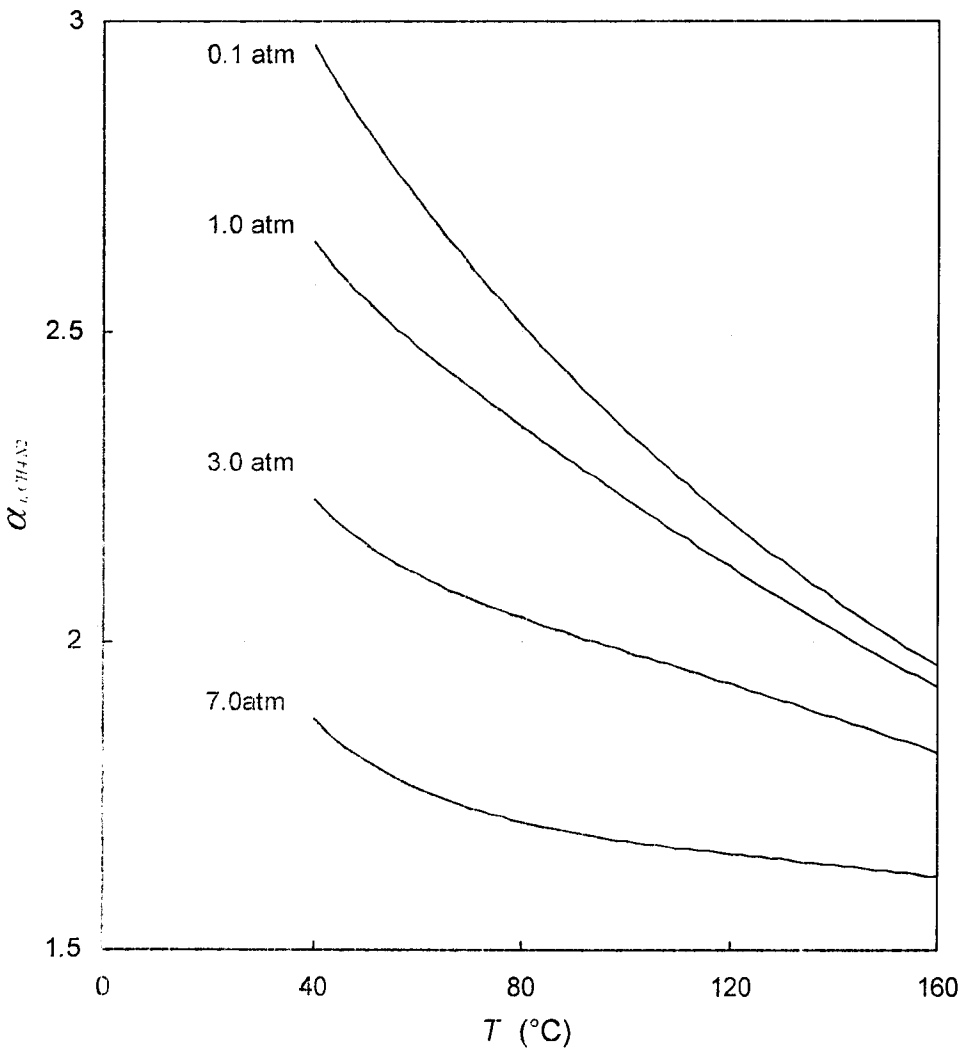

Figure 6.2. Ideal separation factors for CH_4/N_2 on silicalite from pure component data.

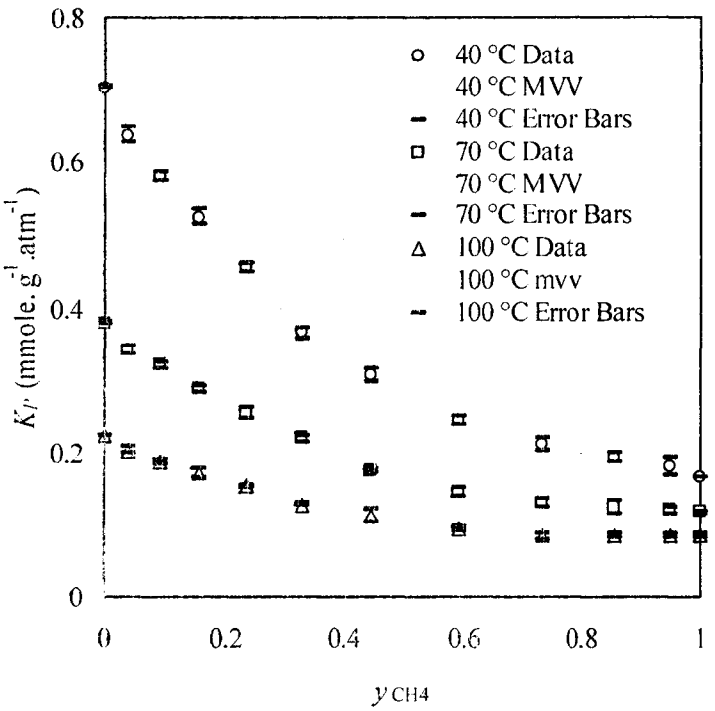

Figure 6.3. Regressions for CH_4/N_2, binary K_p with silicalite by MVV-CPM at different carrier gas compositions at 1atm total pressure

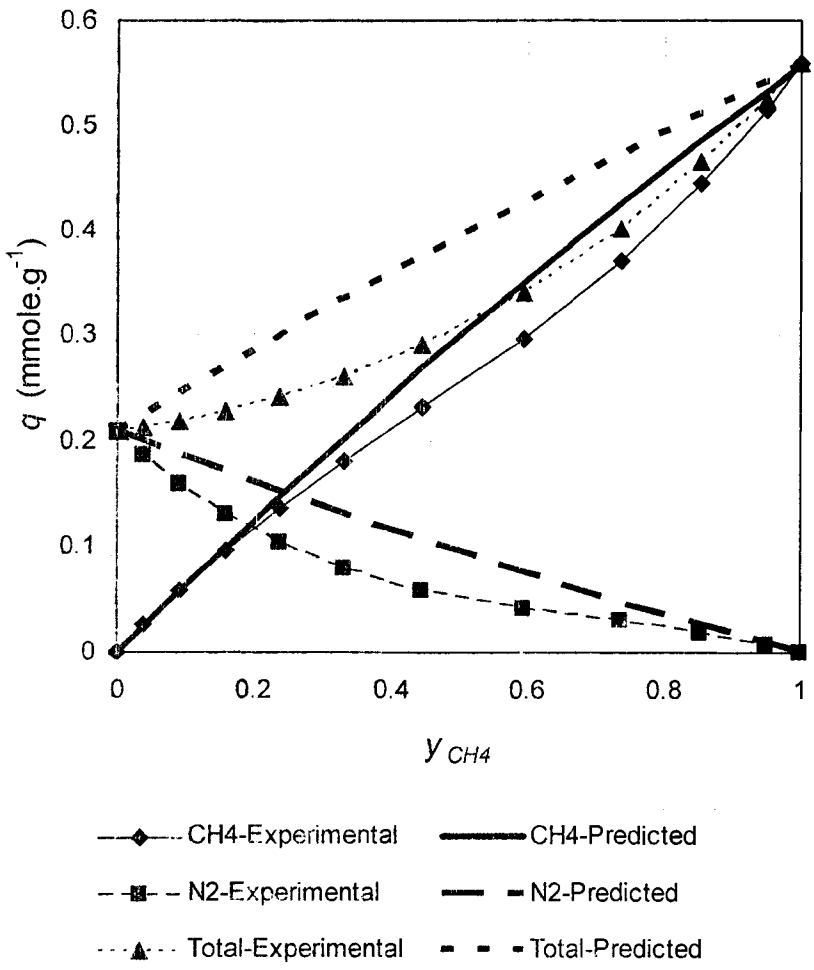

Figure 6.4. CH_4/N_2, binary Isotherms with silicalite at 40 °C and at 1atm total pressure: experimental by MVV-CPM and predicted by Statistical Model

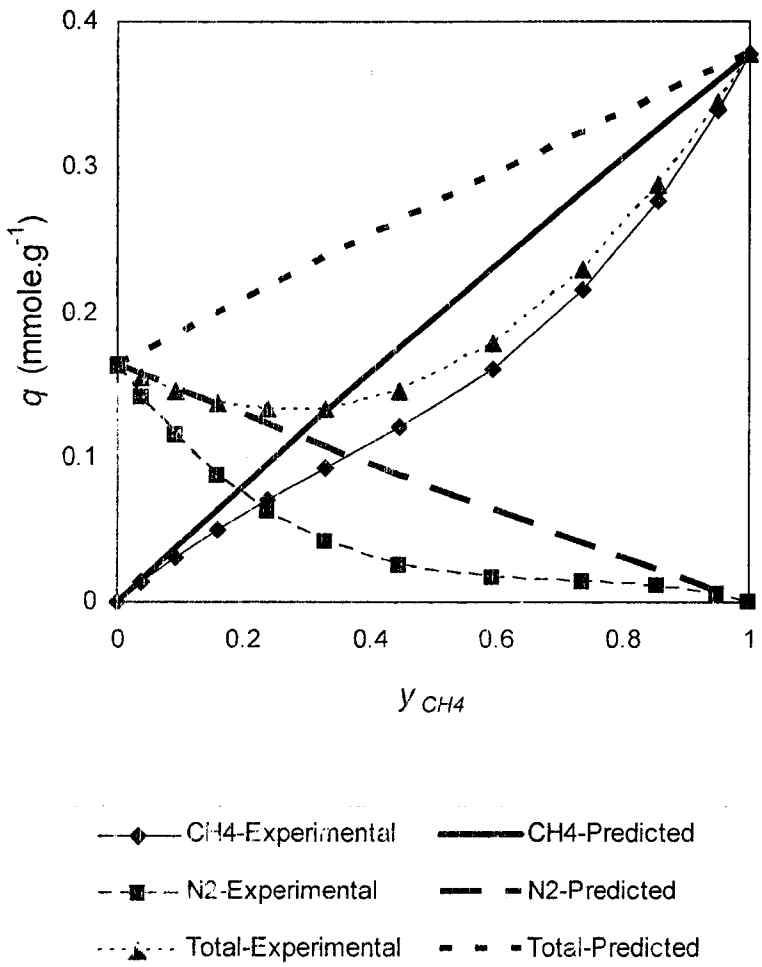

Figure 6.5. CH_4/N_2, binary Isotherms with silicalite at 70 °C and at 1atm total pressure: experimental by MVV-CPM and predicted by Statistical Model

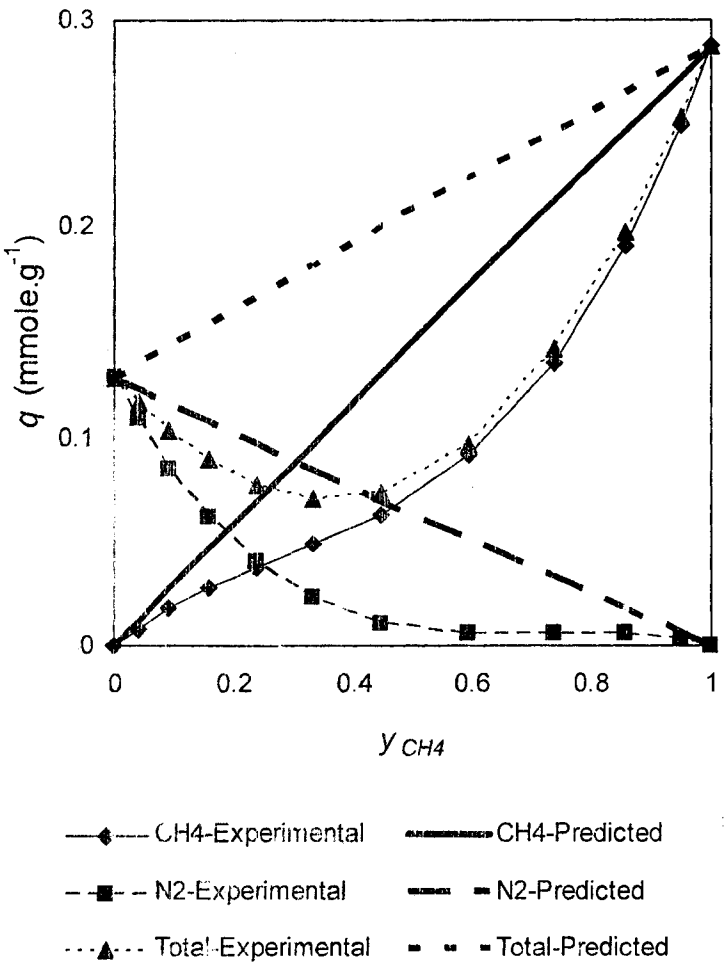

Figure 6.6. CH_4/N_2, binary Isotherms with silicalite at 100 °C and at 1atm total pressure: experimental by MVV-CPM and predicted by Statistical Model

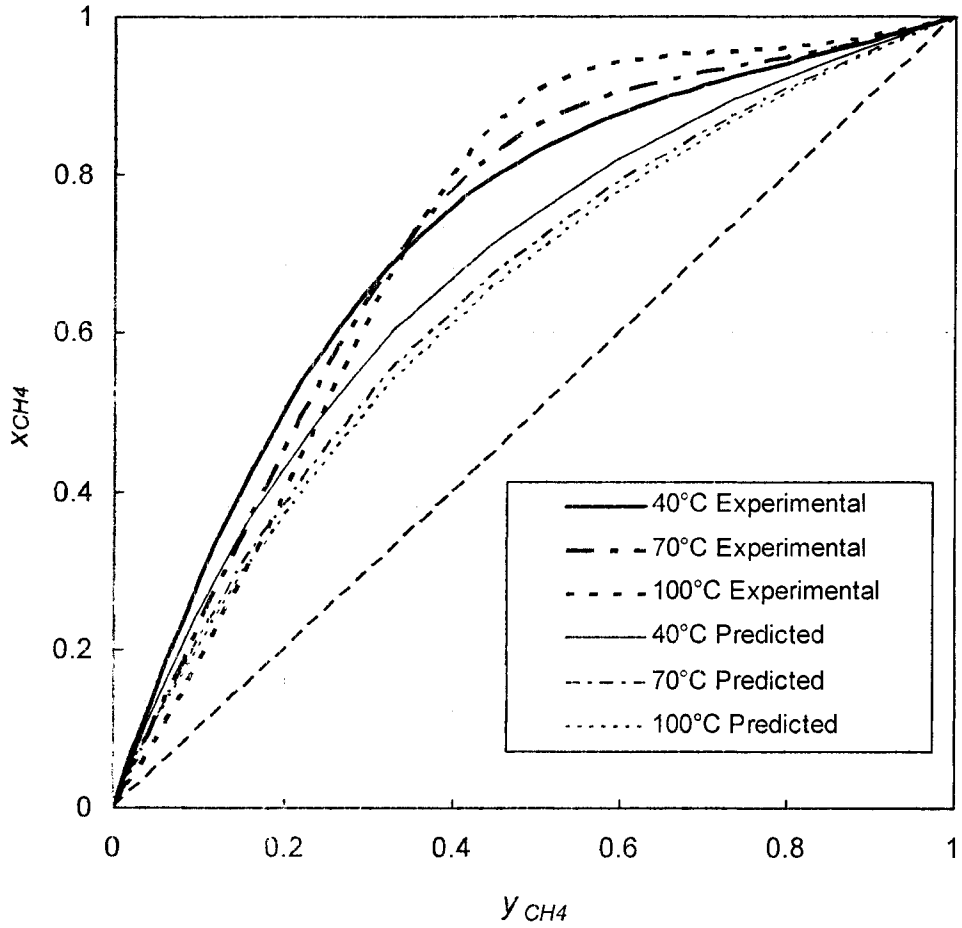

Figure 6.7. x – y diagrams for CH_4/N_2 binary system with silicalite at 1 atm total pressure: experimental and predicted by Statistical Model

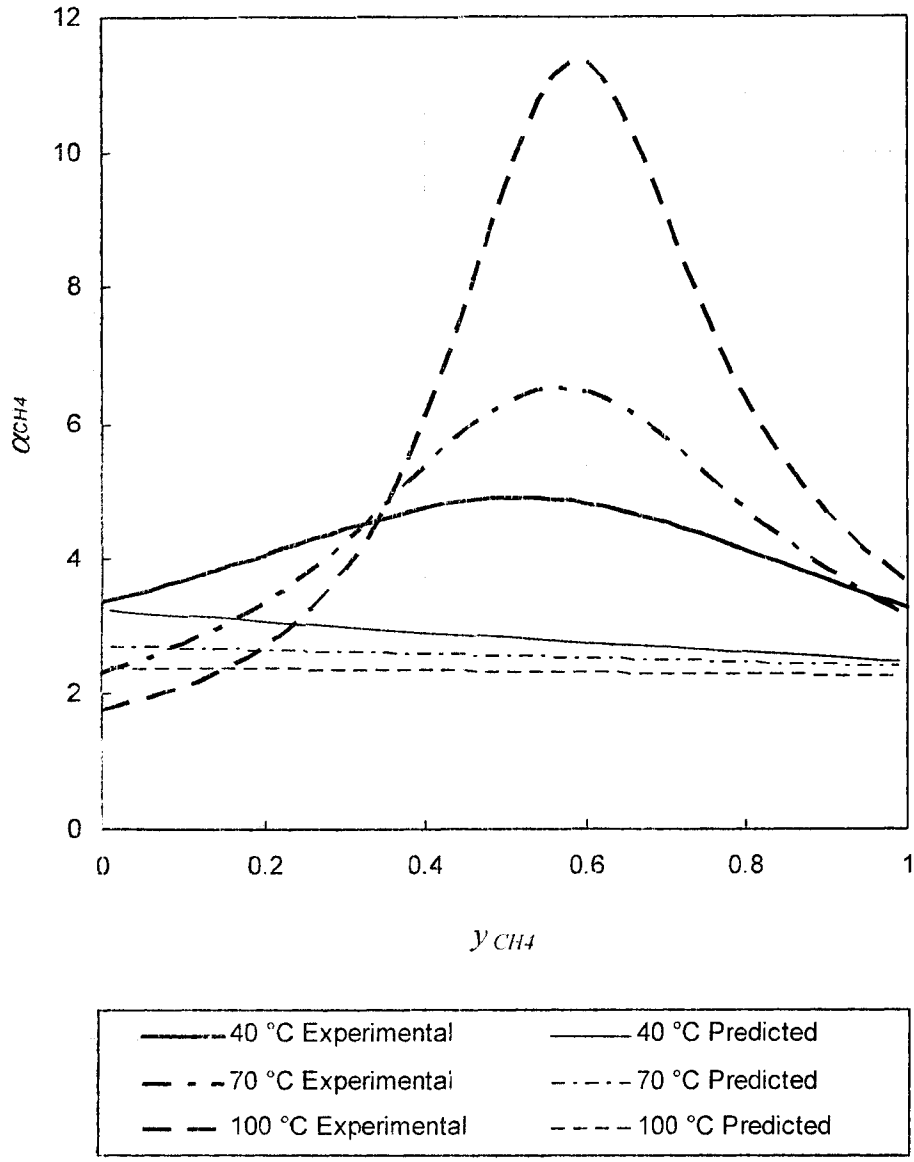

Figure 6.8. Equilibrium separation factor curves for CH_4/N_2 binary system: Experimental by MVV-CPM and predicted from pure component systems

CHAPTER VII

PARAMETRIC ANALYSIS OF ADSORPTION SEPARATION PROCESSES FOR CARBON DIOXIDE / METHANE, CARBON DIOXIDE / NITROGEN AND METHANE / NITROGEN IN SILICALITE

Peiyuan Li and F. Handan Tezel*

Department of Chemical Engineering
Faculty of Engineering
University of Ottawa
161 Louis Pasteur, Ottawa, Ontario K1N 6N5, Canada

* Corresponding author
Tel: 613-562-5800 Ext. 6099
Fax: 613-562-5172
Emai: Handan.Tezel@uottawa.ca

ABSTRACT

Adsorption separation of typical CO_2/CH_4, CO_2/N_2 and CH_4/N_2 gas mixtures were considered for landfill gas, natural gas and flue gas applications with using silicalite as the adsorbent. Henry's law constants were determined experimentally from the pure component isotherms and reported in our previous chapters (Chapters IV, V and VI). External film mass transfer, molecular diffusion and Knudsen diffusion were considered for the estimation of the effective diffusivity for adsorption. Rosen model was used for the determination of the breakthrough curves for the adsorption columns packed with silicalite. Parametric analyses of typical adsorption separation processes for CO_2/CH_4, CO_2/N_2 and CH_4/N_2 gases were carried out and the effects of pressure, particle size, superficial velocity and column length were studied. The economic assessments of typical PSA scenarios were compared with that of membrane systems. Adsorption was found to be an economical method for the three separations considered.

INTRODUCTION

The global environment is a major issue today, and global warming in particular is the focus of much attention. Accumulation of greenhouse gases (GHG) in the atmosphere is responsible for increased global warming of our planet. It is supposed that the increasing concentration of carbon dioxide mainly from flue gas, automobile and landfill emissions in the atmosphere is the major contributor to this problem with more than 80% of total GHG emissions (Cavenati et al., 2005; Hansen et al., 1988). Besides, methane is the most important non-CO_2 GHG responsible for global warming with more than 10% of total GHG emissions. Therefore, any reduction in methane emissions is important in the short- and medium-term atmosphere reconstruction (Cavenati et al., 2005). Landfill gas (LFG) is a multi-component mixture containing mainly methane and carbon dioxide, which constitutes one of the main sources of methane and carbon dioxide emissions, and can be treated as an important resource of directly available methane. This reason, together with a tighter control in emissions to meet Kyoto Protocol targets, puts LFG into consideration for energy production (Cavenati et al., 2004 & 2005). It is therefore obvious to separate CO_2/CH_4 and CH_4/N_2 for landfill gas and CO_2/N_2 for flue gas.

The breakthrough curve for a gas containing a single adsorbate is obtained by the solution of the mass and heat balance equations for both the bed and adsorbent particle, along with the equilibrium isotherm. In principle, a concentration front and a temperature plateau are associated with each adsorbate in the feed mixture. Analytic solutions, though desirable, are available for only a limited number of simple cases involving a single adsorbate. The shape of the breakthrough curve is determined by the nature or type of the adsorption isotherm. In addition, it is influenced by the individual transport processes in the bed and in the particles: All factors tend to make the front more dispersive or less sharp. The front is dispersed by both mass and heat dispersions in the axial direction, and also by the mass and heat transfer resistances in the particle.

In this work, collision integral (Ω_{AB}) in the Lennard-Joned potential-energy function was calculated. Molecular diffusivity (D_m), Knudsen diffusivity (D_K), the total diffusivity (D) and the effect diffusivity (D_e) were solved by studying internal (intra-particle) transport

processes. After that, by using the Rosen Model, the transfer rates were unravelled and the breakthrough curves worked out.

Based on the breakthrough curves related to adsorption dynamics, typical industrial adsorption separation processes for CO_2/CH_4, CO_2/N_2 and CH_4/N_2 were discussed. From the view of economics, including product quality, process productivity, energy efficiency, equipment and material cost, the influences of pressure, particle size, superficial velocity and column length were studied.

THEORY

By using the data from Table 7.1 (Poling et al., 2001), collision integral (Ω_{AB}) in the Lennard-Joned potential-energy function can be calculated, where ε_{AB} is the constant in the Lennard-Jones potential-energy function for the pair AB, k is Boltzmann's constant, T is the temperature in K, $\varepsilon_{AB} = \sqrt{\varepsilon_A . \varepsilon_B}$ and $\varepsilon_A.k^{-1}$ and $\varepsilon_B.k^{-1}$ are listed in Table 7.2 (Poling et al., 2001).

Table 7.1. The accurate relation of Lennard-Joned potential-energy function

$\Omega_{AB} = \frac{A}{T^{*B}} + \frac{C}{e^{DT^*}} + \frac{E}{e^{FT^*}} + \frac{G}{e^{HT^*}}$		
$T^* = \frac{kT}{\varepsilon_{AB}}$	A = 1.06036	B = 0.15610
C = 0.19300	D = 0.47635	E = 1.03587
F = 1.52996	G = 1.76474	H = 3.89411

Table 7.2. Lennard-Jones potentials as determined from viscosity data

Substances	σ, Å	$\varepsilon.k^{-1}$, K
CO_2	3.941	195.2
N_2	3.798	71.4
CH_4	3.758	148.6

Then molecular diffusivity (D_m) for a binary gas mixture can be evaluated by the familiar Chapman-Enskog equation (Bird et al., 1960; Yang, 1987):

$$D_m = 0.0018583 \times \frac{T^{\frac{3}{2}}\left(\frac{1}{M_A}+\frac{1}{M_B}\right)^{\frac{1}{2}}}{P\sigma_{AB}^2\Omega_{AB}} \quad \text{.....(1)}$$

where D_m is the molecular diffusivity of A in B in $cm^2.s^{-1}$, Ω_{AB} is the collision integral, P is the total pressure in atm, T is the temperature in K, and M_A and M_B are the molecular weights, σ_{AB} is the constant in the Lennard-Jones potential-energy function for the pair AB in Å and $\sigma_{AB}=\frac{1}{2}(\sigma_A+\sigma_B)$, where σ_A and σ_B are listed in Table 7.2 (Poling et al., 2001).

Knudsen diffusivity (D_k) is given by (Kauzmann, 1966; Yang, 1987):

$$D_k = 9.7\times10^3 r_p\left(\frac{T}{M}\right)^{\frac{1}{2}} \quad \text{.....(2)}$$

where D_k is the Knudsen diffusivity in $cm^2.s^{-1}$, T is the temperature in K, M is the molecular weight, r_p is the pore radius in cm.

In adsorption process, assuming equimolar counter diffusion, the total pore diffusivity (D_p) can be approximated (Yang, 1987):

$$D_p = \frac{1}{\frac{1}{D_m}+\frac{1}{D_k}} \quad \text{.....(3)}$$

where D_p is the total pore diffusivity in $cm^2.s^{-1}$, D_m is the molecular diffusivity in $cm^2.s^{-1}$, and D_k is the Knudsen diffusivity in $cm^2.s^{-1}$.

The value of D_p can be converted to effective diffusivity (Yang, 1987):

$$D_e = \frac{\alpha D_p}{\tau} \quad \text{.....(4)}$$

where D_p is the total pore diffusivity in cm^2/s, D_e is the effective diffusivity in $cm^2.s^{-1}$, α is the intrapellet void fraction, and τ is the tortuosity factor.

Mass Transfer Coefficient (k) for packed bed can be estimated by (Wakao and Funazkri, 1978):

$$\frac{kd_p}{D_m} = Sh = 2.0 + 1.1Sc^{\frac{1}{3}}\,\mathrm{Re}^{0.6} \quad \text{.....(5)}$$

$$k = \frac{D_m}{d_p}(2.0 + 1.1Sc^{\frac{1}{3}}\,\mathrm{Re}^{0.6}) \quad \text{.....(6)}$$

$$Sc = \frac{\mu}{\rho D_m} \quad \text{.....(7)}$$

$$\mathrm{Re} = \frac{d_p v_s \rho}{\mu} \quad \text{.....(8)}$$

where k is the mass transfer coefficient in $cm.s^{-1}$, d_p is the particle diameter in cm, D_m is the molecular diffusivity of A in B in $cm^2.s^{-1}$, Sh is the Sherwood number, Sc is the Schmidt number, Re is the Reynolds number, μ is the gas viscosity in $g.cm^{-1}.s^{-1}$, ρ is the gas density in $g.cm^{-3}$, and v_s is the superficial velocity in $cm.s^{-1}$.

In treating the mass transfer resistance within the pellet, the Rosen Model is an important diffusion model. In this model, the pellet is treated as a homogenous phase in which diffusion is assumed to be constant. The rate of mass transfer in adsorption within a spherical pellet is assumed to be the combined rate of external film mass transfer around the pellet and internal pore diffusion within the pellet. Simplifying assumptions in the Rosen model are plug flow (no axial dispersion), isothermal process, linear isotherm, constant flow-rate, and constant effective diffusivity. Also the bed is assumed to be clean initially. By using this model, an analytical solution is obtained for the fluid phase composition in the bed as a function of time and distance in the column (Yang, 1987),

$$\frac{C}{C_0} = \frac{1}{2}\left[1 + erf\ \frac{\frac{3U}{2V} - 1}{2\left(\frac{1+5v}{5V}\right)^{\frac{1}{2}}}\right] \quad \text{.....(9)}$$

where

$$U = \frac{2D_e(t - \frac{L\varepsilon}{v_s})}{R_p^2} \quad \text{.....(10)}$$

$$V = \frac{3D_e KL\varepsilon}{v_s R_p^2}(\frac{\varepsilon}{1-\varepsilon}) \quad \text{.....(11)}$$

$$v = \frac{D_e K}{kR_p} \quad \text{.....(12)}$$

where C is the gas-phase concentration in bulk flow, C_0 is the concentration in the feed, v is the dimensionless film resistance parameter, D_e is the effective diffusivity in $cm^2.s^{-1}$, t is the time in s, L is the length of the column in cm, ε is the inter-pellet void fraction, v_s is the superficial velocity in $cm.s^{-1}$. K is the dimensionless Henry's law constant, R_p is the particle radium in cm, k is mass transfer coefficient, $cm.s^{-1}$.

EXPERIMENTAL

The details of the constant volume system used for the determination of pure component isotherms are given in our earlier paper (Li and Tezel, 2007). The sample gases and the details of the adsorbent used in the experiments are listed in Tables 7.3 and 7.4, respectively.

Table 7.3. Details of sample gases.

Gases	Grade	Purity	Supplier
CO_2	Bone Dry 3.0	99.9%	Praxair Inc., Ottawa
N_2	Ultra High Purity 5.0	99.999%	Praxair Inc., Ottawa
He	Ultra High Purity 5.0	99.999%	Praxair Inc., Ottawa

Table 7.4. Details of the adsorbent.

Type	Silicalite
Commercial name	MOLSIV Adsorbents
Commercial number	HISIV 3000
Particle form received	1/16 inch extrudate as received
Size used in the column (Diameter)	Crushed to 20 x 60 mesh
Supplier	Universal Oil Products, Des Plaines, IL, USA

PARAMETRIC ANALYSIS

After industrial separation applications were studied, a set of typical adsorption operating conditions for CO_2/CH_4, CO_2/N_2 and CH_4/N_2 are listed in Table 7.5.

For determination of the breakthrough curves of adsorption dynamics, the isotherms of the three systems were measured by the volumetric method, the experimental data were regressed by the temperature independent Toth, and the parameters are listed in Table 7.6 (Chapters IV and V). With the parameters, the isotherms are obtained for the temperatures and pressures used, and then the slopes of the isotherms are determined and used as the dimensional Henry's law constants (K_p), which are converted to the dimensionless Henry's law constants (K) in Table 7.7 with the following equation:

$$K = RT\rho_p K_p \quad \text{.....(13)}$$

where T is temperature in K, ρ_p is the density of the pellets of the adsorbent in $g.cm^{-3}$, K_p is the dimensional Henry's Law adsorption equilibrium constant in $mmol.g^{-1}.atm^{-1}$, K is the dimensionless Henry's Law adsorption equilibrium constant, and R is gas constant, 82.06 atm. $cm^{-3}.mol^{-1}.K^{-1}$. Then V and v in Equations 11 and 12 can be solved, separately. After that, the normalized concentration at the end of the column at different times (breakthrough curves) are obtained by using Equation 9.

Table 7.5. Adsorption operating conditions

Operating Conditions	CO_2/CH_4	CH_4/N_2	CO_2/N_2
Applications	Landfill gas Natural gas	Landfill gas Natural gas	Flue gas
Adsorbates	CO_2	CH_4	CO_2
Adsorbate Feed composition (%)	40 (CO_2)	80 (CH_4)	15 (CO_2)
Adsorbate Molecular weight, M	44.01	16.04	44.01
Adsorbent	HiSiv 3000	HiSiv 3000	HiSiv 3000
Adsorbent particle diameter (cm)	0.15, 0.30, 0.60	0.15, 0.30, 0.60	0.15, 0.30, 0.60
Intra-pellet void fraction, α	0.45	0.45	0.45
Inter-pellet void fraction, ε	0.39	0.39	0.39
Length of column, L (cm)	400-600	400-600	400- 600
Superficial Velocity ($cm.s^{-1}$)	5-20	5- 20	5- 20
Total pressure, P (atm)	12-16	8-12	16-20
Adsorption temperature, T (°C)	45	45	100
Ambient temperature, T (°C)	25	25	25

For real applications, the effect of pressure, temperature, particle size, superficial velocity, column length and composition was studied.

Table 7.6. Parameters for the temperature independent Toth equation (Chapters IV and V)

Parameters	Units	CO_2	CH_4	N_2
T_0	°C	40	40	40
χ	Dimensionless	0	0	0
q_{m0}	$mmol.g^{-1}$	3.719	2.026	1.441
B_0	atm^{-1} / $atm^{-1/n}$	1.660	0.262	0.123
Q/RT_0	Dimensionless	10.87	4.809	3.278
n_0	Dimensionless	0.494	1.068	1.152
α	Dimensionless	0.869	1.065	4.000

Table 7.7. Henry's law constants, dimensional (K_P) and dimensionless (K)

Adsorbates	Temperature (°C)	Pressure (Atm.)	Kp mmole. $g^{-1}.atm^{-1}$	K (Dimensionless)
CO_2	45	12	0.03919	1.146
CO_2	45	14	0.03244	0.9488
CO_2	45	16	0.02748	0.8038
CH_4	45	8	0.05752	1.6827
CH_4	45	10	0.04157	1.2160
CH_4	45	12	0.03135	0.9170
CO_2	100	16	0.03847	1.320
CO_2	100	18	0.03341	1.146
CO_2	100	20	0.02939	1.008

For the three systems, pressure plays an important role in adsorption dynamics as shown in Figure 7.1, in which, the length of column is 500 cm, the superficial velocity is 10 $cm.s^{-1}$ and the diameter of particles is 0.15 cm. The breakthrough curves for the separation of CO_2/CH_4 at 45 ^0C at y_{CO2} = 0.4 are shown in Figure 7.1a; those for CH_4/N_2 at 45 ^0C at y_{CH4} = 0.8 are shown in Figure 7.1b; those for CO_2/N_2 at 100 ^0C at y_{CO2} = 0.15 are shown in

Figure 7.1c. For all the three systems, the breakthrough curves move to the left and appear early as pressure increases. The change of the parameters is shown below:

- $P \uparrow \Rightarrow D_m \downarrow$ (Equation 1) $\Rightarrow D \downarrow$ (Equation 3) $\Rightarrow D_e \downarrow$ (Equation 4) $\Rightarrow U \downarrow$ (Equation 10)
- $P \uparrow \Rightarrow \rho \uparrow$ (Equation of state) $\Rightarrow \mathrm{Re} \uparrow$ (Equation 8)
- $P \uparrow \Rightarrow K_p \downarrow$ (Experimental data) $\Rightarrow K \downarrow$ (Equation 13)
- $P \uparrow \Rightarrow k \downarrow$ ($D_m \downarrow \Rightarrow k \downarrow\downarrow$ and $\Rightarrow \mathrm{Re} \uparrow \Rightarrow k \uparrow$) (Equation 6)
- $P \uparrow \Rightarrow v \downarrow$ ($K \downarrow \Rightarrow v \downarrow\downarrow$, $D_e \downarrow \Rightarrow v \downarrow$ and $k \downarrow \Rightarrow v \uparrow$) (Equation 12)
- $P \uparrow \Rightarrow V \downarrow$ ($D_e \downarrow \Rightarrow V \downarrow$ and $K \downarrow \Rightarrow V \downarrow$) (Equation 11)
- $P \uparrow \Rightarrow \frac{C}{C_0} \uparrow$ ($V \downarrow \Rightarrow \frac{C}{C_0} \uparrow\uparrow\uparrow$, $U \downarrow \Rightarrow \frac{C}{C_0} \downarrow$ and $v \downarrow \Rightarrow \frac{C}{C_0} \downarrow$) (Equation 9)

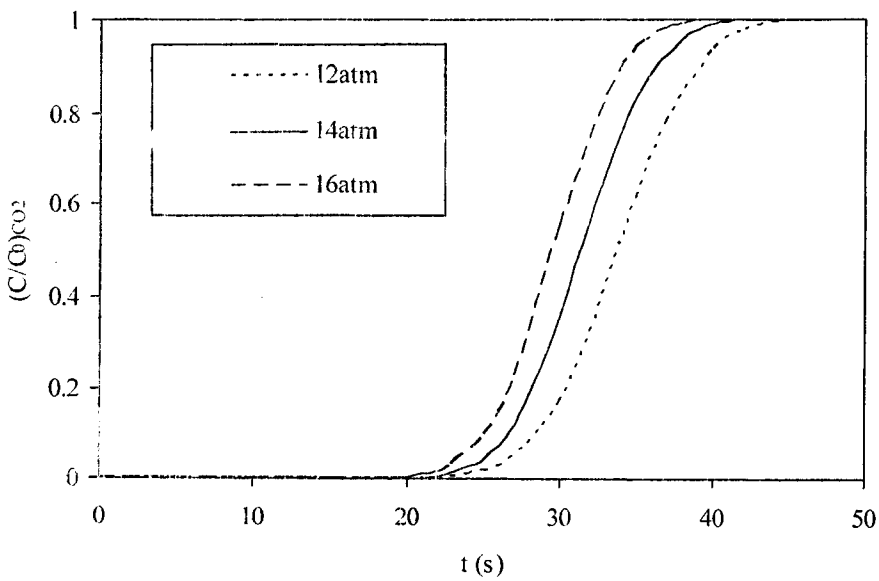

a. CO_2/CH_4, 500 cm column, 10 $cm.s^{-1}$, 45 °C, d_p=0.15cm, y_{CO_2}=0.4

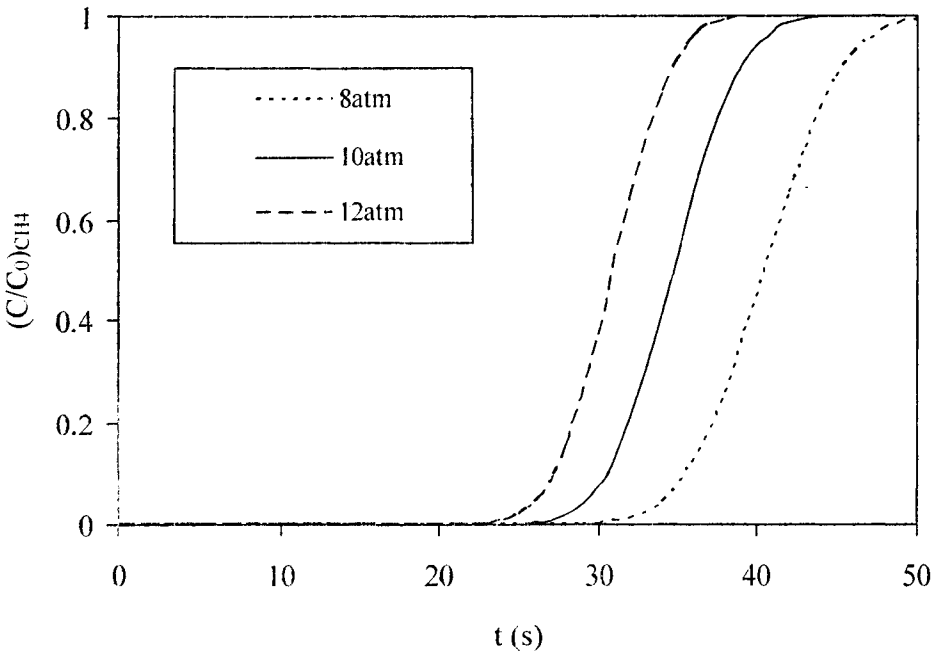

b. CH_4/N_2, 500 cm column, 10 $cm.s^{-1}$, 45 °C, d_p=0.15cm, y_{CH4}=0.8

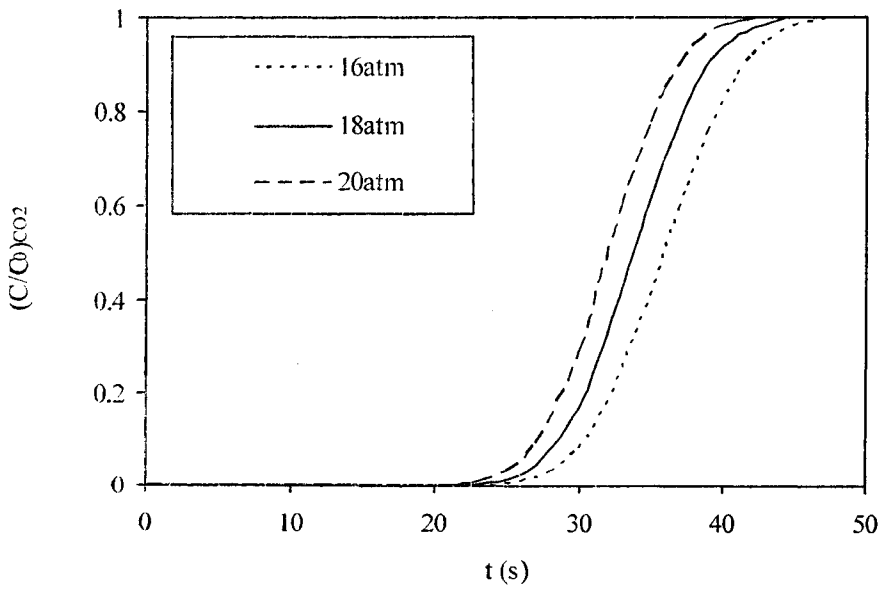

c. CO_2/N_2, 500 cm column, 10 $cm.s^{-1}$, 100 °C, d_p=0.15cm, y_{CO2}=0.15

Figure 7.1. Breakthrough curves at different pressures with silicalite.

For the three systems, particle size influences breakthrough curves greatly, as shown in Figure 7.2, in which, the length of column is 500 cm and the superficial velocity is 10 $cm.s^{-1}$. The breakthrough curves for the separation of CO_2/CH_4 at 45 ^0C at $y_{CO2} = 0.4$ under 14 atm. are shown in Figure 7.2a; those for CH_4/N_2 at 45 ^0C at $y_{CH4} = 0.8$ under 10 atm. are shown in Figure 7.2b; those for CO_2/N_2 at 100 ^0C at $y_{CO2} = 0.15$ under 18 atm. are shown in Figure 7.2c. For all the three systems, the slopes of the breakthrough curves decrease with increasing particle size and the curve becomes sluggish, increasing the length of the mass transfer zone in the column. This decreases the efficiency of the adsorption column. It is better to select reasonable small particle size for good quality products, without increasing the pressure drop through the column. The change of the parameters is shown below:

- $d_p \uparrow \Rightarrow \mathrm{Re} \uparrow$ (Equation 8)
- $d_p \uparrow \Rightarrow k \downarrow$ ($d_p \uparrow \Rightarrow k \downarrow\downarrow$ and $\Rightarrow \mathrm{Re} \uparrow \Rightarrow k \uparrow$) (Equation 6)
- $d_p \uparrow \Rightarrow V \downarrow$ (Equation 11)
- $d_p \uparrow \Rightarrow v \downarrow$ ($d_p \uparrow \Rightarrow v \downarrow\downarrow$ and $k \downarrow \Rightarrow v \uparrow$) (Equation 12)
- $d_p \uparrow \Rightarrow \dfrac{\partial\left(\dfrac{C}{C_0}\right)}{\partial t} \downarrow$ (Equation 9)

Superficial velocity is another important parameter in an adsorption process. For the three systems, it also influences the breakthrough curves, as shown in Figure 7.3, in which, the length of column is 500 cm and the diameter of particles is 0.15 cm. The breakthrough curves for the separation of CO_2/CH_4 at 45 ^0C at $y_{CO2} = 0.4$ under 14 atm. are shown in Figure 7.3a; those for CH_4/N_2 at 45 ^0C at $y_{CH4} = 0.8$ under 10 atm. are shown in Figure 7.3b; those for CO_2/N_2 at 100 ^0C at $y_{CO2} = 0.15$ under 18 atm. are shown in Figure 7.3c. For all the three systems, the breakthrough curves move to the right or appear later and the slopes of the curves decrease with decreasing superficial velocity. The change of the parameters is shown below:

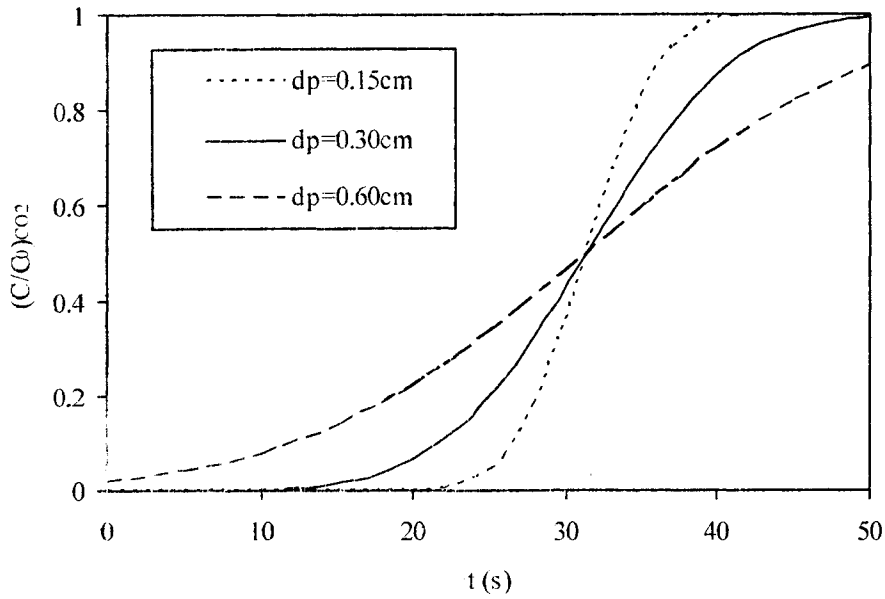

a. CO_2/CH_4, 500 cm column, 10 $cm.s^{-1}$, 45 °C, 14 atm, y_{CO_2}=0.4

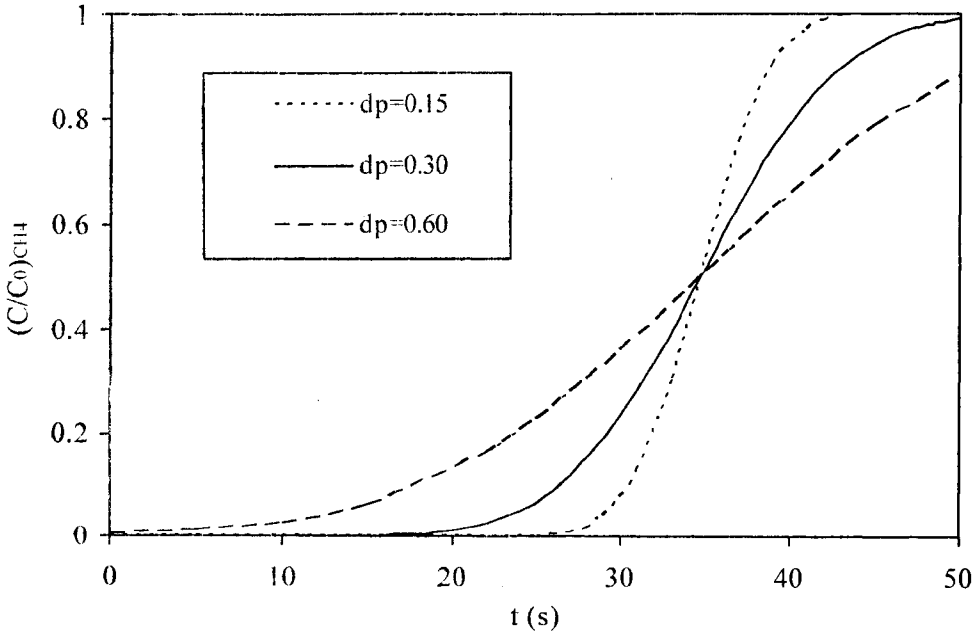

b. CH_4/N_2, 500 cm column, 10 $cm.s^{-1}$, 45 °C, 10 atm, y_{CH_4}=0.8

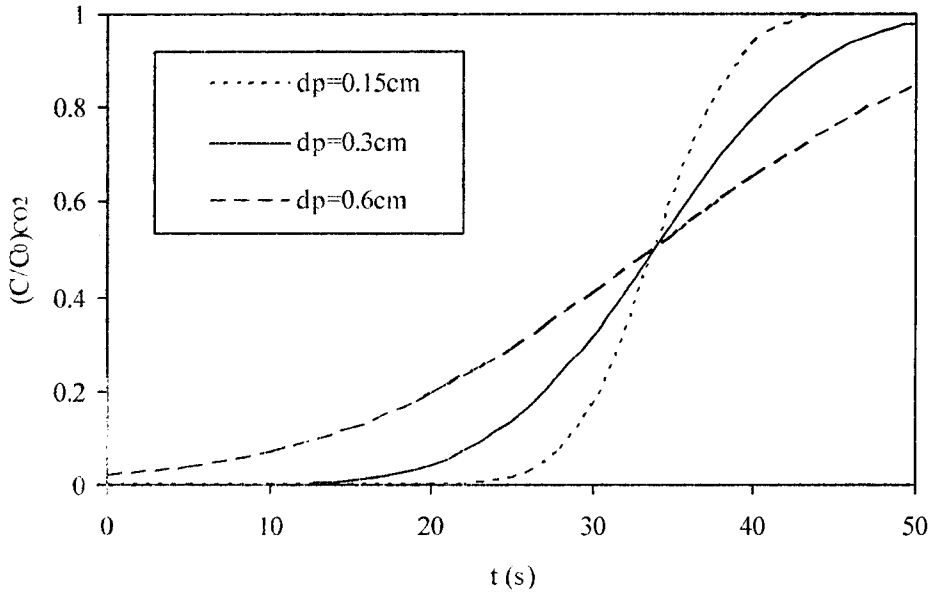

c. CO_2/N_2, 500 cm column, 10 $cm.s^{-1}$, 100 °C, 18atm, y_{CO2}=0.15

Figure 7.2. Breakthrough curves with different particle sizes with silicalite.

- $v_s \uparrow \Rightarrow \mathrm{Re} \uparrow$ (Equation 8) $\Rightarrow k \uparrow$ (Equation 6) $\Rightarrow v \downarrow$ (Equation 12)
- $v_s \uparrow \Rightarrow \mathrm{V} \downarrow$ (Equation 11)
- $v_s \uparrow \Rightarrow \mathrm{U} \uparrow$ (Equation 10)
- $v_s \uparrow \Rightarrow \frac{C}{C_0} \uparrow$ ($V \downarrow \Rightarrow \frac{C}{C_0} \uparrow\uparrow\uparrow$, $U \uparrow \Rightarrow \frac{C}{C_0} \uparrow$ and $v \downarrow \Rightarrow \frac{C}{C_0} \downarrow$)

(Equation 9)

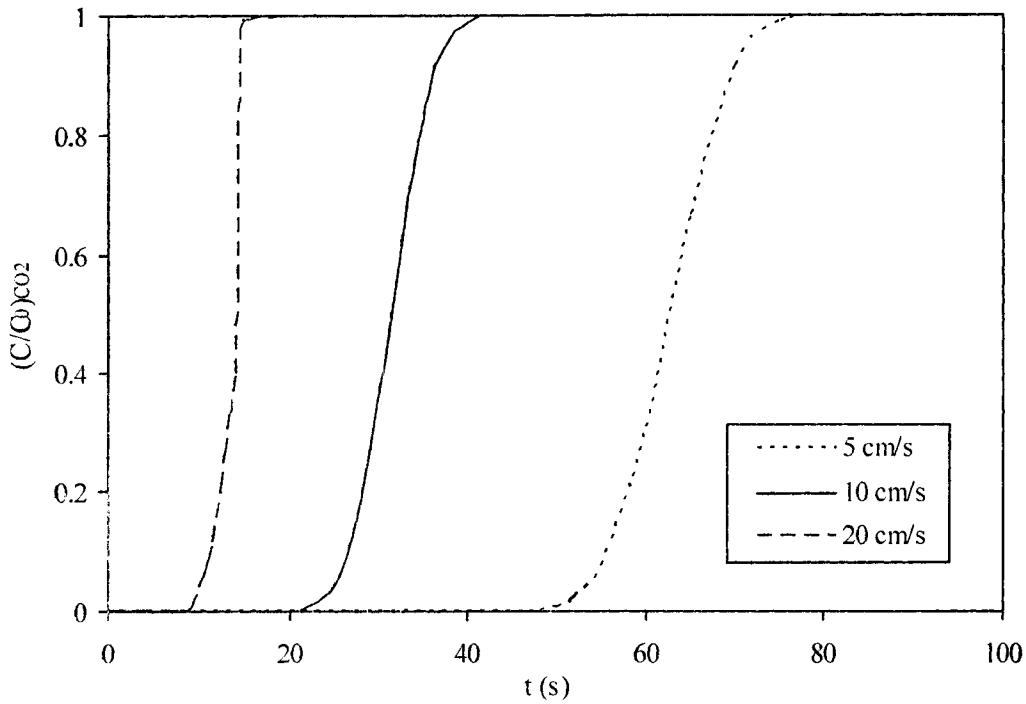

a. CO_2/CH_4, 500 cm column, d_p=0.15 cm, 45 °C, 14 atm, y_{CO_2}=0.4

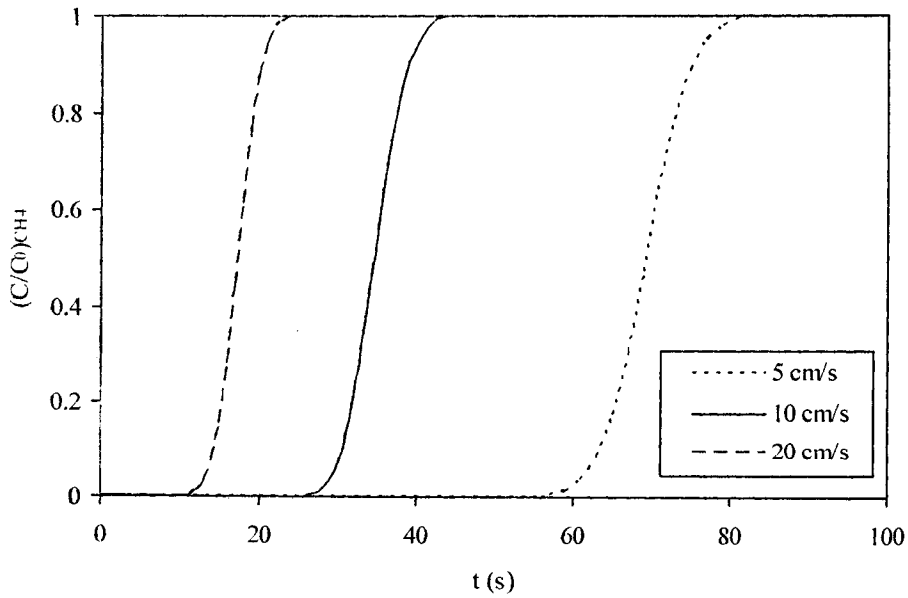

b. CH_4/N_2, 500 cm column, d_p=0.15 cm, 45 °C, 10 atm, y_{CH_4}=0.8

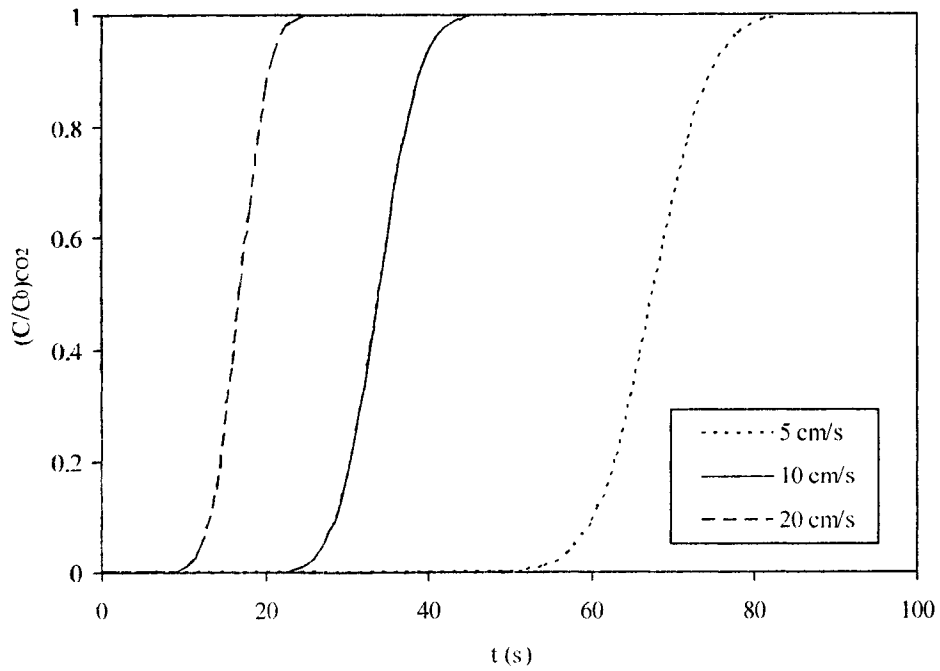

c. CO_2/N_2. 5 m column. d_p=0.15cm. 100 °C. 18 atm. y_{CO2}=0.15

Figure 7.3. Breakthrough curves with different superficial velocities for silicalite.

Column length must be considered for an adsorption process. For the three systems, it also influences the breakthrough curves, as shown in Figure 7.4, in which, the diameter of particles is 0.15 cm and the superficial velocity is 10 $cm.s^{-1}$. The breakthrough curves for the separation of CO_2/CH_4 at 45 ^{0}C at y_{CO2} = 0.4 under 14 atm. are shown in Figure 7.4a; those for CH_4/N_2 at 45 ^{0}C at y_{CH4} = 0.8 under 10 atm. are shown in Figure 7.4b; those for CO_2/N_2 at 100 ^{0}C at y_{CO2} = 0.15 under 18 atm. are shown in Figure 7.4c. For all the three systems, the breakthrough curves move to the right or appear later as column lengths increase. The change of the parameters is shown below:

- $L \uparrow \Rightarrow V \uparrow$ (Equation 11)
- $L \uparrow \Rightarrow U \downarrow$ (Equation 10)
- $L \uparrow \Rightarrow \frac{C}{C_0} \downarrow$ ($V \uparrow \Rightarrow \frac{C}{C_0} \downarrow\downarrow$ and $U \downarrow \Rightarrow \frac{C}{C_0} \downarrow$) (Equation 9)

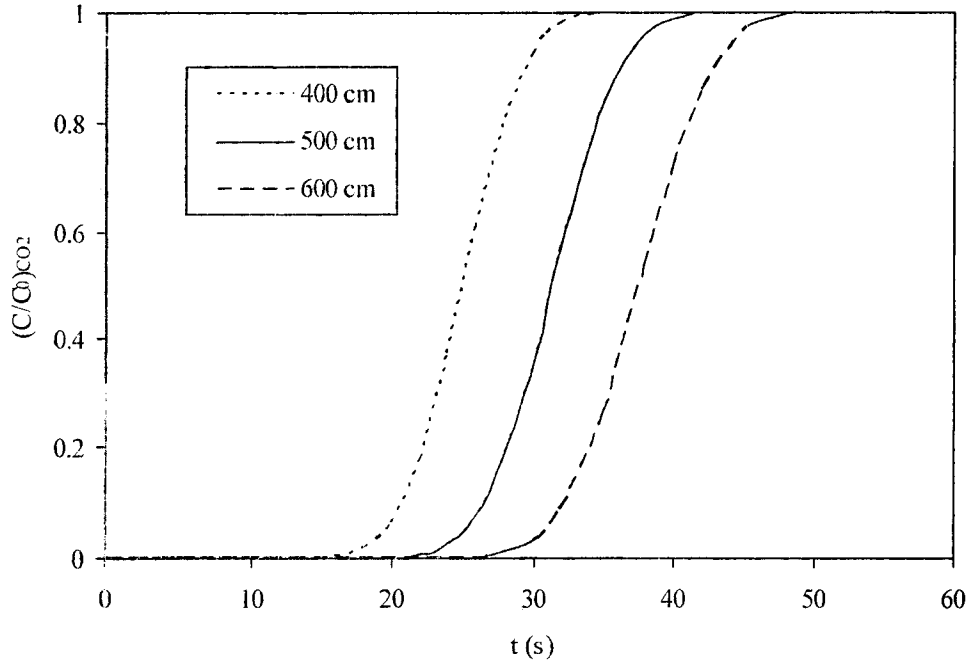

a. CO_2/CH_4, d_p=0.15 cm, 10 $cm.s^{-1}$, 45 °C, 14 atm, y_{CO2}=0.4

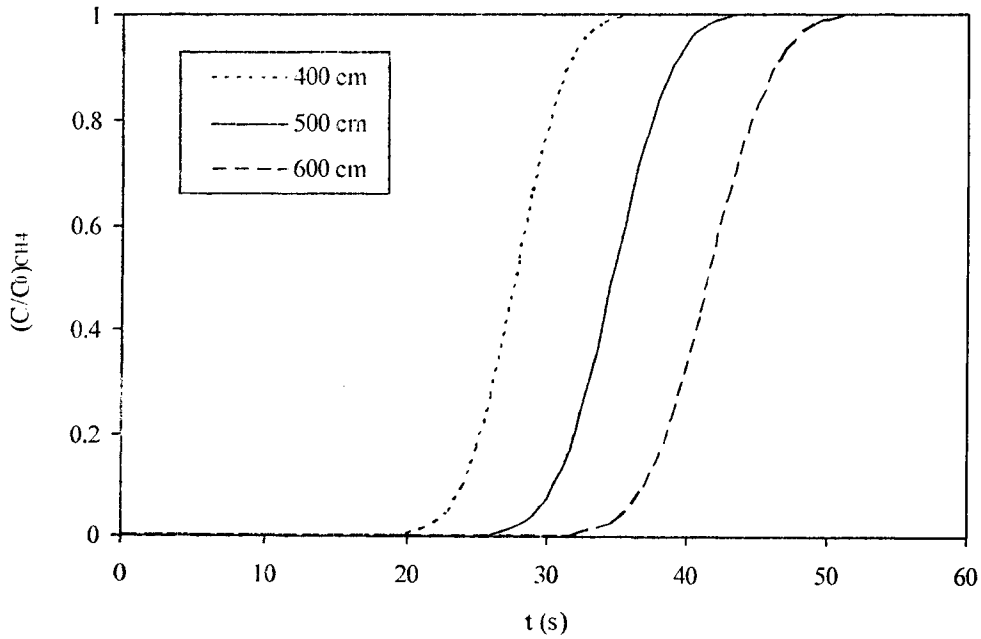

b. CH_4/N_2, d_p=0.15cm, 10 $cm.s^{-1}$, 45 °C, 10 atm, y_{CO2}=0.8

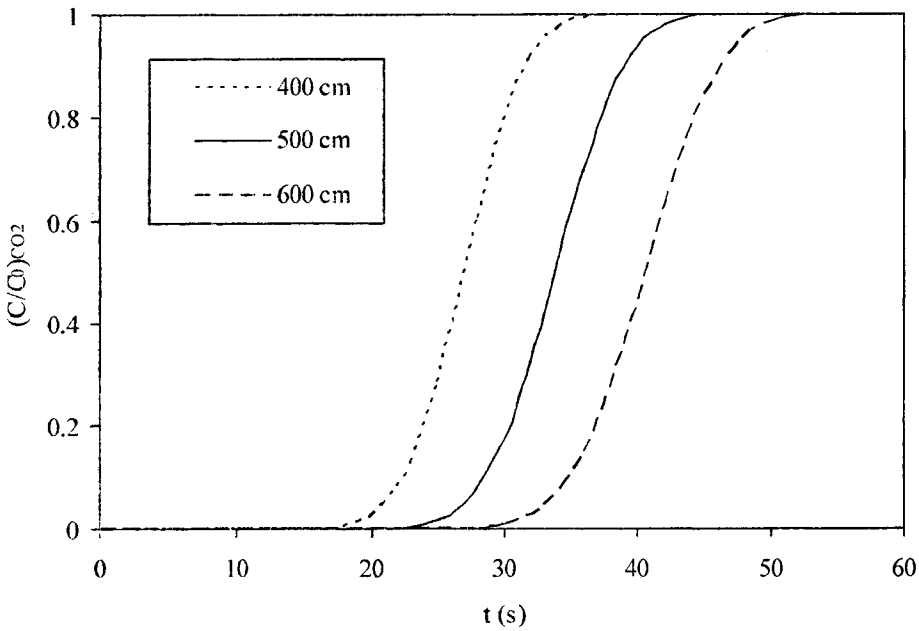

c. CO_2/N_2, d_p=0.15cm, 10 $cm.s^{-1}$, 100 °C, 18 atm, y_{CO2}=0.15

Figure 7.4. Breakthrough curves for different column lengths for silicalite.

TYPICAL CONDITIONS AND ECONOMIC ASSESSMENT

After analyses of the three adsorption separations for industrial applications, a set of typical adsorption operating conditions for CO_2/CH_4, CO_2/N_2 and CH_4/N_2 are listed in Table 7.8. The separation of CO_2/CH_4 can be used in landfill gas and natural gas applications with y_{CO2}=0.4. The separation of CH_4/N_2 can be used in landfill gas and natural gas applications with y_{CH4}=0.8. The separation of CO_2/N_2 can be used in flue gas applications with y_{CO2}=0.15. For the three separations, HiSiv 3000, a silicalite supplied by the Universal Oil Products, can be used. The adsorbent particle diameter is 0.15cm. According to the results obtained, smaller particle size give better results, but on the other hand, much smaller particle sizes will cause high pressure drop and can not be used in a packed column. Therefore the particle size need to be optimized. In the scenarios considered in this work, the smallest particle size available from the supplier is selected. The size of the column and superficial velocities selected are typical in the literature. The total pressures and adsorption temperatures selected

for the three different scenarios are different. The pressures are selected after different pressure runs with the Rosen model to decrease pressure for saving energy for the real application. The temperatures for the three separations are chosen to be the typical ones in real applications to minimize the temperature change for the system.

Table 7.8. Typical adsorption operating conditions
for real applications considered in this study

Operating Conditions	CO_2/CH_4	CH_4/N_2	CO_2/N_2
Applications	Landfill gas Natural gas	Landfill gas Natural gas	Flue gas
Adsorbates	CO_2	CH_4	CO_2
Adsorbent	HiSiv 3000	HiSiv 3000	HiSiv 3000
Adsorbent particle diameter (cm)	0.15	0.15	0.15
Length of column, L (cm)	500	500	500
Diameter of column, D (cm)	60	60	60
Superficial Velocity ($cm.s^{-1}$)	10	10	10
Total pressure, P (atm)	14	10	18
Adsorption temperature, T (°C)	45	45	100

Based on our data and study, after calculation and design and compared with the references in the literature (Tabe-Mohammadi, 1999; Deed et al., 2005), the rough economic assessment of PSA is listed in Table 7.9. For CO_2/CH_4 and CO_2/N_2, adsorption and membrane are popular in real applications. The economic feasibility of adsoption is compared with that of membrane. Because of low selectivities of existing membranes

toward CH_4/N_2, the main technology available for CH_4/N_2 separation is only adsorption (Tabe-Mohammadi, 1999), and to our knowledge, there is no significant improvement until now.

Table 7.9. Economic assessment and comparison with membrane

Operating Conditions	CO_2/CH_4	CH_4/N_2	CO_2/N_2
Feed Capacity (tons / day)	140	70	170
Feed Composition	40% CO_2	80% CH_4	15% CO_2
Purity	90% CO_2	90% CH_4	90% CO_2
Recovery	90% CO_2	80% CH_4	80% CO_2
Number of Two-Bed PSA Systems	4	4	4
Cost of Adsorbent (Canadian $ / kg)	17.7	17.7	17.7
Mass of Adsorbent (kg / two-bed PSA)	1 951	1 951	1 951
Cost of PSA System (Canadian $ / PSA)	32 946	32 946	32 946
Total Cost of Adsorbent (Canadian $)	138 301	138 301	138 301
Total Cost of PSA System (Canadian $)	131 783	131 783	131 783
Total Capital Cost for Adsorption (Canadian $)	270 084	270 084	270 084
Operation & Maintenance Cost (Canadian $ / year)	108 034	108 034	108 034
Operation and Maintenance Cost (Canadian $ / 10 year)	1 080 337	1 080 337	1 080 337
Total Cost of Adsorption (Canadian $ / 10 year)	1 350 421	1 350 421	1 350 421
Total Cost of Membrane (Canadian $ / 10 year)	1 820 684	---	2 021 747

In Table 7.9, feed capacity, feed composition, purity and recovery are typical in real applications in Canada and/or US. Number of two-bed PSA is obtained from our calculation results. Cost of adsorbent was from the supplier (UOP) this year. Cost of PSA system was from the literature (corrected for 2007 from 1996). Mass of adsorbent, total cost of

adsorbent, total cost of PSA system, total capital cost for adsorption, operation & maintenance cost (40% of total capital cost for adsorption), total cost of adsorption are from our calculation. The total capital cost includes those of PSA equipment and adsorbent and the total cost includes the total capital cost and operation and maintenance cost. Total cost of membrane is obtained from the second hand data in the literature and our calculation. According to the assessment, PSA is more economical than membrane. Therefore, adsorption is a feasible method for the three separations.

Here it is noted that the data in Table 7.9 are preliminary results. The rate of transfer in adsorption by a spherical pellet is assumed to be the combined rate of external film diffusion and internal pore diffusion. Simplifying assumptions in the Rosen model are plug flow (no axial dispersion), isothermal, linear isotherm, constant flow velocity, and constant effective diffusivity. The bed is initially clean. Some secondhand data from the literature are used. Therefore, the economic assessment is only preliminary estimation, and further work should be done before a real application.

ACKNOWLEDGMENTS

Financial supports received from the Natural Sciences and Engineering Research Council of Canada (NSERC) Postgraduate Scholarship, the Ontario Graduate Scholarship (OGS) and the Canadian Society for Chemical Engineering (CSChE) Scholarship are gratefully acknowledged.

NOMENCLATURE

C = concentration

d = diameter, cm

D = diffusivity, $cm^2.s^{-1}$; diameter, cm

k = mass transfer coefficient, $cm.s^{-1}$; Boltzmann's constant

K = Henry's law constant

L = length of the bed, cm

M = molecular weight

P = pressure, atm

Q = feed adsorbate amount, m^3/hr

r = pore radium, cm

R = particle radium, cm

Re = Reynolds number, dimensionless

Sc = Schmidt number, dimensionless

Sh = Sherwood number, dimensionless

t = time, s

T = initial, system or ambient temperature, K

u = interstitial velocity, $cm.s^{-1}$

U = parameter in the Rosen Model, dimensionless

v = velocity, $cm.s^{-1}$; film resistance parameter, dimensionless

V = parameter in the Rosen Model, dimensionless

y = mole fraction in the gas phase

Z = position in the column

Greek letters

α = intra-pellet void fraction

ε = inter-pellet void fraction; constant in the Lennard-Jones potential-energy function

μ = gas viscosity, $g.cm^{-1}.s^{-1}$

ρ = density, $g.cm^{-3}$

σ = constant in the Lennard-Jones potential-energy function, Å

τ = tortuosity factor, dimensionless

Ω = collision integral in the Lennard-Joned potential-energy function, dimensionless

Subscripts

0 = Initial

A = Component A

B = Component B

e = effect

k = Knudsen

m = molecular

p = pore or particle

s = superficial

t = total

Abbreviations

GHG = greenhouse gases

LFG = landfill gas

PSA = pressure swing adsorption

REFERENCES

Bird, R. B., W. E. Stewart and E. N. Lightfoot, "Transport Phenomena", Wiley, New York (1960).

Cavenati, S., C. A. Grande and A. E. Rodrigues, "Adsorption Equilibrium of Methane, Carbon Dioxide, and Nitrogen on Zeolite 13X at High Pressures", Journal of Chemical and Engineering Data **49**, 1095-1101 (2004).

Cavenati, S., C. A. Grande and A. E. Rodrigues, "Upgrade of Methane from Landfill Gas by Pressure Swing Adsorption", Energy and Fuels **19**, 2545-2555 (2005).

Deed, C., J. Gronow, R. Smith, A. Rosevear, P. Braithwaite and P. Stanley, "Guidance on Gas Treatment Technologies for Landfill Gas Engines", Environment Agency, Bristol, UK (2002)

Hansen, J., I. Fung, A. Lacis, D. Riud, J.S. Levedeff, R. Ruedy, and G. Russell, "Global Climate Changes as Forecast by Goddard Institute for Space Studies Three-Dimensional Model", Journal of Geophysical Research **93,** 9341-9364 (1988).

Kauzmann, W., "Kinetic Theory of Gases", Benjamin, New York (1966).

Li, P. and F. H. Tezel, "Adsorption Separation of Methane and Carbon Dioxide on Silicalite", submitted to be published in Separation Science and Technology (2007).

Poling, B. E., J. M. Prausnitz and J. P. O'Connell, "Diffusion Coefficients" and "Appendix B: Lennard-Jones Potentials as Determined from Viscosity Data" in "The Properties of Gases and Liquids", B. E. Poling, Eds., McGraw Hill, New York, NY (2001a), pp. 11.1-11.55 and B1-B2.

Tabe-Mohammadi, A., "A Review of the Applications of Membrane Separation Technology in Natural Gas Treatment", Separation Science and Technology **34**, 2095-2111 (1999).

Wakao, N. and T. Funazkri, "Effect of Fluid Dispersion Coefficients on Particle-to-Fluid Mass Transfer Coefficients in Packed Beds: Correlation of Sherwood Numbers", Chem. Eng. Sci. **33**, 1375-1384 (1978).

Yang, R. T., "Gas Separation by Adsorption Process", Butterworths, Boston, MA (1987).

CHAPTER VIII

MEMBRANE GAS SEPARATIONS, THEIR ADSORPTION BEHAVIORS AND SEPARATION MECHANISMS

Peiyuan Li and F. Handan Tezel*

Department of Chemical Engineering
Faculty of Engineering
University of Ottawa
161 Louis Pasteur, Ottawa, Ontario K1N 6N5, Canada

It will be submitted to a journal.

* Corresponding author
Tel: 613-562-5800 Ext. 6099
Fax: 613-562-5172
Emai: Handan.Tezel@uottawa.ca

ABSTRACT

Accumulation of greenhouse gases (GHG) in the atmosphere is responsible for increased global warming of our planet. It is supposed that the increasing concentration of carbon dioxide mainly from flue gas, automobile and landfill emissions in the atmosphere is the major contributor to this problem with more than 80% of total GHG emissions. Landfill gas (LFG) is a multi-component mixture containing mainly methane and carbon dioxide and can be treated as an important resource of directly available methane. It constitutes one of the main sources of methane and carbon dioxide emissions. These reasons, together with a tighter control in emissions to meet Kyoto Protocol targets, put LFG into consideration for energy production.

In this study, the syntheses and application of MFI zeolite membrane were looked at for above mentioned gas systems. Separation of CO_2/N_2 for flue gas application, separation of CO_2/CH_4 for landfill and natural gas applications, separation of CH_4/N_2 for landfill and natural gas applications with MFI zeolite membrane and separation of CO_2/N_2 for flue gas applications with two types of silicone rubber membranes (silicone polycarbonate membrane and dimethyl silicone membrane) were considered. Separation factors and permeability values were measured. Adsorption behaviours of these systems, as well as their separation mechanisms were analyzed.

According to our results, monolayer adsorption, multilayer adsorption and/or capillary condensation dominate the separations of CO_2/N_2, CO_2/CH_4 and CH_4/N_2 with MFI zeolite membrane. The silicone polycarbonate membrane gives better results for the separation of CO_2/N_2 for flue gas applications. It was concluded that adsorption plays an important role in these separations with MFI zeolite and silicone rubber membranes.

INTRODUCTION

The global environment is a major issue today, and global warming in particular is the focus of much attention. Accumulation of greenhouse gases (GHG) in the atmosphere is responsible for increased global warming of our planet.

It is supposed that the increasing concentration of carbon dioxide mainly from flue gas, automobile and landfill emissions in the atmosphere is the major contributor to this problem with more than 80% of total GHG emissions (Cavenati et al., 2005; Hansen et al., 1988). For CO_2-N_2 separation for flue gas applications, there are mainly two methods. One is adsorption (Li and Tezel. 2005 and 2007; Mulgundmath et al., 2007a) and the other is membrane. Some are polymeric membranes: polyimides (Powell and Qiao, 2006; Liu et al., 2004; Heuchel and Hofmann, 2002; Kresse et al., 1999), polyarylates (Powell and Qiao, 2006), polypyrrolones (Powell and Qiao, 2006), polysaccharide/poly(vinyl alcohol) (Kim et al., 2004), polyamide (Petersen and Peinemann, 1997; Kresse et al., 1999; Espeso et al., 2006), polyphosphazene (Orme et al., 2001), poly(4-methyl-2-pentyne) (Morisato and Pinnau, 1996), poly(ethyleneoxide-co-epichlorohydrin) (Sanchez et al., 2002), polysulfones (Powell and Qiao, 2006; Liu et al., 2004; Lee et al., 2006), polycarbonates (Powell and Qiao, 2006) and bis(phenyl)fluorene-based cardo polymer (Kazama et al., 2002). Some are carbon membranes (Katsaros et al., 1997) and carbon molecular sieve membranes (Okamoto et al., 2000). Some are silicone rubber membranes: silicone rubber (Jha et al., 2006) and methyltriethoxysilane (Moon et al., 2005). Others are nanoporous/amorphous silica membranes (Yang et al., 2002; Espeso et al., 2006; Richard et al., 2001) and zeolites membranes, including Y-type zeolites (Mizukami et al., 2001; Kusakabe et al., 1997 and 1998; Hasegawa et al., 2001) and MFI (silicalite and ZSM-5) (Bernal et al., 2004; Ando et al., 1998; Lovallo et al., 1998; Van den Broeke et al., 1999; Masuda et al., 1998; Mase et al., 1998; Hyun et al., 1999; Kwak et al., 2001).

Methane is the most important non-CO_2 GHG responsible for global warming with more than 10% of total GHG emissions. Despite much smaller amounts of methane released to the atmosphere, the greenhouse warming potential (GWP) of this gas is much higher than carbon dioxide's, therefore any reduction in methane emissions is much more important in the short- and medium-term atmosphere reconstruction (Cavenati et al., 2005). Some papers

have been reported on CH_4-N_2 adsorption separation for landfill gas and natural gas (Mulgundmath et al., 2007b; Dong et al., 1999; Jayaramana et al., 2004; Sheikh et al., 1996; Warmuzinski and Sodzawiczny, 1999). Because of low selectivity of existing membranes toward CH_4/N_2, the main technology available for CH_4/N_2 separation is only adsorption (Tabe-Mohammadi, 1999), and to our knowledge, there is no significant improvement until now.

Landfill gas (LFG) is a multi-component mixture containing mainly methane and carbon dioxide and constitutes one of the main sources of methane and carbon dioxide emissions. It can be treated as an important resource of directly available methane. This reason, together with a tighter control on emissions to meet Kyoto Protocol targets, puts LFG into consideration for energy production (Cavenati et al., 2004, 2005). Some techniques have been studied on CH_4-CO_2 separation. The separation of these gases is important for many applications, including the purification of CH_4 from landfill drainage gas, the purification of CH_4 from natural gas and the recovery of CO_2 in enhanced oil recovery. The two popular methods are adsorption (Li and Tezel, 2006; Mulgundmath et al., 2007a) and membranes. Polymeric membranes include polyamide (Espeso et al., 2006; Mohammadi, et al., 1995; Kresse et al., 1999), Polyimide (Thundyil et al., 1999; Ayala et al., 2003 ; Kresse et al., 1999; Bos et al., 2001; Chenar et al., 2006), polysulfone (Bos et al., 2001; Ismail et al., 1999), poly(phenylene oxide) (Sridhar et al., 2006), polybenzimidazole (Pesiri et al., 2003), poly(vinyl chloride) (Tiemblo et al., 2002), poly(lactic acid) (Lehermeier et al., 2001), 2-N, N-dimethyl aminoethyl methacrylate and acrylic acid copolymer (Shen et al., 2006ab), diglycolamine and triethylene glycol (Ito et al., 2001), rubbery amorphous polyphosphazene (Orme et al., 2001) and cellulose (Wu and Yuan, 2002). Some are silicone rubber membranes (Ashworth et al., 1995). Others are zeolite membranes, including SAPO-34 (Li et al., 2004 and 2005; Poseph et al., 1998), DDR type zeolite (Tomita et al., 2004) and MFI (silicalite and ZSM-5) (Leung and Yeung, 2004; Bakker et al., 1996).

In this current work, the syntheses and applications of MFI zeolite membrane were studied. The separations of CO_2/N_2, CO_2/CH_4 and CH_4/N_2 with MFI zeolite membrane and the separation of CO_2/N_2 with two types of silicone rubber membranes (silicone polycarbonate membrane and dimethyl silicone membrane) were looked at. Separation

factors and permeability values were measured, and adsorption behaviours and mass transfer mechanisms were discussed for these systems.

Some properties of the gases studied in this work are given in Table 8.1.

Table 8.1. Properties of gases studied in this work (Breck, 1974; Golden and Sircar, 1994)

Gases	Molecular Weight	Kinetic Diameter (nm)	Dipole Moment X 10^{18} (esu cm)	Quadrupole Moment X 10^{26} (esu cm^2)	Polarizability X 10^{25} (mL^3)
CH_4	16	0.38	0	0	26.0
N_2	28	0.364	0	1.52	17.6
CO_2	44	0.33	0	4.30	26.5

EXPERIMENTAL

Template-Free Secondary Growth Synthesis of MFI type Zeolite Membranes

Silicalite Suspension: Silicalite suspension was prepared according to the following procedure. NaOH-TPAOH (Tetrapropylammonium hydroxide, about 10ml) solution was prepared by dissolving NaOH (1 or 2 pills, 99.99%, Sigma-Aldrich,) pill in 1 M TPAOH (Fluka's Purum, Sigma-Aldrich) solution in a capped Teflon flask (0.014 g NaOH per 1 ml TPAOH solution). A given amount of fumed silica (about 2g, 7nm, Sigma-Aldrich) was dissolved into this NaOH-TPAOH solution at around 80°C with vigorous stirring on a hot plate to obtain a final composition of 1 g SiO_2 - 5 ml (1 M) TPAOH - 0.07 g NaOH.. After a clear solution was obtained, the solution was cooled down to room temperature and kept there for 3 h and then hydrothermally treated in a Teflon lined stainless steel autoclave at 120°C for 12 h. After cooling to room temperature, the seeds in this solution were purified by repeated centrifugation washes with de-ionized water. The final silicalite slurry contained

about 0.12 g silicalite in 1 ml of slurry (measured with a measuring cylinder) with pH =10.

The suspension (about 16.7ml) used for coating was prepared by adding 0.5 wt.% hydroxy propyl cellulose (HPC) (MW = 100,000 g/mol) (Fisher Scientific) solution and de-ionized water in the silicalite slurry in desired amounts with final composition of the suspension: 1 g silicalite - 0.14 g HPC - 94 ml H_2O.

α -Al_2O_3 disks: Homemade porous α -Al_2O_3 disks with thickness of 2 mm and diameter of 20 mm (23mm before sintering; the magnitude of shrinking depends on the sintering temperature) were used as the supports. The α - Al_2O_3 disks were prepared according to the following procedure: 84 wt. % α -Al_2O_3 nano powder (about 60g, average particle size (APS) was 150 nm from BET SSA and SEM, grain size was about 40 nm from X-ray line broadening, BET multi-point specific surface area (SSA) was about 10 $m^2.g^{-1}$) , the catalogue number was 26N-0802A, and it was supplied by Inframat Advanced Materials LLC) and 16 wt. % de-ionized water were fully mixed and made mud in a mortar and kept for an hour (more percentage of water made the moulding process difficult, less percentage caused the sintered disk to be fragile; the smaller the particle size, the higher the percentage of water). 2.7g of this mixture is filled in a stainless steel mould and pressed at force of 10.000 pound for 1 min by a lab press. These raw disks were dried at 40°C for two days. Then they were polished carefully for the first time by a knife (although they could be polished after calcination, it was difficult to do that as the sintered disk was hard). The dried disks were sintered in a programmed furnace to a maximum temperature of 1500 °C (the permeability of the disk was lower at higher temperature while the strength of the disk was lower at lower temperature) with setting at 10 $^0C.min^{-1}$ for increasing temperature and at 1 $^0C.min^{-1}$ for decreasing temperature (the disk was easy to be broken at a higher cooling rate).

Coating: Before coating, two sides of the α -Al_2O_3 supports were polished for the second time with sandpaper (#400), the smoother side of the α -Al_2O_3 supports was polished finally with fine sandpaper (#800) to obtain a smooth surface for membrane preparation, and then the α -Al_2O_3 supports were washed for 10 min, followed by drying at 40°C for two days. The polished α -Al_2O_3 supports were dip coated with the silicalite suspension as uniformly as possible for four times with drying for 5 minutes after each dipping in ambient air, and then dried at 40°C in the oven for two days. It was difficult to coat the silicalite layers on the alumina support by dip coating from the silicalite suspension at pH of about

10. Therefore, the silicalite layer was readily coated on the alumina support using the silicalite suspension with pH modified to 3 by adding 1 drop of 1N HNO_3 (Sigma-Aldrich). The dried supported silicalite membranes were calcined at 450°C for 8 hours and subsequently at 650°C for 8 hours with a heating and cooling rate of 0.3 °C/min (the membrane seed layer had more defects at a higher heating and cooling rate). The calcination was done to enhance the bonding between the zeolite layer and the support. Template was also removed from the zeolite pores in this step.

Secondary Grown Membrane: Silica sol for secondary grown membrane was prepared by adding a given amount of fumed silica powder into 1.5 wt. % NaOH solution at around 80°C with vigorous stirring on a hot plate to obtain a composition of 0.16 g NaOH - 1 g SiO_2 - 10.5 g H_2O. After cooling down and aging for 1.5 h, a viscous silica sol was obtained. It was subsequently dispersed in water to be washed for 30 min. No template was used in the synthesis sol with silica concentration of 0.1 g/ml and pH value was measured to be 12. The dip-coated silicalite membranes, as the seed layers, were put at the bottom of Teflon lined stainless steel autoclave (Parr Acid Digestion Bomb, VWR International) filled with the silica sol with the zeolite layer on top. The autoclave was closed and placed in an oven at 150°C (the crystallization was mostly done at 120-180 °C in the literature) for a specified time (3, 12 or 36 hours). When the crystallization was tried at 180°C it was observed that the membrane did not show good properties. After cooling to the room temperature, the membranes were removed from the autoclave and washed with water for 10 min. Then membranes were dried at 40°C for two days. The membrane layer formed in the secondary growth step did not require the calcination at 450°C or 650°C since no organic template was used.

Separation Process

A schematic diagram of the experimental apparatus is shown in Figure 8.1. After drying at 40°C for two days, the zeolite membrane sample was mounted in a stainless steel membrane cell with the zeolite layer on the feed side, and sealed by 4 O-rings cut out from parafilm. The permeation area of the membranes was 2.27 x 10^{-4} m^2. The feed pressure was 791kPa and the permeate pressure was 101.3 kPa. The flow rates of the feed (the mixture gas or the

pure gas) were controlled at 100 cc.min^{-1}. A gas chromatograph (GC) with an 80/100 mesh Porapak Q column, a TCD detector and He as carrier gas was used on-line to analyze the permeate composition. The thickness of the membrane was measured by a microscope. The waiting time for a new run to reach steady state was 24 hours or longer and it was determined by measuring permeate flow rate and composition. For pure systems, the run for the less adsorbed gas was done first. For N_2/CO_2 binary gas system, the order was 15%, 30%, 50%, 70%, and then 85% of CO_2 concentrations. After a run for more adsorbed gas, such as CO_2, a longer time desorption was followed. The desorption lasted even for several days, depending on the systems. When an equilibrium reached, the permeate concentration and flow rate were steady.

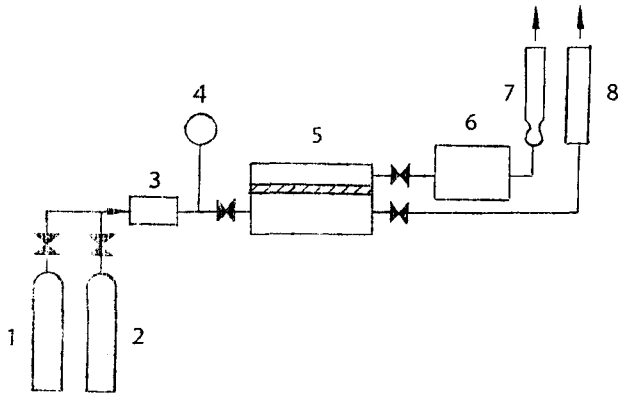

Figure 8.1. Schematic diagram of the experimental set-up of separation process.

1 – Sample gas cylinder 1 2 – Sample gas cylinder 2
3 – Mixing chamber 4 – Pressure gauge
5 – Membrane cell 6 – GC
7 – Bubble meter 8 – Rotameter

Volumetric System

An AccuSorb 2100E Physical Adsorption Analyzer supplied by Micromeritics Instrument Corporation was equipped with precise pressure transducers and thermocouples. Data acquisition was performed using a National Instruments based data acquisition card and Labview 6.1. The adsorbent sample was regenerated at approximately 350 °C under vacuum for approximately 20 hours before use. Helium, with a negligible adsorption on the

adsorbent, was used to measure the dead volume in the gas phase.

Materials

The gases used in the experiments are listed in Table 8.2.

Table 8.2. Details of gases

Gases	Grade	Purity	Supplier
CH_4	Ultra High Purity 3.7	99.97 %	Praxair Inc., Ottawa
N_2	Ultra High Purity 5.0	99.999 %	Praxair Inc., Ottawa
CO_2	Bone Dry 3.0	99.9 %	Praxair Inc., Ottawa
He	Ultra High Purity 5.0	99.999 %	Praxair Inc., Ottawa

The membranes and adsorbent used in the experiments are listed in Table 8.3.

Table 8.3. Details of the materials used

Products	Commercial Number	Size	Supplier
Dimethyl Silicone Membrane	SSP-M823	0.003 " (thickness) 12"x12" (sheet)	Specialty Silicone Products, New York, NY, USA
Silicone Polycarbonate Membrane	SSP-M213	0.001 " (thickness) 12"x12" (sheet)	Specialty Silicone Products, New York, NY, USA
MFI zeolite	HiSiv-3000	1/16 " extrudate as received Crushed to 20 x 60 mesh	Universal Oil Products, Des Plaines, IL, USA

RESULTS AND DISCUSSION

Adsorption plays an important role in the separation processes involving zeolite membranes. In order to quantify this role, adsorption capacities of CO_2, CH_4 and N_2 gases were considered for MFI zeolite at 24 °C under pressures up to 800 kPa. In order to do that, experimental adsorption capacities obtained from our previous data (Chapters 4, 5 and 6) with the same adsorbent were used. By using the temperature independent Toth isotherm model parameters obtained from this experimental data, adsorption capacities at 24°C were estimated up to 800 kPa pressure and results are shown in Figure 8.2 for these gases. The order of adsorption capacity as well as the slopes of the isotherms is $CO_2 > CH_4 > N_2$ mainly because of their dipole moments, polarizabilities and kinetic diameters.

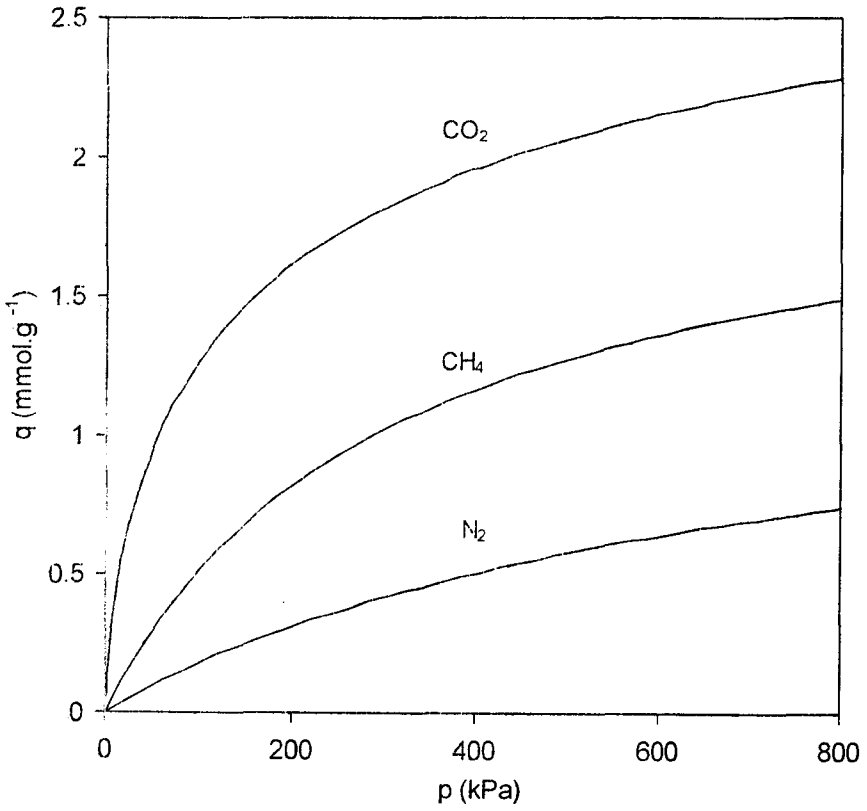

Figure 8.2. Temperature independent Toth isotherms for CO_2, CH_4 and N_2 on silicalite at 24 °C

Zeolite membranes are micro-porous inorganic membranes that have been used in a wide variety of applications. The affinity of the permeating molecules toward the zeolite material and the difference between the size of these molecules and that of the membrane pores are the factors that play the key roles in these separations. Most of the zeolite membranes investigated to date belong to the MFI type (silicalite and ZSM-5) although other membrane materials, such as mordenite and zeolites A and Y, have also been studied (Bernal et al., 2004).

For the separation of N_2/CO_2 with MFI zeolite membrane, the compositions of permeate are measured by GC and are shown in Figure 8.3, where "No mem" is for the disk after coating and calcinations but before the secondary grown crystallization. The periods of secondary grown crystallization are 3, 12, and 36 hours. The compositions of feed and permeate for N_2/CO_2 mixture are compared for the different periods of secondary grown crystallization. As can be seen from this figure, the disk without the secondary grown crystallization hardly separates these gases, as feed and permeate compositions are very similar. The difference between feed and permeate compositions increases with decreasing time of secondary grown crystallization. The experiments for shortening the secondary grown crystallization time have failed as the data were neither repeatable nor reliable because of defects, pinholes and/or uneven crystallization layer. For MFI zeolite membrane, making a super thin and uniform crystallization layer without defects and pinholes is a challenging task.

The primary requirement for an economic separation process is a membrane with sufficiently high permeability and selectivity. The permeability (coefficient) is defined in terms of the steady-state flux J_i and the pressure or fugacity driving force, Δp_i or Δf_i, normalized by the membrane thickness l,

$$P_i = \frac{J_i l}{\Delta p_i} = \frac{J_i l}{p_{iF} - p_{iP}} = \frac{J_i l}{px_i - py_i} \quad \text{.....(1)}$$

where J_i is the flux of Component i in cm^3 (STP).$cm^{-2}.s^{-1}$, l is the membrane thickness in cm, p is the total pressure in cmHg, Δp_i is the difference between upstream partial pressure and downstream partial pressure of Component i in cmHg, p_{iF} and p_{iP} are the upstream and

downstream partial pressure of Component i, respectively, in cmHg, x_i and y_i are the feed and the permeate compositions of Component i, respectively, and P_i is the permeability coefficient of Component i in cm^3 (STP).cm/(cm^2.s.cm Hg) (Ho and Sirkar, 1992). In general, the common unit of P is Barrer, 10^{-10} cm^3 (STP).cm/(cm^2.s.cm Hg).

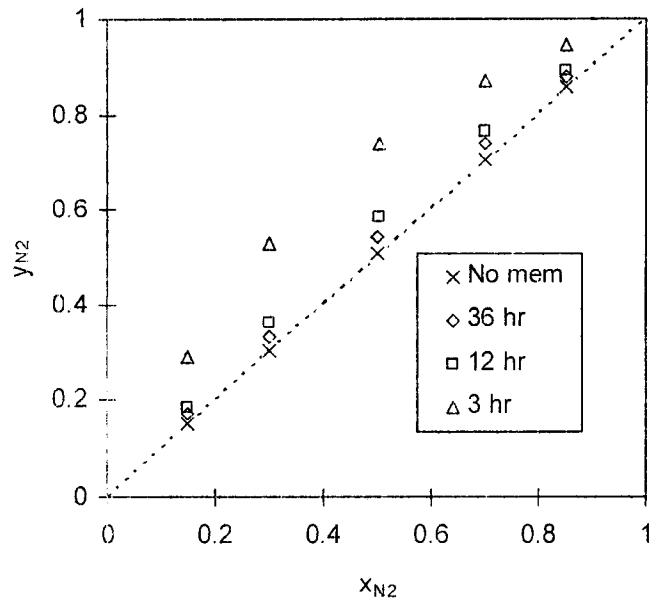

Figure 8.3. Relation between feed (x_{N2}) and permeate (y_{N2}) compositions for N_2/CO_2 through MFI membrane at 24 °C under 721.7 kPa feed and 101.3 kPa permeate pressures for different times of secondary grown crystallization.

The permeabilities of total mixture and individual gases in the mixing permeate are given in Table 8.4 and Figure 8.4 for different compositions in the feed. The permeabilities decrease dramatically after the secondary grown crystallization. Before the secondary grown crystallization, the permeability of CO_2 is only a little smaller than that of N_2, but the difference of the permeabilities is rather large after the secondary grown crystallization. The difference of the permeabilities increases with decreasing the period of time of secondary grown crystallization.

The ability of the membrane to separate gases is characterized by the separation factor,

$$\alpha_{A/B} = \frac{y_A / y_B}{x_A / x_B} \quad \text{..... (2)}$$

where y_A, y_B and x_A, x_B refer to the mole fraction of Components A and B in the permeate and feed streams, respectively (Ho and Sirkar, 1992). When the downstream pressure is absolute vacuum, the separation factor may be determined by ideal separation factor:

$$\alpha^*_{A/B} = \frac{P_A}{P_B} \quad \text{..... (3)}$$

where $\alpha^*_{A/B}$, the ratio of permeability coefficients, is the ideal separation factor. For the special case in which the absolute downstream pressure is close to zero, the ideal separation factor is equal to the separation factor (Ho and Sirkar, 1992).

Table 8.4. Permeabilities (Barrer) for mixture, CO_2 and N_2 compositions in the permeate

1 Barrer = 10^{-10} cm^3 (STP).cm/(cm^2.s.cm Hg)

Period of Time (secondary grown crystallization)	Gases	N_2 Compositions in the Feed						
		0	0.15	0.30	0.50	0.70	0.85	1.00
No Membrane (before the secondary grown crystallization)	Mixture	9224	10167	10720	11244	11673	12122	12923
	N_2	-	10398	10925	11408	11781	12189	12923
	CO_2	9244	10127	10634	11079	11422	11743	-
36 Hours	Mixture	6.57	34.3	48.6	57.9	65.7	77.3	96.6
	N_2	-	40.0	55.3	63.6	69.8	80.2	96.6
	CO_2	6.57	33.3	45.9	52.4	56.1	60.9	-
12 Hours	Mixture	6.45	35.2	50.7	59.0	64.5	69.8	75.3
	N_2	-	45.1	62.9	70.0	71.3	73.4	75.3
	CO_2	6.45	33.5	45.7	48.4	49.2	49.9	-
3 Hours	Mixture	6.24	21.4	27.7	36.5	45.4	53.5	62.4
	N_2	-	48.2	55.5	57.8	58.3	60.2	62.4
	CO_2	6.24	17.4	17.7	17.8	18.2	18.7	-

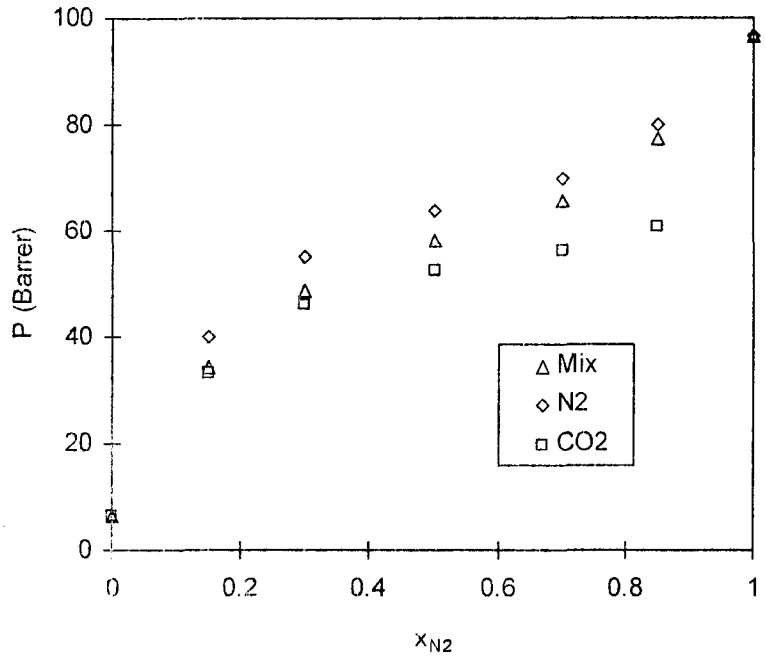

a. 36 hours for secondary grown crystallization

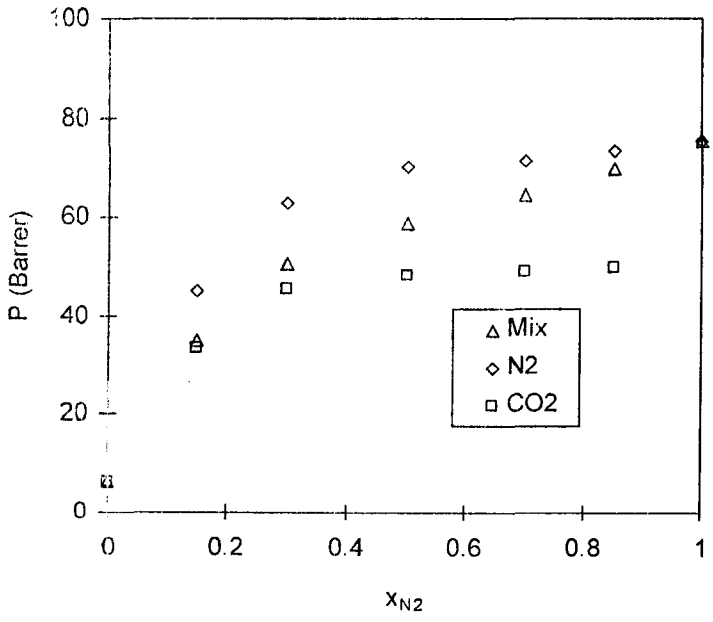

b. 12 hours for secondary grown crystallization

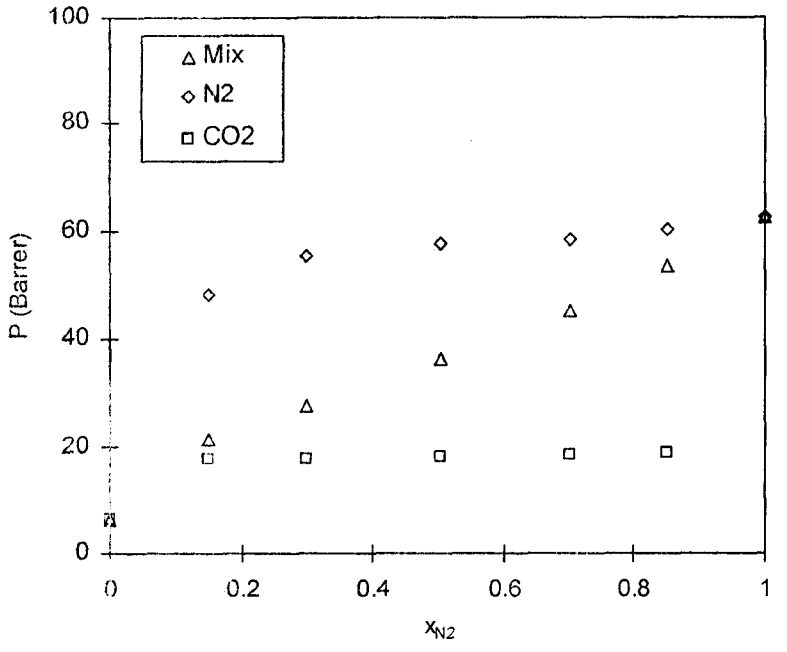

c. 3 hours for secondary grown crystallization

Figure 8.4. Relation between the permeability and the composition of feed (x_{CO2}) for N_2/ CO_2 through MFI membrane at 24 °C under 721.7 kPa feed and 101.3 kPa permeate pressures

The real and ideal separation factors are given as a function of the composition of feed (x_{N2}) for N_2/CO_2 through MFI membrane at 24 °C in Figure 8.5. As can be seen in this figure, the real and ideal separation factors are a little higher than 1 before the secondary grown crystallization. The real and ideal separation factors increase with decreasing time of secondary grown crystallization. Ideal separation factors are slightly bigger than real ones. Decreasing downstream pressure or applying vacuum downstream does not increase the real separation factor by much. Therefore, decreasing downstream pressure is not a good solution for improving ideal separation factors since vacuuming increase operational cost.

For checking the values of the real and ideal separation factors from the experiments carried out, there is a relation between the two separation factors (Barbari et al., 1989; King, 1980; Ho and Sirkar, 1992).

$$\alpha_{A/B} = \alpha^{*}_{A/B}\left(\frac{x_A(\alpha_{A/B}-1)+1-x_A\left(\frac{p_P}{p_F}\right)}{x_A(\alpha_{A/B}-1)+1-\frac{p_P}{p_F}}\right) \quad \text{.....(4)}$$

where $\alpha_{A/B}$ and $\alpha_{A/B}^{*}$ are the real and ideal separation factors, respectively, x_A is the fraction of Component A in the feed stream, and p_P and p_F are the permeate stream and feed stream pressures, respectively. With Equation (4), the experimental ideal and real separation factors are checked and the results showed that the difference between these values is rather small.

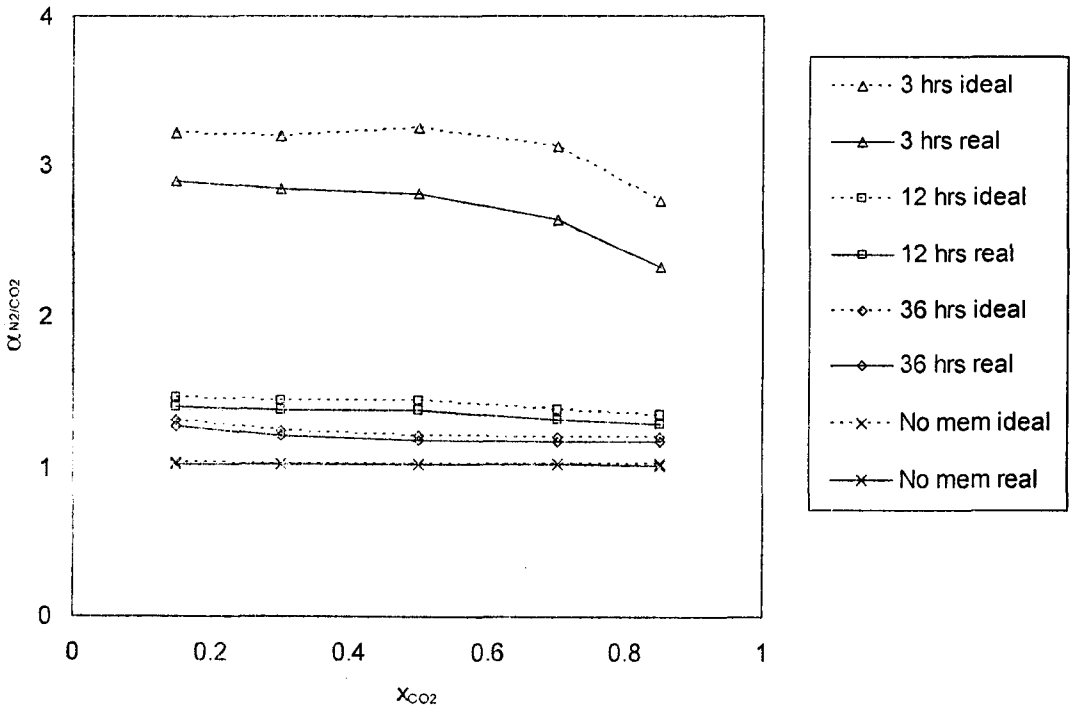

Figure 8.5. Separation factor for N_2/CO_2 through MFI membrane at 24 °C under 721.7 kPa feed and 101.3 kPa permeate pressures

Since the isotherm curves for the three gases are nonlinear in Figure 8.2, the adsorption of gases in MFI zeolite membrane may obey a more complex adsorption

isotherm, which is well described by a combination of Henry's law and Langmuir terms. Furthermore, this dual mode adsorption of gases into a MFI zeolite membrane impacts the diffusion process itself, and the model developed by Vieth and Sladek (1965) to account for diffusion in membrane is the widely accepted dual mode adsorption theory, which postulates the existence of two types of adsorption sites in a membrane. One, which accommodates mobile gas molecules following Henry's law, is the Henry's law adsorption site. The other type of adsorption site, in which gas molecules are much less mobile than those in Henry's law adsorption site, is the Langmuir site. In general, the second mode of adsorption may be associated with any mechanism which immobilizes penetrant molecules in a micro-heterogeneous medium (Vieth et al., 1976). As the kinetic part of the dual adsorption theory, the adsorption of mobile or diffusible species obeys Henry's law for gas adsorption in a membrane. The adsorption of immobilization at a fixed number of sites within the membrane can be represented by a nonlinear Langmuir expression. The penetrant adsorbed by the second mode is completely immobilized and, therefore, does not contribute to the diffusive flux. Only diffusion of the mobile species occurs, and it is driven by its concentration gradient or pressure gradient (Vieth and Sladek, 1965; Kesting and Fritzsche, 1993).

Gas transport in porous membranes might occur by viscous (Poiseuille) flow, Knudsen diffusion, surface diffusion, and molecular sieving with decreasing pore size and depending on pore-penetrant interactions. Surface diffusion has few subcategories: surface diffusion (in a narrow sense), capillary condensation, multilayer adsorption and monolayer adsorption. This order also follows with decreasing pore size and depending on pore-penetrant interactions. The fluxes through the gas phase and the adsorbed phase are to a first approximation independent and therefore additive so that the diffusivity will be given by the sum of the pore and surface contributions (Karger and Ruthven, 1992):

$$D = D_p + K\left(\frac{1-\varepsilon_p}{\varepsilon_p}\right)D_s \quad \text{.....(5)}$$

where D is the total diffusivity in $cm^2.s^{-1}$, D_s is the surface diffusivity in $cm^2.s^{-1}$, K is the dimensionless adsorption equilibrium constant, D_p denotes the contributions from Knudsen and other diffusions in $cm^2.s^{-1}$, and ε_p represents the porosity. When the first term is negligibly small, adsorption and surface diffusion control the process. The form of Equation

(5) is similar to that equation for solution-diffusion mechanism of non-porous membranes. It is noted that adsorption and solution have the similarity from the microcosmic view. If the adsorption and/or surface diffusion are very low, or the second term is extremely small, the case is a regular membrane process.

For MFI membranes, there are numerous micropores in the membrane and a strong interaction between membrane and gases. Because of the strong interaction, the dimensionless adsorption equilibrium constant is extremely high. Besides, surface diffusion is very high as the inside surface area of pores per unit volume is large due to small and numerous pores. Since the last term of Equation (5) is very high, the total diffusivity mainly depends on surface diffusion and adsorption (and desorption).

Before the secondary grown crystallization, the pore size is rather large, so Knudsen diffusion mainly dominates the separation of N_2/CO_2. Therefore, the separation factor is very small. According to the values, the separation factors from the experiments are even smaller than those of Knudsen diffusion because of adsorption and desorption.

After the secondary grown crystallization, there is a thin zeolite membrane on top of the disk, so the permeability is much lower since the pore size of the zeolite membrane is much smaller. As the pore size is much smaller, the specific surface is much larger, and surface diffusion becomes more important, while Knudsen diffusion cannot dominate the separation of N_2/CO_2. The calculated Knudsen diffusivities are about two orders of magnitude larger than the apparent diffusivities. It proves that apparent surface diffusivity is much lower than calculated Knudsen diffusivity and the process of surface diffusion does not follow Knudsen mechanism (Do and Do, 2001).

In surface diffusion, gas molecules interact with the surface, adsorb on surface sites and be mobile on the surface. If a pressure gradient exists, a difference in surface occupancy will occur. Therefore, a surface composition gradient is created and transport along the surface will occur if the molecules are mobile. However, there is a contradiction since the more the molecules are adsorbed the less the likelihood of them being mobile. This effect was clearly demonstrated by Uhlhorn et al. (1989). It was shown that CO_2 exhibits surface diffusion on γ-alumina membranes. When the amount of CO_2 adsorbed on the surface increased, the mobility decreased. Due to this lower mobility, effectively less CO_2 was transported through the membrane although more adsorption occurred.

After the secondary grown crystallization in these experiments, N_2 is transported through the MFI zeolite membrane more than CO_2 although the amount of CO_2 adsorbed is larger than that of N_2. According to the dual adsorption theory, the nonlinear isotherms of CO_2 can explain the reason why the molecules of N_2 are more mobile than those of CO_2. The main reasons are higher quadrupole moment and polarizability of CO_2 than those of N_2. Actually, the adsorbed phase can exhibit multilayer adsorption, capillary condensation, and surface diffusion (in a narrow sense) as well as monolayer adsorption.

After 36 hours of secondary grown crystallization, the layer of MFI zeolite membrane is very thick, so the pressure gradient (p/l) is very small. As diffusion of the mobile species is driven by its pressure gradient, most molecules of both CO_2 and N_2 are immobile, and the molecules of CO_2 block those of N_2 (Bernal et al., 2004). These are the reasons why the separation factors are smaller if the period of secondary grown crystallization is longer. If secondary grown crystallization is shortened, there are more mobile molecules of N_2 while most molecules of CO_2 are still immobile.

From Figure 8.2, the ratio of the adsorption capacity of CO_2 to N_2 can be calculated to be 3.2. Therefore, the number of CO_2 molecules on the surface of the micro-pores is much higher than that of N_2 molecules. This causes CO_2 molecules to be more immobile than N_2 molecules, causing higher N_2 permeability, compared to CO_2.

In Table 8.4, pure CO_2 permeability is very low, but the mixture permeability is much higher, even the mixture with small amount of nitrogen. Because nitrogen is much more mobile than carbon dioxide, it becomes a carrier gas for the CO_2 diffusion.

In addition to decreasing the pore size, there are two other ways to increase the contribution of the surface diffusion to total transport: altering the amount adsorbed and promoting surface mobility. For CO_2, the amount adsorbed is rather large, so the possible way to increase surface diffusion will be to increase surface mobility. A thinner membrane will have a higher pressure gradient. Probably, the best results with MFI membranes have been reported by Ando et al. (1998), who found a separation factor of 25.5 at a CO_2 permeance of 6.6×10^{-7} mol / (m^2.s.Pa), but another set of data they obtained is a separation factor of 10 at a CO_2 permeance of 5.0×10^{-8} mol / (m^2.s.Pa) at the same conditions (Mase et al., 1998). They made an excellent progress although their data are not repeatable. It is also noted that CO_2 was transported faster than N_2 in their experiments. The reason is that their

super thin membranes cause extremely high pressure gradient (p/l). so most molecules of CO_2 become mobile.

For the separation of CH_4/CO_2 with MFI zeolite membrane, the parameters are given in Table 8.5. When the membrane is thick, the separation of CH_4/CO_2 is not satisfactory, even worse than that of N_2/CO_2. On the conditions of the membrane separation process, the ratio between the adsorption capacity of CO_2 and CH_4 is 1.6 from Figure 8.2, so the number of CO_2 molecules is larger than that of CH_4 molecules on the surface of micro-pores. Because CO_2 molecules are much more immobile than those of CH_4, at the end, CH_4 can be transported faster than CO_2. In fact, CO2 is still immobile in the MFI membrane for CH_4/CO_2 separation. Therefore, for this separation, super thin membranes for causing extremely high pressure gradient are needed to make most molecules of CO_2 mobile.

Table 8.5. Parameters of separation of CH_4/CO_2 (50%/50% feed) through MFI membrane at 24 °C under 721.7 kPa feed and 101.3 kPa permeate pressures

Parameters	No membrane	36 hours	12 hours	3 hours
y_{CO2}	0.49	0.47	0.45	0.40
$\alpha_{CH4/CO2}$ Separation factor	1.04	1.12	1.22	1.49
$\alpha^*_{CH4/CO2}$ Separation factor	1.05	1.14	1.25	1.58
P (Barrer) Permeability	13559	63.4	57.2	49.9
P_{CO2} (Barrer) Permeability	13243	59.1	50.8	39.0
P_{CH4} (Barrer) Permeability	13875	67.6	63.7	61.4

For the separation of N_2/CH_4 with MFI zeolite membrane, the parameters are given in Table 8.6. When the membrane is thick, the separation of N_2/CH_4 is not good. In this case, apparently, Knudsen diffusion cannot dominate the separation of N_2/CO_2 as y_{N2} is even lager

than y_{CH4}. Therefore, surface diffusion, including monolayer adsorption and/or multilayer adsorption, and/or capillary condensation dominate this process and N_2 are more mobile than CH_4. Because surface diffusion and Knudsen diffusion have the opposite separation effect, the separation factors are so low. This case can help us explain the mechanism although it doesn't seem to have much meaning for real applications. On the conditions of the membrane separation process, the ratio between the adsorption capacity of CH_4 and N_2 is 2.1 from Figure 8.2, so the number of CH_4 molecules is larger than that of N_2 molecules on the surface of micro-pores. Because CH_4 molecules are much more immobile than those of N_2, at the end, N_2 can be transported faster than CH_4.

Table 8.6. Parameters of separation of N_2/CH_4 (50%/50% feed) through MFI membrane at 24 °C under 721.7 kPa feed and 101.3 kPa permeate pressures

Parameters	No membrane	36 hours	12 hours	3 hours
y_{N2}	0.50	0.52	0.54	0.57
$\alpha_{N2/CH4}$ Separation factor	1.00	1.07	1.18	1.34
$\alpha^*_{N2/CH4}$ Separation factor	1.00	1.08	1.20	1.40
P (Barrer) Permeability	15352	140	126	113
P_{CH4} (Barrer) Permeability	15353	135	115	94
P_{N2} (Barrer) Permeability	15351	145	138	132

For explaining the diffusion process theories more clearly for MFI membranes mentioned above, the main points are summarized below:

- The diffusion process of MFI membranes is different from that of regular membranes.

- The diffusion of the MFI membrane process can be assessed by Equation (5). In it the related parameters can be determined by experiments (Karger and Ruthven, 1992).
- Surface diffusion, including monolayer adsorption, multilayer adsorption, capillary condensation, can dominate the diffusion process of the MFI membrane.
- Dual mode adsorption theory is applicable to the diffusion process of the MFI membrane.
- Adsorption behaviors and parameters, such as Henry's law constant and isotherms, are important for MFI zeolite membranes
- These main points (theories, mechanisms, equations and views) memtioned above are compatible as a bridge between adsorption and membrane. It can be named the Li-Tezel Adsorption and Membrane Bridge or briefly named the Li-Tezel Bridge. It can be used for MFI zeolite membranes, maybe for other zeolite membranes, and even for non-zeolite and non-porous membranes.

Silicone rubber membranes, in general, are more permeable than non-silicone stable polymers. They possess the unique ability to allow various gases to permeate rapidly through it. This phenomenon is due primarily to the flexible silicone-oxygen-silicone linking sites of the silicone chain and an absence of crystallization in silicone rubber. The process of permeation through a non-porous membrane is actually a three stage activity. Whereas a porous material uses size exclusion as its method of separation, the process by which a non-porous membrane allows a separation to occur is a much more complex means to an end. These steps are: adsorption in, diffusion through and desorption from the membrane by the permeating gas. The rate of permeation is the product of diffusivity and solubility coefficients of the permeating gas. The solubility coefficients for gases into the silicone are comparable to those of most polymers but the diffusion rates through the silicone are nearly an order of magnitude greater than other membrane polymers. Therefore, silicone owes its rapid transport of gases to the high rate of diffusion, not solubility (Jha et al., 2006).

For the separation of CO_2/N_2 with two silicone rubber membranes, the parameters are given in Table 8.7. Here dimethyl silicone membrane is a modified silicone membrane, which has methyl-silicon-methyl group. These methyls are branches of silicone rubber

molecules. They increase the space between molecular chains, so gases can be transported through the membrane fast and easy. The other membrane is silicone polycarbonate membrane, another modified silicone membrane. According to the literature, most polycarbonates tend to have a high carbon dioxide selectivity ranging from 15 to over 25 (Powell and Qiao, 2006).

Table 8.7. Parameters of separation of CO_2 (15%feed) / N_2 through silicone rubber membranes at 24 °C under 101.3 kPa permeate pressure

Parameters	Dimethyl Silicone Membrane		Silicone Polycarbonate Membrane	
Feed Pressure (kPa)	446.1	790.8	446.1	790.8
y_{CO2}	0.351	0.402	0.449	0.534
$\alpha_{CO2/N2}$ Separation factor	3.12	3.90	4.73	6.65
$\alpha^*_{CO2/N2}$ Separation factor	4.57	4.86	8.61	9.43
P (Barrer) Permeability	17.2	16.4	119	132
P_{CO2} (Barrer) Permeability	57.2	54.3	617	648
P_{N2} (Barrer) Permeability	12.5	11.2	71.6	68.8

In comparison with the separation behaviours of the three membranes, the separation factor and permeability of the silicone polycarbonate membrane are better than those of both the dimethyl silicone membrane and the MFI membrane. Therefore, the silicone polycarbonate membrane is more practical in industrial applications in the separation of CO_2/N_2 for flue gases.

In Table 8.7, the parameters of dimethyl silicone membrane change only a little when feed pressure changes because diffusion dominates the separation process. However, the parameters of silicone polycarbonate membrane change more when feed pressure changes. As the permeability of silicone polycarbonate membrane is much higher than that of dimethyl silicone membrane, diffusion of silicone polycarbonate membrane is faster than that of dimethyl silicone membrane, so the rate of diffusion is so high that it is close to the rates of adsorption and desorption. Therefore, diffusion cannot control the separation process very well. At that time, adsorption and desorption play an important role in the separation process. According to the data in Table 8.7, at a higher pressure, the rates of adsorption and desorption increase more than the rates of diffusion. Therefore, the separation factor and permeability of silicone polycarbonate membrane are higher at a higher pressure.

CONCLUSIONS

1. Monolayer adsorption, multilayer adsorption, capillary condensation, and/or surface diffusion (in a narrow sense) dominate the separations of CO_2/N_2, CO_2/CH_4 and CH_4/N_2 with MFI zeolite membrane.
2. Among the three membranes studied, the silicone polycarbonate membrane gave the best separation factor to be used in industrial applications for the separation of CO_2/N_2 mixture for flue gas applications.
3. Adsorption plays an important role in the separations with MFI zeolite membrane and silicone rubber membranes.
4. The Li-Tezel (Adsorption and Membrane) Bridge is a tool suitable for MFI zeolite membranes, maybe for other zeolite membranes, and even for non-zeolite membranes.

ACKNOWLEDGMENTS

We wish to thank Mr. Al Kuiper, Dr. Dogan Paktunc and Mr. Rolando Lastra at the Natural Resources Canada for providing us with the high temperature furnace and its technical support to manufacture the alumina disks.

Financial supports received from the Natural Sciences and Engineering Research Council of Canada (NSERC), the Ontario Graduate Scholarship (OGS) Program, and the Canadian Society for Chemical Engineering (CSChE) are gratefully acknowledged.

NOMENCLATURE

D = (total) diffusivity, $cm^2.s^{-1}$

D_p = diffusivity in pores, $cm^2.s^{-1}$

D_s = surface diffusivity, $cm^2.s^{-1}$

J_i = flux of Component I, cm^3 (STP).$cm^{-2}.s^{-1}$

K = dimensionless adsorption equilibrium constant

l = membrane thickness, cm

p = (total) pressure, kPa, Pa or cm Hg

p_i = pressure of Component i, kPa, Pa or cm Hg

p_F = feed stream (upstream) pressure, kPa, Pa or cm Hg

p_P = permeate stream (downstream) pressure, kPa, Pa or cm Hg

p_{iF} = feed stream (upstream) partial pressure of Component i, cm Hg

p_{iP} = permeate stream (downstream) partial pressure of Component i, cm Hg

Δp_i = difference between upstream partial pressure and downstream partial pressure of Component I, cmHg

P = permeability, Barrer, 10^{-10} cm^3 (STP).cm/(cm^2.s.cm Hg)

P_i = permeability of Component i, Barrer, 10^{-10} cm^3 (STP).cm/(cm^2.s.cm Hg)

P_A = permeability of Component A, Barrer, 10^{-10} cm^3 (STP).cm/(cm^2.s.cm Hg)

P_B = permeability of Component B, Barrer, 10^{-10} cm^3 (STP).cm/(cm^2.s.cm Hg)

q = amount adsorbed, $mmol.g^{-1}$

x_i = mole fraction of Component i in the upstream, dimensionless

x_A = mole fraction of Component *A* in the upstream, dimensionless

x_B = mole fraction of Component *B* in the upstream, dimensionless

y_i = mole fraction of Component *i* in the downstream, dimensionless

y_A = mole fraction of Component *A* in the downstream, dimensionless

y_B = mole fraction of Component *B* in the downstream, dimensionless

Greek letters

α = separation factor, dimensionless

$\alpha_{A/B}$ = separation factor of Component *A* over Component *B*, dimensionless

α^* = ideal separation factor, dimensionless

$\alpha^*_{A/B}$ = ideal separation factor of Component *A* over Component *B*, dimensionless

ε_p = porosity, dimensionless

Abbreviations

APS = average particle size

GC = gas chromatography

GHG = greenhouse gases

GWP = greenhouse warming potential

HPC = hydroxy propyl cellulose

LFG = landfill gas

MW = molecular weight

SSP = Specialty Silicone Products

STP = standard temperature and pressure

TPAOH = tetrapropylammonium hydroxide

TCD = thermal conductivity detector

REFERENCES

Ando, Y., Y. Hirano, S. Mase and H. Taguchi, "Preparation and Characterization of Monolithic and Planar Elements of Zeolite Membranes", Proc. ICIM' 98, Nagoya, Japan, p.124 (1998).

Ashworth, A. J., B. J. Brisdon, R. England, A. G. W. Hodson and A. R. Watts, "The Permeability of Carbon Dioxide and Methane in Poly(organosiloxane) Membranes Containing Mono- and Di-ester Functionalities", Journal of Membrane Science **101**, 109-115 (1995).

Ayala, D., A. E. Lozano, J. Abajo, C. Garcia-Perez, J. G. Campa, K.-V. Peinemann, B. D. Freeman and R. Prabhakar, "Gas Separation Properties of Aromatic Polyimides", Journal of Membrane Science **215**, 61-73 (2003).

Barbari, T. A., W. J. Koros and D. R. Paul, "Polymeric Membranes based on bisphenol-A for Gas Separation", Journal of Membrane Science **42**, 69-86 (1989).

Bakker, W. J. W., F. Kapteijn, J. Poppe and J. A. Moulijn, "Permeation Characteristics of a Metal-Supported Silicalite-1 Zeolite Membrane", Journal of Membrane Science **117**, 57-78 (1996).

Bernal, M. P., J. Coronas, M. Menendez and J. Santamaria, "Separation of CO_2/N_2 Mixtures Using MFI-Type Zeolite Membranes", AIChE Journal **50**, 127-135 (2004).

Bos, A., I. Punt, H. Strathmann and M. Wessling, "Suppression of Gas Separation Membrane Plasticization by Homogeneous Polymer Blending", AIChE Journal **47**, 1088-1093 (2001).

Cavenati, S., C. A. Grande and A. E. Rodrigues, "Adsorption Equilibrium of Methane, Carbon Dioxide, and Nitrogen on Zeolite 13X at High Pressures", Journal of Chemical and Engineering Data **49**, 1095-1101 (2004).

Cavenati, S., C. A. Grande and A. E. Rodrigues, "Upgrade of Methane from Landfill Gas by Pressure Swing Adsorption", Energy and Fuels **19**, 2545-2555 (2005).

Chenar, M. P., M. Soltanieh, T. Matsuura, A. Tabe-Mohammadi and K. C. Khulbe, "The Effect of Water Vapor on the Performance of Commercial Polyphenylene Oxide and Cardo-type Polyimide Hollow Fiber Membranes in CO_2/CH_4 Separation Applications", Journal of Membrane Science **285**, 265–271 (2006).

Cuffe, L., J. M. D. MacElroy, M. Tacke, M. Kozachok and D. A. Mooney, "The Development of Nanoporous Membranes for Separation of Carbon Dioxide at High Temperatures", Journal of Membrane Science **272**, 6–10 (2006).

Do, D. D., "Adsorption Anatysis: Equilibria and Kinetics", Imperial College Press, London, UK, pp. 1-148 (1998).

Do, D. D. and H. D. Do, "Surface Diffusion of Hydrocarbons in Activated Carbon: Comparison between Constant Molar Flow, Differential Permeation and Differential Adsorption Bed Methods", Adsorption **7**, 189-209 (2001).

Dong, F., H. Lou, A. Kodama, M. Goto and T. Hirose, "The Petlyuk PSA Process for the Separation of Ternary Gas Mixtures: Exemplification by Separation a Mixture of CO_2-CH_4-N_2", Separation and Purification Technology **16**, 159-166 (1999).

Espeso, J., A. E. Lozano, J.G. Campa and J. Abajo, "Effect of Substituents on the Permeation Properties of Polyamide Membranes", Journal of Membrane Science **280** 659–665 (2006).

Golden, T. C. and S. Sircar, "Gas Adsorption on Silicalite", Journal of Colloid Interface Science **162**, 182-188 (1994).

Hasegawa, Y., K. Watanabe, K. Kusakabe and S. Morooka, "The Separation of CO_2 Using Y-Type Zeolite Membranes Ion-Exchanged with Alkali Metal Cations", Desalination **22-23**, 319–325 (2001).

Heuchel, M. and D. Hofmann, "Molecular Modelling of Polyimide Membranes for Gas Separation", Desalination **144**, 67–72 (2002).

Ho, W. S. W. and K. K. Sirkar, "Membrane Handbook", Van Nostrand Reinhold, New York, NY, USA (1992)

Hyun, S. H., J. K. Song and B. I. Kwak, "Synthesis of ZSM-5 Zeolite Composite Membranes for CO2 Separation", Journal of Materials Science **34**, 3095–3103 (1999).

Ismail, A. F., I. R. Dunkin, S. L. Calliven and S. J. Shilton, "Production of Super Selective Polysulfone Hollow Fiber Membranes for Gas Separation", Polymer **40**, 6499–6506 (1999).

Ito, A., S. Duan, Y. Ikenori and A. Ohkawa, "Permeation of Wet CO_2/CH_4 Mixed Gas through a Liquid Membrane Supported on Surface of a Hydrophobic Microporous Membrane", Separation and Purification Technology **24**, 235–242 (2001).

Jayaramana, A., A. J. Hernandez-Maldonadoa, R. T. Yanga, D. Chinnb, C. L. Munsonb and D. H. Mohrb, "Clinoptilolites for Nitrogen/Methane Separation", Chemical Engineering Science **59**, 2407 – 2417 (2004).

Jha, P., L. W. Mason and J. D. Way, "Characterization of Silicone Rubber Membrane Materials at Low Temperature and Low Pressure Conditions", **272** 125–136 (2006).

Karger, J. and D. M. Ruthven, "Diffusion in Zeoites and Other Microporous Solids", John Wiley & Sons, New York, NY, USA (1992).

Katsaros, F. K., T. A. Steriotis, A. K. Stubos, A. Mitropoulos, N. K. Kanellopoulos and S. Tennison, "High Pressure Gas Permeability of Microporous Carbon Membranes", Microporous Materials **8**, 171–176 (1997).

Kazama, S., T. Teramoto and K. Haraya, "Carbon Dioxide and Nitrogen Transport Properties of Bis(phenyl)fluorene-based Cardo Polymer Membranes", Journal of Membrane Science **207**, 91–104 (2002).

Kesting, R. E. and A. K. Fritzsche, "Polymeric Gas Separation Membranes", John Wiley & Sons, New York, NY, USA (1993).

Kim, M., Y. Park, K. Youm and K. Lee, "Gas Permeation Through Water-Swollen Polysaccharide/Poly(vinyl alcohol) Membranes", Journal of Applied Polymer Science **91**, 3225–3232 (2004).

King, C. J., "Model for Sorption of Mixed Gases in Glassy Polymers", 2nd ed., McGraw-Hill Book, New York, NY, USA (1980).

Kresse, I., A. Usenko, J. Springer and V. Privalko, "Gas Transport Properties of Soluble Poly(amide imide)s", Journal of Polymer Science Part B: Polymer Physics **37**, 2183 - 2193 (1999).

Kusakabe, K., T. Kuroda, A. Murata and S. Morooka, "Formation of a Y-Type Zeolite Membraneona Porousr-Alumina Tube for Gas Separation", Ind. Eng. Chem. Res. **36**, 649-655 (1997).

Kusakabe, K., T. Kuroda and S. Morooka, "Separation of Carbon Dioxide from Nitrogen Using Ion-Exchanged Faujasite-Type Zeolite Membranes Formed on Porous Support Tubes", Journal of Membrane Science **148**, 13-23 (1998).

Kwak, B. I., S. H. Hyun and G. T. Kim, "CO_2 Separation Characteristics of ZSM-5 Composite Membranes Synthesized by the Hydrothermal Treatment", Journal of Materials Science Letters **20**, 1893–1896 (2001).

Lee, Y., I. Song, Y. Lee, S.-B. Lee and J.-H. Kim, "Numerical Simulation on Separation of Carbon Dioxide from Nitrogen by Hollow Fiber Membrane of Poly(ethersulfone)", Desalination **200**, 169–172 (2006).

Lehermeier, H. J., J. R. Dorgan and J. D. Way, "Gas Permeation Properties of Poly(lactic acid)", Journal of Membrane Science **190**, 243–251 (2001).

Leung, Y. L. A. and K. L. Yeung, "Microfabricated ZSM-5 Zeolite Micromembranes", Chemical Engineering Science **59**, 4809–4817 (2004).

Li, P. and F. H. Tezel, "Equilibrium and Kinetic Analysis of CO_2-N_2 Adsorption Separation by Concentration Pulse Chromatography", 40th IUPAC Congress, Beijing, P. R. China (2005), p61, 1-O-034.

Li, P. and F. H. Tezel, "Adsorption separation of methane and carbon dioxide from landfill gas", AICHE (American Institute of Chemical Engineers) Annual Meeting, San Francisco, USA, 333c (2006).

Li, P. and F. H. Tezel, "Adsorption Separation of N_2, O_2, CO_2 and CH_4 Gases by β-Zeolite", Microporous & Mesoporous Materials **98**, 94–101 (2007).

Li, S., J. L. Falconer and R. D. Noble, "SAPO-34 membranes for CO_2/CH_4 separation", Journal of Membrane Science **241**, 121–135 (2004).

Li, S., G. Alvarado, R. D. Noble and J. L. Falconer, "Effects of Impurities on CO_2/CH_4 Separations through SAPO-34 Membranes", Journal of Membrane Science **251**, 59–66 (2005).

Liu, L., A.Chakma and X. Feng, "Preparation of Hollow Fiber Poly (etherblockamide) / Polysulfone Composite Membranes for Separation of Carbon Dioxide from Nitrogen", Chemical Engineering Journal **105**, 43–51 (2004).

Lovallo, M. C., A. Gouzinis and M. Tsapatsis, "Synthesis and Characterization of Oriented Membranes Prepared by Secondary Growth", AIChE J. **44** 1903-1913 (1998).

Mase, S., Y. Ando, Y. Hirano and H. Taguchi, "Planar Type Module with Zeolite (MFI) Membranes", Proc. ICIM' 98, Nagoya, Japan, p.652 (1998).

Masuda, T., K. Hashimoto, F. Kapteijn and J. A. Moulijn, "Selective Permeation of CO_2 from Mixture Gas of CO_2 and N_2 through ZSM-5 Zeolite Membrane", Proc. ICIM' 98, Nagoya, Japan, p.128 (1998).

Mizukami, K., H. Takaba, Y. Kobayashi, Y. Oumi, R. V. Belosludov, S. Takami, M. Kubo and A. Miyamoto, "Molecular Dynamics Calculations of CO_2/N_2 Mixture through the NaY Type Zeolite Membrane", Journal of Membrane Science **188**, 21–28 (2001).

Mohammadi, A. T., T. Matsuura and S. Sourirajan, "Gas Separation by Silicone-Coated Dry Asymmetric Aromatic Polyamide Membranes", Gas. Sep. Purif. **9**, 181–187 (1995).

Moon, J., Y. Park, M. Kim, S. Hyun and C. Lee, "Permeation and Separation of a Carbon Dioxide/Nitrogen Mixture in a Methyltriethoxysilane Templating Silica/α-alumina Composite Membrane", Journal of Membrane Science **250**, 195–205 (2005).

Morisato, A. and I. Pinnau, "Synthesis and Gas Permeation Properties of Poly(4-methyl-2-pentyne)", Journal of Membrane Science **121**, 243–250 (1996).

Mulgundmath, V. P., P. Li, F. H. Tezel, T. Saatcioglu, T. C. Golden, J. Mogan and B. Morin, "Adsorption separation of CO_2/N_2 and CO_2/CH_4 by zeolites", FOA9 (9th International Conference on Fundamentals of Adsorption), Sicily, Italy (2007a).

Mulgundmath, V. P., P. Li, F. H. Tezel, F. Hou, T. C. Golden, J. Mogan and B. Morin, "Binary adsorption behavior of methane and nitrogen gases", FOA9 (9th International Conference on Fundamentals of Adsorption), Sicily, Italy (2007b).

Okamoto, K., M. Yoshino, K. Noborio, H. Maeda, K. Tanaka and H. Kita, "Preparation of Carbon Molecular Sieve Membranes and Their Gas Separation Properties", in "Membrane Formation and Modification" edited by I. Pinnau and B. D. Freeman, American Chemical Society, Washington, DC, USA (2000).

Orme, C. J., M. K. Harrup, T. A. Luther, R. P. Lash, K. S. Houston, D. H. Weinkauf and F. F. Stewart, "Characterization of Gas Transport in Selected Rubbery Amorphous Polyphosphazene Membranes", Journal of Membrane Science **186**, 249–256 (2001).

Pesiri, D. R., B. Jorgensen and R. C. Dye, "Characterization of Gas Transport in Selected Rubbery Amorphous Polyphosphazene Membranes", Journal of Membrane Science **186**, 249–256 (2001).

Pesiri, D. R., B. Jorgensen and R. C. Dye, "Thermal Optimization of Polybenzimidazole Meniscus Membranes for the Separation of Hydrogen, Methane, and Carbon Dioxide", Journal of Membrane Science **218**, 11–18 (2003).

Petersen, J. and K.-V. Peinemann, "Novel Polyamide Composite Membranes for Gas Separation Prepared by Interfacial Polycondensation", Journal of Applied Polymer Science **63**, 1557 - 1563 (1997).

Poseph, J. C., V. A. Tuan, J. L. Falconer and R. D. Noble, "Synthesis and Permeation Properties of SAPO-34 Tubular", Ind. Eng. Chem. Res. **37**, 3924-3929 (1998).

Powell, C. E. and G. G. Qiao, "Polymeric CO_2/N_2 Gas Separation Membranes for the Capture of Carbon Dioxide from Power Plant Flue Gases", Journal of Membrane Science **279**, 1-49 (2006).

Richard, V., E. Favre, D. Tondeur and A. Nijmeijer, "Experimental Study of Hydrogen, Carbon Dioxide and Nitrogen Permeation through a Microporous Silica Membrane", Chemical Engineering Journal **84**, 593-598 (2001).

Sanchez, J.,C. Charmette and P. Gramain, "Poly(ethyleneoxide-co-epichlorohydrin) membranes for carbon dioxide separation", Journal of Membrane Science **205**, 259–263 (2002).

Sheikh, M. A., M. M. Hassan and K. F. Loughlin, "Adsorption Equilibria and Rate Parameters for Nitrogen and Methane on Maxsorb Activated Carbon", Gas Separation and Purification **10**, 161-168 (1996).

Shen, J., J. Qiu, L. Wu and C. Gao, "Facilitated Transport of Carbon Dioxide through Poly(2-N, N-dimethyl aminoethyl methacrylate-co-acrylic acid sodium) Membrane", Separation and Purification Technology **51**, 345–351 (2006).

Shen, J., L. Wu, L. Zhang, Y. Dong, H. Chen and C. Gao, "Selective Permeation of CO_2 through a Composite Membrane witha Separation Layer of 2-N, N-Dimethyl Aminoethyl Methacrylate and Acrylic Acid Copolymer", Desalination **193**, 327–334 (2006).

Sridhar, S., B. Smitha, M. Ramakrishna and T. M. Aminabhavi, "Modified Poly(phenylene oxide) Membranes for the Separation of Carbon Dioxide from Methane", Journal of Membrane Science **289**, 202–209 (2006).

Tabe-Mohammadi, A., "A Review of the Applications of Membrane Separation Technology in Natural Gas Treatment", Separation Science and Technology **34**, 2095-2111 (1999).

Thundyil, M. J., Y. H. Jois and W. J. Koros, "Effect of Permeate Pressure on the Mixed Gas Permeation of Carbon Dioxide and Methane in a Glassy Polyimide", Journal of Membrane Science **152**, 29-40 (1999).

Tiemblo, P., J. Guzman, E. Riande, C. Mijangos, M. Herrero, J. Espeso and H. Reinecke, "Diffusion of Small Molecules through Modified Poly(vinyl chloride) Membranes", Journal of Polymer Science: Part B: Polymer Physics **40**, 964–971 (2002).

Tomita, T., K. Nakayama and H. Sakai, "Gas Separation Characteristics of DDR Type Zeolite membrane", Microporous and Mesoporous Materials **68**, 71–75 (2004).

Uhlhorn, R. J. R., K. Keizer and A. J. Burggraaf, "Gas and Surface Diffusion in (Modified) γ-alumina Systems", Journal of Membrane Science **46**, 225-246 (1989).

Van den Broeke, L. J. P., W. J. W. Bakker, F. Kapteijn and J. A. Moulijn, "Transport and Separation Properties of a Silicalite-1 Membrane—II.Variable Separation Factor", Chemical Engineering Science **54**, 259-269 (1999).

Vieth, W. R. and K. J. Sladek, "A Model for Diffusion in a Glassy Polymer", Journal of Colloid Science **20**, 1014–1033 (1965).

Vieth, W. R., J. M. Howell and J. H. Hsieh, "Dual sorption theory", Journal of Membrane Science **1**, 177-220 (1976).

Warmuzinski, K. and W. Sodzawiczny, "Effect of Adsorption Pressure on Methane Purity during PSA Separations of CH_4/N_2 Mixtures", Chemical Engineering and Processing **38**, 55–60 (1999).

Wu, J. and Q. Yuan, "Gas Permeability of a Novel Cellulose Membrane", Journal of Membrane Science **204**, 185–194 (2002).

Yang, S. M., Y. E. Lee, S. H. Hyun and C. H. Lee, "Organic-Templating Approach to Synthesis of Nanoporous Silica Composite Membranes (I): TPA-Templating and CO_2 Separation", Journal of Materials Science **37**, 2519–2525 (2002).

CHAPTER IX

CONCLUSIONS, CONTRIBUTIONS AND RECOMMENDATIONS

CONCLUSIONS

CONTRIBUTIONS

RECOMMENDATIONS

CONCLUSIONS

The general conclusions, which integrate the material addressed in the papers, excluding the two papers in the appendices, are provided as follows:

1. The initial adsorption equilibrium separation factors decrease as column temperatures increase for all the adsorbents and separations studied.
2. The four zeolites studied, 13X, NaY, β and silicalite all have good separation factors for the separation of CO_2/N_2 for equilibrium processes. The order of the equilibrium separation factors is 13X (Ceca) > 13X (Zeochem) > NaY > β > Silicalite in the temperature range studied.
3. Micro-pore diffusion resistance is the definite dominant mass transfer mechanism for all the adsorbents and separations studied. The order of the contributions of three mass transfer resistances is micro-pore diffusion >> macro-pore diffusion > external film mass transfer, which is identical with the results for other similar systems from the literature.
4. According to the pure gas isotherm data on silicalite, the order of pure gas adsorption capacity is $CO_2 > CH_4 > N_2$. The pure gas adsorption capacity decreases with increasing temperature on silicalite in the systems studied as expected from physical adsorption systems.
5. Among the three concentration pulse chromatographic methods, generally the MVV-CPM is good, but when the difference between the adsorption capacities of the two adsorbates is big, the HT-CPM and the MTT-CPM are much better.
6. For the binary systems, the capacities of all the adsorbates increase with decreasing temperature. Therefore, temperature is a very important factor for these separations.
7. For predicting the binary system behaviour from pure component data, most models used often cannot describe the real binary system accurately and they can be used only at low temperatures or for rough estimation when the experimental binary data are not available.
8. The binary adsorption data on silicalite at low temperatures satisfy the integral thermodynamic consistency test fairly well. The thermodynamic consistency becomes worse as temperature increases.

9. Silicalite has good selectivity for the adsorption separations of CO_2/N_2, CO_2/CH_4 and CH_4/N_2. It is very promising as an adsorbent in industrial applications for the three separations for landfill gas, flue gas and natural gas applications.
10. From the economic analyses carried out, it was shown that it is practical to operate adsorption separations of CO_2/N_2, CO_2/CH_4 and CH_4/N_2 with silicalite.
11. Adsorption plays an important role in the separations with MFI zeolite membrane and silicone rubber membranes.
12. The Li-Tezel (Adsorption and Membrane) Bridge is a tool suitable for MFI zeolite membranes, maybe for other zeolite membranes, and even for non-zeolite membranes.

CONTRIBUTIONS

The main contributions of this thesis are summarized as follows:

Adsorption kinetics and equilibrium behaviours are studied at three temperatures with zeolites as adsorbents by using concentration pulse chromatography for adsorption separations. Henry's law constants are calculated from the corrected first moment of the response peaks. The heat of adsorption and the pre-exponential factors are obtained by using the Van't Hoff equation. The micro-pore diffusion (D_c/r_c^2) is determined from the corrected first and second moment of the response peaks, and the three different mass transfer mechanisms are discussed. From the data, adsorption separation factors are obtained for the adsorption separation processes. Adsorption applications and fundamentals are benefit from these Henry's law constants, diffusivities and other parameters and behaviors obtained from our study. Carbon dioxide, nitrogen, methane and oxygen adsorption with β-zeolite are investigated in Chapter II and carbon dioxide and nitrogen adsorption with silicalite, NaY and 13X are investigated in Chapter III. The first paper in Chapter II has been already published in Microporous and Mesoporous Materials and presented at 55th CSChE Conference. The second paper transcript in Chapter III has been accepted to Journal of Colloid and Interface Science to be published and presented at 40th IUPAC Conference.

Adsorption separations are studied on silicalite by both the constant volume method and the concentration pulse chromatographic techniques to determine pure and mixture

adsorption behaviour. Seven pure adsorption isotherm models are considered for the experimental isotherms of the pure systems obtained by the constant volume method in the pressure range from 0 and 5 atmospheres at 40, 70 and 100 °C. The ranges of temperature and pressure are extended to other operating conditions by using two temperature independent isotherm models. Ideal separation factors are also obtained from the isotherms for the pure systems. Experimental binary isotherms at different concentrations are determined at 40, 70 and 100 °C and 1 atmosphere total pressure by using three concentration pulse chromatographic techniques: HT-CPM (Harlick and Tezel-Concentration Pulse Method), MTT-CPM (Modified Triebe and Tezel-Concentration Pulse Method) and MVV-CPM (Modified Van der Vlist and Van der Meijden-Concentration Pulse Method). By using seven prediction models most often used, difference between real and predicted adsorption behaviors for mixtures is shown for a warning: this type of prediction is often not reliable although it is widely used in the present. Equilibrium phase diagrams and separation factors are obtained from the experimental binary isotherms. The integral thermodynamic consistency tests are also shown and discussed. Carbon dioxide/nitrogen, carbon dioxide/methane and methane/ nitrogen studies carried out with silicalite are given in Chapters IV-VI, respectively. The third paper transcript given in Chapter IV has been revised to be published in Separation Science and Technology and has been presented at 2006 AIChE Conference. The fourth paper transcript in Chapter V has been submitted to the Journal of Chemical and Engineering Data and has been presented at 56th CSChE Conference. The fifth paper transcript in Chapter VI will be submitted to the Journal of Chemical and Engineering Data and has been presented at 56th CSChE Conference.

In Chapter VII, dynamics of adsorption separation of carbon dioxide/nitrogen, carbon dioxide/methane and methane/nitrogen with silicalite adsorbent are studied with the parameters and data obtained from the results of experiments carried out in this work and in the literature. Henry's law constants are taken directly from the results obtained in this study. By using the Rosen Model, the rates of transfer in the adsorption are unravelled and the breakthrough curves of adsorption dynamics are worked out. The parametric analyses of adsorption separation processes for carbon dioxide/nitrogen, carbon dioxide/methane and methane/nitrogen are carried out. For real applications, the effects of pressure, particle size,

superficial velocity and column length are discussed. At the end, the economic assessments of PSA processes are compared with that of membrane systems. It was concluded that, adsorption is an economical method for these three separations. The sixth paper transcript Chapter VII will be submitted to a journal.

For explaining the contributions of Chapters IV-VII more clearly, the main points are summarized below:

- New mixture adsorption behaviours for different separation applications.
- Difference between real and predicted adsorption behavior for mixtures.
- Benefit for designing and building adsorption columns for the three separations considered

In Chapter VIII, the syntheses and applications of MFI zeolite membrane are studied. Following separations are considered: CO_2/N_2 for flue gas applications, CO_2/CH_4 for landfill gas and natural gas applications and CH_4/N_2 for landfill gas and natural gas applications with MFI zeolite membrane and CO_2/N_2 for flue gas applications with two types of silicone rubber membranes (silicone polycarbonate membrane and dimethyl silicone membrane). The separation factors and permeability values are measured. Their adsorption behaviours in the separation processes are analyzed and separation process mechanisms are discussed. The Li-Tezel (Adsorption and Membrane) Bridge is a tool suitable for MFI zeolite membranes, maybe for other zeolite membranes, and even for non-zeolite membranes. The seventh paper transcript Chapter VIII will be submitted to a journal.

RECOMMENDATIONS

During the period of research, a number of interesting topics arose and the most important are presented here as recommendations for further work. Some initial ideas that would allow carrying on these studies are discussed below.

Pure component adsorption kinetics and equilibrium behaviours for methane gas with silicalite, NaY and 13X can be studied for further research to be able to predict the separations of CO_2/CH_4 and CH_4/N_2 with the data in this thesis, to compare the other

adsorption separation techniques and to study membrane mass transfer mechanisms. For methane and nitrogen, flow rates of carrier gas should be as slow as 2 – 5 $cc.min^{-1}$. Additionally, the Zero Length Column Chromatography (ZLC) technique can be applied for extending research on diffusivities.

For binary adsorption isotherms, more adsorbents should be studied. Higher pressure can be tried if possible and the effect of pressure can be studied with several different pressures. Moreover, ternary system is a good topic for future research for more complex systems.

For membrane applications, MFI olefin/paraffin separation with zeolite membrane is a potential topic and extending the research and applications of the Li-Tezel (Adsorption and Membrane) Bridge is also a valuable topic.

In the adsorption research lab, a regulated power supply should be equipped for GCs, volumetric system, binary gas adsorption system, membrane shell system, and adsorption equilibrium and kinetic system to obtain more accurate and more precise data.

A better switch for recording the starting time on GCs should be equipped for decreasing the change of electric resistance during switching it.

Furthermore, it is better to use a more precise TCD (Thermal Conductivity Detector) for adsorption equilibrium and kinetic studies.

APPENDIX I

ADSORPTION SEPARATION OF CO_2/N_2 AND CO_2/CH_4 BY ZEOLITES

Mulgundmath, V.P [a]., Li, P [a]., Tezel, F.H [a]., Saatcioglu, T [a].,

Golden, T.C [b]., Mogan, J [c]., Morin, B [c]

a Department of Chemical Engineering, University of Ottawa,
161 Louis Pasteur, Ottawa. K1N 6N5. CANADA

b Air Products and Chemicals, Inc.,
7201 Hamilton Blvd., Allentown, PA USA 18195-1501, USA.

c Alcan Specialty Aluminas,
1000 Development Drive, P O Box 250, Brockville. ON K6V 5V5. CANADA

Accepted to be presented in FOA9 (Fundamentals Of Adsorption 9th International Conference) in Sicily, Italy on May 20-25, 2007 (Paper is available).

It will be submitted to a journal.

ABSTRACT

Accumulation of greenhouse gases in the atmosphere is responsible for increased global warming of our planet. The increasing concentration of carbon dioxide mainly from flue gas, automobile and landfill emissions in the atmosphere is the major contributor to this problem with more than 80% of total GHG emissions. On the other hand, landfill gas (LFG) is a multi-component mixture containing mainly methane and carbon dioxide. It can be treated as an important resource of directly available methane, and constitutes one of the main sources of methane and carbon dioxide emissions. For these reasons, together with a tighter control in emissions to meet Kyoto Protocol targets, separations of CO_2/N_2 and CO_2/CH_4 gases need to be realized for different applications. In this work, adsorption separations of these gases on zeolite 13X and silicalite were studied by determining pure and binary mixture behavior using constant volume and concentration pulse chromatographic techniques.

Several theoretical adsorption models were discussed for their applications for the pure gas behavior of carbon dioxide, methane and nitrogen gases in the range of 0-5 atmospheres at 40 °C and 100 °C.

Mixture adsorption isotherms and separation factors for the above mentioned 2 binary systems were also determined experimentally at 40 °C and 100 °C under 1 atmosphere total pressure and compared to predicted binary behavior.

The effect of the ratio of Si / Al in the adsorbent was discussed and the two adsorbents, 13X and silicalite, were compared for their potential use in separating CO_2, N_2 and CH_4 gases.

APPENDIX II

BINARY ADSORPTION BEHAVIOR OF METHANE AND NITROGEN GASES

Mulgundmath, V.P [a]., Li, P [a]., Tezel, F.H [a]., Hou, F [a]., Mogan, J [b]., Golden, T.C [c]., Morin, B [b]

a Department of Chemical Engineering, University of Ottawa, 161, Louis Pasteur, Ottawa. K1N 6N5. CANADA

b Alcan Specialty Aluminas, 1000 Development Drive, P O Box 250, Brockville. ON K6V 5V5. CANADA

c Air Products and Chemicals, Inc., 7201, Hamilton Blvd., Allentown, PA USA 18195-1501, USA.

Accepted to be presented in FOA9 (Fundamentals Of Adsorption 9th International Conference) in Sicily, Italy on May 20-25, 2007 (Paper is available).

It will be submitted to a journal.

ABSTRACT

In this work, adsorption separation of methane and nitrogen by 13X, Actiguard Activated Aluminas and Silicalite has been studied by constant volume method and concentration pulse chromatographic technique to obtain the pure and mixture adsorption isotherms at 40 and 100 °C.

Several adsorption isotherm models have been discussed for their application to the pure gas isotherms of methane and nitrogen. Also, ideal separation factors were calculated from the pure component isotherms.

Mixture adsorption isotherms for the binary system of methane and nitrogen at 40 and 100 °C under 1 atmosphere total pressure have been determined using three concentration pulse methods: HT- CPM (Harlick and Tezel Concentration Pulse Method), MTT - CPM (Modified Triebe and Tezel Concentration Pulse Method) and MVV - CPM (Modified Van der Vlist and Van der Meijden Concentration Pulse Method). The applications of some theoretical models for binary adsorption systems have also been discussed.

For the systems studied, the integral thermodynamic consistency test between pure and binary equilibrium adsorption data has been carried out. Different adsorbents, 13X, Actiguard Activated Aluminas and Silicalite, have been compared for their potential in industrial applications for this separation.

APPENDIX III

THE UNIT OF HENRY'S LAW CONSTANT AND THE RELATION BETWEEN THE TWO HENRY'S LAW CONSTANTS

Dimensionless Henry's law constant $K_{dim} = q^*/ c$ or $K_{dim} = q / c$ (Karger and Ruthven, 1992; Yang, 1987), where q (q*) is (equilibrium) adsorbate amount adsorbed per unit volume of the pellets of the adsorbent in cm^3 (adsorbate) / cm^3 (adsorbent) or in m^3 (adsorbate) / m^3 (adsorbent) (Yang, 1987; Karger and Ruthven, 1992; Nokerman etc., 2005); c is adsorbate concentration in vapor phase or bulk flow in mol (adsorbate) / mol (vapor phase or bulk flow) (Yang, 1987; Karger and Ruthven, 1992; Nokerman etc., 2005)
So the unit of K_{dim}:

$$\frac{cm^3\ (adsorbate) / cm^3\ (adsorbent)}{mol\ (adsorbate) / mol\ (vapor\ phase\ or\ bulk\ flow)}$$

When the total pressure is 1 atm., adsorbate concentration in vapor phase or bulk flow is the adsorbate pressure in atm. in vapor phase or bulk flow, so the unit of K_{dim}:

$$\frac{cm^3\ (adsorbate) / cm^3\ (adsorbent)}{atm\ (adsorbate)}$$

So the unit of K_{dim}:

$$K_{dim}\left(\frac{cm^3\ (adsorbate) / cm^3 (adsorbent)}{atm\ (adsorbate)}\right) = K\left(\frac{cm^3\ (adsorbate) / g(adsorbent)}{atm\ (adsorbate)}\right) \times \rho\left(\frac{g(adsorbent)}{cm^3 (adsorbent)}\right)$$

$$K_{dim}\left(\frac{cm^3\ (adsorbate) / cm^3 (adsorbent)}{atm\ (adsorbate)}\right) = K\left(\frac{mmol\ (adsorbate) / g(adsorbent)}{atm\ (adsorbate)}\right) \times 22.4\left(\frac{cm^3}{mmol}\right) \times \rho\left(\frac{g(adsorbent)}{cm^3 (adsorbent)}\right)$$

Therefore, at standard temperature and pressure, the relation between the two Henry's law constants is

$$K_{dim} = 22.4 \times \rho[g.cm^{-3}(adsorbent\ pellet)] \times K_p[mmol\ (adsorbate).g^{-1}(adsorbent).atm^{-1}\ (adsorbate)]$$

Or under any conditions,

$$K_{\text{dim}} = RT\rho K_p$$

where T is the absolute temperature, ρ is the density of the pellets of the adsorbent and K_p is the dimensional Henry's Law adsorption equilibrium constant.

Usually, the unit

$$[\text{mmol (adsorbate)}.\text{g}^{-1}\text{(adsorbent)}.\text{atm}^{-1}\text{ (adsorbate)}]$$

for dimensional Henry's law constant, K_p, can be used.

RERERENCES

Karger, Jorg and D. M. Ruthven, "Diffusion in Zeolited", John Wiley and Sons, Inc., Toronto, Ontario, Canada (1992), p225, 233, 275, 291, 294-295, xxv.

Nokerman, J., X. Canet, P. Mougin, S. Limborg-Noetinger and M. Frere, "Comparative Study of the Dynamic Gravimetric and Pulse Chromatographic methods for the Determination of Henry constants of Adsorption for VOC-Zeolite Systems", Measurement Science and Technology, 16, 1802-1812 (2005).

Yang, R. T., "Gas Separation by Adsorption Process", Butterworth Publishers, Stoneham, MA (1987), p102, 135, 136, 143-148, 196-197, 223.

APPENDIX IV

ZERO LENGTH COLUMN (ZLC) METHOD[1]

INTRODUCTION

ADVANTAGES

PRINCIPLE

EXPERIMENT SYSTEM

THOERY

OPERATING CONDITIONS

REFERENCES

INTRODUCTION: A variety of different flow methods have been developed in which the diffusivity, or the diffusional time constant, is determined from measurements of the dynamic response of an adsorption column to a perturbation in the sorbate concentration at the inlet. Numerous experimental studies have been reported in which diffusion measurements have been made by both chromatographic and sorption rate measurements for the same system. Such methods include conventional chromatographic measurements using a pulse or a step injection of sorbate (in Chapters II and III), frequency response measurements using a sinusoidal variation of sorbate concentration and zero length column or ZLC method (short column measurements) carried out under limiting conditions of high flow rate such that the column behaves as a differential bed. These techniques were originally developed for gaseous systems, but they have been successfully extended to liquid phase sorption systems.

The conventional chromatographic technique offers advantages of speed and simplicity and when properly applied it can provide reasonably accurate measurements of intracrystalline diffusivities in both gas and liquid systems. However, to ensure reliable results a wide range of checks including variation of fluid velocity and particle size are needed. In the conventional chromatographic method the main difficulty is to eliminate or allow for axial dispersion and this is the most likely source of error where unrealistically small apparent diffusivities have been reported. The ZLC method avoids the problem of axial dispersion although the problem in that method is to ensure the absence of external film resistance. While this is normally not a severe restriction it may cause difficulty with strongly adsorbed and rapidly diffusing species.

ADVANTAGES: The major advantage of the chromatographic method is that by maintaining a relatively high carrier flow rate through the column, external mass and heat transfer resistances can be eliminated more easily than in a static system. The major disadvantage is that the dispersion of the response depends on both mass transfer resistance and axial dispersion. In order to determine the mass transfer resistance, and hence the intraparticle diffusivity, it is necessary to either eliminate or allow for the contribution from axial dispersion. This imposes an upper limit on the diffusional time constant (r^2/D) that can be measured since, if intraparticle diffusion is too rapid the contribution from axial

dispersion becomes dominant and it is then impossible to extract reliable kinetic data. The ZLC method was developed in an attempt to retain the basic advantages of the chromatographic method while eliminating the limitations imposed by axial dispersion. The method is especially useful for measuring intracrystalline diffusion in zeolites since only a very small sample of adsorbent is required and relatively high diffusivities can be measured (D/R^2 >0.01 s^{-1}). It has been applied to a wide range of hydrocarbons in NaX, 5A, and silicalite.

PRINCIPLE: The principle of the ZLC method is straightforward. A small sample of the adsorbent is equilibrated at a uniform sorbate concentration, preferably within the Henry's Law range, and then desorbed by purging with an inert gas at a flow rate high enough to maintain essentially zero sorbate concentration at the external surface of the particles or crystals. The desorption rate is measured by following the composition of the effluent gas. This requires a sensitive detector since the concentration is very low. For organic sorbates a flame ionization detector is particularly useful since it has the required sensitivity and can be used without interference with any inorganic purge gas. It has the further advantage that it is not sensitive to moisture which may be present as a trace impurity or even added in controlled quantities to investigate the effect on the diffusional behavior of the system. Although developed originally for gaseous systems, the method has been extended to the study of liquid systems using an ultraviolet absorption detector to follow the desorption of aromatics into a purge of saturated hydrocarbon.

EXPERIMENT SYSTEM: The basic experimental system for vapor phase measurements is shown schematically in Figure A4.1. The cell contains a very small quantity of zeolite crystals (or other adsorbent) placed between two porous sinter discs. The individual crystals are dispersed approximately as a monolayer across the area of the sinter to ensure good contact with the purge gas stream, thus minimizing external resistance to heat and mass transfer. Changing the purge gas from He to Ar offers a convenient way of testing for the intrusion of extracrystalline resistances since, if such resistances are significant a change in the molecular diffusivity (and thermal conductivity) of the gas should affect the mass transfer rate and thus the desorption curve.

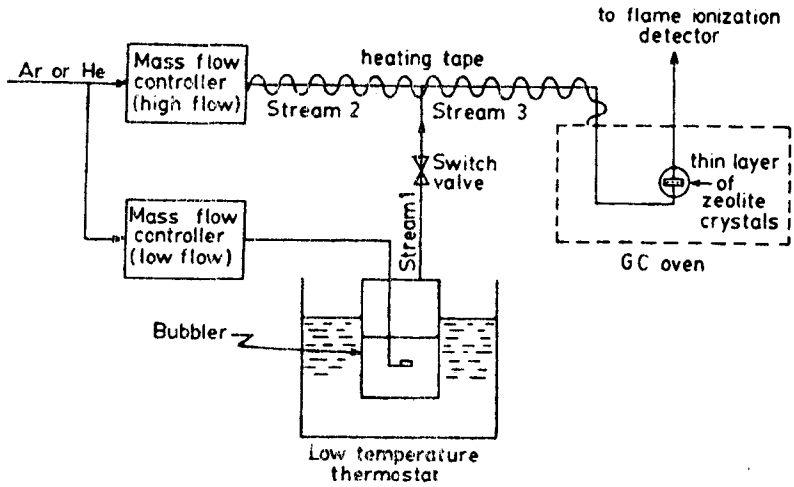

Figure A4.1. Schematic diagram showing the experimental system for ZLC measurements.[2]

Although the principle of the method is straightforward, to achieve reliable results detailed attention must be paid to the design of the experimental system. Since the quantity of adsorbent is very small it is important to minimize any extraneous adsorption on tube walls, in valves and so on. It is best to provide completely separate lines for saturation and purge streams and to minimize the length of the common line between the ZLC cell and the detector. Blank runs can be made with the adsorbent removed to confirm the successful elimination of extraneous adsorption and to determine the response time of the system.

THOERY: In the absence of significant external resistance to mass transfer, equilibrium will be maintained between the purge gas and the sorbate at the external surface of the crystal. By solving the Fickian diffusion equation together with a mass balance over the ZLC cell we obtain the expression for the effluent concentration:

$$\frac{c}{c_0} = 2L\sum_{n=1}^{\infty}\frac{\exp(-\beta_n^2 Dt/r_c^2)}{[\beta_n^2 + L(L-1)]} \quad \text{.....(A4.1)}$$

where β_n is given by the roots of the transcendental equation,

$$\beta_n \cos\beta_n + L - 1 = 0 \quad \text{.....(A4.2)}$$

$$L = \frac{\varepsilon v r_c^2}{3(1-\varepsilon)KDl} = \frac{1}{3}\frac{PurgeFlowRate}{CrystalVolume}\frac{r_c^2}{KD} \quad \text{.....(A4.3)}$$

For $L \rightarrow 0$. Equation A4.1 approaches the limiting solution for qquilibrium control:

$$\frac{c}{c_0} = \exp\left[\frac{-\varepsilon vt}{(1-\varepsilon)Kl}\right] \quad \text{.....(A4.4)}$$

Under these conditions the desorption curve contains no kinetic information. If the objective is to measure the intracrystalline diffusivity this regime must obviously be avoided.

For large values of L, $\beta_n \rightarrow n\pi$ and Eq. 10.62 reduces to

$$\frac{c}{c_0} = 2L\sum_{n=1}^{\infty} \frac{\exp(-n^2\pi^2 Dt/r_c^2)}{\left[n^2\pi^2 + L(L-1)\right]} \quad \text{.....(A4.5)}$$

which, in the long time region simplifies to

$$\frac{c}{c_0} = \frac{2}{L-1}\exp(-\pi^2 Dt/r_c^2) \quad \text{.....(A4.6)}$$

If external mass transfer resistance is significant the analysis is basically similar except that the value of L is modified to

$$\frac{1}{L} = \frac{3lKD}{vr_c^2}\left(\frac{1-\varepsilon}{\varepsilon}\right) + \frac{2}{Sh}\frac{KD}{D_m} = DK\frac{3\times CrystalVolume}{r_c^2 \times PurgeFlowRate} + \frac{2}{ShD_m} \quad \text{.....(A4.7)}$$

Intracrystalline diffusivities can be measured even in the presence of film resistance provided that the latter is not dominant.

The diffusional time constant can be extracted from the desorption curves in several different ways. If measurements can be made at a sufficiently high flow rate so that L is large, the value of D/r_c^2 may be derived directly from a plot of $ln(c/c_0)$ versus time, according to Equation A4.6. With rapidly diffusing sorbates, however, it is not always possible to operate at sufficiently high L values. An alternative approach is to work directly with Equation A4.1 and A4.3 using as high a flow rate as is practically convenient. According to Equation A4.1 a plot of $ln(c/c_0)$ versus time, in the long time region, should yield a slope $\beta_1^2 D/r_c^2$ and an intercept given by $2L/[\beta_1^2 + L(L-1)]$. Since L and β_1 are related through Equation A4.3 we have three equations that can be solved for the three unknowns (β_1, L, and D/r_c^2). If this approach is adopted an independent estimate of the L value may be obtained from measurements at very low flow rates in the equilibrium regime. Such measurements yield directly $\varepsilon/(1-\varepsilon)Kl$ (from Equation A4.4) so the value of LD/r_c^2 at

any other velocity can be found directly. Further confirmation of the consistency of the data may be obtained by varying the crystal size and the nature and flow rate of the purge gas as illustrated in Figure A4.2. It is noteed that the curves obtained with He and Ar at the same flow rate are essentially identical, confirming the absence of extracrystalline resistance to mass transfer. The curves for 100 μm and 50 μm crystals show the fourfold difference in time constants which is expected for intracrystalline diffusion control. Consistency of the derived diffusivity values with the values obtained directly from gravimetric sorption rate measurements has been confirmed for several systems.

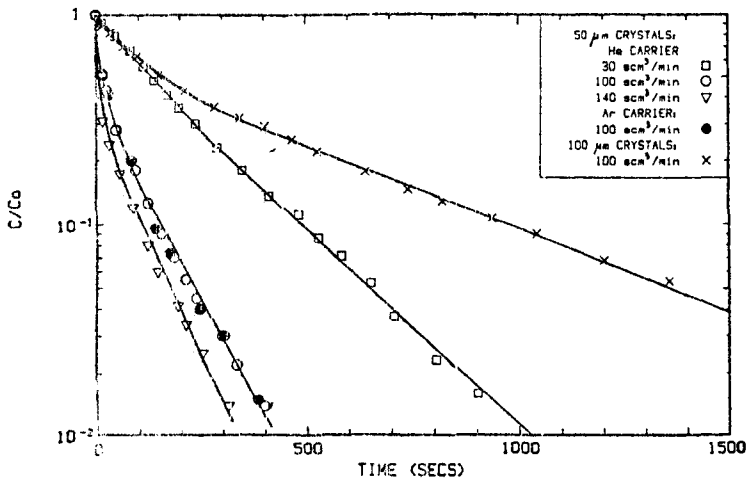

Figure A4.2. ZLC response curves for o-xylene in NaX crystals at 200°C with changing crystal size, purge rate and the nature of the purge gas. (All curves are consistent with $D_c = 0.9 \times 10^{-8}$ cm^2 s^{-1}).[3]

OPERATING CONDITIONS: To ensure kinetic control requires L > 1.0 and this requirement imposes, in principle, a limit on the fastest process that can be measured. It follows from Equation A4.7 that the maximum possible L value is given by $L \approx ShD_m / 2KD$, and taking Sh=2.0 as a conservative estimate this gives $L_{max} \approx D_m / KD$. This is not a serious limitation for vapor phase systems as KD is generally much smaller than D_m. However, for liquid phase systems this restriction can be important.

To eliminate external film resistance it is necessary to operate under conditions such that

$$\frac{r_c^2}{15RD} >> \frac{r_c}{3k_f} \quad \text{(A4.8)}$$

which, taking Sh = 2.0, reduces to

$$\frac{D_m}{KD} >> 1.0 \quad \text{(A4.9)}$$

This condition is easily fulfilled for weakly adsorbed species but can be critical when the sorbate is very strongly adsorbed. The most serious limitation on the choice of operating conditions is generally the requirement that the rate of the process be slow enough to measure without intrusion of extraneous time delays resulting from the inevitable dead volume in the system. A reasonable criterion is

$$\frac{D}{r_c^2} << 0.05s^{-1} \quad \text{(A4.10)}$$

REFERENCES

[1] J. Karger and D. M. Ruthven, Diffusion in Zeolites and other Microporous Solids, John Wiley and Sons Inc., New York, NY, pp.328-333 (1992).

[2] M. Eic and D. M. Ruthven, Zeolites 8, 327 (1988).

[3] D. M. Ruthven and M. Eic, ACS Symp. Ser. **368**, 362 (1988).